Study of cellular mechanisms allowing dendritic cell migration in restricted spaces

Lucie Barbier

université PARIS-SACLAY

Study of cellular mechanisms allowing dendritic cell migration in restricted spaces

Thèse de doctorat de l'université Paris-Saclay

École doctorale n°577 : Structure et Dynamique des Systèmes Vivants (SDSV)
Spécialité de doctorat : Sciences de la Vie et de la Santé
Unité de recherche : UMR144 Biologie Cellulaire et Cancer, Institut Curie, 75005, Paris
Référent : Faculté des sciences d'Orsay

Thèse présentée et soutenue à l'Institut Pierre-Gilles de Gennes, Paris, le 15 Octobre 2020, par

Lucie BARBIER

Composition du Jury

Guillaume MONTAGNAC CR, HDR, Institut Gustave Roussy, Université Paris-Saclay	Président
Marie-Emilie TERRET DR, HDR, Collège de France	Rapporteur & Examinatrice
Tim LÄMMERMANN DR, Max Planck Institute of Immunobiology and Epigenetics	Rapporteur & Examinateur
Florence NIEDERGANG DR, HDR, Institut Cochin	Examinatrice
Pablo VARGAS CR, HDR, Institut Curie	Directeur de thèse
Matthieu PIEL DR, HDR, Institut Curie	Co-Directeur de thèse

Thèse de doctorat

NNT : 2020UPASL028

« Être docteur, ce n'est pas simplement un manuscrit et une soutenance, c'est un état d'esprit. »

Benoît

ACKNOWLEDGMENTS

Je souhaiterais commencer ce manuscrit en remerciant toutes les personnes qui y ont participé, qui m'ont soutenue et sans qui ce travail n'aurait pas abouti.

À mon jury, Guillaume Montagnac, Florence Niedergang et particulièrement aux rapporteurs, Marie-Emilie Terret, Tim Lämmermann, merci d'avoir pris le temps d'évaluer mon travail.

À mon comité de thèse, Danijela Vignjevic, Stéphanie Descroix et Manuel Théry, merci pour vos conseils tout au long de ces quatre ans.

Au Ministère de l'Enseignement supérieur de la Recherche et de l'Innovation et aux donateurs de la Fondation pour la Recherche Médicale, merci d'avoir financé mes quatre années de recherches doctorales.

À Matthieu P., merci de m'avoir accueillie dans votre laboratoire, pour vos nombreuses idées et votre soutien scientifique tout en me laissant la liberté de mener mes projets au laboratoire et en dehors.

À Pablo V., merci de m'avoir encadrée pendant ces quatre ans, de m'avoir appris tous les secrets des DCs et à chuchoter à l'oreille des microscopes. Tu m'as accompagnée avec bienveillance vers l'indépendance, j'espère que tu pourras t'épanouir et mener à bien tes projets avec tes prochains doctorants.

À tous les membres actuels et passés de l'équipe Bio6, merci pour toute l'aide que vous m'avez apportée des premières manips jusqu'à la présentation de thèse et pour les nombreuses discussions pas toujours scientifiques mais à chaque fois passionnées et intenses ; Pablo S., Mathieu D., Aastha et Mathilde pour les longues discussions du lundi matin et tous les conseils scientifique et technique ; Olivier (Jian), Li et Rafaele pour la micro-fabrication, Juanma pour le partage de ton enthousiasme indéfectible pour les sciences, Larisa et Bianca pour être toujours prête à aller prendre un verre, Ghuuuuilerme pour ton expertise sur les lovely WB et dynamic confiner, Alice (pour l'orthographe de ces remerciements) et Zahraa pour les séances salon de thé dans le labo, Damien pour rester simplement toi-même, Nishit pour tes blagues que je comprendrai un jour, Ido et Valentin pour le regard différent que vous avez porté sur mon travail, et Nico pour l'analyse d'image et surtout pour permettre au labo de continuer à tourner avec tous ce petit monde.

À l'équipe des Lennon et en particulier Anna et Doriane, merci pour l'aide que vous m'avez

apportée sur les DCs.

Aux personnels des plateformes de l'IPGG et de Curie : Guillaume(s), Olivier, Nawel, Bertrand, Kevin, Nhung et Ludovic, merci pour votre disponibilité et votre aide au cours de mes longues séances en salle de microscopie.

Aux personnels administratifs : Caroline, Gabriela, Edwige N, Edwige, Sylvia et Rolie, merci pour votre support qui a facilité mon quotidien à l'IPGG et à Curie.

À Perrine et Manon, merci pour votre sourire et votre positivisme et merci de m'avoir accueilli dans votre bureau de la bonne humeur durant ma dernière année de thèse. En particulier, merci Perrine pour toute l'énergie que tu donnes pour faire vivre l'IPGG et pour m'avoir initiée à la Com'-Innovation.

Aux autres membres du 3ème étage de l'IPGG : l'équipe Micromégas, Jacques et son équipe, Tommaso et sa futur équipe, merci pour l'atmosphère sympathique et ouverte que vous avez su créer lors de nos discussions de couloirs et des soirées de Noël.

À l'équipe du 4ème et en particulier à Steph, merci d'avoir été toujours présent pour papoter, m'apporter votre soutien scientifique et personnel, et surtout pour partager vos gâteaux.

Un merci particulier à Larisa, Juanma, Léa et Elodie avec qui j'ai traversé cette période de thèse et qui l'ont égayée de Saint-Marc, jambon espagnol, séances de bad et goûters. Bonne chance à tous les quatre pour la suite et j'espère que nos chemins se recroiseront.

À mes amis d'enfance, de Bio, du BDE, du YRLS et du Palais, merci pour tous les bons moments et aventures partagés au cours de ces quatre ans, de vrais bols d'air qui m'ont fait relativiser les déboires de la thèse.

À ma famille et mes proches, merci de m'avoir soutenue tout au long de ces longues études qui ont pu vous paraître sans fin !


migration
Cells
Actin
Dendritic
motility
mDCs
nucleus
Immune
MyosinII
Microchannels
movement
confinement
interstitial
deformation
MTOC
lysosomal
lysosomes
lymphatic
membrane
cytoskeleton
organization
contractility
microtubules
microtubule
microchannel
remodeling
actomyosin
Arp2/3
ROCK
cluster
chemokine
adhesion
microenvironment
molecular
dendritic
speed
Golgi
antigens
antibodies
MDCs
mDC
length
vessels
inflammatory
lymphocytes
lysosome
pathogens
coordination
blood
tissues
formins
ECM
PDMS
confined
F-actin
proteins
tissue
properties
cortical
rapid
cortex
force
Cell
antigen
forces
innate
flow
pore
cytokines
signals
irregular
polymerization
polarization
channels
neutrophils
constrictions
leukocytes
velocity
extracellular
recruitment
lymph
system
gels
Physical
CCL21
lamin
narrow
immature
signal
adaptive
constriction
maturation
mechanism
BMDCs
LPS
MHCII
CD4
retractioninfection
microfabricated
Arp2/3
cluster
ROCK
contractile
interaction
MyoII-GFP
pathogen
protrusions
mechanisms
migrate
migrating
matrix
environment
environments
mechanical
Y-27632
microenvironments
protrusion
molecules

Table of content

METHODS

FIGURE LIST

ABBREVIATIONS

2D: 2 dimensions

3D: three dimensional

ABP: actin-binding protein

ATP: Adenosine Triphosphate

BCR: B Cell Receptor

BMDC: bone marrow-derived dendritic cell

CD4+ LT: CD4-positive T lymphocyte

CD8+ LT: CD8-positive T lymphocyte

cDC: Conventional dendritic cell

DAMP: danger-associated molecular pattern

DC: dendritic cell

ECM: extracellular matrix

ELC: essentials light chain

ER: endoplasmic reticulum

ERM: Ezrin, radixin and Moesin

ESCRT: Endosomal Sorting for Transport

F-actin: Filamentous actin

FMNL1: formin-like 1

FRC: Fibroblastic reticular cells

FRET: fluorescence resonance energy transfer

G-Actin: monomeric actin

GAP: GTPase activator protein-

GDI: GDP-dissociation inhibitor-

GDP: Guanosine diphosphate

GEF: GTP-exchange factor

GFP: Green fluorescent protein

GM-CSF: granulocyte-macrophage colony-stimulating factor

GPCR: G-protein coupled receptors

GTP: Guanosine triphosphate

IDC: Immature dendritic cell

IF: Immunofluorescence

Ii: invariante chain

KO: Knock out

LINC: Linker of Nucleoskeleton and cytoskeleton

LN: lymph nodes

LPS: lipopolysaccharide

MAP: Microtubules associated portein

MDC: Mature dendritic cell

MHC I: Major histocompatibility complex class I

MHC II : Major histocompatibility complex class II

MHC: **Major histocompatibility complex**

MLCK: myosin light chain kinase

MTOC: microtubule organizing center

mTOR: mechanistic target of rapamycin

MyoII: Non-musle myosin Class II

NLS: nuclear localization sequence

PAMP: pathogen-associated molecular pattern

PDMS : Polydimethylsiloxane

PRR Pattern-recognition receptors

RLC: regulatory light chain

ROCK: Rho-associated coiled-coil containing kinase

ROI: regions of interest

SD: standard deviation

SEM: standard error of the mean

Sema3: class 3 semaphorins

TCR: T cell Receptor

TFEB: Transcription factor EB

TLR: Toll-Like Receptor

TRPML1: Transient Receptor Potential cation channel, Mucolipin subfamily, Member 1

WASH: WASP and SCAR homolog

WASP: Wiskott–Aldrich Syndrome protein

WGA: Wheat Germ Agglutinin

WT: Wild-type

INTRODUCTION

CHAPTER 1: DENDRITIC CELL MIGRATION DURING IMMUNE RESPONSE

The immune system facilitates the elimination of pathogens and damaged cells. Its proper functioning is essential for maintaining the integrity of the organism. It is a molecular and cellular system that detects and eliminates pathogens. Unlike conventional organs, the immune system is made up of billions of cells scattered throughout the body. The coordination of their function involves a strict regulation of their movement within the body. The immune response is the main physiological process that involves cell migration at the adult stage. In this first introductory chapter, I present an overview of the immune system organization and the migration processes involved in the immune response and highlight the central role of dendritic cells (DCs)—the focus of my doctoral research.

I. Principles and organization of the immune system

A. Two types of immune response

Two types of immune responses have been described on the basis of their activation process.

1. Innate immune response

The innate immune response detects a limited set of conserved features associated with pathogens: the pathogen-associated molecular patterns (PAMPs) or, with tissue damage: the danger-associated molecular patterns (DAMPs). PAMPs are common to a family of pathogens—for example, the gram-negative bacterial cell wall component lipopolysaccharide (LPS) or viral nucleic acids—whereas DAMPs include mainly cytosolic components, such as adenosine triphosphate (ATP), released into the extracellular medium upon non-controlled cell death (Alberts et al., 2002a).

The innate immune cells detect PAMPs and DAMPs through pattern-recognition receptors (PRRs), which are cytosolic or present on the cell surface. The different classes of PRRs trigger different immune signals depending on the type of pathogens encountered. For example, the toll-like receptor (TLR) 4 binds to LPS on the plasma membrane and triggers an anti-bacterial immune response. TLR3, TLR7, TRL8, and TLR9 bind to different types of viral nucleic acids in endolysosomes and trigger an antiviral response (Mogensen, 2009). The combined expression of PRRs by a large number of cells facilitates the direct pathogen sensing upon infection. Thus, the innate immune response occurs almost immediately after pathogen entry into the body.

Pattern-recognition receptors are hereditary; effective pathogen recognition is based on host-pathogen co-evolution. Thus, the innate immune response evolves at the population level (Alberts et al., 2002a).

2. Adaptive immune response

The adaptive immune response is based on the specific detection of each pathogen by a vast and diverse repertoire of receptors present on effector cells. A particular receptor recognizes a specific peptidic marker of a pathogen—the antigen—and is present in very small numbers in the body. Thus, the adaptive immune response requires a step of activation and expansion of pathogen-specific effector cells; this activation step is crucial for an effective immune response (Alberts et al., 2002b).

The receptor repertoire is formed by a random gene rearrangement and is not hereditary. Successive activation and clonal expansion events shape the repertoire over the lifetime of an individual (Alberts et al., 2002b).

B. Steady-state organization of the immune system

The immune system comprises more than a billion cells with specific functions. Immune cells are not all assembled in the same compartment as conventional organs. They are localized in specialized lymphoid organs, circulate in the blood or lymphatic system, or infiltrate tissues for immune surveillance (Mescher, 2016).

The primary lymphoid organs—bone marrow and thymus—produce immune cells, whereas the secondary lymphoid organs generate the immune response. They ensure the immune surveillance of extracellular fluids: the spleen for blood, lymph nodes for lymph, and unencapsulated

lymphoid organs for tissue fluid from the intestine or mucosa (Mescher, 2016). In the context of my doctoral research, I will elaborate on the immune response in the lymph nodes.

Immune cell scattering in different compartments involves cell movement throughout the body and communication between cells. The immune cells interact through direct cell-to-cell contact or by secretion of soluble factors—the cytokines (Xie et al., 2013). In the following section, I present the different cell types involved in the immune response.

C. Innate immune cells

Innate immune cells detect and respond directly to pathogen entry with their set PRRs. They form the first line of warning and defense (Alberts et al., 2002a). I will first describe the non-antigen-presenting innate cells.

Granulocytes are short-lived leukocytes circulating in the blood. They include eosinophils, basophils, and neutrophils, the most abundant white blood cells. Neutrophils are recruited within a few hours at the site of infection. They contain specialized granules and can engulf pathogens by phagocytosis. They are essential for the immune response against extracellular pathogens (bacteria, fungi, or parasites) (Luster et al., 2005).

Mast cells are tissue-resident sentinels. They are in close proximity to arterioles and venules. Upon detecting pathogens or sensing inflammatory signals, they release a substantial quantity of cytokines through degranulation. They are essential for leukocyte recruitment at the site of infection (Luster et al., 2005).

Natural killer cells are lymphocytes circulating in the blood vessels. They detect and eliminate infected or stressed cells. They play a central role in anti-viral and anti-cancer immunity (Luster et al., 2005).

D. Adaptive immune cells

Adaptive immunity is a pathogen-specific response mediated by B and T lymphocytes. A fraction circulate in the bloodstream. However, their activation occurs mainly in the secondary lymphoid organs. This section provides an overview of the specificity and effector functions of these two main types of lymphocytes (Alberts et al., 2002b).

T lymphocytes express a T-cell receptor (TCR), and B lymphocytes express a transmembrane

immunoglobulin, the B-cell receptor (BCR). There is a wide variety of TCRs and BCRs, each specifically recognizing one antigen. Each T or B cell expresses only one type of TCR or BCR. Thus, they detect one antigen specific to one pathogen. Estimates suggest that each TCR or BCR is present on approximately only hundred cells in an adult. Because of this very restrictive number, they cannot directly detect and eliminate a pathogen. Their immune action relies on a critical step of activation and expansion (Alberts et al., 2002b).

1. T lymphocytes

In T lymphocytes, TCRs form a complex with the transmembrane molecule CD4 or CD8. They interact with antigens bound to the major histocompatibility complex (MHC) of a presenting cell (Abbas et al., 2017a).

CD4-positive T lymphocytes ($CD4^+$ TLs) recognize antigens presented on MHC class II (MHC II) molecules. Upon activation by the cognate antigen, they differentiate into helper T cells. The helper T cells stimulate CD8-positive T lymphocytes ($CD8^+$ TLs) or B lymphocytes and orchestrate the adaptive immune response (Abbas et al., 2017b).

$CD8^+$ TLs recognize antigens presented on MHC class I (MHC I) molecules. Their activation requires an interaction with both the cognate antigen and helper T cells. They differentiate into cytotoxic T cells and migrate to the site of infection. They induce specific apoptosis of infected cells or tumor cells presenting the cognate antigen on their MHC I molecules (Abbas et al., 2017c).

2. B lymphocytes

B cell activation requires two signaling events. First, the BCR interacts with the cognate antigen in soluble form or on a presenting cell. The BCR–antigen complex is internalized, and the cognate antigen is loaded onto MHC II molecules. The second activation step involves the interaction between the B cell and a helper T cell specific for the antigen presented on MHC II. Activation of B cells leads to their differentiation into plasma cells. They release a substantial amount of a soluble version of their BCR in the bloodstream. These antibodies bind the pathogens with high affinity and promote their recognition and elimination by other effector molecules or immune cells (Abbas et al., 2017d).

The adaptive immune response relies on the specific interaction between an antigen and its BCR or TCR counterpart. The probability of a random interaction throughout the body is low. Cellular

organization and communication in the lymph nodes optimize the rate of this encounter and facilitate effective activation of the adaptive response. $CD8^+$ TL activation leads to a cellular immune response, whereas B cell activation leads to a humoral immune response. During activation, B and T cells also detect co-stimulatory molecules and cytokines produced by antigen-presenting cells. They trigger the differentiation of effector cells into specific subtypes, which I have not presented in detail here. They facilitate the fine-tuning and adaptation of the immune response to the pathogen characteristics and the inflammatory context (Hilligan and Ronchese, 2020). Upon activation, a subset of cells differentiates into long-lived memory cells, which facilitate a faster response in the event of a second infection with the same pathogen. Finally, the integrity of the organism requires a tolerance mechanism that eliminates B or T cells reacting to self-antigens (Alberts et al., 2002b). This process will not be described in this thesis.

E. Antigen-presenting cells

Antigen-presenting cells link the innate immune response to the adaptive immune response. They have the ability to process external antigens on the MCHII and to detect infection through PRRs. Thus, they restrict the adaptive immune response to a pathogenic context. They are also migratory cells that transfer antigens from the site of infection to the lymph node. Most antigen-presenting cells are tissue resident; however, a fraction of these cells circulate in the blood. Macrophages and dendritic cells (DCs) are considered professional antigen-presenting cells (Kambayashi and Laufer, 2014). The present doctoral research focuses on DCs, which are the major antigen transporters from the periphery to the lymph nodes.

1. Macrophages

Macrophages are tissue-resident cells. They originate from embryonic precursors or are differentiated from monocytes after entering tissues. They are highly phagocytic and can directly eliminate pathogens. They also play a critical role in resolving inflammation and tissue homeostasis by removing cellular debris or apoptotic vesicles (Perdiguero and Geissmann, 2016).

2. Dendritic cells

There are four main types of DCs. Despite the lack of a common precursor, they are

characterized by their common ability to activate T lymphocytes (Ueno et al., 2007).

Langerhans cells—the first DC type described—are located in the dermis where they form long extensions scanning the tissue (Ueno et al., 2007).

Conventional DCs (cDCs) can be divided into two groups: resident cDCs populate lymphoid organs and participate in maintaining tolerance, whereas interstitial cDCs are located in tissues throughout the body. These are the main antigen transporters to the lymph nodes upon pathogen detection.

Plasmacytoid DCs circulate in the bloodstream and secrete large quantities of type 1 interferon, which activates the effectors of the anti-viral response (Ueno et al., 2007).

Monocyte-derived DCs differentiate from monocytes after they enter inflamed tissues. They ensure the renewal of the interstitial cDC population (Ueno et al., 2007).

In the present thesis, I focus on the interstitial cDCs, as they are the main migratory cells that activate the adaptive immune response. Henceforth, the general term DCs is used to refer to interstitial cDCs.

Figure 1 Schematic summary of the organization of the immune system in a steady-state condition

(Top panel) Presentation of the different cells of the innate (left: orange) and adaptive (right: green) immune systems. Antigen presenting cells (middle: blue) link the innate and adaptive immune systems. Image from the Servier Medical ART database.

(Bottom panel) Distribution of immune cells in the body. Innate immune cells circulate in the bloodstream and infiltrate tissues to ensure immune monitoring with antigen-presenting cells. Adaptive immune cells circulate in the bloodstream and colonize the secondary lymphoid organs (only lymph nodes and spleen represented here). At steady state, antigen-presenting cells residing in the secondary lymphoid organs ensure adaptive immune tolerance.

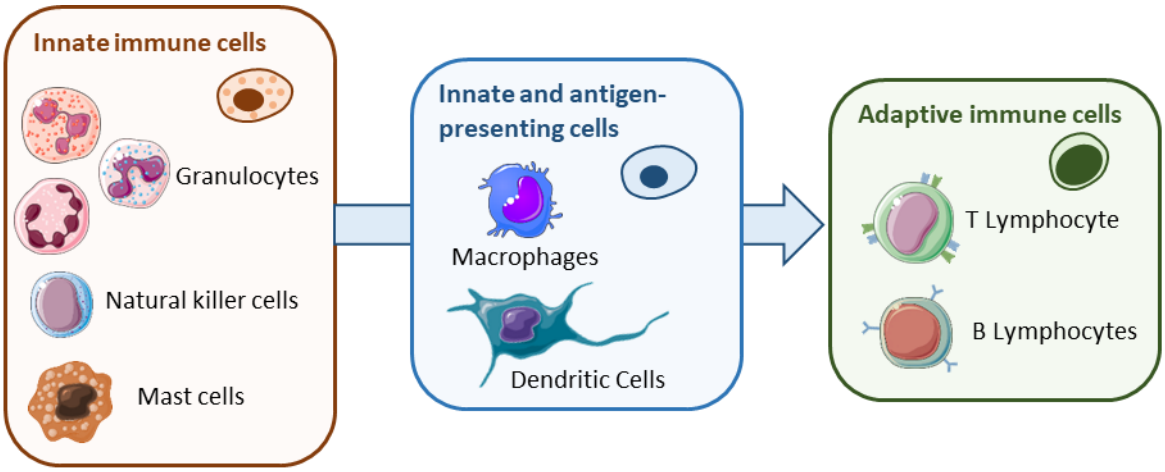
Innate immune cells
Granulocytes
Natural killer cells
Mast cells
Innate and antigen-presenting cells
Macrophages
Dendritic Cells
Adaptive immune cells
T Lymphocyte
B Lymphocytes

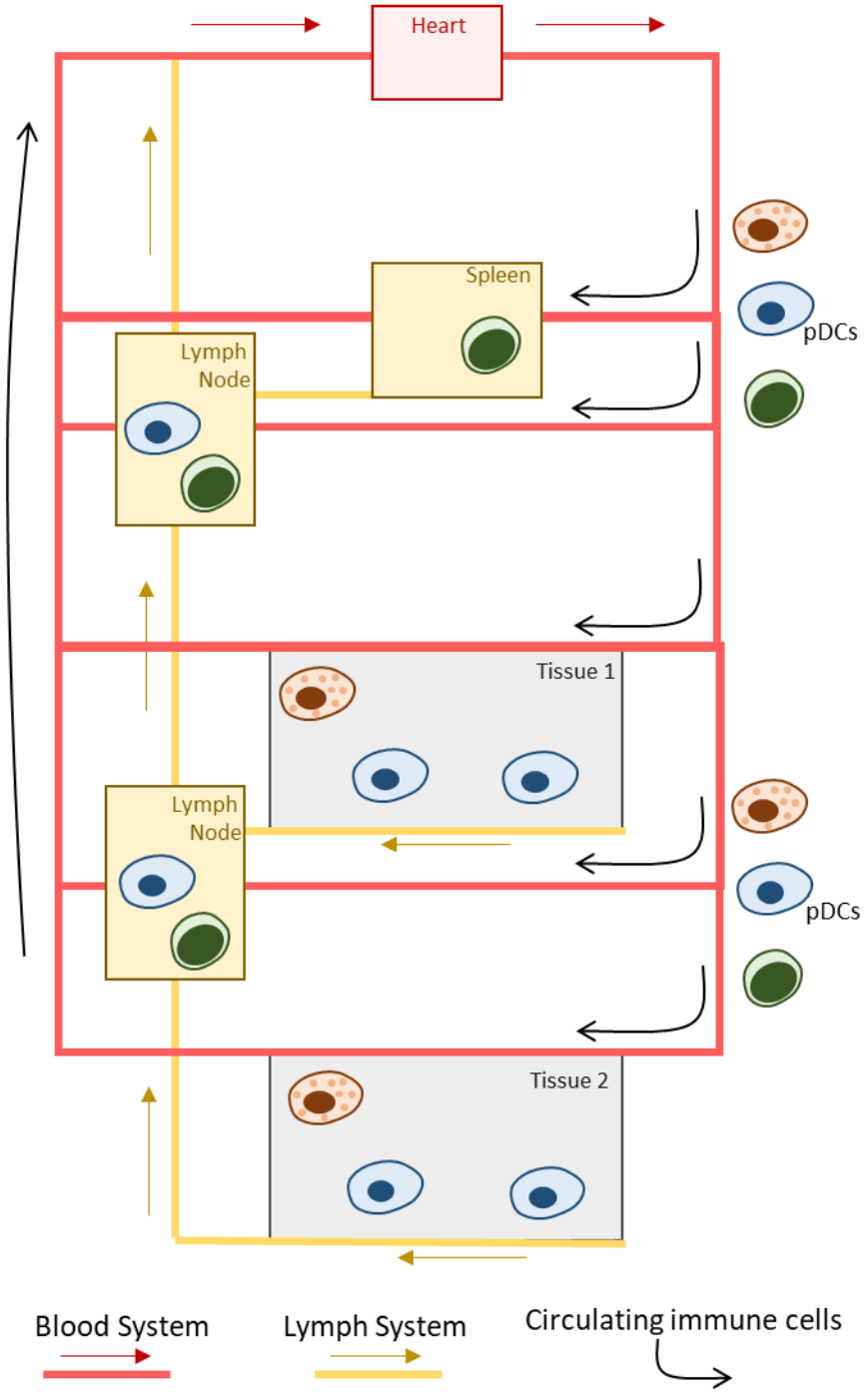
Heart
Spleen
Lymph Node
pDCs
Tissue 1
Lymph Node
pDCs
Tissue 2
Blood System
Lymph System
Circulating immune cells

This first section provides a brief description of the main actors of the immune system and their location in a steady-state condition. Next, I describe how the immune response is orchestrated in case of infection and focus on the central role of DCs as a link between the innate and adaptive immune responses (Banchereau and Steinman, 1998).

II. Local immune response: activation of the innate system

The innate immune response involves tissue-resident and blood-circulating immune cells. It is fast and restricted to the site of pathogen entry. The main function of this first line of defense is to detect the pathogen and to contain the infection.

A. Inflammation

Inflammation is a local and immediate response to an injury or pathogen entry. Tissue-resident immune cells—mainly DCs, macrophages, and mast cells—detect pathogens or damaged cells through their PRRs. The engagement of PRRs triggers signaling pathways, leading to the secretion of pro-inflammatory cytokines. The set of cytokines secreted depends on the type of PAMPS or DAMPs detected and is therefore specific to a family of pathogens. The release of pro-inflammatory cytokines corresponds to an alarm system that modifies the local environment to recruit effector immune cells (Mogensen, 2009).

Some cytokines can guide leukocytes in tissue to the site of infection; these chemoattractant molecules are named chemokines (Zlotnik and Yoshie, 2012). Another group of inflammatory cytokines acts on the blood vessel endothelium. They cause endothelial cells to increase blood flow, increase endothelial barrier permeability, and express adhesion molecules on the luminal surface of the blood vessels. This blood vessel endothelial activation promotes the entry of circulating leukocytes into the inflamed tissue (Pober and Sessa, 2007).

B. Leukocyte recruitment: from blood to the site of infection

The recruitment of blood leukocytes to the site of infection in tissues involves several steps of migration through the blood vessel endothelium and into the interstitial space. Neutrophils—the most abundant blood leukocytes—are essential for pathogen clearance, and their recruitment to

the site of infection is the most studied (Weninger et al., 2014).

1. Transendothelial migration

The transendothelial migration of neutrophils in inflamed tissues involves a well-established multi-step adhesion cascade. Selectin expression on activated endothelial cells allows neutrophils to slow down and roll along the walls of inflamed blood vessels. Integrin engagement and chemokine sensing leads to firm adhesion of neutrophils, followed by their transmigration through the endothelial cell monolayer (Vestweber, 2015). After transmigration, the neutrophils crawl into the subendothelial space confined by the dense basement membrane and pericytes surrounding the blood vessels. The neutrophils extravasate into the tissue through low-density regions of extracellular proteins in the basement membrane. Chemokines secreted by the perivascular immune cells guide the neutrophil extravasation (Vestweber, 2015).

Blood leukocyte transmigration is a limiting step that requires specific signaling events triggered by inflammation. Thus, leukocyte infiltration is limited to the site of infection (Pober and Sessa, 2007).

2. Interstitial migration

Once in the interstitial space, leukocytes navigate in a three-dimensional environment composed of a network of cross-linked extracellular matrix fibers (Lämmermann and Germain, 2014). To reach the site of infection, they integrate chemoattractant signals from tissue-resident immune cells, damaged cells, or pathogens. The neutrophil population exhibits coordinated chemotactic migration, leading to the formation of a dense cell cluster that contains the injury (Kienle and Lämmermann, 2016; Ng et al., 2011). This swarming behavior relies on the secretion of chemokines that act as a paracrine signal among the neutrophils. This process of self-amplification of a local inflammatory signal facilitates neutrophil recruitment throughout the tissue at a long distance from the site of injury (200–300 µm) and in a short time (~20 min) (Lämmermann et al., 2013).

Leukocyte migration into the interstitial space does not require high-affinity integrin signaling. Thus, immune cell recruitment is mainly orchestrated by chemokines secreted during the inflammation process and is independent of the composition and structure of the extracellular matrix. This migration mechanism, which will be described in detail later in this thesis, is a critical step in the immune response that requires leukocytes to be able to rapidly reach any type of tissues

upon detection of inflammatory signals (Lämmermann et al., 2008). Integrins transduce signals of arrest rather than migration during the immune response. They induce leukocyte adhesion on the inflamed blood vessels (Vestweber, 2015) and are necessary for neutrophil accumulation at the site of injury (Lämmermann et al., 2013).

At the site of infection, innate immune cells release molecules and enzymes that directly eliminate the pathogen or prevent its spread (Alberts et al., 2002a). The molecules are specific to the pathogen family. Phagocytic cells, mainly neutrophils and macrophages, engulf pathogens and remove cellular debris. This process is essential for the resolution of inflammation at a later stage of the immune response (Westman et al., 2020). While innate immune cells control the spread of pathogens, they release a second set of cytokines that orchestrate the activation of an adaptive immune response (Iwasaki and Medzhitov, 2015).

C. Dendritic cell maturation

Antigen transport from the injury site to the lymph nodes is essential for the initiation of an adaptive immune response. Microbial detection triggers DC maturation, a multi-step process that leads to mature DCs (mDCs) capable of activating T lymphocytes. This process involves antigen uptake and presentation on MHC, integration of the inflammatory context to activate appropriate adaptive immune cells, and acquisition of the ability to migrate to the lymph node (Cella et al., 1997a).

1. Antigen uptake and processing

Before microbial detection, immature DCs (iDCs) scan the tissues for harmful particles. Tissue surveillance is ensured by projecting long cell protrusions in random directions or by active cell migration. *In vitro* studies suggest that the migration patterns of iDCs follow an intermittent random walk model. They alternate between rapid migration phases and arrest phases when sampling their surroundings; this behavior optimizes the pathogen search in the environment (Chabaud et al., 2015).

Direct pathogen detection through PRRs or inflammatory chemokine sensing transiently increases the ability of DCs to internalize extracellular components by endocytosis, phagocytosis, or macropinocytosis. Subsequently, internalized pathogenic particles are degraded into antigenic peptides and loaded onto MHC II for presentation to $CD4^+$ TLs and onto MHC I for presentation to

$CD8^+$ TLs (West et al., 2004).

MHC II binds to antigens degraded in the lysosomal pathway. In the absence of antigens, the invariant chain (Ii) stabilizes MHC II. After pathogen detection, the lysosomal protease cathepsin-S cleaves Ii and allows peptide loading onto MHC II. The complex is then transported to the plasma membrane to present the antigen to T lymphocytes (Neefjes et al., 2011).

MHC I binds to antigens degraded by cytosolic and nuclear proteasomes. Cytosolic peptides are transported to the endoplasmic reticulum (ER) where they are loaded onto MHC I molecules (Neefjes et al., 2011). Extracellular antigen presentation on MHC I requires a process called cross-presentation. There are two main pathways. In the vacuolar route, MHC I vesicles encounter the lysosomal pathway, and antigens degraded in the lysosomes are loaded onto MHC I. The second pathway is cytosolic: internalized particles escape from endosomes and are degraded by the cytosolic proteasome before being loaded onto MHC I in the ER (Alloatti et al., 2016).

Antigen processing is tightly regulated to avoid the presentation of self-antigens in an inflammatory context. Maturation of DCs increases MHC expression and translocation to the cell surface (Cella et al., 1997b) and modulates the lysosomal activity to process antigens properly (Trombetta et al., 2003). Increasing lysosomal acidification promotes antigen processing on MHC II, whereas maintaining a high pH promotes cross-presentation on MHC I (Samie and Cresswell, 2015). Cytokines and PRRs such as TLRs are known to signal from the endolysosomal compartments. PRRs directly modulate antigen presentation by co-trafficking with pathogenic endocytic particles (Watts et al., 2010) and locally regulate lysosomal activity to promote pathogen particle degradation into antigens (Roche and Furuta, 2015). Thus, he endolysosomal compartment plays a role as a signaling platform that integrates the inflammatory context to control antigen presentation.

2. Cytokine and co-stimulatory molecules

Antigens are not the only type of information acquired by DCs at the site of infection; they also integrate PAMPs and DAMPs present in the microenvironment and cytokines secreted by other immune cells. These factors provide information on the pathogenicity and location of the microbe as well as the level of tissue damage. This inflammatory context shapes the cytokine profile secreted by the mDCs and the nature of the co-stimulatory molecules expressed on their surface (Iwasaki

and Medzhitov, 2015).

Figure 2 Schematic representation of the integration of the inflammatory context during dendritic cell maturation

Internalized pathogenic particles are degraded to form antigens and presented on MHC II in the endolysosomal pathway (right) or on MHC I by cross-presentation (left). Engagement of PRRs and cytokine sensing at the site of infection induce signaling events that control antigen processing and trigger the expression of a specific set of cytokines and co-stimulatory molecules

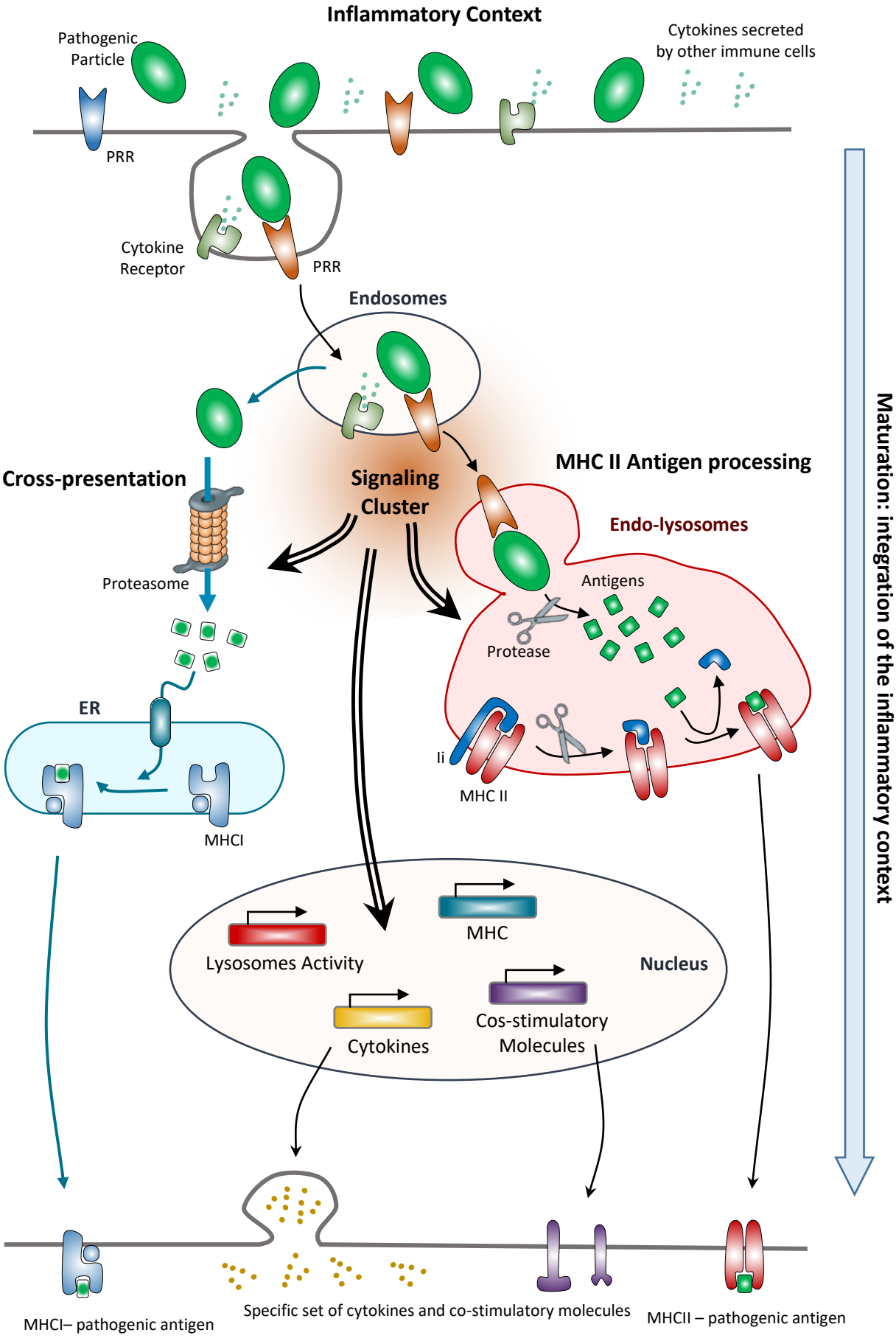
Inflammatory Context
Pathogenic Particle
Cytokines secreted by other immune cells
PRR
Cytokine Receptor
PRR
Endosomes
Cross-presentation
Signaling Cluster
MHC II Antigen processing
Endo-lysosomes
Proteasome
Antigens
Protease
ER
Ii
MHC II
MHCI
MHC
Lysosomes Activity
Nucleus
Cytokines
Cos-stimulatory Molecules
Maturation: integration of the inflammatory context
MHCI– pathogenic antigen
Specific set of cytokines and co-stimulatory molecules
MHCII – pathogenic antigen
Mature dendritic cell

3. Migration to the lymph nodes

The final stage of maturation leads to the migration of DCs to the draining lymph node via the lymphatic system. It is characterized by reduced internalization of extracellular components, loss of adhesion, and increased cell motility (Ueno et al., 2007). A key event is the expression of CCR7 chemokine receptors (Sallusto et al., 1998). It allows the detection of the chemokine CCL21, which is essential for guiding the mDCs in the lymphatic system (Ohl et al., 2004). Endothelial lymphatic cells secrete CCL21 and form a chemokine gradient that guides the mDCs into the interstitial space (Weber et al., 2013). CCL21 is additionally released at the site of transmigration and promotes the entry of mDCs into the lymphatic vessels (Vaahtomeri et al., 2017). Finally, the CCL21 gradient within the vessels promotes the migration of mDCs to the lymph node (Russo et al., 2016).

As for other leukocytes, mDCs migration into the interstitial space is independent of specific integrin engagement. This mode of motility promotes flexible migration across any tissue context (Lämmermann et al., 2008). However, mDCs move away from the site of infection in the opposite direction to other innate immune cells. Thus, within the same infected tissue, immune cells exhibit specific migration patterns depending on their function (Vargas et al., 2017). Therefore, coordination of immune function and migration requires the correct interpretation of signals from the pathogen, other immune cells, and tissue microenvironment.

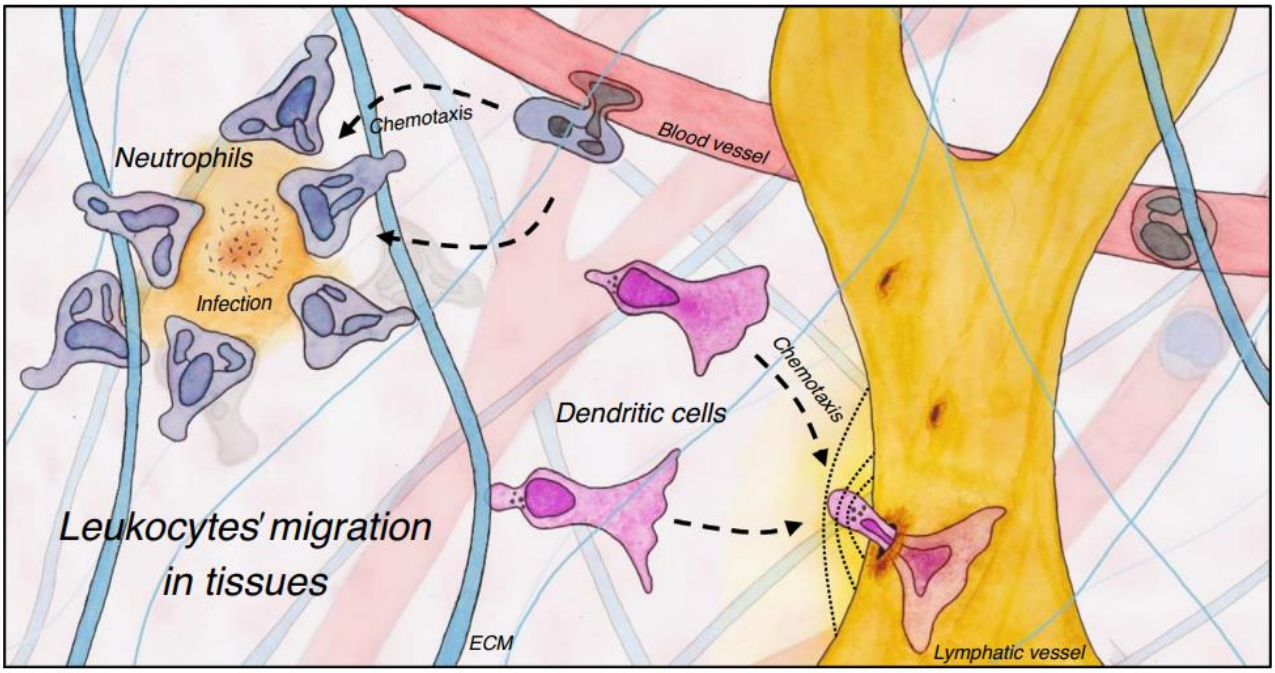

Figure 3 Leukocyte migration in the interstitial space

In infected tissue, neutrophils cross the blood vessel endothelium and migrate to the site of infection. They form a cell cluster that contains the infection. The inflammation also activates the DCs. After maturation and antigen uptake, they acquire the ability to migrate toward the lymphatic vessels and activate the adaptive immune response in the lymph nodes. In the same environment, the two cell types follow different migration patterns depending on their immune function. This coordination requires specific migration machinery and the correct interpretation of signals from the microenvironment. From Vargas *et al.*, 2017

In vitro, DC maturation requires 16 to 20 h before the co-stimulating molecules, MHC II and CCR7, are expressed on the cell surface (Alloatti et al., 2016). During this process, DCs integrate both the pathogen nature through antigen presentation and the inflammatory context through the expression of cytokines and co-stimulatory molecules. Once DCs have assimilated this information, they acquire the ability to migrate to the lymph nodes. The mDCs carry the information necessary to instruct T lymphocytes and activate the appropriate effectors of the adaptive immune response

III. Systemic immune response: activation of the adaptive system by dendritic cells

The adaptive immune response is specific to the pathogen encountered at the injury site. It allows the elimination of the infection and the establishment of memory cells. They facilitate the activation step and trigger a rapid response if the same pathogen is encountered a second time. In this section, I describe the key role of mDCs in triggering this immune response in the lymph nodes.

A. Antigen presentation to CD4+ T cells

The antigen-specific activation of $CD4^+$ T cells is the first step in triggering the adaptive immune response. Expansion of pathogen-specific $CD4^+$ T cells and their differentiation into appropriate helper T cells are essential to orchestrate the action of effector cells (Abbas et al., 2017b). $CD4^+$ T cell antigen priming requires physical contact with mDCs presenting their cognate antigen (Bousso, 2008). The probability of an encounter is very low (~1 in 1 million). The microarchitecture of the lymph nodes optimizes the contact between mDCs and their cognate T cells (Lämmermann and Sixt, 2008). Within the lymph nodes, B cells and T cells are compartmentalized and separated. B cells form follicles in the outer cortex, whereas T cells reside primarily in the inner cortex, below the B cell zone.

The mDCs enter the lymph nodes through the afferent lymph vessel and actively migrate to the T-cell-rich cortex. This area is a cell-rich environment, densely populated with T cells and fibroblastic reticular cells (FRCs), which form a three-dimensional scaffold (Lämmermann and Germain, 2014). The FRCs produce CCL21 and thus regulate the intranodal movement of T cells and mDCs, both expressing CCR7 (Worbs et al., 2007). The $CD4^+$ T cells migrate randomly along the FRC tracks (Bajénoff et al., 2006), while mDCs can adhere to the cellular scaffold (Lindquist et al., 2004). This organization optimizes the scanning of the antigen-presenting mDCs by the T cells. Other work suggests that the mDCs migrate to the lymph node entry site of the T cells from the bloodstream. Thus, mDCs effectively scan all incoming T cells and retain the T cells specific to their antigen (Bajénoff et al., 2003). The mDCs also have specific shape dynamics in the lymph nodes, forming long cell extensions (Bousso and Robey, 2003), which increase the area of contact with T cells. This behavior is essential for T cell priming (Benvenuti et al., 2004) and allows a single mDC to simultaneously present its antigens to more than 10 T cells simultaneously (Bousso and Robey, 2003).

B. Differentiation of $CD4^+$ T cells and activation of the specific immune cell effectors

Once the cognate mDCs encounter $CD4^+$ T cells, they form a strong interaction (Bousso, 2008). This facilitates information transfer from the mDCs to the $CD4^+$ T cells. This information includes not only the pathogen-specific antigen but also a specific set of co-stimulating molecules

and cytokines, which summarize the inflammatory environment at the site of infection (Kambayashi and Laufer, 2014). The interaction with mDCs leads to the activation and proliferation of the antigen-specific $CD4^+$ T cells and their differentiation into context-specific $CD4^+$ helper T cells (Hilligan and Ronchese, 2020).

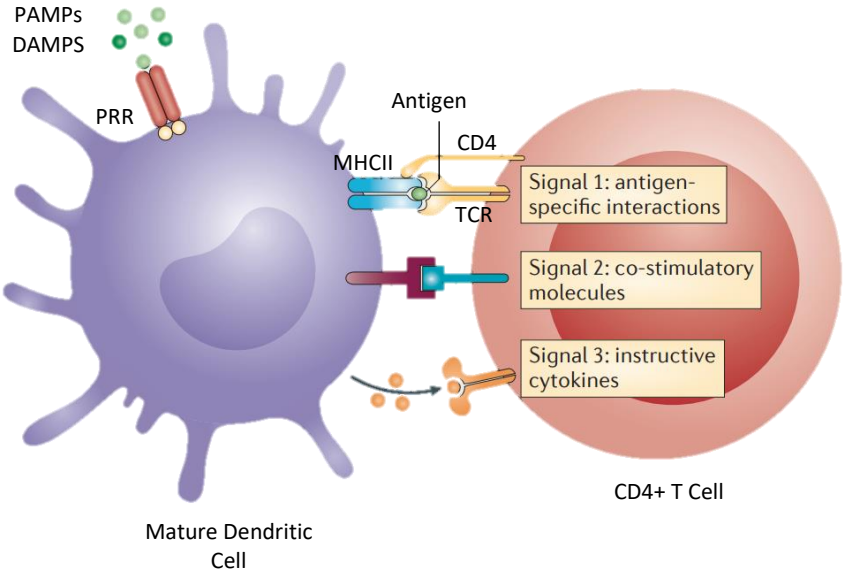

Figure 4 Information transfer during contact between mature dendritic cells (mDCs) and $CD4^+$ T cells

Mature DCs carry antigens to the lymph nodes that enable the activation and expansion of pathogen-specific T-lymphocytes. They also express a specific set of cytokines and co-stimulatory molecules that summarize the inflammatory context at the site of infection. They induce the differentiation of $CD4^+$ T lymphocytes into helper T lymphocytes specific to the inflammatory context. From Taku Kambayashi and Terri M. Laufer, 2014.

The $CD4^+$ helper T cells then orchestrate the pathogen-specific immune response. They secrete a precise set of cytokines that activate the appropriate immune effectors (Iwasaki and Medzhitov, 2015).

Depending on their immune phenotype, $CD4^+$ helper T cells can activate $CD8^+$ T cells to differentiate into cytotoxic T cells or B cells to differentiate into plasma cells. Both cell types also require antigen-specific priming. $CD8^+$ T cell activation involves antigen presentation on the mDC MHC I molecules. B lymphocytes can interact with soluble antigens or antigens presented on DC plasma membrane (Alberts et al., 2002b). The specific mDC localization in the lymph node cortex may result in preferential activation of $CD8^+$ T cells or B cells and thus shape the immune response (Gerner et al., 2017; Kissenpfennig et al., 2005).

Finally, pathogen elimination by effector T cells requires their subsequent migration from the lymph node to the site of infection. Effector T cells recirculate in the blood; as with innate

immune cells, their transmigration through the blood vessel endothelium of infected tissues requires specific adhesion molecules and signaling pathways (Abbas et al., 2017b). Effector T lymphocytes can acquire some of these homing receptors when primed by mDCs (Pejoski et al., 2019). Thus, mDCs also carry the signature of the tissues in which they encountered the pathogenic antigen. The mechanism underlying the effector T cell tropism towards infected tissues is not completely understood and remains an obstacle to the development of effective vaccination against cancer or human immunodeficiency virus, which requires a T cell-based immune response (Fu et al., 2016).

Figure 5 Schematic summary of the immune cell movements in response to infection.

Tissue Infection results in coordinated steps of immune cell movement that ensure pathogen elimination. Pathogen detection induces a local infiltration of innate immune cells. They trigger a local inflammation and limit the pathogen spread. The inflammation activates dendritic cells, and they migrate to the lymph node. In the lymph node, mature dendritic cells trigger the activation, expansion, and differentiation of specific effectors of adaptive immunity (top panel - image from Servier Medical ART database). The adaptive effector cells recirculate in the bloodstream and migrate into the infected tissue where they mediate pathogen elimination. All these steps of immune cell migration are tightly regulated to limit the inflammation and cell infiltration to the infected tissue only and to avoid the damage of healthy tissue.

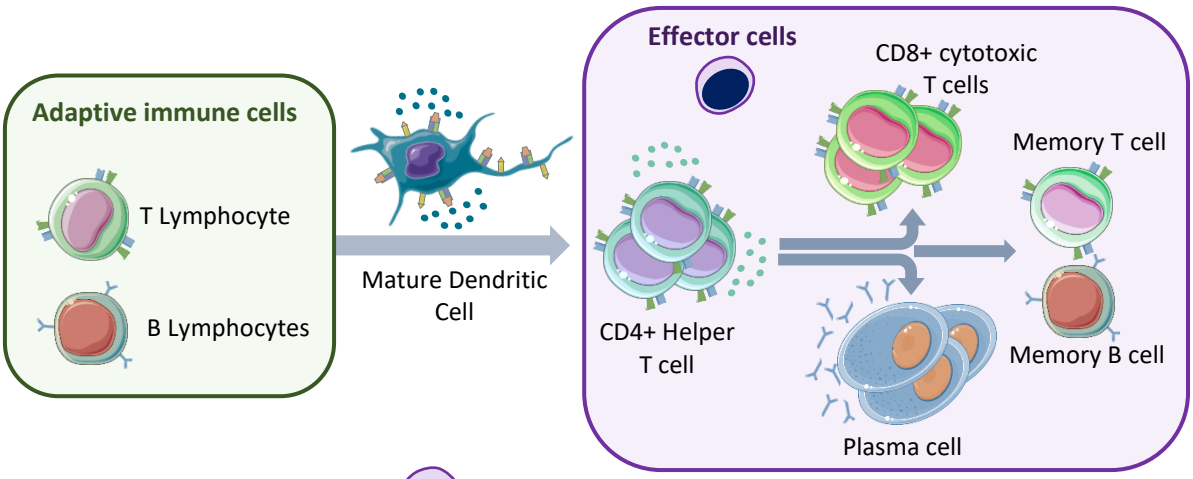
Adaptive immune cells
T Lymphocyte
B Lymphocytes
Mature Dendritic Cell
Effector cells
CD8+ cytotoxic T cells
Memory T cell
CD4+ Helper T cell
Memory B cell
Plasma cell

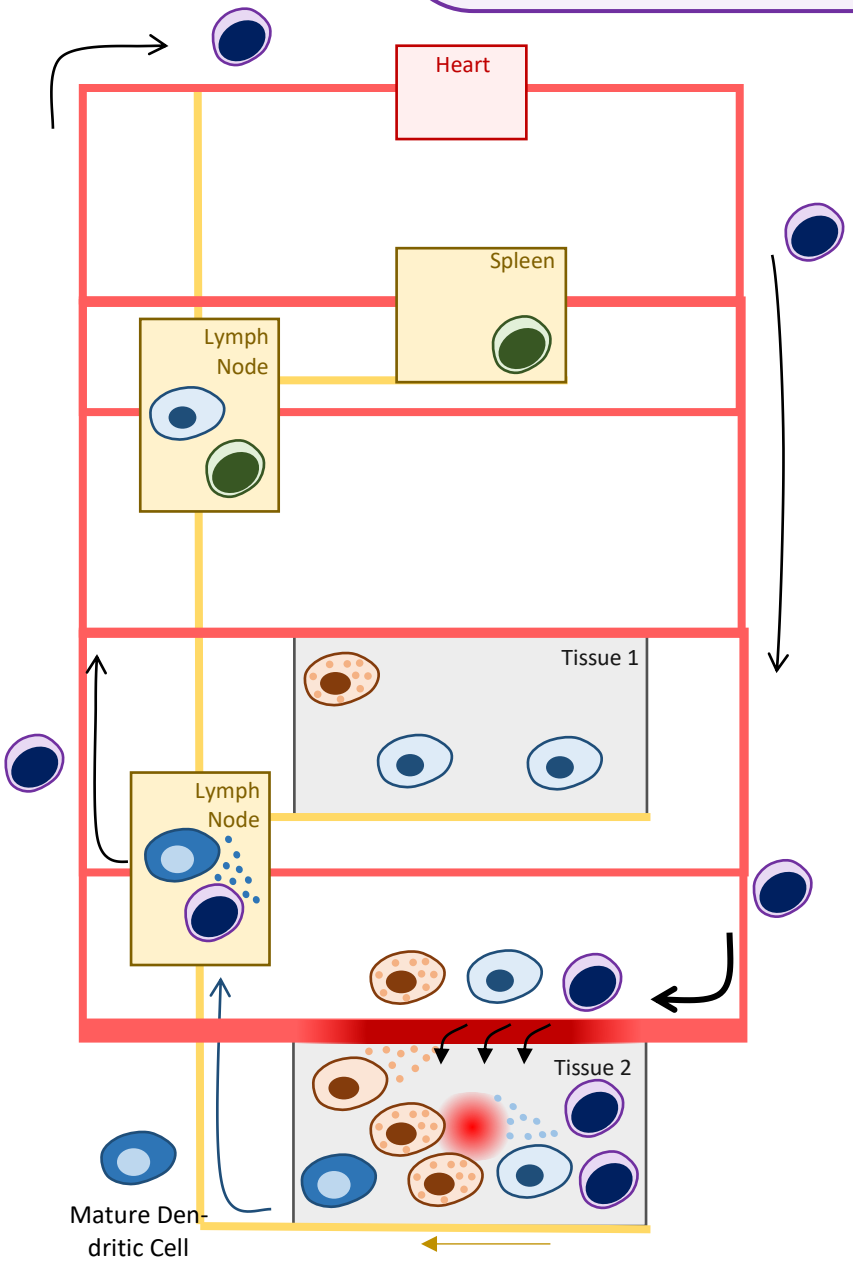
Heart
Spleen
Lymph Node
Tissue 1
Lymph Node
Tissue 2
Mature Dendritic Cell

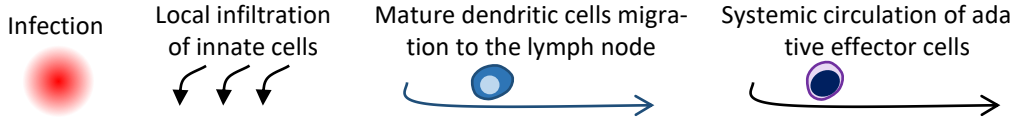
Infection
Local infiltration of innate cells
Mature dendritic cells migration to the lymph node
Systemic circulation of adaptive effector cells

Dendritic cells play an essential role in the immune system activation by linking the innate and adaptive response. They uptake information on the pathogen and inflammatory microenvironment and transport it to the lymph nodes, where they activate pathogen-specific immune effectors.

Their function involves multiple stages of migration from different tissues to the lymph nodes. They are optimized to migrate efficiently in different physical and chemical contexts. They are, therefore, an appropriate model to study cell migration. In my doctoral research, I focus mainly on the interstitial migration of mDCs. Indeed, the physical and chemical properties of this environment can vary among tissues and require an adaptation of mDC migration mechanisms. Moreover, neutrophils and T lymphocytes also migrate in the interstitial space to perform their immune function. Therefore, a comparison between different immune cells could highlight the migration mechanisms shared by rapidly moving leukocytes in the interstitial space and the specific mechanisms required for the immune function of antigen-transporting mDCs. Finally, understanding the mechanisms controlling mDC migration from the site of infection to the lymph nodes could provide molecular tools to modulate the activation of the adaptive response. This is particularly relevant in the context of vaccine and cancer immunotherapy development.

CHAPTER 2: MECHANISMS OF CELL MIGRATION

As described in the previous chapter, cell migration is an essential process for the immune response. It is also involved in other physiological or pathological events such as embryonic development or metastasis progression. Thus, the mechanisms underlying cell migration have been studied in a variety of different contexts (Yamada and Sixt, 2019). They are dependent on the properties of both the cell and its environment. In this chapter, I will describe globally the different mechanisms involved in single-cell migration. Then, in the following section, I will put them in the context of DCs interstitial migration.

Cell migration relies on internal forces that drive cell movement. Previous studies have highlighted different strategies developed by cells to meet the requirements for cell migration (Vicente-Manzanares et al., 2005). This chapter will focus on describing how internal forces are generated in cells, transmitted to the substrate and further polarized inside cells to result in single-cell displacement to a particular direction.

I. Intracellular forces for cell deformation

In most animal cells, the actomyosin cytoskeleton generates the forces necessary for cell motion. Its expansion by polymerization is associated with pushing forces and membrane protrusion while its shrinkage causes pulling forces and membrane retraction (Svitkina, 2018). In this section, I will first describe the molecular organization of the actomyosin network and then discuss on how its remodeling leads to cell movement

A. Acto-Myosin Cytoskeleton

1. Actin filament

Actin filament (F-actin) assembles from monomeric actin proteins (G-Actin). It forms a polar filament with a "barbed" end and a "pointed" end. F-actin diameter is ~7 nm, and its persistence

length is ~10 µm. As compared to other cytoskeleton elements, actin filaments are more flexible and dynamic, with structural changes in the time scale of minutes (Blanchoin et al., 2014).

In the cell, the concentration of G-actin allows spontaneous and asymmetric polymerization of F-actin. Single filaments elongate ten-times faster at the barbed end than at the pointed end. However, actin-binding proteins (ABPs) modulate this spontaneous elongation rate by interacting with G-actin and F-actin. APBs such as profilin bind directly to G-actin and promote the assembly reaction or sequester actin monomers. Capping proteins stabilize the barbed ends, preventing both polymerization and depolymerization. Cofilin interacts with F-actin, cleaves the filament and, increases its dynamics (Pruyne et al., 2002). The binding sites of the different ABPs partially overlap, resulting in competition for F- or G-actin interaction and tight regulation of filament elongation.

While the elongation of F-actin is spontaneous, the nucleation step of the first three monomers is thermodynamically unfavorable and prevented by the interaction with profilin. Thus, the formation of new F-actin is dependent on actin nucleating factors. Their nucleation and regulation properties lead to different organizations of the actin network.

2. Actin network organization

a) Branched network – Arp2/3

Arp2/3 is a complex of seven subunits. Among them, Arp2 and Arp3 are actin-related proteins and mimic an actin dimer. The complex acts as a template for further F-actin elongation and overcomes the limiting step of nucleation (Goley and Welch, 2006). It binds to the side of pre-existing filaments and branches a new F-actin at an angle of 70°. The new filament grows from its barbed end, while interactions with capping proteins limit its length (Amann and Pollard, 2001).

Nucleation by Arp2/3 leads to the formation of a branched network of short actin filaments. The WASP family and the WAVE family are the main regulators of its activity (Molinie and Gautreau, 2018).

b) Non-Branched Network – Formins

Formin family proteins share conserved FH1 and FH2 domains and their activity is controlled by the Rho family GTPases. The FH1 domain is known to interact with profilin and the FH2 domain with actin. Formins promote both nucleation and elongation of F-actin. They interact processively with the barbed end of the growing filament and protect it from capping proteins (Higashida et al.,

2004).

Nucleation by formins leads to long, unbranched actin filaments. Actin crosslinkers further organize this network. They bridge two actin filaments and form actin bundles with parallel, antiparallel or mixed F-actin depending on the crosslinker (Blanchoin et al., 2014).

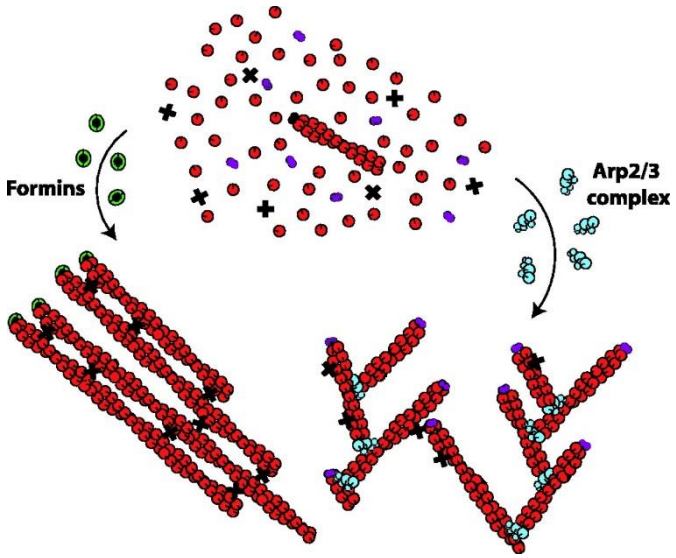

Figure 6 Different organization of actin networks polimerized by Arp2/3 or formins.

From the same pool of G-actin (red), Arp2/3 (blue) and formins (green) polymerize actin networks with different structures. Arp2/3 leads to short, branched filaments due to the interraction of capping proteins (violets) with free filaments barbed end. Formins protect the growing end from the capping proteins, resulting in long filaments that are bundled by crosslinkers (cross). Adapted from Michael Bindschadler and James L. McGrath 2004.

Formin and Arp2/3 are the best described actin nucleators, which give rise to distinct network organizations with specific properties. Their functions are not exclusive, and they can cooperate to generate complex actin networks. Actin elongation also involves other proteins such as Spires or members of the Ena/Vasp family, adding another level of complexity to the network dynamics.

3. Myosin

Other key players in the dynamics of the actin cytoskeleton are members of the myosin family. Myosins are molecular motors characterized by a globular domain that interacts with actin and has ATP hydrolysis activity. Depending on their structure, they are involved in different processes: cross-linking of F-actin with the cell membrane (class I), F-actin contraction (class II), or transport of vesicles along F-actin (class V) for the conventional myosins (Sellers, 2000).

Non-muscular class II myosin (MyoII) produces contractile force by sliding antiparallel actin bundles through the energy of ATP hydrolysis. MyoII is a heterodimer complex composed of two heavy chains encompassing the globular domain, two regulatory light chains (RLC), and two essentials light chains (ELC). MyoII alone is unipolar and, therefore, ineffective in producing contractile forces. It must assemble into a bipolar mini-filament to interact with antiparallel actin bundles and cause their gliding (Vicente-Manzanares et al., 2009).

Phosphorylation of the RLC controls MyoII ATPase activity and its assembly into filaments. More than a dozen kinases have been identified to phosphorylate the RLC. The most characterized are the myosin light chain kinase (MLCK) and the Rho-associated coiled-coil containing kinase (ROCK). The signals triggering these kinases are different, MLCK is activated by calcium via calmodulin, while the GTP binding protein RhoA activates ROCK. They also differ in their specificity, MLCK seems specific to the regulatory light chain, while ROCK can phosphorylate several substrates in the cell (Vicente-Manzanares et al., 2009).

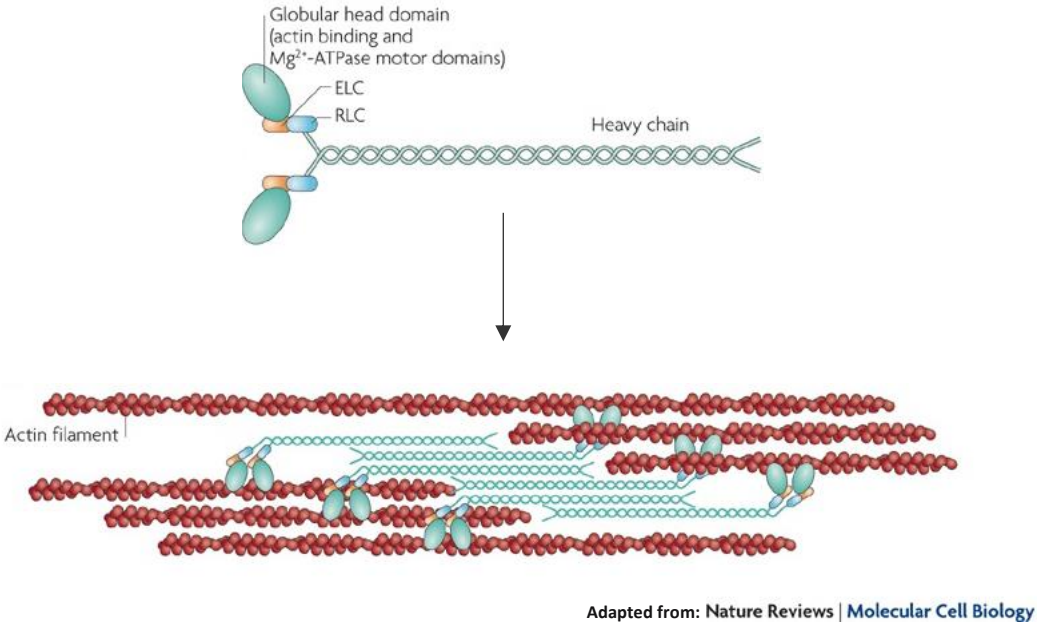

Figure 7 MyoII structure and organization in bipolar mini-filaments.

The subunits of the MyoII form a unipolar complex. Mini filaments are formed by anti-parallel interaction of the MyoII via their heavy chains. This bipolar organization allows the interaction with antiparallel actin bundles and their sliding with the movement of globular domains. Adapted from Vicente-Manzanares M *et al* 2009.

The interaction between F-actin, actin nucleators and myosin gives rise to a dynamic and tightly regulated actomyosin network. Its elongation and contraction generate pushing and pulling forces capable of deforming the cell membrane. At the cellular level, the actomyosin network is

integrated into large structures that lead to movement. I will describe these structures in the next section.

B. Different types of cell protrusions

1. Actin-rich protrusion

F-actin assembly produces picoNewton forces (Kovar and Pollard, 2004); thus, the growing of an actin network underneath the plasma membrane is sufficient to push it and create a protrusion (Pollard and Borisy, 2003).

Actin-rich protrusions have a variety of shapes (Ridley, 2011). The most well-described is a thin (~200nm thick) veil assembled by cells on a 2D surface, named lamellipodia. Such actin-rich lamellar ruffles protruding in the free space have also been observed on cells migrating in 3D environments (Fritz-Laylin et al., 2017). In these structures, F-actin elongation occurs mainly against the plasma membrane. The formation of a branched network by Arp2/3 is essential for lamellipodia extension (Bailly et al., 2001), being WAVE the main Arp2/3 activator (Takenawa and Miki, 2001).

Another protrusion involved in cell movement is filopodia, described as a finger-like structure. They are formed by the elongation of unbranched actin bundles towards the plasma membrane nucleated by formins and Ena/VASP at the tip of the filopodia (Faix and Rottner, 2006). Actin crosslinkers further modulate the stability of these structures (Khurana and George, 2011). N-WASP mediated Arp2/3 activation also promotes filopodia formation (Miki et al., 1998).

Branched and unbranched actin networks are not mutually exclusive in the different protrusions. Studies inhibiting actin elongation mediated by Arp2/3 or by formins have revealed their collaboration in the formation of complex structures. For example, the formin mDia2 generates long actin filaments essential for the maintenance of lamellipodia (Fig.8) (Yang et al., 2007). Similarly, the formins FMNL2 and FMNL3 are not essential for the formation of the lamellipodia, but they enhance the density and the mechanical stability of the network and are required for efficient force generation (Kage et al., 2017a). At the cellular level, distinct actin networks polymerized by formins or Arp2/3 have also been observed in migrating cell protrusions (Ponti et al., 2004; Wilson et al., 2013). Generally, Arp2/3 and formins have specific roles in leukocytes that help to coordinate their migration and immune functions. For instance, cell motility requires only the formin-dependent network (Vargas et al., 2016; Wilson et al., 2013), while Arp2/3

activity is essential for space exploration and sensing of environmental cues (Fritz-Laylin et al., 2017; Leithner et al., 2016; Vargas et al., 2016).

Finally, in specific conditions, cells can also form actin-rich protrusionS named invadopodia and podosomes. They are defined by well-described architecture and their capacity to degrade the extracellular matrix (Ridley, 2011).

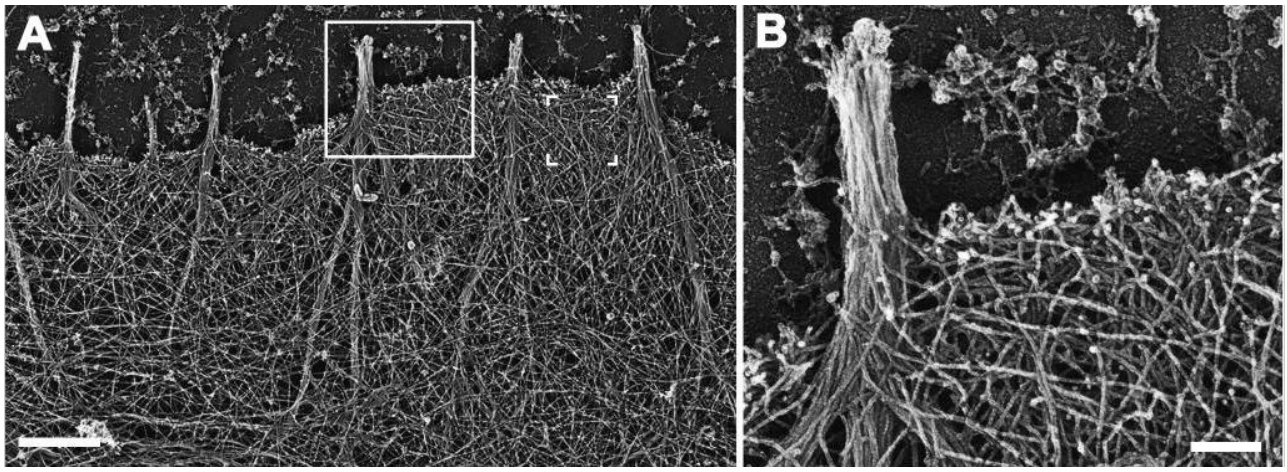

Figure 8 Platinum replica electron microscopy of the lamellipodia of B16F1 cell.

Overview (A) and zoom (B) of the actin network organization at the leading edge. Parallel actin bundles form filipodes and are integrated into a dense and branched actin network. Scale bars: 1µm in (A), 0.2µm in (B). Adapted from Ynad C *et al*, 2007

The balance in the activity of the different actin nucleators confers to protrusions different mechanical and biochemical properties and, therefore, specific functions.

2. "Bleb" protrusion

Blebs are rounded protrusion of the plasma membrane containing a limiting amount of cytoplasm and detached from the cell cortex (Bovellan et al., 2010).

The cortex is a layer mainly composed of actin and myosins underneath the cell membrane (Salbreux et al., 2012). Contractile activity of MyoII in this structure generates a hydrostatic pressure on the cytoplasm. A local rupture in the cortex or a local dissociation of the cell membrane from the cortex leads to cytoplasmic flow that rapidly pushes the membrane outwards due to the hydrostatic pressure. Then, re-formation of the actin cortex in the newly formed protrusion induces bleb retraction (Charras and Paluch, 2008). Eventually, sustained MoyII contraction can lead to bleb stabilization (Liu et al., 2015).

Of note, the force leading to bleb protrusion is based on hydrostatic pressure and not on

filament polymerization as for actin protrusions. Thus, the level of MyoII activity is a major factor regulating bleb formation. Modulation of the cortex anchorage with the plasma membrane can also promote or prevent bleb initiation (Ridley, 2011).

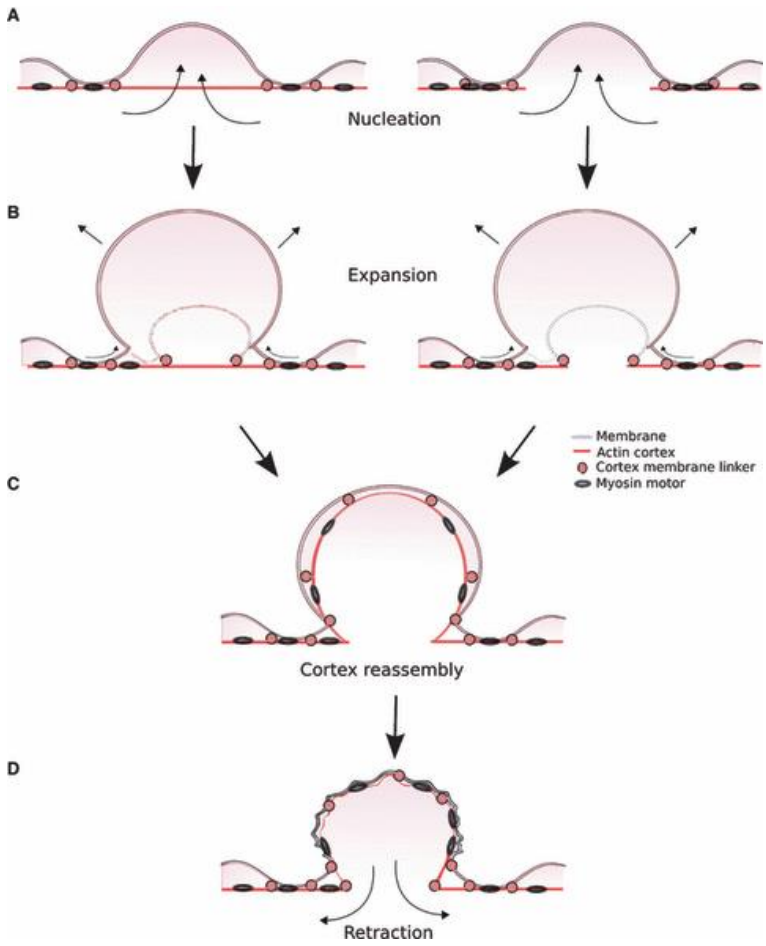

Figure 9 Schematic diagram of the different steps of bleb formation and retraction.

(A) Bleb initiation results from local detachment of the membrane (left) or rupture of the cortex (right). (B) Hydrostatic pressure (black arrows) causes cytoplasmic flow and extension of the bleb. (C) The actin cortex reformed in the protrusion, resulting in retraction of the bleb (D). From Bovellan M *et al*, 2009.

Cells can form a wide variety of protrusions with different force generators and actomyosin organizations. Thus, the type of protrusion depends on the intracellular balance between MyoII contractility and actin elongation (Yoshida and Soldati, 2006). Surprisingly, cells are able to switch from one type of protrusion to another either spontaneously (Bergert et al., 2012), by specific inhibition of the actomyosin cytoskeleton (Lämmermann et al., 2008; Obeidy et al., 2020) or as a result of a change in their microenvironment (Bergert et al., 2012; Liu et al., 2015). This suggests that both hydrostatic pressure and actin polymerization cooperate to drive cell protrusion (Bergert et al., 2012; Lämmermann and Sixt, 2009)

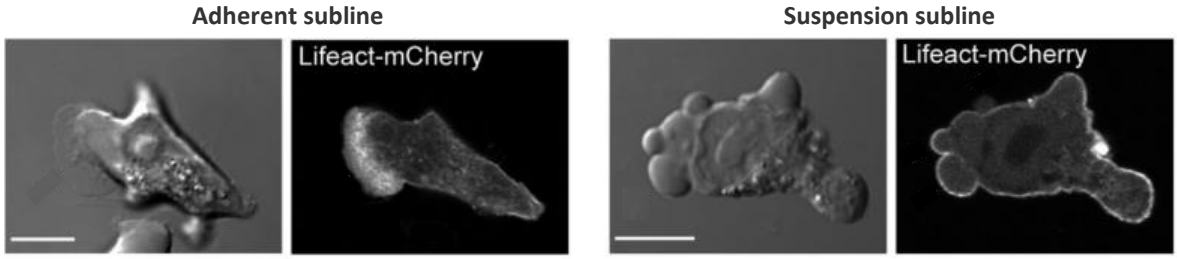

Figure 10 Walker 256 carcino-sarcoma sublines from different type of protrusion.

Sublines were selected by culture on adherent (left) or non-adherent (right) surfaces. The adherent subline forms actin-rich lamelipodia while the suspension subline forms blebs. Scale bars: 10µm on the left panel, 5µm on the right. From Bergert *et al*, 2012.

C. Mechanisms of cell retraction

In addition to the pushing force that drives cell protrusions, the actomyosin cytoskeleton also generates pulling forces associated with cell retraction (Cramer, 2013).

MyoII contributes significantly to cell retraction. This molecular motor generates a contractile force by sliding actin bundles at the cell cortex. The coupling between the membrane and the cortex causes the cells to retract (Vicente-Manzanares et al., 2009). Ultimately, the compressive stress exerted by MyoII on F-actin might cause their disassembly (Vogel et al., 2013). This, in turn, induces the compaction of the cortical actin and reinforces the retraction of the cells (Wilson et al., 2010).

However, several studies show that cells can retract without MyoII activity (Lämmermann et al., 2008; Wessels et al., 1988). They revealed that actin disassembly, mainly driven by ADF/cofilin (Mseka and Cramer, 2011) and compaction of the actin network by crosslinkers, produce sufficient tensile force to cause cell retraction (Sun et al., 2010).

D. Generation of an actin flow

The mechanisms of cell movement described above highlight the central role of actin turnover in this process. Actin assembly at the protrusion sites and simultaneous disassembly at the retraction sites result in actin flow. Mechanically, the plasma membrane opposes resistance to F-actin assembly; thus, when a filament polymerizes against it, it is pushed back while the membrane protrudes (Cramer, 1997). MyoII activity is not required for this flow but further enhances the retrograde movement of the cortex (Renkawitz et al., 2009; Wilson et al., 2010). It can be observed

along the entire cell length (Renkawitz et al., 2009) or limited to the protruding area (Svitkina et al., 1997; Theriot and Mitchison, 1991). This actin flow generates the driving force that leads to cell migration (Pollard and Borisy, 2003). However, its transduction into traction force on the substrate and polarization across the cell are necessary to induce a net displacement (Vicente-Manzanares et al., 2005). I will describe this mechanism in the following parts.

II. Force transmission to the substrate

A. Adhesion-dependent interaction

Adhesion receptors, such as integrins, can mediated force transduction. Integrins are transmembrane heterodimers without intrinsic catalytic activity that link the cell-substrate to the actin cytoskeleton (Campbell and Humphries, 2011).

Upon engagement with specific extracellular ligands, integrins cluster and recruit adaptor proteins leading to the formation of focal adhesions linked with the actin cytoskeleton. These structures form "molecular clutches", which transmit forces generated by the actin flow on the cell substrate. Force transduction counteracts the retrograde flow resulting in a net protrusion and exerts traction forces leading to cell displacement (Case and Waterman, 2015).

This mode of force transmission requires an active turnover of the focal adhesions with the formation of new ones at the protrusion while they are disassembled at the retraction sites. Contractile forces generated by MyoII are required to breakdown adhesions and retract the cell (Parsons et al., 2010).

Thus, on adhesive substrates, MyoII inhibition leads to decreased velocity due to impaired focal adhesion breakdown (Wessels et al., 1988).

Furthermore, in integrin-based migration, cell speed is dependent on the adhesion strength to the surface. Too strong or weak adhesions prevent migration. Thus force transduction efficiency is highly dependent on integrin-ligand interaction properties, such as their respective concentration and binding affinities (Palecek et al., 1997).

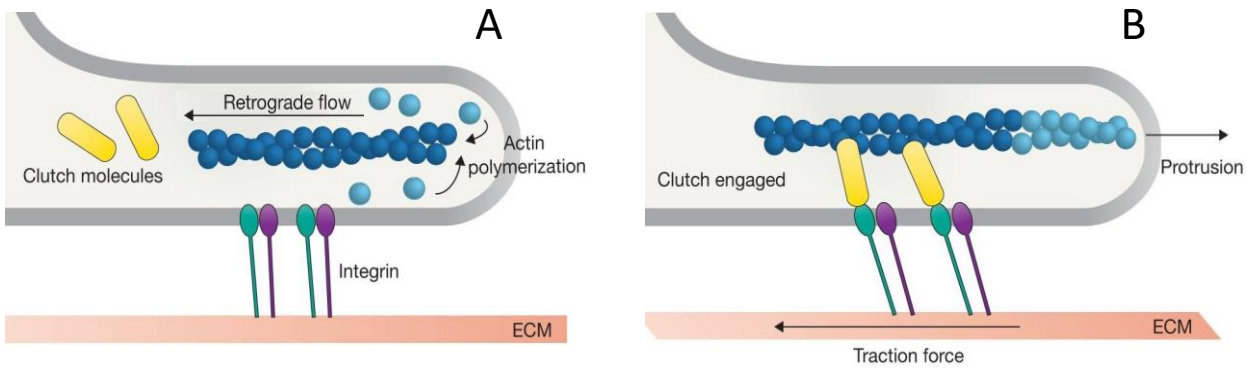

Figure 11 Force transmission in adherent migration

The engagement of integrins on the substrate triggers molecular clutch recruitment and interaction with actin filaments. The molecular clutch counteracts the retrograde flow of actin, which induces the transmission of traction forces to the substrate and a net protrusion of the cell. Adapted from Case LB and Waterrman CM, 2015.

B. Anchorage-independent

At the cell scale, gravity is negligible. Thus, on a 2D flat surface, specific integrin-mediated anchorages are necessary to mediate cell interaction with the surface. However, in 3D environments, confinement imposes this interaction, and specific adhesion becomes not necessary for motility (Lämmermann et al., 2008; Malawista et al., 2000).

1. Actin flow friction

In the absence of integrin engagement, the backward movement of the F-actin is not limited, resulting in a retrograde flow along the cell length (Renkawitz et al., 2009). This flow can create enough friction with the substrate to propel the cell (Bergert et al., 2015).

Non-specific transmembrane interactions with the surface mediate the friction. This frictional interface can involve integrins without the formation of focal adhesions. Another study suggests the role of charged glycocalyx and electrostatic interactions (Friedl and Bröcker, 2000).

In the total absence of transmembrane force coupling, cells can take advantage of the topography of their environment. The texture of the substrate deflects the actin flow and creates retrograde shear forces sufficient to propel the cell (Reversat et al., 2020).

This friction-based migration suggests that the retrograde actin flow may be sufficient to maintain cell movement in specific environments. MoyII is not necessary even if contractile forces increase cell speed by supporting the retrograde flow (Lämmermann et al., 2008).

2. Hydrostatic pressure and 'Chimneying.'

The high pressure inside the cell also increases friction with the substrate and converts the actin flow into motion. Actin polymerization or contraction of the cortex by MyoII generates this pressure. This model is known as "Chimneying", where cells exert normal forces on their environment (Heuzé et al., 2013).

In an extreme case, when the cell is polarized and exerts a pressure gradient, friction and actin flow can be dispensable, and normal forces, perpendicular to the surface, could be sufficient to drive movement. This force transduction mechanism can be applied to blebbing protrusions, where cortical contraction by MyoII generates hydrostatic pressure (Charras and Paluch, 2008).

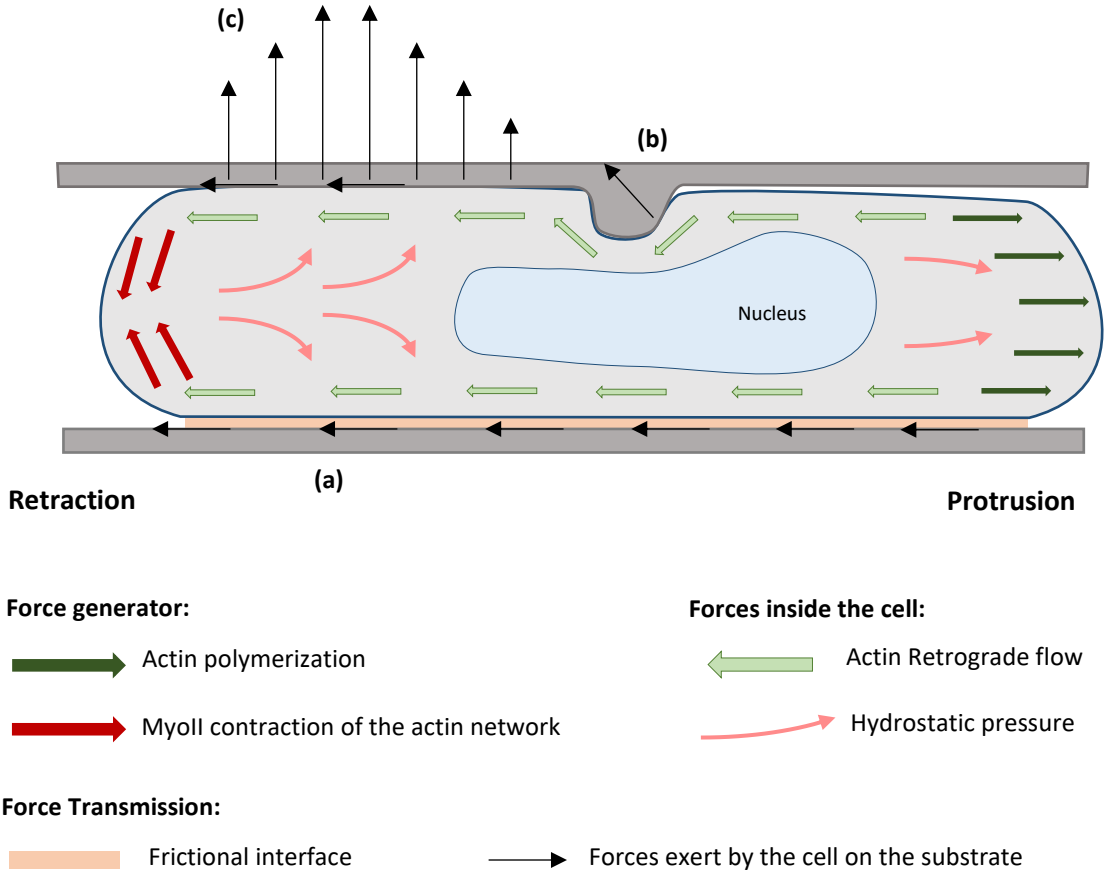

Figure 12 Schematic summary of force generation and transmission in a non-adherent migrating cell.

Actin polymerization associated with MyoII contractility generates a retrograde flow of actin and hydrostatic pressure within the cell. The retrograde flow of actin can exert a traction force on the substrate if there is sufficient friction **(a).** In absence of force coupling across the membrane, **(b)** the surface topography lead to shear forces. **(c)** Hydrostatic pressure or actin polymerization exert normal forces on the substrate, they enhance friction or may be sufficient for movement if there is a pressure gradient.

Surprisingly, despite their apparent simplicity, 2D flat surfaces are very restrictive models for cell migration because cell adhesion is strictly required. On the contrary, the 3D environment seems more permissive since migration modes independent of integrins, actin-flow or MyoII are conceivable in confined spaces. As a striking example, DCs are barely motile on open chambers but migrate efficiently once compressed between two surfaces (Heuzé et al., 2013).

The mechanism of force transduction is dependent on cell adhesion, contraction, and actin polymerization rate. As for the different modes of protrusion, cells can switch upon changes in their environment (Liu et al., 2015; Renkawitz et al., 2009). This incredible flexibility is essential for cells that migrate within tissues with variable properties.

III. Maintenance of front-rear polarization

Finally, efficient migration relies on the spatial and temporal coordination of protrusion and retraction within a cell. Net displacement requires cell movement persistence with the stable organization of a protruding "front" domain and a retracting "rear" domain, also called the leading and trailing edge, respectively. Thus, the initiation of cell migration depends on a triggering event of symmetry breaking, leading to the establishment of these distinct domains. Symmetry breaking can be spontaneous or induced by external signals such as chemokines, but I will not present this initial step. I will focus here on the mechanisms allowing the maintenance of cell polarity.

A. Definition of front and rear domains

1. Rho family of small GTPases paradigm

The members of the Rho GTPase family are key cytoskeletal regulators. They govern both MyoII contractility and actin polymerization. They are central components of the signaling pathway controlling the spatio-temporal activity of the actomyosin machinery (Lawson and Ridley, 2018).

Rho-GTPase proteins act as molecular switches: they alternate between an active state, bound to GTP, and an inactive state, bound to GDP. The transition between GTP- and GDP-bound states is fast and tightly regulated by activators (GTP-exchange factors - GEFs) and inhibitors (GDP-dissociation inhibitors-GDIs and GTPase activator proteins- GAPs) (Tybulewicz and Henderson, 2009). The most characterized members of the Rho-GTPase family are RhoA, Rac, and Cdc42. They are involved in complex and intricate signaling networks (Devreotes and Horwitz, 2015). I will

provide here a very simplified view of their role in the establishment of cell polarity.

Rac and Cdc42 coordinate protrusions at the leading edge. They activate WAVE and WASP, and promote actin polymerization generating distinct cellular macrostructures, i.e., lamellipodia and filopodia, respectively (Benvenuti et al., 2004; Lämmermann et al., 2009; Vargas et al., 2016). At the rear, RhoA activates formins and ROCK, leading to MyoII-dependent contraction and cell retraction (Hind et al., 2016; Vargas et al., 2016). The maintenance of these two distinct spacial domains requires a mutual exclusion at the cell scale and a local positive feedback loop (Tsai et al., 2019; Weiner et al., 2002). I will detail the mechanisms of front-rear coupling in a following paragraph.

2. Cortical polarization

The cell cortex is a thin network of actomyosin underneath the plasma membrane. The linker proteins, Ezrin, Radixin and Moesin (ERM), reversibly bind the plasma membrane to the cortex. Modification of the cell cortex organization, contractility, and anchoring controls the cell shape and is involved in the front-to-back asymmetry (Salbreux et al., 2012). High local cortical tension at the rear can support retraction and counteract inefficient protrusion, while low local tension at the front facilitates efficient protrusion (Shi et al., 2018). Cortical polarization is particularly relevant for blebbing cells since a local weakening of the membrane-cortex attachment initiates this type of protrusion (Charras and Paluch, 2008).

Recently, Bisaria and her colleagues reported asymmetric actin organization in the cortex. The density of actin near the membrane is higher at the cell back, and the low density at the front favors protrusions (Bisaria et al., 2020). Ramalingam and colleagues also characterized a formin-dependent resilient actin network at the cell back. This network resists to contractile forces and prevents backward blebbing (Ramalingam et al., 2015).

In addition to actin polarization, ERM proteins concentrate at the back of the cell during migration (Prentice-Mott et al., 2016). They prevent bleb formation at the rear (Lorentzen et al., 2011) and can sustain Rho activation (Lee et al., 2004). Consequently, their miss-localization or deregulation affects cell migration *in vitro* and *in vivo* (Diz-Muñoz et al., 2010; Liu et al., 2012).

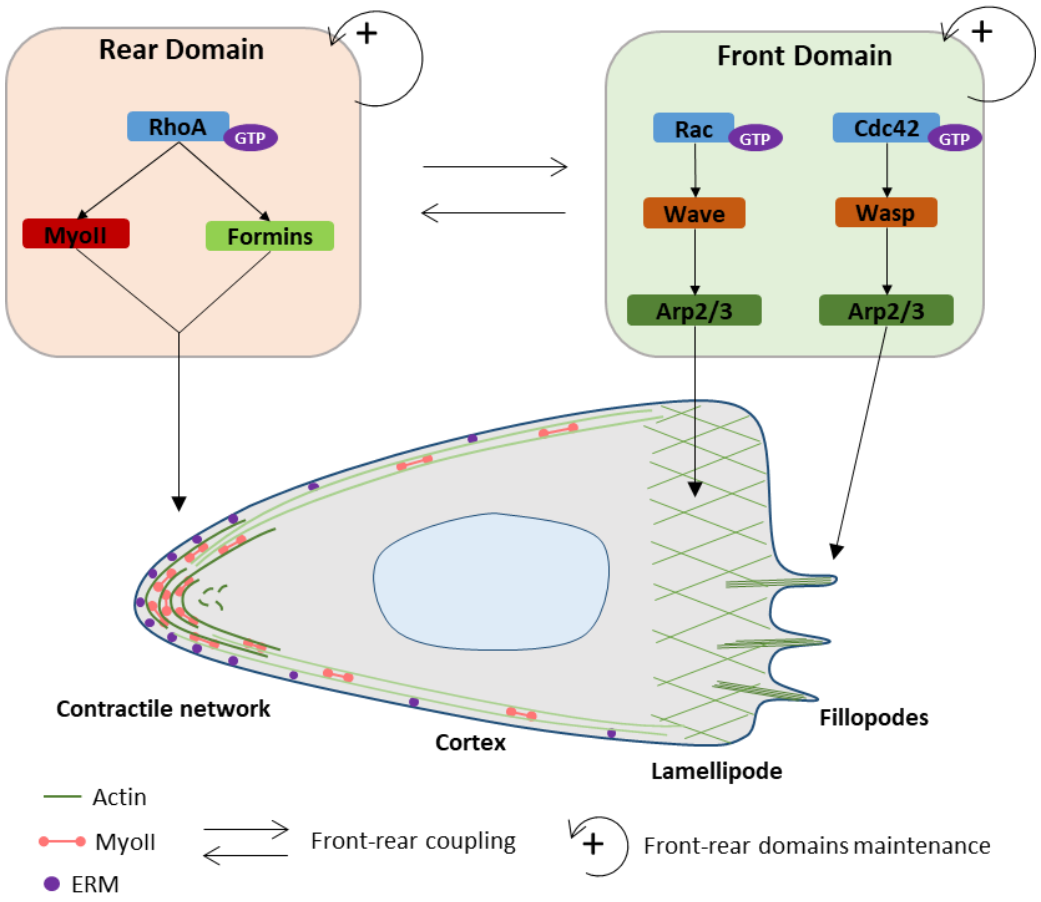

Figure 13 Simplified front and rear domain diagram in an actin-prutrusive cell

The differential activation of the small RhoGTPases and the cortical structure define a protruding front and a retractile back. At the back, RhoA activation and the accumulation of ERM proteins cause cells retraction and prevent protrusions. The front is characterized by the activation of Rac and Cdc42 which promote the formation of lamellipodia and filopodia, respectively. The front and back domains must be coupled to ensure coherent movement and be maintained over time for persistent migration.

The differential activation of Rho GTPases and the asymmetric cortex define front and back domains that spatially restrict protrusion and retraction, resulting in cell polarization. In the next section, I will describe how they are maintained and coupled during cell migration to ensure coherent and persistent movement.

B. Front-to-rear coupling during migration

1. Membrane tension

A first model proposes that the membrane can directly couple the protruding front with the rest of the cell. Simply, if we consider the membrane as an inextensible bag, a protrusion on one side will automatically cause the opposite side to retract. A caterpillar from a tank illustrates

this model. It recapitulates well the amoeba migration of Dictyostelium (Copos et al., 2017) and the shape variations of motile keratocytes (Keren et al., 2008).

A second model considers the lateral tension of an extensible membrane as a long-range inhibitor. During neutrophil migration, protrusion leads to an overall increase in membrane tension that inhibits actin assembly. This overall negative feedback loop prevents the formation of secondary protrusions in other parts of the cell (Diz-Muñoz et al., 2016; Houk et al., 2012).

However, this coupling mechanism requires rapid propagation of membrane tension across the cell, and the cortical cytoskeleton can prevent this homogenization (Shi et al., 2018). In this line, Hetmanski and colleagues reported that the tension in the back is rather lower than in the rest of the cell. The low local tension recruits caveolae and triggers membrane retraction by Rho activation (Hetmanski et al., 2019). The front-to-back coupling mechanism by membrane tension is well accepted for small cells; however, elongated or branched cells would require other coupling mechanisms.

2. Sustained actin flow

In the late 1990s, Verhovsky and colleagues used lamellar fragments of keratocytes devoid of organelles and microtubules to study the front-to-back asymmetry during migration. The retrograde flow of actin and myosin combined with the anterograde movement of the fragment was sufficient to maintain backward MoyII accumulation. This work showed that a positive feedback loop intrinsic to actomyosin can maintain polarized locomotion (Verkhovsky et al., 1999).

Several researchers have confirmed this concept. The retrograde actin flow, associated with cell migration, results in the retrograde transport of actin-binding regulatory factors. Their accumulation at the cell back enhances cell polarity and persistent migration (Maiuri et al., 2015). Among them, MyoII is a crucial protein transported across the entire cell length. This leads to a gradient of MyoII concentration sustained by the actin flow and essential to restrain contractility to the cell rear (Liu et al., 2015; Ruprecht et al., 2015). This front-rear coupling has also been observed in migrating neutrophils *in vivo* (Tsai et al., 2019).

Moreover, MyoII accumulation, along with cofilin, contracts and disassembles the actin network at the rear. This results in a positive feedback loop that further maintains the actin-flow polarity and the rear domain (Yolland et al., 2019).

3. Long-range cytoskeleton structures: microtubule network

a) Organization of the microtubule network

Microtubules are polymers of heterodimeric subunits made of α-tubulin and β-tubulin. The filament width is about 25 nm, and its length can vary from a few to hundreds of micrometers. The subunits are oriented in the same direction, resulting in a polarized filament with a "minus" end and a "plus" end (Lodish et al., 2000).

In most cells, microtubules are organized with their stable "minus" end at the Microtubule Organizing Center (MTOC), and their dynamic "plus" end towards the periphery of the cell (Muroyama and Lechler, 2017). Microtubules plus ends alternate between phases of rapid growth (called rescue) and phases of rapid shrinkage (called catastrophes); this behavior is known as "dynamic instability". Microtubule Associated Proteins (MAP) can interact with the dynamic plus end or the filament's side. They regulate the dynamic turnover of the network (Cassimeris, 2009).

Microtubules serve as a lattice for the transport of vesicles, proteins or mRNA within the cell. Kinesins and dyneins are molecular motors that connect the cargoes with the microtubule lattice and ensure their directed transport to the microtubules plus or minus end (Lodish et al., 2000).

b) The role of microtubules in cell polarization

The actin network forms local structures at the back and front of the cell. In contrast, the microtubules radiate from the MTOC and form a unique long-range network that reaches the front and back of the cell. This continuity makes it a central player in maintaining cell polarity (Etienne-Manneville, 2013), highlighted by the oscillatory phenotype presented by cells treated with microtubule destabilizing-drugs (Zhang et al., 2014).

In migrating cells, microtubules network is globally aligned with the font-back axis and has an asymmetric organization with stable and persistent microtubules towards the leading edge and few filaments growing towards the cell back (Li and Gundersen, 2008). They are involved in the maintenance of front and back domains through their interaction with actomyosin regulators and the directed transport of proteins on the network (Etienne-Manneville, 2013).

At the front, microtubule growth leads to the accumulation of plus-end MAPS that can also activate Rac-specific GEFs and trigger actin protrusion (Kawasaki et al., 2000). Directed transport of vesicles toward the microtubules plus end is also responsible for the concentration of active Cdc42 at the leading edge (Osmani et al., 2010).

At the rear, microtubule depolymerization triggers the local release of RhoA-specific GEFs, leading to increased contractility and cell retraction (Kopf et al., 2020).

Small Rho GTPases can also affect microtubule growth, resulting in local positive feedback loops that enhance cell polarity. At the front, activation of Rac stabilizes the pioneer microtubules growing in the lamellipodia (Wittmann et al., 2003), and at the back, activation of RhoA further destabilizes microtubules (Takesono et al., 2010).

Two force generators produce cell movement: actin polymerization and MyoII contractility. When confined, cells exhibit a wide diversity in their protrusion mode and force transduction mechanisms, allowing rapid adaptation of cell migration to microenvironments of varied topography, density and geometry. The front-back domains that limit protrusion and retraction within the cell are maintained and coupled by different mechanisms acting at different scales. These mechanisms can be specific to different cellular parameters (e.g., length, number of branches) or substrates. Thus, the extracellular environment affects the mechanisms of cell migration. Small molecules can activate protrusion or retraction in a part of the cell, changing the polarity axis and leading to guided migration. Physical properties can also affect protrusion or force transmission, resulting in switches between different migration mechanisms. Thus, the constant crosstalk between the cell and its surrounding environment will ultimately affect the mechanisms of cell migration, cell behavior and function. Therefore, efficient cell motility requires the integration of physical and chemical signals from the environment to optimize the mechanisms underlying cell motility. The last chapter of this introduction will describe the different aspects of this adaptation in the context of interstitial mDCs migration, the major subject of investigation of my thesis project.

.

CHAPTER 3: MECHANISMS OF RAPID DENDRITIC CELL MIGRATION IN THE INTERSTITIAL SPACE

As described in the first chapter, a key event in triggering the adaptive immune response is the migration of mDCs from the site of inflammation to the lymph node. Thus, mDCs have evolved to migrate efficiently through the interstitial space and represent an excellent model for studying the mechanisms that allow cell migration in complex environments. In this last part of the introduction, I will present the physical and chemical properties of the interstitial space and, focusing on the impact of confinement, how mDCs migration mechanisms are adapted to overcome the challenges imposed by the environment.

I. Physical and chemical properties of the interstitial space: challenges for cell migration

After activation, mDCs navigate through the interstitial space to reach the lymphatic system. During this process, they may encounter a wide range of extracellular environments with different chemical and physical properties.

A. Chemical properties

1. The extracellular matrix

The extracellular matrix (ECM) is the main non-cellular component of the interstitial space. It forms a fibrous protein meshwork, and its composition may vary locally or between different organs. It is mainly composed of type I collagen, which forms a scaffold for other proteins such as proteoglycans, elastin, and non-collagenous glycoproteins such as fibronectin (Kular et al., 2014).

Inflammation leads to ECM remodeling, such as a reduction in collagen fiber density or an increase in fibronectin deposition (Overstreet et al., 2013). Changes in the chemical composition of the ECM affect its physical properties. They also alter the capacity of cells to interact with the matrix through integrin-dependent adhesions. Consequently, ECM remodeling might result in modulation

of adhesion-dependent force transmission during cell migration.

2. Chemokines

Chemokines are small molecules that bind to G-protein coupled receptors (GPCRs) of immune cells. They trigger downstream signaling that results in increased cell speed (chemokinesis effect) or directional migration (chemo-attractive or repulsive effect) (Lämmermann and Kastenmüller, 2019).

CCL21 is the primary chemokine that regulates mDCs migration in the interstitial space. It is secreted by lymphatic endothelial cells and binds non-covalently to heparan sulfate in the ECM. It forms a steep gradient over 100µm in the interstitial space (Weber et al., 2013).

The CCL21 gradient is always present in the interstitial space. However, DCs can only detect the chemokine after maturation and expression of its receptor, CCR7. Thus, only mDCs exhibit guided migration to the lymphatic vessels (Sallusto et al., 1998). My PhD work does not focus on the sensing of CCL21; however, the context of directed migration is essential as it may force mDCs to migrate into challenging microenvironments.

B. Physical properties

Interstitium represents a porous and heterogeneous three-dimensional (3D) meshwork. Its main physical characteristics that can affect cell migration are its rigidity, topology, adhesive properties and confinement level. They depend on the quantity and cross-linking levels of the different components of the ECM (Charras and Sahai, 2014). During my PhD work, I mainly focused on the effect of confinement on mDCs migration.

Confinement can be indirectly characterized by the typical pore size between the ECM fibers. It represents the "free" space in which cells can evolve. The pore size *in vivo* can vary from 2 µm to more than 20 µm. This heterogeneity is due to the variation in density, thickness, and bundling of collagen fibers. Strikingly, these different collagen patterns can be observed within the same tissue (Wolf et al., 2009).

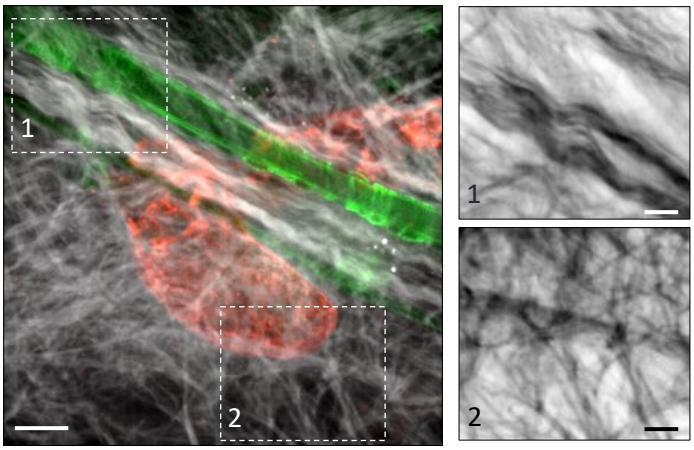

Figure 14 Collagen heterogeneity in mouse ear explant

Immunofluorescence (IF) of the collagen structure in the interstitial space. The insets show areas with wavy collagen bundles (1) or a loose reticulated network (2). Scale bar: 30µm on the left and 15µm on the inserts.

The variation in confinement can affect the force transmission mechanisms, creating in some cases enough friction that facilitates adhesion-independent migration. High confinement also limits cell protrusion and causes both cell and nuclear deformation where cells squeeze into pores smaller than their typical size. Migration in this physical context may require specific adaptation of the migratory machinery.

C. Challenges for DCs interstitial migration

1. *In vitro* models of the interstitial migration

In order to study the mechanisms underlying mDCs migration in the interstitial space, *in vitro* devices arise as an alternative to fine-tune specific physical parameters of the microenvironment. Collagen gels are commonly used as a model. Mesh organization and pore size vary according to the collagen concentration and polymerization conditions. However, collagen gels can be heterogeneous, and pore size cannot be precisely controlled (Wolf et al., 2009).

Microfabricated devices allow precise control of pore size at the submicron scale. Examples of common designs include, among others, a two-dimensional array of obstacles separated by an accurate distance as well as a simpler one-dimension microchannel (Irimia and Ellett, 2016) (see Methods).

These different configurations allow precise control of the confinement and complexity of the cellular microenvironment. Thus, they provide a versatile alternative to identify mechanisms

specifically required for mDCs migration in confined *in vivo* microenvironments, such as the interstitial space.

2. Main characteristics of mDCs migration in 3D confined-environment and limiting factors

Mature DCs movement in the interstitial space is characterized by a constant change in cell shape. This flexible morphology is called the "amoeboid" mode of migration (De Bruyn, 1946), which is an order of magnitude faster than typical mesenchymal locomotion (~10 µm/min and ~0.5 µm/min, respectively) (Binamé et al., 2010). In confined spaces, this migration mode is independent of integrins (Lämmermann et al., 2008) and matrix degradation. Thus, changes in the chemical composition of ECM do not affect mDCs movement, but it is sensitive to pore size and spatial distribution (i.e., environmental complexity).

Using an *in vitro* set-up with varying levels of confinement and complexity, previous studies have shown that cell body deformation (Lämmermann et al., 2008) and protrusion coordination (Lämmermann et al., 2009) are limiting factors in complex 3D migration, but can be dispensable in 2D environments without restriction. In the next sections, I will describe the mechanisms by which mDCs can overcome these major challenges of interstitial migration.

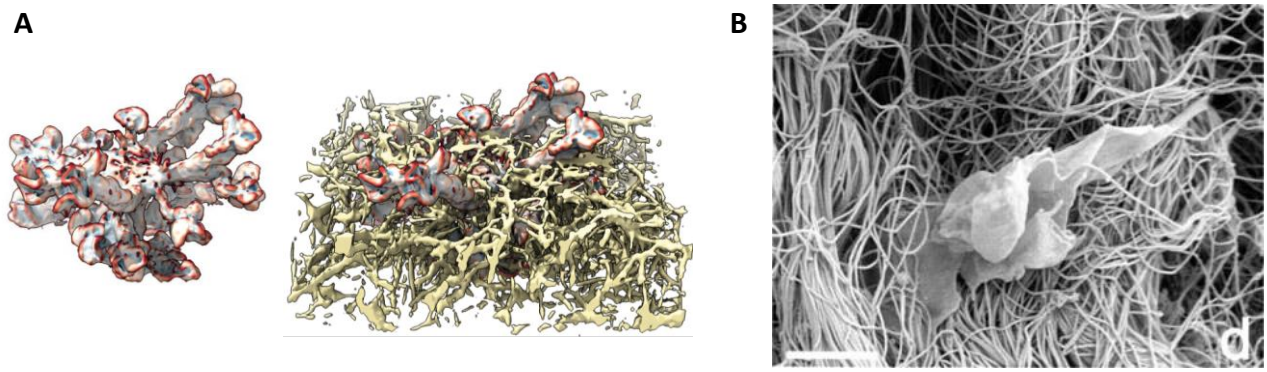

Figure 15 Protrusions coordination and cell deformation are necessary for mDCs migration in 3D complex environments.

(A) Light sheet microscopy of a DC embedded in a 3D collagen gel with (right) and without (left) the surrounding matrix. The cell forms multiple branches inserted in different pores. Efficient migration requires the coordination of the protrusions to lead to the passage of a "winning" arm followed by the rest of the cell and thus avoid cell bottleneck. From Renkawitz J. et al, 2019 (B) Scanning electron microscopy of a DC migrating within the interstitial space of the dermis. The passage of cells through the collagen network requires an important cellular deformation; From Stoitzner P. et al 2002.

II. Maturation optimizes DCs migration machinery for rapid and directed migration

A. Remodelling of the actomyosin cytoskeleton

Upon immune detection, DCs switch from patrol function to antigen presentation. This maturation process requires crucial changes to adapt DCs to their new function. The main modification is the expression of CCR7, allowing the sensing of CCL21 and directional migration to lymphatic vessels. However, chemokine detection must be accompanied by changes in the cytoskeleton to allow rapid and persistent migration into the dense and irregular interstitial space.

Maturation induces the expression of the actin-bundling protein fascin-1 and stabilization of filamins, both of which are involved in the disassembly of the podosomes (Lamsoul et al., 2013; Yamakita et al., 2011). Podosome disassembly is a key factor in DCs transition from mesenchymal to amoeboid migration with no adhesion nor matrix degradation. Podosome disassembly is induced by LPS-treatment but may be specific to the maturation signal (Cougoule et al., 2018).

Parallel to de-adhesion, maturation induces a complete reorganization of the actomyosin cytoskeleton in DCs. This process was analyzed using microchannels. In the immature state, both actin and myosin are transiently recruited at the cell front to allow antigen sampling by macropinocytosis. This process is associated with slow migration phases (Chabaud et al., 2015; Vargas et al., 2016). In the mature state, macropinocytosis is down-regulated, and the actomyosin cytoskeleton concentrates at the back of the cell. Thus, the speed of mDCs is higher than iDCs (Bretou et al., 2017; Vargas et al., 2016). This remodeling is essential for the rapid and persistent migration of mDCs along the CCL21 gradient in the interstitial space and their arrival at the lymph node (Vargas et al., 2016). This phenomenon was observed following either LPS or ATP activation (Sáez et al., 2017; Vargas et al., 2016).

Interestingly, the rear and front actin pools do not depend on the same nucleator: Arp2/3 is responsible for the front actin, while the formin mDia1 polymerizes the rear actin. Maturation signaling favors the activity of mDia1 over Arp2/3 via modulation of RhoGTPases: activation of RhoA and down-regulation of Cdc42. However, the two nucleators are in equilibrium at the different maturation states and can compensate each other in case of inhibition. Inhibition of formins in mDCs brings actin back to the front with slow migration phases, while inhibition of Arp2/3 in iDCs induces rapid migration similar to mDCs (Vargas et al., 2016).

DCs maturation leads to a complete remodeling of their migratory mechanism through changes in actin bundling, RhoGTPase signaling, and actin nucleator activity. Mature DCs are characterized by decreased adhesion and increased retrograde flow of actomyosin relative to iDCs. These modifications are not required for detection and orientation toward CCL21, but for rapid and persistent migration along the gradient in the interstitial space. Thus, the mDC migration machinery is optimized for situations where chemokine guidance imposes a series of physical restrictions.

B. Coordination of antigen capture and rapid migration

Coordination of antigen sampling and DC migration is essential for proper activation of the immune system. Indeed, DCs arriving at the lymph node without antigen loaded on their MHCII cannot trigger a specific adaptive immune response. As already mentioned in the previous section, antigen sampling and rapid DC migration are mutually exclusive by the common MyoII requirement (Chabaud et al., 2015). The two processes are also coordinated by signals from the lysosomes, where antigens are processed (Bretou et al., 2017).

In the immature state, the invariant chain (Ii) recruits MyoII at the front of the cell (Faure-André et al., 2008), and with the activation of Arp2/3 by Cdc42, they are both necessary for macropinocytosis (Vargas et al., 2016). During maturation, the protease Cathepsin S is activated and cleaves Ii to allow antigen loading on the MHCII in the lysosomes (Riese et al., 1998). Degradation of Ii and negative regulation of Cdc42 decrease macropinocytosis (Chabaud et al., 2015; Vargas et al., 2016). Macropinocytosis reduction results in (i) inhibition of the mammalian target of rapamycin complex 1 (mTORC1) and (ii) release of calcium from lysosomes via the Transient Receptor Potential cation channel, Mucolipin subfamily, Member 1 (TRPML1). Calcium signaling activates MyoII at the back of the cell. At the same time, mTORC1 inhibition and TRPML1 activation induce translocation of transcription factor EB (TFEB) into the nucleus, thereby promoting lysosomal activity and expression of lysosomal genes, including TRPML1 itself (Bretou et al., 2017).

Thus, lysosomal signaling establishes a positive feedback loop via the TFEB-TRPML1 axis that maintains activation of MyoII at the back of the cell and is essential for the arrival of mDCs at the lymph node (Bretou et al., 2017).

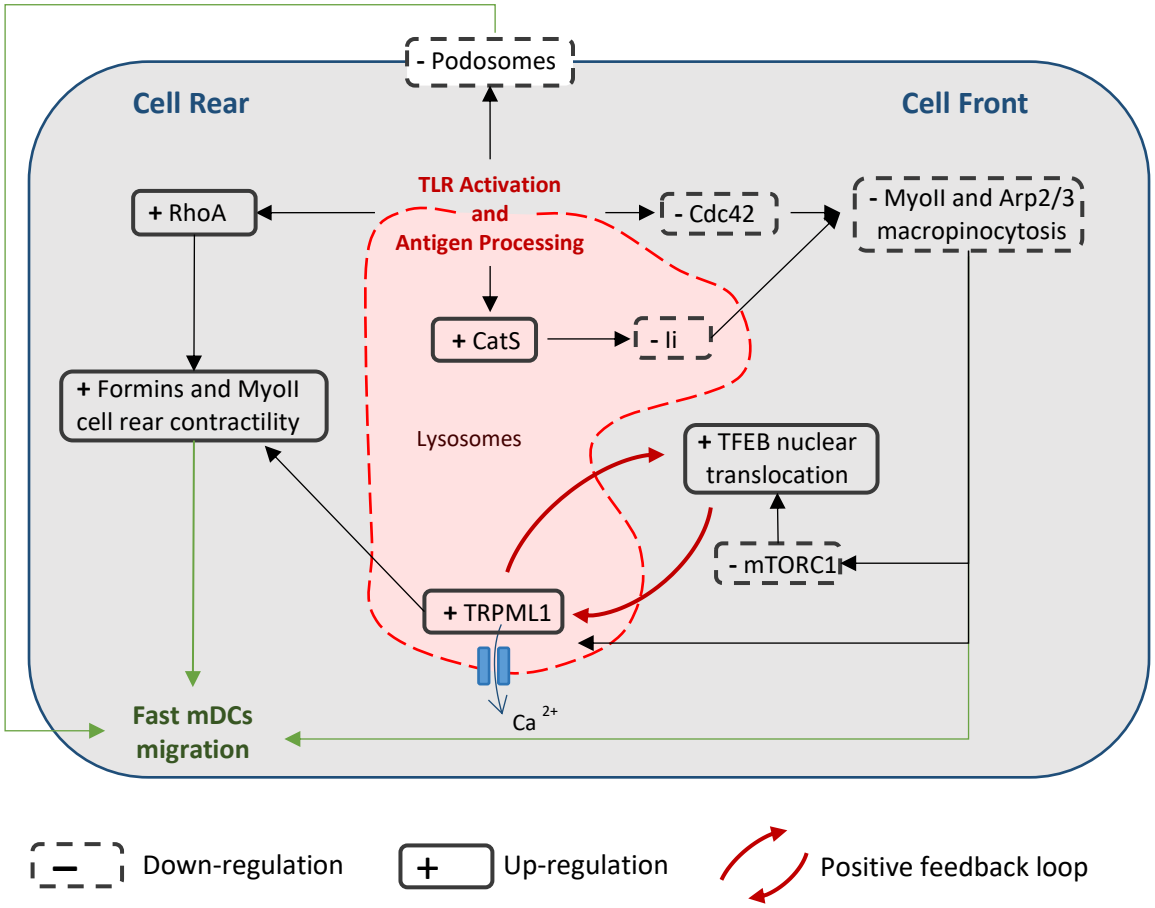

Figure 16 Schematic summary of the signaling pathway coupling microbial detection with reorganization of mDC migration machinery

TLR activation by LPS results in (i) a decrease in macropinocytosis due to negative regulation of MyoII and Arp2/3 at the cell front and (ii) rapid amoeboid migration due to disassembly of the podosomes, and positive regulation of MyoII and formin at the back of the cell. Cytoskeletal remodeling is initiated and sustained over time by antigen processing-induced lysosome signaling.

Microbial detection leads to a complete remodeling of the actomyosin cytoskeleton. Cell adhesion is reduced while the retrograde flow of actomyosin is increased, thus optimizing a fast amoeboid migration mode. This remodeling is triggered by antigen processing and calcium signaling by lysosomes, allowing coordination between antigen uptake and mDC migration into the interstitium. The last part of the introduction will describe how this reorganization of actomyosin facilitates the rapid and directed migration of mDCs in a complex and confined 3D environment, such as the interstitial space.

III. DCs strategies to overcome physical obstacles

A. Cell branching coordination in a porous environment

Cell morphology in the interstitial space is characterized by an elongated and branched cell immersed into the multiple pores of the microenvironment. Thus, cell branching coordination is essential for mDCs chemokine sensing and migration in complex 3D environments.

1. Rac and Cdc42 control front protrusions in mDCs

As mentioned in the previous chapter, the Rac and Cdc42 axes are the main regulators of actin protrusions at the cell front. Their role in DCs interstitial migration has been characterized using knock-out approaches.

In the absence of the Cdc42, cells form a multipolar front. This phenotype induces a moderate migration defect in unimpeded 2D confinement chambers. However, in 3D collagen gels, the cells are stopped, with multiple protrusions leading to cell entanglement in the porous environment (Lämmermann et al., 2009). The deletion of the upstream activator of Cdc42, DOCK8, leads to a similar defect, with elongated cells eventually fragmenting in collagen gels (Harada et al., 2012). Overall, the deletion of each member of the DOCK8-Cdc42-Wasp axis leads to defects in the *in vivo* migration of mDCs and cells do not reach the lymph node after activation (de Noronha et al., 2005). Indeed, human immune deficiencies are associated with both DOCK8 and Wasp mutations (Harada et al., 2012; de Noronha et al., 2005).

In contrast to the Cdc42 axis, Rac deletion decreases the ability of DCs to extend protrusions but also decreases cell migration (Benvenuti et al., 2004). Similarly, Wave null mDCs do not form lamellar protrusions, and only thin filipodia are present at the cell front. These cells show normal migration in straight microchannels, while their speed is reduced in 3D collagen gels and in the interstitial space (Leithner et al., 2016). Furthermore, the deletion of the Eps8 capping protein, which participates in the Rac signaling pathway, also abolishes the formation of protrusions in 3D collagen gels, which causes the cells to oscillate in place, while, as with other phenotypes, the 2D migration speed remains unaffected (Frittoli et al., 2011).

Therefore, the impact of deletion in the Rac and Cdc42 axes depends on the physical context. The effect is weak in an unimpeded environment, while migration in 3D collagen gels or in the interstitial space is considerably reduced. Thus, the Rac and Cdc42 axes are not necessary for mDCs motility *per-se*, but are specifically required for the regulation of branching in complex geometries. In porous 3D environments, branching dynamic presents an optimum: the formation of stable protrusions is necessary for cell migration, but too many impede mDCs movement. Surprisingly, the direct inhibition of Arp2/3 does not affect mDCs motility in the interstitial space (Vargas et al., 2016).

Thus, the coordination of its activity at the cell front appears to be critical, but other mechanisms may compensate for the loss of branched actin and allow efficient migration.

2. Microtubule network coordinate protrusion and retraction

Mature DCs protrusions must also be coupled to cell retractions to ensure coherent migration. In a porous environment, the formation of one main branch should be associated with the withdrawal of the others, to allow translocation of the entire cell body through the same path.

As described in the previous chapter, membrane tension is unlikely to allow this front-to-back coordination in long and branched cells such as mDCs. Recent work has shown the essential role of the microtubule network in this process in mDCs (Kopf et al., 2020).

The MTOC follows the nucleus after the choice of a path; this promotes microtubules polymerization in the main branch and microtubules depolymerization in the other branches and at the cell back. Microtubules depolymerization releases the RhoA GEF, Lfc, and triggers local phosphorylation of MyoII light chain, leading to branches retraction. Destabilization of the microtubule network by pharmacological microtubules depolymerization leads to cell fragmentation in collagen gels, and as a consequence, mDCs are unable to reach the lymphatic vessels in tissue explants (Kopf et al., 2020).

Branch coordination is, therefore, a key factor for mDCs motility in complex 3D environments and a deficiency in this process leads to cell fragmentation and immunodeficiency. The RhoGTPases Rac and Cdc42 regulate front protrusion, while the coordination between protrusions and retraction relies on the microtubule network. In immature DCs, Arp2/3 is often highlighted as the coordinator between branching events and chemokine detection (Leithner et al., 2016). However, migration and directionality of mDCs are not dependent on Arp2/3 in microchannels, nor in 3D collagen gels (Vargas et al., 2016). The microtubule network appears to be particularly necessary for mDCs to coordinate protrusions-retraction and detection of CCL21. Indeed, local control of MyoII activation triggered by microtubules depolymerization is essential for migration into interstitial spaces (Kopf et al., 2020), which is consistent with the formin- and contractility-dependent migration machinery of mDCs (Vargas et al., 2016). However, the mechanism linking chemokines sensing with microtubule network polarization remains unknown for mDCs.

B. mDCs migration in confined environments

The dense structure of the interstitial space with pores smaller than the typical cell size limits cell migration. A mechanism developed by cells to overcome these obstacles is based on the generation of paths by ECM proteolysis (Wolf et al., 2013). Such matrix degradation is associated with slow mesenchymal cells and leads to long-term remodeling of the interstitial space. Thus, this mechanism is related to pathological situations such as cancer metastasis and is not compatible with homeostatic migration of immune cells. Non-proteolytic cells, such as mDCs, develop mechanisms to adjust their migration to the physical constraints of their environment. This flexible behavior involves both the adaptation of cell mechanics to deform the cell body and the nucleus in confined areas and the adaptation of the migration path to avoid obstacles (Yamada and Sixt, 2019).

Figure 17 The structure of the ECM limits mDCs migration in the interstitial space.

The ECM (blue) forms a dense and porous network in the interstitial space. Thus, rapid migration in this physical context requires mDCs to coordinate cell branches and overcome pores smaller than the typical cell size. The cell nucleus (dark purple) appears to be the main factor limiting cell deformation in confined environments. Adapted from Vargas *et al* 2017 .

1. The mechanical properties of the nucleus will limit cell migration

The deformability of the cells depends on their mechanical properties. I will focus on the nucleus since it has been described as the main factor limiting cell migration in different models (Wolf et al., 2013), including DCs (Thiam et al., 2016).

The main component of the nucleus is the chromatin surrounded by the nuclear lamina and two lipid bilayers: the inner and outer nuclear membrane. The lamina is composed of two distinct filamentous networks of intermediate filaments, either type A or type B lamins. In mammalian cells,

type A lamins comprise lamin A and C, while type B lamins comprise lamin B1 and B2. As in the cell cortex, both lamina networks are anchored to the inner nuclear membrane and can then induce nuclear tension. Moreover, the Linker of Nucleoskeleton and cytoskeleton (LINC) complex mechanically binds the lamina with the cytoskeleton and allows force transduction across the nuclear membrane (Lele et al., 2018).

In simple mechanical models of the nucleus, the lamin B mainly governs the elastic strength, while the lamin A/C network and chromatin determine the viscous strength (Lele et al., 2018). In the case of large deformation, the lamin A/C plays a major role in nuclear resistance (Lammerding et al., 2006; Stephens et al., 2017). Thus, the level of lamin A/C determines the nuclear rigidity and the ability of the cells to deform through small pores (Harada et al., 2014). Some cells, such as neutrophils, express a low level of lamin A/C. They have a soft nucleus that promotes their migration through narrow pores (Rowat et al., 2013). However, reduced lamin A/C is also associated with a short lifespan (Harada et al., 2014) (~24 hours for neutrophils). DCs must combine interstitial space migration and long-term survival to present antigens to T-lymphocytes. Thus, they express a higher level of lamin A/C compared to neutrophils and develop different strategies to allow the movement of their rigid nucleus in dense extracellular matrices (Thiam et al., 2016).

2. Selection of the path of least resistance

A first mechanism that promotes mDCs migration in dense interstitial spaces relies on the integration of physical signals to follow an optimal migration path with the lowest number of obstacles that can block their nucleus. Recent work has shown that mDCs can detect the local and global resistance of a tissue.

a) Hydraulic resistance

Hydraulic resistance is the force required to displace the fluid surrounding the cell. It depends on both the viscosity of the fluid and the structure of the microenvironment. The hydraulic resistance is a key parameter since it integrates the physical resistance of the tissues over a long distance.

Most studies on hydraulic resistance have been performed in microchannels in which the cells fill the entire channel and must move the fluid in front of them (Belotti et al., 2020; Moreau et al., 2019; Prentice-Mott et al., 2013). In this configuration, mDCs can detect the hydrostatic pressure difference and thus select the shortest path in a maze. At a bifurcation with a difference in hydraulic

resistance, mDCs extend arms into both channels. However, local accumulation of actomyosin cytoskeleton amplifies the small force imbalance and leads to the retraction of the arm in the more resistive channel. Detection of hydraulic resistance could allow the long-range optimization of mDC migration to lymphatic vessels via the path of least resistance (Moreau et al., 2019). However, the presence of local differences in hydraulic resistance in tissues remains unknown, as does the interaction with chemokine guidance.

b) Pore size selection

During interstitial migration, mDCs face several pores simultaneously. In the previous section, I discussed how mDCs coordinate their different arms to pass through a single pore, but I did not discuss how they decide which pore they pass through. Recent work has shown that during this decision-making process, mDCs integrate the local pore size to select the largest one (Renkawitz et al., 2019).

For example, in heterogeneous collagen gels, mDCs locally avoid dense areas of the matrix. The mechanisms of this mechanical guidance have been studied in microchannels. Mature DCs are guided to a decision point where they encounter a series of channels of different dimensions. At the decision point, the cell nucleus is inserted into the different paths before the cell makes its choice. The nucleus positioned at the front of the cell is used as a mechanical sensor to select the largest pore. The MTOC directly follows the nucleus after the decision-making. This triggers the retraction of the other branches inserted into the narrowest pores, as described above (Renkawitz et al., 2019).

The mechanical properties of the nucleus are essential for the pore size selection. Indeed, only pores narrower than the size of the nucleus bias cell migration. Moreover, this process is affected by the modification of the nuclear lamina. Cells with a more rigid nucleus (lamin A overexpression) are more biased towards the wide pores (Renkawitz et al., 2019).

Nuclear probing of the pore size would allow the cell to avoid trapping of its nucleus in a narrow pore during migration in the interstitial space. Overall, nuclear probing is a general characteristic of non-proteolytic and fast migrating cells, which are all characterized by a “nucleus-first” configuration (Renkawitz et al., 2019).

The molecular mechanism linking the nucleus insertion into the different pores and the selection of the largest one remain unknown. Recent work has shown that stretching of the nucleus during confinement increases cell contractility through MyoII activation (Lomakin et al., 2019; Venturini et al., 2019). We could hypothesize that inserting the nucleus into a small pore could

trigger a local MoyII activation and retraction of the cell. However, migration of MoyII-inhibited cells is still biased by pore sizes, even though the decision process is longer (Renkawitz et al., 2019). Thus, pore size selection could also be a passive mechanism depending only on the viscous properties of the nucleus.

Pore size and hydraulic resistance detection allow mDCs to choose the local and global path of least resistance. However, when mDCs migrate in chemotactic gradients, mechanical guidance only allows them to avoid dense local areas of the matrix. If they encounter large dense regions, they are able to move through and maintain their direction of migration (Renkawitz et al., 2019). Thus, mDCs develop mechanisms to overcome physical limitations and maintain their ability to migrate despite changes in their environment. Until now, the study of these mechanisms has focused on the deformation of the cell nucleus.

3. Mechanism of Nuclear deformation

The shape of mDCs'nucleus changes during interstitial migration, highlighting the presence of forces deforming it. The force generator has been studied in microchannels with micro-scale constrictions of precise dimensions (Thiam et al., 2016). DCs use the force generated by both MyoII-based contractility and Arp2/3-induced actin polymerization to deform their nuclei (Lämmermann et al., 2008; Thiam et al., 2016).

a) MyoII-based contractility

MyoII-based contractility leads to pushing forces on the nucleus. These forces can create a pressure gradient between the front and back of the nucleus as it fills the pore. MyoII activity imposes nuclear deformation by pressing the nucleus onto the narrow pore. In dense collagen gels, MyoII inhibition leads to elongated mDCs with a spherical nucleus immobilized at the back of the cell. In loose collagen gels, mDCs exhibit residual migration based on actin protrusion forces. MyoII-Inhibited cells reach the same peak velocity values as untreated cells, probably in the area where the spacing of the fibers is large enough to allow the nucleus to pass through without deformation. This result shows that actomyosin contraction at the back of the cell propels the nucleus when confronted with narrow pores (Lämmermann et al., 2008).

b) Arp2/3-dependent actin network

The second mechanism described for nuclear deformation involves the nucleation of an Arp2/3-dependent actin network around it. This specific lattice triggers lateral compressive forces on the nucleus at the channel narrowing. Strikingly, under compression by this actin structure, the nucleus reaches a diameter smaller than the narrowing width. Thus, the Arp2/3-dependent actin network allows the deformation of the rigid nucleus. However, unlike contractility by MyoII, it does not induce forward pushing forces (Thiam et al., 2016).

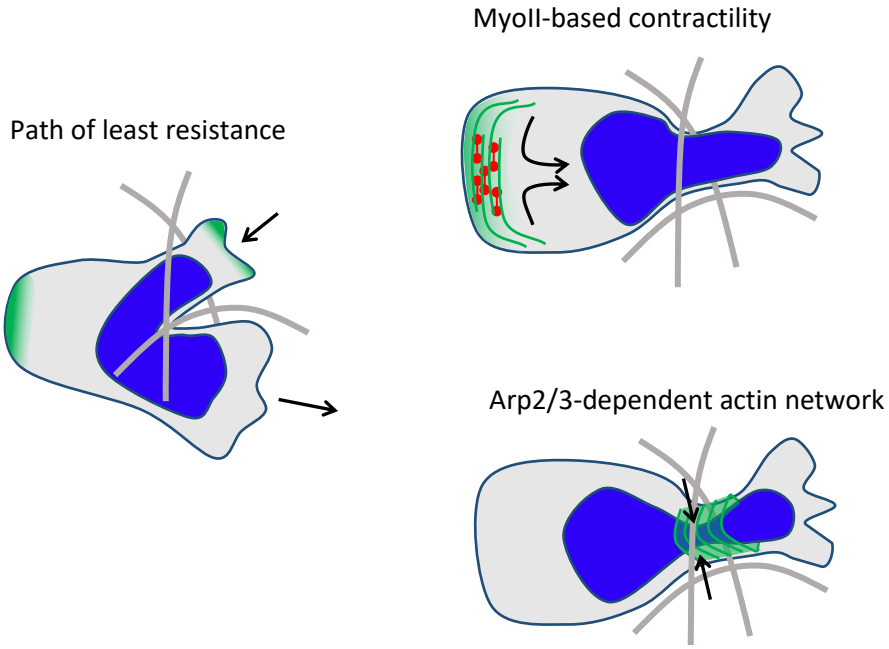

Figure 18 Schematic diagram of the mechanism used by DCs to overcome small pores in the interstitial space.

(Left)Nuclear probing can allow mDCs to avoid nuclear compression through small pores. This process must be coupled with branch coordination to avoid cell trapping between pores.

(Right) In some situations, mDCs do not bypass physical barriers and apply forces on their nucleus to deform it through narrow pores. Two main nuclear deformation mechanisms have been characterized: (Top) MyoII-based contractility (red) can push the nucleus through the narrowing. Arp2/3-dependent actin (green) network can exert lateral compressive forces on the nucleus at the restriction site.

c) Different requirements for nuclear deformation

The requirement for these distinct mechanisms depends on the pore size and mechanical properties of the nucleus. In immature DCs, MyoII-based contractility determines the speed of passage, while the Arp2/3-dependent actin network determines the level of nuclear deformation. The actin structure around the nucleus appears in constrictions of less than 12 µm² cross-section area and is both necessary and sufficient to deform the nucleus without MyoII contractility (Thiam et al., 2016).

Nuclear deformation through these narrow pores transiently breaks the laminar A/C lattice (Thiam et al., 2016). This promotes high nuclear deformation, and may also lead to ruptures of the nuclear envelope. The Endosomal Sorting for Transport (ESCRT) complex III can repair these nuclear ruptures, but they still result in transient DNA damage and exposure of genetic material to the cytosol (Raab et al., 2016). Since immature DCs express different DNA sensors, nuclear deformation can, therefore, trigger specific intracellular signaling that impacts their immune function (Chen et al., 2016).

In laminA/C-depleted immature DCs, there is no longer any actin accumulation around the nucleus in the constrictions, whereas the removal of the LINC complex alone does not affect this actin structure. Thus, the deformation of a soft nucleus does not trigger Arp2/3-dependent actin polymerization. In this condition, MyoII-based contractility is necessary and sufficient to deform the nucleus without Arp2/3-dependent compressive forces. Thus, the modification of the mechanical properties of the nucleus switches the force generators necessary for its deformation (Thiam et al., 2016).

The nuclear deformation requirements for mDCs have been studied in less detail than for immature cells. As already mentioned, in collagen gels, the propulsion of the mDCs nucleus requires MyoII-based contractility (Lämmermann et al., 2008), and the overall migration of mDCs is independent of Arp2/3-mediated actin nucleation (Vargas et al., 2016). However, in microchannels, the presence of the Arp2/3-dependent actin network around the deformed nucleus has not been characterized. In this set-up, Wave-null mDCs squeeze their nuclei through 7.5 µm² cross-section area constrictions while MyoII inhibition blocks their passage (Leithner et al., 2016). Thus, mature DCs use similar mechanisms to those of immature DCs depleted for laminA/C, with MyoII-based contractility being both necessary and sufficient to deform their nuclei without Arp2/3-dependent compressive forces. The reason for the differences between immature DCs and mature DCs is unknown. We do not know whether DCs maturation affects lamin A/C expression and the mechanical properties of the nucleus. The difference could also be related to the modification of the mDCs migration machinery and, more precisely, the down-regulation of Arp2/3.

d) Specific mechanisms for mDCs entry into the lymphatic vessels

After interstitial migration, mDCs pass through the lymphatic endothelium to reach the lymphatic system. This barrier consists of a discontinuous basement membrane composed of laminin and collagen IV, surrounding a layer of lymphatic endothelial cells (Pflicke and Sixt, 2009).

Mature DCs entry in the lymphatic vessel involves strong nuclear deformation. However, mDCs do not require cell-cell or integrin-mediated matrix-cell interaction to cross this endothelium (Lämmermann et al., 2008). Thus, they use a different mechanism than the well-established adhesion cascade used by leukocytes to cross the blood endothelium (Vestweber, 2015).

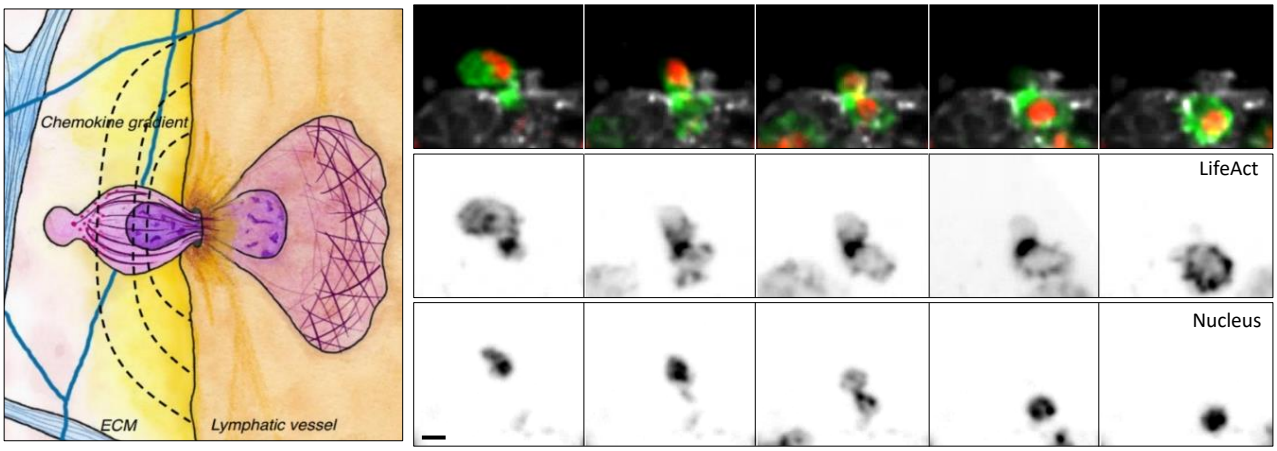

Figure 19 MDCS migration through the lymphatic endothelium causes a strong deformation of the nucleus

(Left) Drawing of an mDC passing through the basement membrane. Adapted from Vargas *et al* 2017. (Right) Image sequence of an exogenous LifeAct-mDC (actin, top panel in green and central panel) crossing lymphatic endothelial cells (top panel in grey). Mature DC transmigration is characterized by a strong deformation of the nucleus (top panel in red and lower panel) and rearrangement of the actin cytoskeleton. Time lapse=2 min, scale bar=5µm.

Firstly, mDCs preferentially pass through pre-formed pores present in the discontinuous basement membrane (Pflicke and Sixt, 2009). Interestingly, nuclear probing could help to select the largest pre-existing portal and optimize mDCs passage through the basement membrane. Mature DCs are also able to enlarge these pre-existing pores to facilitate their translocation. This process is independent of ECM proteolysis (Pflicke and Sixt, 2009).

Moreover, mDCs transendothelial migration in lymphatic vessels appears to require the engagement of specific receptors to promote cell deformation. Mature DCs express the C-type lectin receptor CLEC-2, which binds to the glycoprotein podoplanin on the lymphatic endothelium. This interaction activates Rac1, and decreases the activity of RhoA and MyoII, leading to mDCs spreading on lymphatic vessels and promotes their transmigration (Acton et al., 2012; de Winde et al., 2018).

Class 3 semaphorins (Sema3) are soluble proteins also involved in mDCs transendothelial migration. Lymphatic endothelial cells secrete Sema3 A. It promotes mDCs entry by local activation of MyoII contractility at the back of the cell via its plexin-A1/neuropilin 1 receptor (Takamatsu et al., 2010). Additionally, neuropilin-2 is known to have a dual role in mDC migration. It facilitates the binding of CCL21 to CCR7 and promotes chemotaxis, but also facilitates the binding of Sema3s to

plexins and promotes transwell migration by modulation of the actomyosin cytoskeleton. Thus, neuropilin-2 signaling may promote nuclear deformation when mDCs follow chemotactic gradients (Curreli et al., 2016). This is particularly relevant at the site of mDCs transmigration since lymphatic endothelial cells secrete Sema3 A and also release CCL21 when interacting with mDCs (Vaahtomeri et al., 2017).

Thus, while mDCs nuclear deformation during interstitial migration appears to be primarily controlled by cell-intrinsic mechanisms, transendothelial migration requires additional signaling provided by the lymphatic endothelium. The basement membrane structure and the state of the lymphatic endothelial cells can, therefore, control mDCs transmigration and modulate the immune response. However, studies of both steps of mDCs migration highlight the crucial need for MyoII-based contractility to deform the nucleus.

To conclude, DCs migration into different microenvironments is essential for the initiation of the adaptive immune response. Consequently, their migration mechanisms exhibit high plasticity and are directly coordinated with their immune function.

DCs use both actin polymerization and MoyII contractility as the driving forces for their movement. Strikingly, inhibition of either leads to residual migration instead of completely blocking it, thus highlighting their adaptive capacity. Pathogens or cellular damage sensing switches both DCs function and migration mechanisms. Tissue patrolling and extracellular sampling by immature DCs require slow migration phases associated with Arp2/3-dependent actin polimerization and Ii-dependent recruitment of MyoII at the cell front. Rapid and persistent migration to lymphatic vessels of mDCs requires mDia1-dependent actin and increased MyoII activity at the back of the cell. On the other hand, lysosomes appear as a central signaling platform controlling both immune function and mDC migration. They integrate chemical signals from pathogens and the inflammatory context to coordinate antigen processing, expression of cytokines and co-stimulatory molecules, as well as actomyosin machinery remodeling.

In DCs, force transmission to the substrate is mainly independent of integrin-specific interactions. Thus, their movement is independent of the chemical composition of the ECM, and mainly characterized by rapid shape changes with a "flowing and squeezing" behavior. This mode of migration imposes cell deformation as a critical factor limiting cell movement, especially for mDCs guided by chemokine gradients that can force their passage into dense matrix areas. Previous studies on cell deformation have focused on the nucleus. They have shown that nuclear deformation

in immature DCs relies on an Arp2/3-dependent actin ring to weaken transiently the lamina A/C shell. However, after maturation, nuclear deformation depends on MyoII-based contractility. The reasons for this switch and the precise requirements for mDCs nuclear passage through small pores have not been fully characterized. Moreover, mDCs migration in dense microenvironments imposes cell-wide strains. Understanding how mDCs respond to global confinement and its impact on cell movement, migration mechanisms, and immune function are the main objectives of my Ph.D. To answer these questions, I combined a series of approaches, from microfabricated devices to *ex vivo* skin models, to dissect the cytoskeletal rearrangements triggered by mDCs confinement, and their functions in overcoming the physical barriers imposed by the tissue microenvironment.

METHODS

I. Bone marrow-derived dendritic cells as a cell model

A. Culture protocol

We used bone marrow-derived dendritic cells (BMDCs) as a cellular model for DCs. The BMDCs were obtained by differentiation of bone marrow precursors for 10 days in a medium composed of IMDM-Glutamax, fetal calf serum (10%), penicillin-streptomycin solution (100 U ml^{-1}), and β-mercaptoethanol (50 µM) supplemented with granulocyte-macrophage colony-stimulating factor (GM-CSF)-containing supernatant (50 ng ml^{-1}) obtained from transfected J558 cells, as previously described (Faure-André et al., 2008)

At day 10 of differentiation, semi-adherent DCs were treated with LPS (100 ng ml^{-1}) for 30 min. After three washes with medium, cells were maintained in culture overnight until they reached full maturation. The migration of mDCs was recorded between 16 and 36 h post LPS treatment. During this period, the expression level of classical surface maturation markers CD86, MHC II, and CCR7 remains constant (Alloatti et al., 2015).

Wild-type (WT), LifeAct-GFP, and MyoII-GFP precursors were obtained from 6–10-week-old C57BL/B6 mice (Charles River), LifeAct-GFP mice (Riedl et al., 2010), and myosin IIA heavy Chain-GFP knock-in mice (Zhang et al., 2012), respectively.

B. Characteristics of bone marrow-derived dendritic cells

The generation of DCs from bone marrow cultures supplemented with GM-CSF is a well-established protocol that produces a large number of primary cells and does not require purification steps (Inaba et al., 1992). The BMDCs are characterized by the expression of CD11c integrin and MHC II, high motility, and ability to activate antigen-specific T cells. However, GM-CSF promotes the differentiation of three myeloid cell lineages: granulocytes, macrophages, and DCs (Helft et al., 2015). The three cell types are separated according to their adhesion properties. Granulocytes are not adherent and are eliminated during cell culture. Macrophages are more adherent than DCs. Thus, DCs are enriched by recovering only the semi-adherent cells for further LPS activation. However, for experiments using iDCs, it is important to retain the adherent fraction because it

promotes the maintenance of the inactivated state. The DCs are further enriched during the migration assay as they enter the chamber more rapidly, whereas the macrophages remain adherent in the cell-loading well.

C. Visualization of the cytoskeleton components and cellular compartments in live BMDCs

Similar to other primary cells, BMDCs are difficult to transfect. In addition, they are highly endocytic and tend to accumulate fluorescent probes or transgenic proteins in their endolysosomes. Thus, most of the live cell migration assays included in the present thesis were performed using transgenic mice. The actin cytoskeleton was visualized mainly using LifeAct-GFP mice. LifeAct is a small peptide derived from a yeast actin-binding protein. It binds non-covalently to F-actin and does not interfere with cellular processes such as DC migration along chemokine gradients (Riedl et al., 2010). To visualize MyoII, we used the MyoIIA heavy chain-GFP knock-in mice. The transgenic myosin IIA heavy chain-GFP protein is expressed at the endogenous level. It localizes in the cytoplasm or is incorporated in MyoII contractile filaments (Zhang et al., 2012). LifeAct-GFP and myosin IIA heavy chain-GFP are hereafter referred to as LifeAct and MyoII-GFP, respectively.

To visualize the lysosomal compartment, we exploited the endocytic properties of DCs. The plasma membrane was stained with a pulse of fluorescently conjugated wheat germ agglutinin (WGA; 0.25 µg ml^{-1} for 30 min). After a few hours, the stained plasma membrane is fully internalized and renewed; thus, the fluorescent WGA accumulates in the lysosomal compartment. The WGA staining colocalizes with the lysosomal-associated membrane protein 1 (LAMP-1) (Bretou et al., 2017). The nuclear compartment is classically stained with Hoechst 33342 (referred to as Hoechst; 200 ng ml^{-1}).

II. Microfabricated devices to study mDCs migration under different degrees of confinement.

To address specific aspects of cell migration, our laboratory has developed a series of microfabricated devices. This technique allows us to design *in vitro* chambers with precise and controlled dimensions and chemical composition. They mimic specific parameters of the *in vivo* microenvironment and are compatible with high spatiotemporal resolution imaging (Garcia-Arcos

et al., 2019). This reductionist approach facilitates the analysis of the contribution of the physical and chemical microenvironments to cell migration (Le Berre et al., 2013; Liu et al., 2015).

A. Manufacturing protocol

To study the effect of physical confinement on mDC migration, we designed a series of microfabricated devices with dimensions ranging from 1 to 8 µm. Molds were made on silicon wafers by photolithography by the laboratory engineer using a previously described protocol (Heuzé et al., 2011). Photolithography facilitates the construction of micro-sized structures with very few limitations and accuracy of 0.5 µm in their X and Y dimensions. However, the height of the structure is determined by the height of the spin-coated photoresist on the wafer. Therefore, it cannot be precisely pre-determined and is the main limitation of this technique.

Reproducible microfabricated chambers are produced by casting a silicon-based organic polymer—polydimethylsiloxane (PDMS)—onto the molds. After curing, the molded PDMS pieces are bonded to a glass-bottom dish to form the migration chamber with precise dimensions (Sáez et al., 2018). Because PDMS is biocompatible transparent and can shape nano-sized structures, it is the most commonly used silicone in bioengineering. However, its main disadvantage is its absorption of small hydrophobic molecules such as many drugs (van Meer et al., 2017). Thus, microfabricated PDMS chambers are compatible with long-term live cell migration assays and microscopic imaging, but the use of pharmacological inhibitors requires a pre-incubation step.

All PDMS chambers were coated with bovine plasma fibronectin (10 µg ml^{-1}), except where specific treatments are indicated. They were used within 48 h of manufacture. At least 1 h before cell loading, PDMS chambers were incubated with the culture medium containing pharmacological inhibitors, when indicated (Sáez et al., 2018).

The following section describes the series of microfabricated devices that we designed during my doctoral research, the specific aspects of mDC migration that can be studied using them, and their limitations.

B. MDCs migration in microchannels of different dimensions

The first series of devices is based on microfabricated straight channels. The microchannel forms a tube that confines DCs from the top and sides. Dendritic cells are seeded at the entrance of

the channels, and they spontaneously migrate inside. The microchannel limits the direction of migration to a single dimension (Faure-André et al., 2008). They provide an optimized model to evaluate the effect of physical constraints on mDC speed and cellular organization, independently of the effect of cell branching, which may also affect mDC migration in dense extracellular matrices.

1. Devices for live-cell imaging

The device that I mainly used during my Ph.D. is composed of six microchannel arrays distributed on each side of 3 wells allowing cell loading. In each zone, the microchannels have a specific width of 3, 4, 5, 6, 7, or 8µm, and their height is fixed at 4µm (Fig.20 A). This device allows us to evaluate mDCs migration in different confinement levels. In the largest microchannel of this assay (8x4µm), mDCs shape is already constrained in the X and Z-dimensions. Mature DCs lengthen with the microchannels shrinkage: from 50µm mean cell length in the 8x4 microchannels to 80µm in the 3x4 microchannels (Fig.20 B and C). The average projected cell surface area is preserved in the different microchannels (Fig.20 D). However, the projected area is measured from the LifeAct signal and does not allow accurate assessment cell volume changes since the front protrusion does not fill the channels (Fig.20 A).

The reduction in the width of the microchannel also affects the nuclear shape. It looks like a folded bean in the 8x4 microchannel while it elongated without folds in the 3x4 microchannel (Fig.20 B). This change in shape is characterized by an increase in the nucleus major axis length, aspect ratio, and solidity with the microchannel narrowing, while the projected area remains constant (Fig.20 E). The nuclear shape may fluctuate in the 8x4 microchannel, whereas it is constrained by the geometry of the 3x4 microchannel.

This device allows us to evaluate the effect of different levels of cell and nucleus confinement on migration mechanisms. The impact of nuclear squeezing is particularly interesting to study as it is described as the main mechanically resistive organelle.

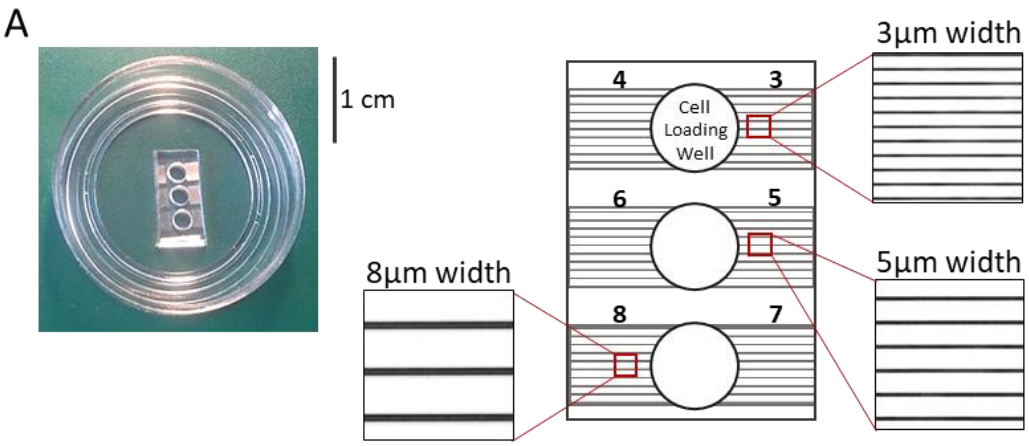
A
1 cm
3µm width
8µm width
5µm width
Cell Loading Well
4
3
6
5
8
7

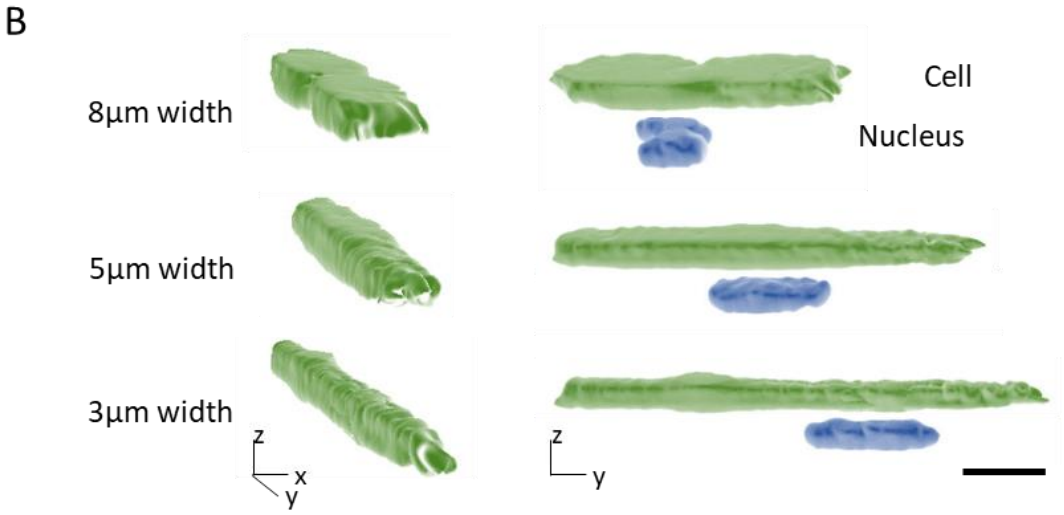
B
8µm width
5µm width
3µm width
Cell
Nucleus
z
x
y
z
y

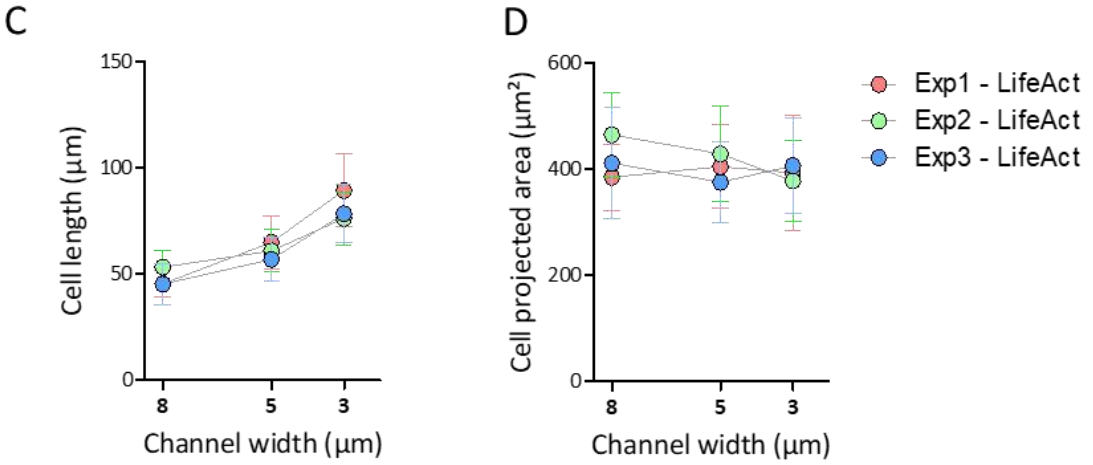
C
Cell length (µm)
150
100
50
0
8
5
3
Channel width (µm)
D
Cell projected area (µm²)
600
400
200
0
8
5
3
Channel width (µm)
Exp1 - LifeAct
Exp2 - LifeAct
Exp3 - LifeAct

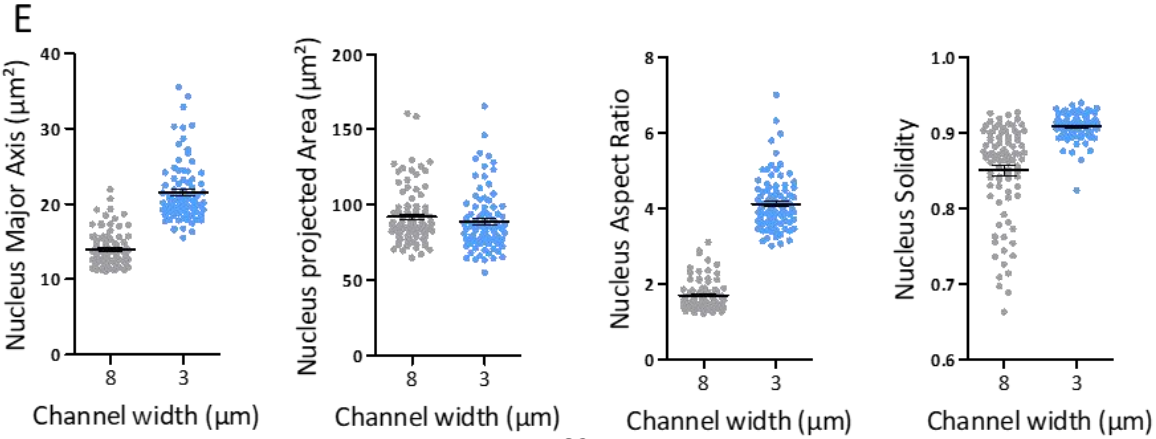
E
Nucleus Major Axis (µm²)
40
30
20
10
0
8
3
Channel width (µm)
Nucleus projected Area (µm²)
200
150
100
50
0
8
3
Channel width (µm)
Nucleus Aspect Ratio
8
6
4
2
0
8
3
Channel width (µm)
Nucleus Solidity
1.0
0.9
0.8
0.7
0.6
8
3
Channel width (µm)

Figure 20 Physical constraints imposed by microchannels of different sizes

(A) Image (left) and schematic representation (right) of a microfabricated device with channels of different sizes. The numbers indicate the width of the microchannels in the area below. Inserts show phase contrast images of areas with the 8 × 4 µm, 5 × 4 µm, and 3 × 4 µm microchannels. **(B)** Perspective views of a three-dimensional iso-surface reconstruction from z-stack spinning disk images (63×; 0.2 µm z-step) of LifeAct-mDCs migrating inside the 8 × 4 µm, 5 × 4 µm, and 3 × 4 µm microchannels. Nucleus 3D iso-surface is obtained using the Hoechst signal. Scale bar = 10 µm. **(C-D)** Quantification of cell length **(C)** or cell projected area **(D)** from LifeAct signal of mDCs migrating inside the 8 × 4 µm, 5 × 4 µm, and 3 × 4 µm microchannels. Each dot and error bar represent the mean and standard deviation (SD), respectively, of one independent experiment. **(E)** Quantification of the nuclear shape indexes from Hoechst signal in mDCs migrating in the 8 × 4 µm and 3 × 4 µm microchannels. Each dot represents the value for one cell, the line and the error bar correspond to the mean and the standard error of the mean (SEM), respectively. Data were pooled from two independent experiments.

2. Microscopic set-up and image analysis

Migrating cells were recorded for 8 to 16 h, with one image taken every 2 or 3 min. Recording began 2 h after the cells were seeded in the loading well, to allow the first cells to enter the microchannels. LifeAct cells were recorded using a DMi8 inverted microscope (Leica) and a 20× dry objective (NA 0.75). MyoII-GFP cells were recorded on a spinning disk confocal CSU X1 inverted microscope (Leica) and a 20× dry objective (NA 0.75) because the cytoplasmic signal is too high to distinguish the MyoII structures on a standard microscope.

After reconstruction, image sequences of isolated cells migrating in a single direction were extracted from the video recordings to allow single cell quantification of the parameters of interest. If a cell changed directions, only the image sequence preceding the first turning event was taken into account. Sequences of less than 20 min were excluded from the analysis (Fig.21 A). Following cell isolation, a mask was made for the different fluorescent signals recorded. Triangle, Li, Yen, or Otsu thresholding methods were used depending on the signal-to-noise ratio. The same thresholding method was used for all conditions in a single experiment. Single-cell image sequences and masks were automatically extracted from the video recording using a custom program and manually verified. Then, parameters to quantify the cell speed and shape and the LifeAct or MyoII-

GFP signal were extracted using custom ImageJ macros (Fig.21 B).

Cell speed at a given time t is defined as the cell geometric center position at time t+1 minus the cell geometric center position at time t divided by the time interval of the image sequence.

To quantify the LifeAct or MyoII-GFP signal distribution in the cells, we used signal density maps and quantification of signal accumulation in the regions of interest (ROIs). we used an already established ImageJ macro to produce the density maps (Vargas et al., 2016). In brief, the density map of each cell was obtained by averaging the projection of all images of an individual cell after normalizing the size and signal. Then, the behavior of the population was obtained by the average projection of all the individual density maps (Fig.22 A). The signal accumulation in an ROI is defined as the average signal intensity in the ROI normalized by the average signal intensity in the entire cell (Fig.22 B).

All parameters were measured on each image of an individual cell and then averaged to obtain one value per cell. The mean value for the population and errors were calculated for each independent experiment and plotted using GraphPad-Prism software. Microchannel arrays enable the analysis of at least 20 isolated cells per condition per experiment, allowing for a robust comparison of the populations. The number of cells analyzed is indicated when it was less than 20 (Fig.21 B-C-D).

Figure 21 Overview of the image analysis workflow and an example of cell length quantification .

(A) Image of the entire field of view obtained after the reconstruction of a video film recorded in the 8 × 4 µm microchannel area. The image shows an overlay of the LifeAct signal in green, the Hoechst signal in blue, and phase contrast. **(B)** Example of a single-cell image sequence and mask automatically extracted from the film. The image shows an overlay of the LifeAct signal in green and the Hoechst signal in grey. Cell length was measured using ImageJ on each frame of the sequence and then averaged to obtain a mean value per cell**. (C)** The average cell length (line) for the population and standard error (error bar) were calculated for each channel width in three independent experiments using GraphPad-Prism software. Microchannel arrays allow the analysis of at least 20 isolated cells per channel width per experiment. Each dot represents a cell value. **(D)** The mean cell length (point) and the standard error (error bar) of each independent experiment are plotted on the same graph. This is the typical design of the graphs used *in the results chapter.* Each dot and error bar represent the mean and the standard deviation, respectively, of one independent experiment.

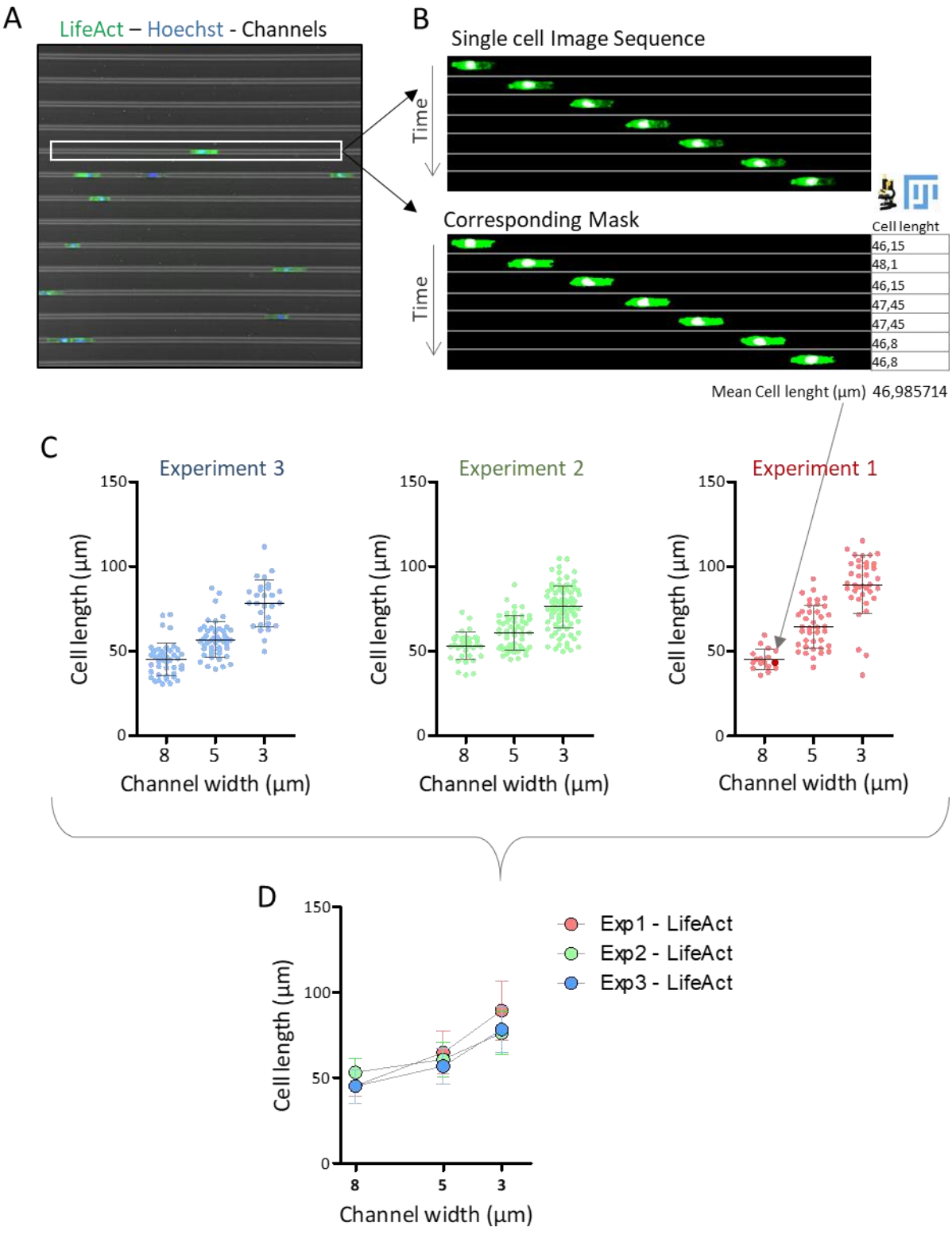
A
LifeAct – Hoechst - Channels
B
Single cell Image Sequence
Time
Corresponding Mask
Time
Cell lenght
46,15
48,1
46,15
47,45
47,45
46,8
46,8
Mean Cell lenght (µm) 46,985714
C
Experiment 3
Experiment 2
Experiment 1
Cell length (µm)
150
100
50
0
8
5
3
Channel width (µm)
D
Exp1 - LifeAct
Exp2 - LifeAct
Exp3 - LifeAct
Cell length (µm)
Channel width (µm)

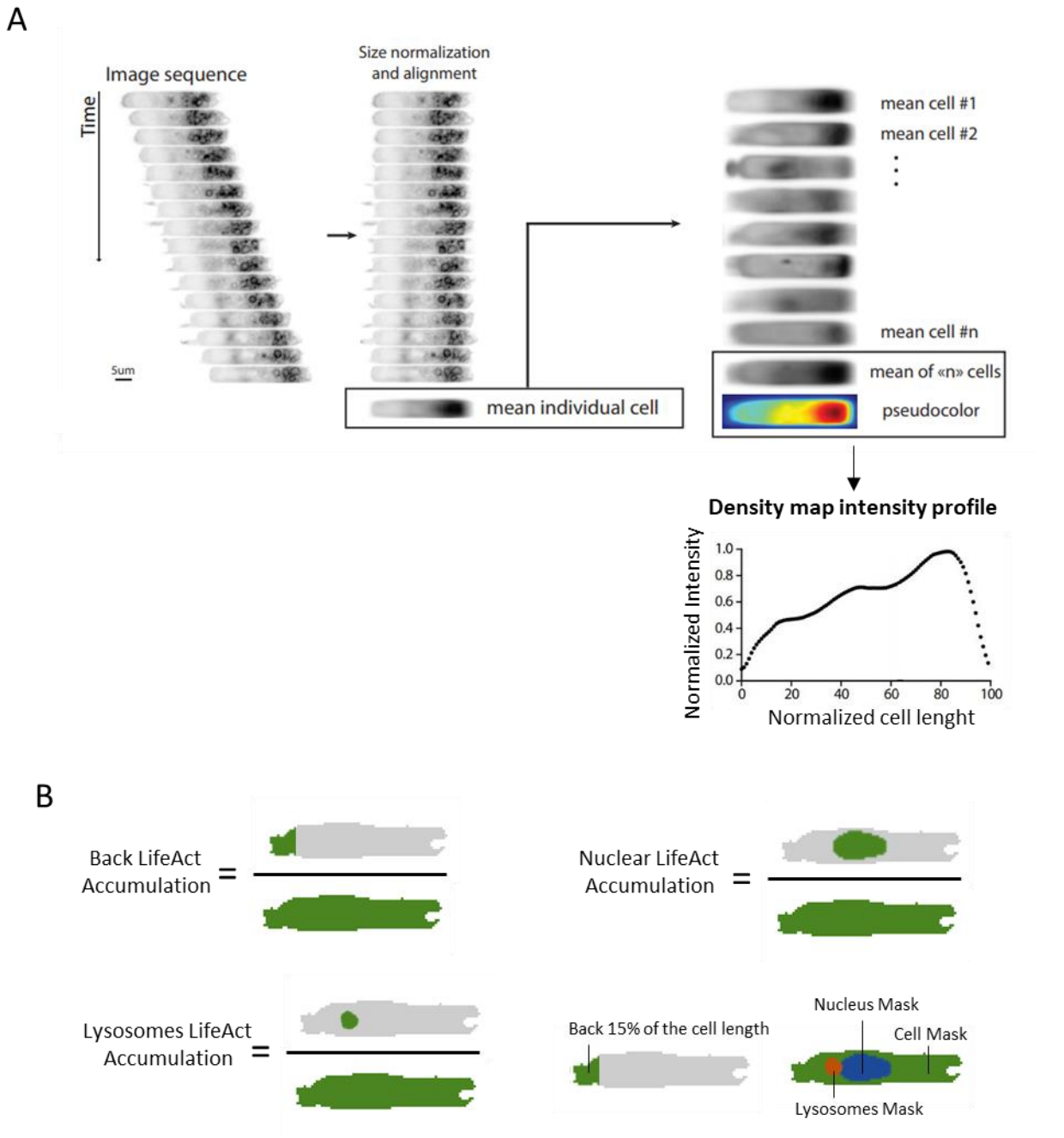

Figure 22 Quantitative method to analyze the organization of the LifeAct or MyoII-GFP signal in cells

(A) Method used to obtain a density map. An average signal map was first made for each cell. Then, the population behavior was obtained by projecting the average of all individual mean cells. The intensity profile of the density map was measured using ImageJ. The integrated intensity signal and the cell length were normalized to allow comparison between different conditions. Adapted from Vargas *et al.*, 2016. **(B)** Signal accumulation in a region of interest (ROI) is defined as the average signal intensity in the ROI normalized by the average signal intensity in the entire cell. The ROIs were defined as the back 15% of the cell length, nuclear and lysosomal mask.

3. Device developed for immunofluorescence staining of cells

Live cell analysis helps to establish a correlation between cell organization and migration parameters. However, the number of cytoskeletal components and cell compartments that can be investigated is limited by the need for a live fluorescent probe or transgenic mice expressing fluorescent proteins. To gain access to a wide range of structures, we optimized a device that facilitates immunofluorescence (IF) staining of cells fixed within the microchannels. The main limitation is the low diffusion rate of solutions inside the channels. Previous IF protocols established in the laboratory require the removal of the PDMS chamber after cell fixation to allow staining with antibodies. However, this step detaches and deforms many cells, and the yield is very low. Therefore, we developed a device that allows cell fixation and IF staining inside the PDMS chamber. The limitation of low diffusion rates was overcome by using microchannels only 100 µm in length distributed around a large channel (> 50 × 100 µm), which facilitates rapid exchange between different solutions (Fig.23).

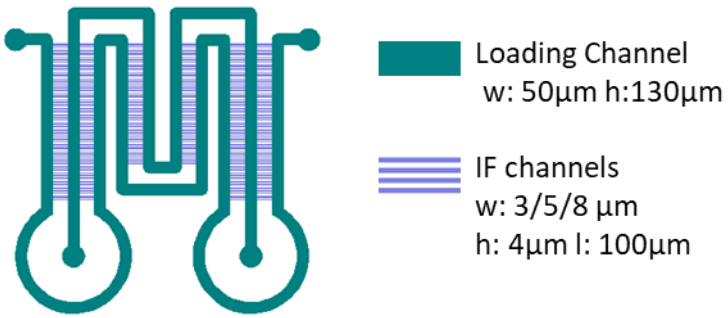

Figure 23 Diagram of the microfabricated device used to perform immunofluorescence staining within microchannels

W: width, h: height, l: length

In brief, cells were allowed to migrate within the microchannels for 4 h. Then, the medium was exchanged with a fixing solution (4% paraformaldehyde in phosphate-buffered saline [PBS]). Rapid exchange is crucial for preserving the cell membrane structure. After three washes, the chamber was incubated with the antibodies in PBS with 2% bovine serum albumin and 0.02% saponin overnight at 4°C for primary antibodies and 2 h at room temperature for secondary antibodies. The limitation of this protocol is antibody absorption by PDMS; however, optimization of the surface coating may reduce this effect. In addition, experiments to control the homogeneous diffusion of the antibodies over the entire cell length have not yet been performed. Therefore, we used this device to characterize the structural organization of cell components, but we removed the

PDMS chamber for the quantification of signal intensity.

C. Mature DCs migration in microchannels of varying dimensions

1. Design of the microfabricated devices

To study the dynamic adaptation of mDC migration at different degrees of confinement, we designed channels with varying widths. The microchannels impose a directional movement and thus guide the cell to the obstacle. When the constrictions are shorter than the cell length, they induce local deformation; this type of constrictions have already been used in the laboratory to study the nuclear mechanics of iDCs (Thiam et al., 2016). On the other hand, when the constrictions are longer than the cell length, they impose a global deformation and thus facilitate the study of cell deformation and adaptation to increasing confinement.

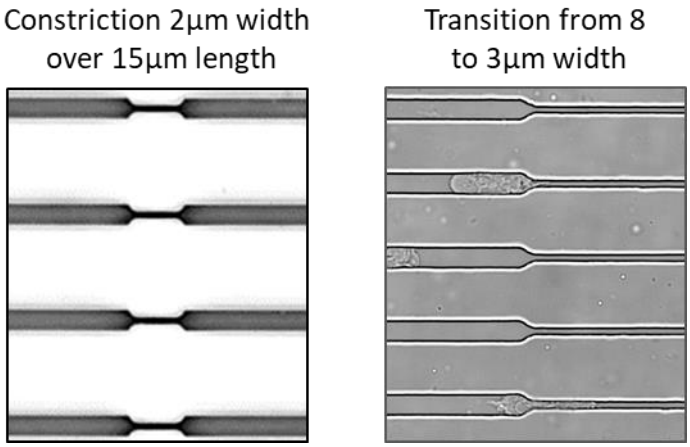

Figure 24 Example of devices with constrictions in the microchannels

(Left) Phase contrast image of 8µm wide channels with short constrictions. (Right) Bright background image of microchannels with widths ranging from 8 to 3 µm.

2. Microscopic set-up and image analysis

The purpose of this device is to understand the evolution of the migration parameters and the cytoskeletal organization when cells pass through the constriction. Thus, the analysis differs from straight microchannels mainly in the following aspects: (i) the temporal resolution is higher, with an image taken every 30 s, and (ii) the parameters measured are not averaged per cell but as a function of the distance to the constriction.

After extracting the image sequence from the video recording, different parameters were measured for each cell and plotted as a function of the cell distance from the constriction (Fig.25 A and B). Direct averaging over the cell population would give more weight to slow-moving cells as they appear more times over the channel length. To overcome this bias, I performed a data binning so that, for each cell, one data point is obtained in each bin. If, in the image sequence, the cell does not appear in a bin (fast-moving cell), the value is extrapolated as the average of the previous and the next bin. If the cell appears more than once (slow-moving cell), the data points are replaced by the average (Fig.25 C). The values are then averaged to obtain the mean behavior of the cell population during the passage through the constriction (Fig.25 D). In the present analysis, a bin represents a 10 μm interval.

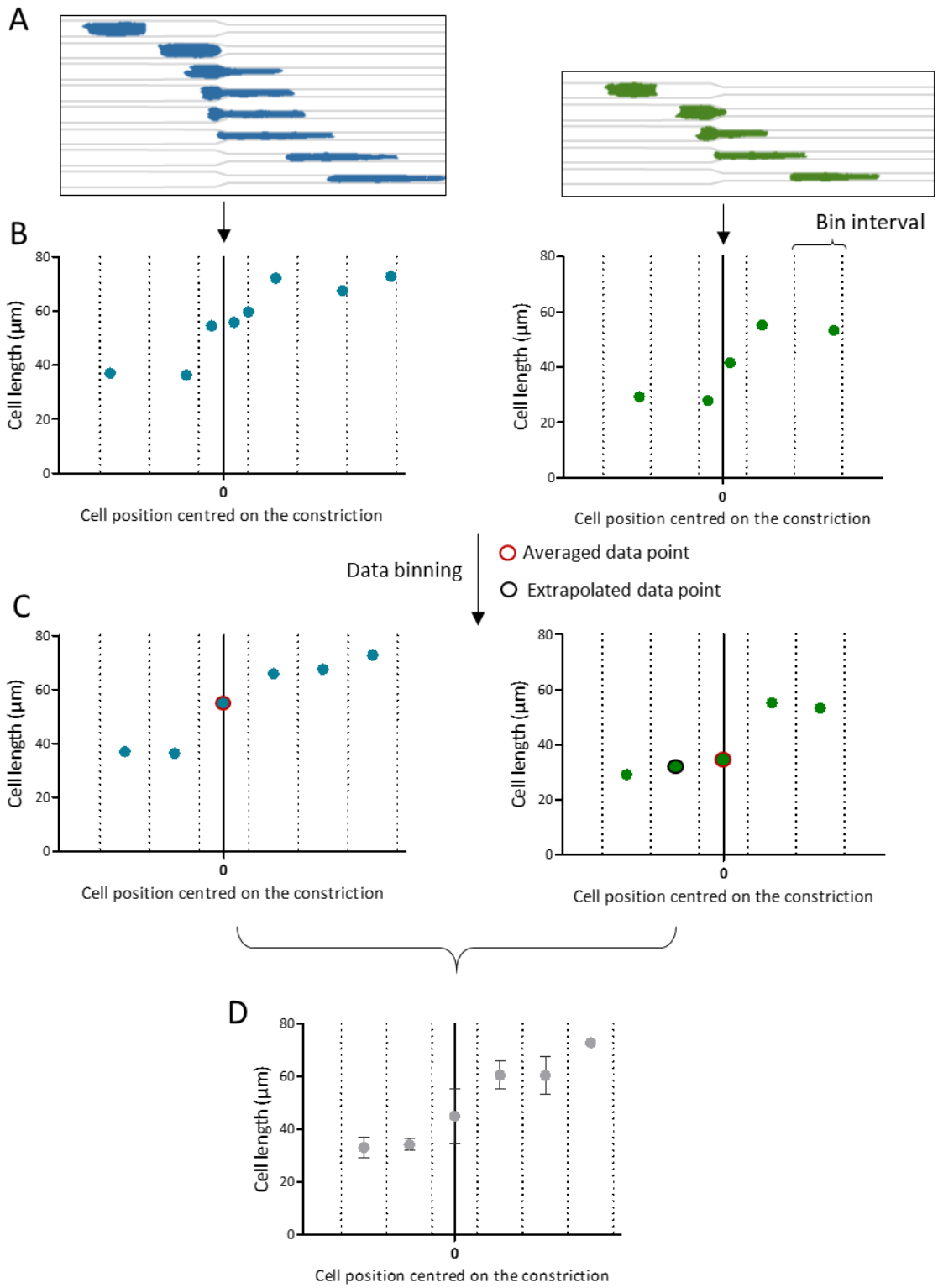

Figure 25 Overview of the data processing workflow applied to analyze cell migration through constrictions

(A) Simplified example: a slow-moving (left: blue) or fast-moving (right: green) cell mask extract from the video recording (the entire image sequence is not shown here). **(B)** The cell length is measured according to the distance between the cell center and the constriction. **(C)** Data binning is performed on each cell to obtain one data point per bin. **(D)** Cell length measurements are averaged over the cell population after binning.

D.Arrays of pillars combining cell constraints and branching

Microchannels are powerful tools for studying the effect of physical constraints on mDC migration mechanisms. However, they do not summarize the full complexity of the interstitial space, in particular its porous structure, which requires cell branching coordination. To mimic this aspect in combination with confinement, we designed a series of devices composed of arrays of hexagonal or circular pillars with a specific spacing of 2, 4, 6, or 8 µm. Hexagonal pillars form an array of bifurcated channels with uniform widths, whereas circular pillars lead to width variations in the network. They are also compatible with the generation of chemokine gradients and are used by other team members to study the effect of confinement on guided migration of mDCs (Fig.26).

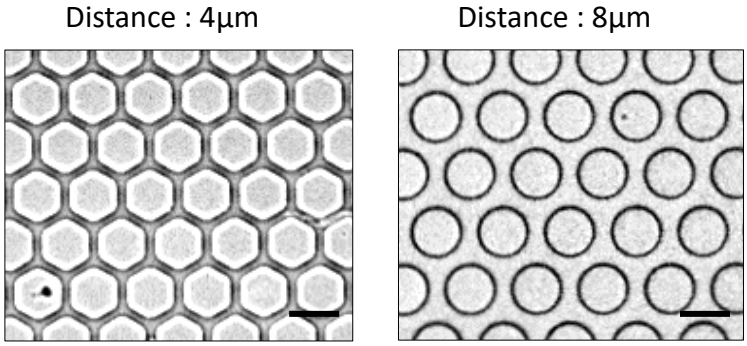

Figure 26 Examples of microfabricated devices with pillar networks

Bright-field images of hexagonal (left) and circular (right) pillar arrays. They form branched channels of uniform (left) and variable (right) widths, respectively. The pillar diameter is 20 µm (graduated bar); different devices have been designed with a spacing of 2 to 8 µm for each pillar shape.

III. From microfabricated devices to ex-vivo tissue explants

Ex-vivo tissue explants provide an opportunity to perform a physiological assay to study mDC migration in the interstitial space. This approach is more versatile than intravital imaging because tissue dissection allows the staining of different extracellular molecules and cell types. However, it can alter tissue structure and trigger inflammation due to cell damage. In the present study, we employed this assay to confirm the importance of the migration mechanism studied using the microfabricated devices.

A. Mature DC migration assay in mouse ear explant

We used mouse ear skin as a tissue model, following a well-established protocol (Weber and Sixt, 2013). In the mouse ear skin explant, the CCL21 gradient secreted by lymphatic endothelial cells is conserved, and exogenous mDCs show a directed migration to the lymphatic vessels (Weber et al., 2013). In brief, the ear skin was dissected to expose the inner part of the dermis. Lymphatic endothelial cells were stained with fluorescently labeled primary antibodies against the LYVE-1 molecule. Exogenous fluorescently labeled mDCs were incubated on the open explant. After 1 hour incubation, cells that have not crawled in were removed by gentle washes. The ear was then either mounted on a fluorodish for live imaging on a spinning disk confocal CSU X1 inverted microscope (Leica) and a 20× dry objective (NA 0.75) or fixed to simply assess the number of mDCs inside and outside the lymphatic vessels as an end-point assay (Fig.27).

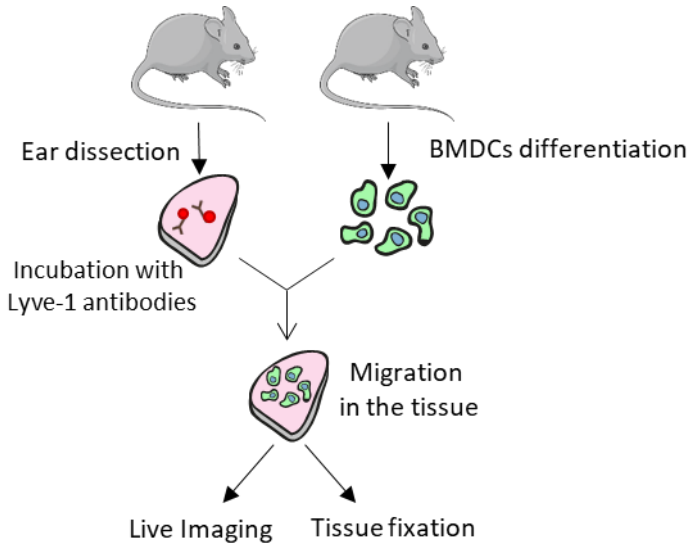

Figure 27 Overview of the mature dendritic cell (mDC) migration assay protocol in mouse ear explant.

Exogenous labelled mDCs are incubated on a pre-stained mouse ear sheet. This protocol allows the live imaging of mDCs migrating into the interstitial space of the skin or an end-point assay after tissue fixation.

B. A simple method to image tissue collagen structures without second harmonic generation

As a last point in the section on methods, I developed a protocol for staining collagen structures in skin explants. Indeed, fibrillar structures are usually visualized by second harmonic generation. However, this method was not feasible on the spinning disk confocal microscope

available in the laboratory. I used SureCoat bovine collagen type I (Advanced BioMatrix) as this collagen solution is optimized for surface coating but not for gel formation. Thus, SureCoat collagen molecules can bind to the tissue collagen matrix without forming de novo structures. Mouse ear sheets were stained with fluorescently labeled SureCoat, and the collagen network in the skin was observed. The collagen network was characterized by a high heterogeneity with dense wavy collagen bundles and loose reticulated areas (Fig.28) Therefore, visualization of the collagen network is crucial to study mDC migration at different degrees of confinement in tissue models

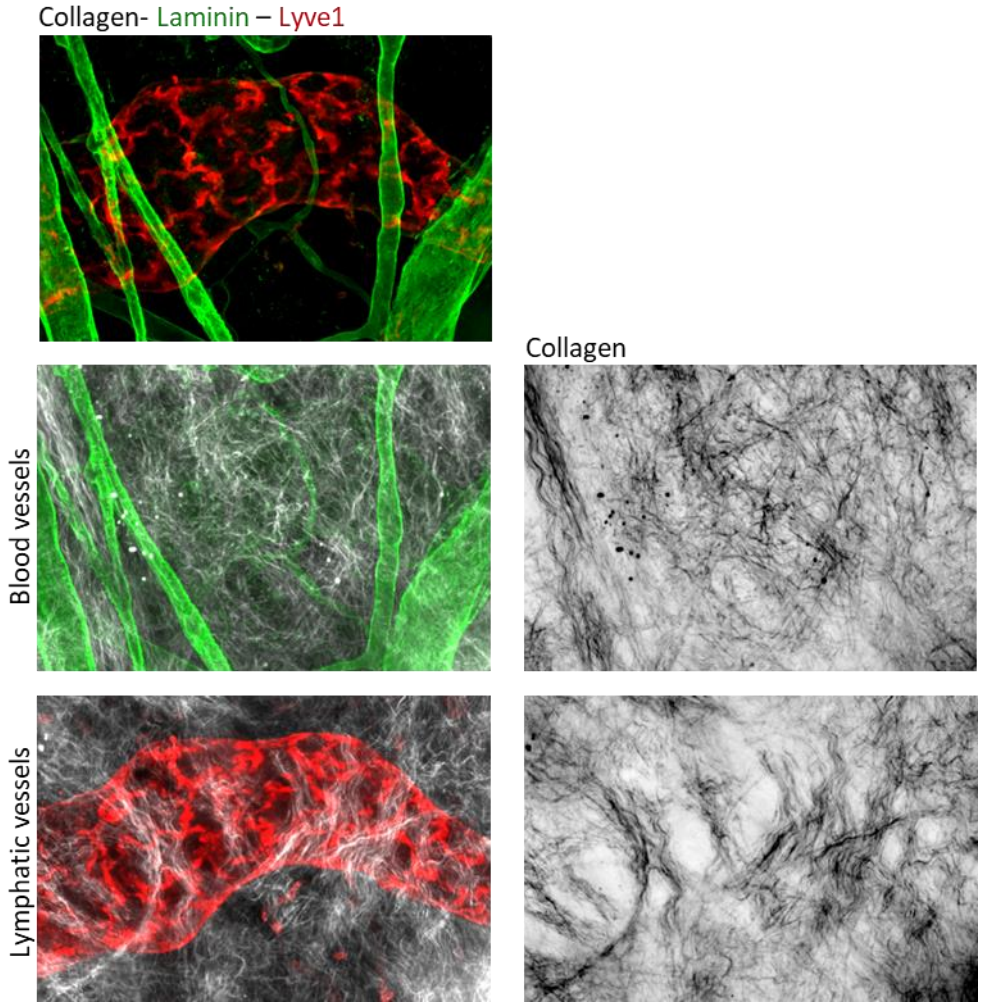

Figure 28 Collagen staining in a mouse ear explant with fluorescently labelled SureCoat collagen

Immunofluorescence staining of collagen (grey), blood vessels (green, anti-laminin antibody), and lymphatic vessels (red, anti-LYVE-1 antibody) in the interstitial space. The collagen matrix surrounding the vessels has a variable structure and density with wavy collagen bundles and loose reticulated areas.

RESULTS

I include at the beginning of this chapter a first-authored article published in 2019. It presents a detailed analysis of mDCs migration in microchannels of different sizes and MyoII requirements according to the degrees of confinement. In brief, we show that MyoII activity, which is increased during DCs activation, is necessary for mDCs migration to lymphatic vessels in the interstitial space. Using collagen gels, we confirmed that this defect is due to a decrease in mDC migration capacity but not to chemokines sensing. As previously demonstrated (Lämmermann et al., 2008), MyoII inhibited-cells still show residual movement in the collagen matrix, suggesting that it could affect a specific step of mDCs migration in complex environments. Thus, we used microchannels of different dimensions to accurately characterize the role of MyoII-dependent contractility in mDCs movement and deformation. Despite strong deformation, mDCs speed is only slightly influenced by the microchannel sizes. In addition, MyoII-dependent contractility is specifically critical for mDC movement in confined areas. Indeed, the effect of MyoII inhibition on cell speed and deformation increases with the narrowing of the microchannels and constrictions. It has a strong impact on cell movement in 3x4µm microchannels and on the cell passage through constrictions less than 2µm wide.

This work reveals the high plasticity of mDC migration. It is only slightly affected by confinement, and MyoII-activity might be dispensable in unrestricted spaces. However, extreme confinement requires a specific migration mechanism based on cell contractility. This raises the question of whether there is an adaptation of mDCs migration mechanisms to confinement and whether there is a mechano-response in these cells. Following this publication, I continued my work to answer these questions. The results of this complementary study are presented following the article.

I. Myosin II activity is selectively needed for migration in highly confined microenvironments in mature dendritic cells

Original Research Article
Front. Immunol., 12 April 2019 | https://doi.org/10.3389/fimmu.2019.00747

Running title: Requirements for cell migration under strong confinement

Lucie Barbier[1,2,3], Pablo J Sáez[1,2], Rafaele Attia[1,2], Ana-Maria Lennon[4], Ido Lavi[1,2], Matthieu Piel[1,2] and Pablo Vargas[1,2,*]

[1]Institut Curie, PSL Research University, CNRS, UMR 144, F-75005, Paris, France.

[2]Institut Pierre-Gilles de Gennes, PSL Research University, F-75005 Paris, France

[3]Université Paris Sud, Université Paris-Saclay, F-91405 Orsay, France

[4]Institut Curie, PSL Research University, INSERM U932, F-75005, Paris, France.

* Correspondence: Pablo Vargas: pablo.vargas@curie.fr

Keywords: cell migration, dendritic cell, confinement, myosin II, contractility, microfabrication, microfluidics, chemotaxis

Abstract

Upon infection, mature dendritic cells (mDCs) migrate from peripheral tissue to lymph nodes (LNs) to activate T lymphocytes and initiate the adaptive immune response. This fast and tightly regulated process is tuned by different microenvironmental factors, such as the physical properties of the tissue. Mechanistically, mDCs migration mostly relies on acto-myosin flow and contractility that depend on non-muscular Myosin IIA (MyoII) activity. However, the specific contribution of this molecular motor for mDCs navigation in complex microenvironments has yet to be fully established. Here, we identified a specific role of MyoII activity in the regulation of mDCs migration in highly confined microenvironments. Using microfluidic systems, we observed that during mDCs chemotaxis in 3D collagen gels under defined CCL21 gradients, MyoII activity was required to sustain their fast speed but not to orientate them toward the chemokine. Indeed, despite the fact that mDCs speed declined, these cells still migrated through the 3D gels, indicating that this molecular motor has a discrete function during their motility in this irregular microenvironment. Consistently, using microchannels of different sizes, we found that MyoII activity was essential to maintain fast cell speed specifically under strong confinement. Analysis of cell motility through micrometric holes

further demonstrated that cell contractility facilitated mDCs passage only over very small gaps. Altogether, this work highlights that high contractility acts as an adaptation mechanism exhibited by mDCs to optimize their motility in restricted landscapes. Hence, MyoII activity ultimately facilitates their navigation in highly confined areas of structurally irregular tissues, contributing to the fine-tuning of their homing to LNs to initiate adaptive immune responses.

Introduction

Antigen delivery from peripheral tissues to LNs by mDCs is critical to initiate the adaptive immune response (1). To ensure its adequacy, this antigen transport needs to occur within a few hours. Consequently, DCs migration to LNs is boosted by signals that trigger their activation, such as pathogen-associated and damage-associated molecular patterns (PAMPs and DAMPs, respectively) (2–5). In this context, we have recently shown that DCs activation leads to a fast and persistent mode of migration, which is linked to the concentration of the acto-myosin cytoskeleton at the cell rear (4–6). MyoII activity generates the force required for mDCs migration in 3D confined microenvironments (7) and is needed for fast and persistent motility during chemotaxis in a dense extracellular matrix (4). Accordingly, failure in inducing MyoII activity is sufficient to delay mDCs homing to draining LNs, with important consequences in the development of immune responses (8).

Importantly, during navigation from the infected tissue to the draining LN, mDCs need to adapt their morphology to the evolving geometrical properties of their microenvironment (9). Recently, several articles have evidenced that distinct cell types increase their MyoII-dependent contractility to migrate in confined microenvironments (10–13). In mesenchymal cells, we have shown that combination of high confinement and low adhesion result in MyoII-dependent fast cell motility in vitro (13). In analogy to this observation, fully mature DCs are intrinsically non-adhesive in vitro and do not require specific adhesions to migrate in dense 3D microenvironments in vivo (7). However, how MyoII activity regulates mDCs motility in response to the degree of confinement remains unexplored.

Here, we combined the use of ex vivo imaging and precise in vitro microfabricated tools to demonstrate that MyoII activity is important to sustain efficient mDCs navigation exclusively in highly confined microenvironments. Since migratory mDCs possess a high basal level of MyoII activity (6), we propose that this property allows them to adapt their motility to irregular microenvironments found in different tissue compartments. This property might be key to bypass natural physical obstacles in

order to reach efficiently the draining LN, ensuring the prompt initiation of the adaptive immune response.

Inhibition of cell contractility reduces mDCs migration speed in a dense extracellular matrix

To assess the contribution of MyoII to cell migration in a complex microenvironment, we first used an ex vivo model tissue. For that, we evaluated the capacity of exogenous mDCs to reach the LVs in mouse ear explants (4, 14). Briefly, in vitro differentiated bone marrow-derived DCs were activated with bacterial lipopolysaccharide (LPS), labeled and seeded in the dermal side of open ear explants either in the absence or presence of the MyoII inhibitor Blebbistatin (**Figure 1A**). After one hour of migration, the tissue was fixed and imaged to quantify the number of mDCs that reached the LVs (**Figure 1B**). Control cells were mostly observed near the lymphatic system or overlapping it, reflecting their strong capacity to migrate towards the LVs. Conversely, in the presence of Blebbistatin, the localization of mDCs was mainly restricted to the area surrounding the LVs (**Figure 1B**). Accordingly, the ratio of mDCs overlapping the LVs over those remaining in the interstitial space decreased upon MyoII inhibition (**Figure 1C**). Importantly, these differences were not due to changes in the expression of CCR7, chemokine receptor responsible for driving mDCs migration towards the lymphatic system (**Figure 1D**). Altogether, these data indicate that MyoII activity is required for the migration of mDCs from the interstitial space towards the LVs in the confined microenvironment of this model tissue.

One limit of this experimental setup is that migration of mDCs in both, the absence or presence of Blebbistatin, cannot be evaluated in the exact same tissue. In addition, despite the short duration of the experiment, the drug might have adverse effects on the tissue itself. Thus, we decided to confirm this result by evaluating the capacity of MyoII conditional knock-out mice mDCs to reach the LVs ex vivo (15). For that, exogenous mDCs derived from MyoII-flox/flox/CD11c-Cre- (WT) and MyoII-flox/flox/CD11c-Cre+ (KO) mice were differentially labeled, mixed 50%-50% and seeded in the dermal side of the open ear explants (**Sup. Figure 1A and 1B**). In our *in vitro* cultures, we observed a reduction by half in the total amount of MyoII, as measured by western blot (**Sup. Figure 1C**). However, this drop was sufficient to reduce significantly the number of mDCs reaching the LVs (**Sup. Figure 1D**).

Altogether, these results indicate that MyoII activity is needed for the proper migration of mDCs in ear explants, and a partial decrease in the protein abundance is enough to impair their arrival at LVs, highlighting the relevance of this molecule for mDCs migration in tissues.

Based on these observations, we hypothesized that the decreased mDCs arrival at the lymphatic system might be due to a) reduced directional migration towards CCL21, the chemokine that guides mDCs toward the lymphatic vessels (14) and/or to b) a diminished efficiency of mDCs to migrate in the dense extracellular matrix. To test these hypothesis, we used an in vitro chemotactic assay in which we assessed the capacity of mDCs to follow a gradient of CCL21 in a dense 3D collagen gel (7,16). Since MyoII depletion was incomplete in the KO mice, we decided to restrict our experiments to different small inhibitors of this molecular motor. In the control condition, mDCs migrated directionally towards CCL21 (**Figure 1E**), while in areas of the same gel that were not exposed to the chemokine, their motility remained random (**Figure 1E**). In Blebbistatin-treated mDCs, directionality towards the chemokine was not affected (**Figure 1E, Sup. Figure 1E and Sup. Movie 1**) while cell speed was markedly reduced (**Figure 1F**). Slower cell migration was also observed during random motility, indicating that MyoII activity is required for fast cell migration in the 3D extracellular matrix, but is dispensable for sensing or orientation of mDCs towards CCL21 (**Sup. Figure 1F**). Similar results were obtained from inhibiting the rho-activated kinase (ROCK) using Y27632 (Y27), which also leads to decreased MyoII activity (**Figure 1E, 1F and Sup. Figure 1F**). These results indicate that MyoII inhibition causes a strong decrease in mDCs migration in 3D microenvironments.

Myosin II is required for mDCs migration in highly confined microenvironments

A striking property of 3D collagen gels is the geometrical irregularity imposed to cells, which forces them to transit through zones of variable confinement. Interestingly, inhibition of MyoII activity in mDCs reduces their migration speed in the 3D gel, but without stopping completely their movement (**Sup. Movie 1**). Based on this observation, we hypothesized that MyoII activity could influence specific steps of mDCs motility depending on the degree of confinement encountered in irregular 3D landscapes.

To test this idea, we took advantage of the precise and diverse geometries that can be generated by using microfabrication (17,18). With this technology, we designed microchannels of different sizes (8, 5 or 3 µm width by 4 µm height) to challenge cells to migrate in microenvironments with increasing degrees of confinement (**Figure 2A**). First, we observed that mDCs were able to migrate

spontaneously independently of the degree of confinement. Strikingly, despite a strong effect on the cell shape due to the confinement in small microchannels (i.e 3 µm) (**Figure 2B**), mDCs speed was only slightly reduced in these tubes (**Figure 2C and Sup. Figure 2A**). This suggests that mDCs activate a specific cellular machinery to maintain efficient migration in very confined geometries. Surprisingly, mDCs treatment with Blebbistatin did not significantly affect their speeds in larger channels (i.e 8 µm) (**Figure 2C, Sup. Figure 2A**), but decreased them only under higher confinement (30% and 50% speed reduction in 5 and 3 µm channels, respectively) (**Figure 2C, Sup. Figure 2A**). Similar results were obtained from using the ROCK inhibitor Y27, indicative of the phenotype robustness (**Sup. Figure 2B)**. For us, the simplest interpretation of this result is that large channels impose little resistance to migration, and thus the force provided by MyoII is not needed. In contrast, MyoII becomes critical to maintain cell speed in small channels, which impose more resistance to their motility. These results suggest that mDCs regulate MyoII activity depending on the degree of confinement.

MyoII activity is required for mDCs passage through small gaps

The constant confinement provided by straight microchannels does not recapitulates the complex geometry of dense extracellular matrices, which display multiple irregularities (19). Thus, we decided to study mDCs migration in microchannels coupled to micrometric constrictions, to evaluate the precise contribution of MyoII activity to migration through an irregular landscape (Figure 2D) (9,16). For that, we used 8 µm width microchannels and added constrictions of different sizes, ranging from 4 µm to 1.5 µm width, over 15 µm length (**Figure 2D**) (9). Since in these channels MyoII inhibition does not affect cell speed (**Figure 2B and Sup. Figure 2A**), this system allowed us to evaluate the specific role of cell contractility in the passage of mDCs through small pores (**Figure 2E**). First, we evaluated the percentage of cells effectively passing through the different constrictions (**Figure 2F**). Our experiments showed that in control cells, more than 80% of the mDCs passed through 4 µm and 3 µm width constrictions, while 60 % and 40 % of them were able to overcome 2 µm and 1.5 µm pores, respectively (**Figure 2F**). No significant effect was observed on the fraction of cells migrating through 4 µm width constrictions upon MyoII inhibition with Blebbistatin (**Figure 2F**). However, the drug impact intensified progressively with the constriction narrowing, ending up with a 75% inhibition of the passage through the smallest pores (1.5 µm width) (**Figure 2F**). A similar effect was induced by the ROCK inhibitor Y27 (**Sup. Figure 2C**). Altogether, these data indicate that MyoII activity in mDCs is needed exclusively to pass through narrow gaps smaller than 3 µm in width.

Next, as an indicator of the cell efficiency in deforming and passing through the small gaps, we calculated the time spent by each cell inside a constriction, only if they succeeded to migrate through it. In the analysis, we observed that this time also increased with the pore narrowing, starting at 5 min in average for the 4 µm constriction, and ending with 10 min when moving through the 2 µm gaps (**Figure 2 G**). These observations indicate that unlike straight microchannels, the pore size of an irregular microenvironment can be determinant to restrict mDCs migration. In this setup, MyoII inhibition using blebbistatin systematically increased the time spent by mDCs in the constriction as compared to the control condition, independently of gap size (**Figure 2G, 2E and 2H**). Similarly, ROCK inhibition also doubled the passage time of cells through the constrictions for all pore sizes (**Sup. Figure 2D**). Of note, due to the low proportion of mDCs able to pass through the 1.5 µm constrictions upon MyoII inhibition, the passage time was not considered for this specific condition.

Collectively, these data indicate a dual role of MyoII activity in the migration of mDCs through small gaps: *i)* it is required for cell passage through very small holes and *ii)* to maintain cell speed while squeezing and deforming in an irregular landscape. Combined with the data obtained from collagen gels and straight microchannels, our experiments demonstrate that MyoII activity in mDCs helps them to adapt their migration to irregular and restrictive microenvironments. This suggests a specific adaptation of mDCs that ensures fast homing from infected tissues to LNs, a situation that imposes a series of physical constrains as cells translocate between distant locations in the organism.

Discussion

Migration from peripheral tissues to lymph nodes is a challenging function for mDCs, which must constantly move through different body compartments adapting to the changing properties of the tissues. Here, we found that MyoII activity in mDCs is required specifically to maintain their speed and squeeze through highly confined microenvironments. In ear explants, MyoII inhibition impaired mDCs arrival at the lymphatic system, which was not due to a defect in the detection of CCL21 gradient but rather to a defect in their intrinsic motile capacity, as measured in collagen gels. This is in agreement with data showing that cell speed can be dissociated from directionality during chemotaxis, having as consequence a decrease in the quality of cell migration in vitro and ex vivo (4,20,21). Interestingly, partial depletion of MyoII was enough to decrease cell migration of mDCs in ear explants. Recently, similar observations were obtained in neutrophils, in which partial depletion of MyoII diminished migration in confinement (36). Together with our data, these evidences indicate

that motility of mDCs and neutrophils in confinement is highly sensitive to the levels or activity of MyoII.

Interestingly, inhibition of MyoII reduces the speed, but does not fully stops cells as they migrate in a collagen gel. Cell speed during random motility and chemotaxis decreases in both cases, but cells are still able to move. Since the microenvironment in a 3D gel is irregular, this can be explained by a specific role of MyoII during migration in the more restricted areas of the gel. In agreement with this idea, recent articles have shown MyoII activation under compression (10-13).

Surprisingly, in our experiments, migration speed in large channels was not affected by MyoII inhibition. One possibility to explain this result is that MyoII is simply not required for their movement in such a microenvironment. However, in previous studies obtained by our group, we have seen that MyoII inhibition triggers a global reorganization of the actin cytoskeleton in mDCs when migrating in large channels (6). This suggests the existence of distinct modes of motility that can operate in these cells, resulting in both cases in fast migration in vitro when confinement is not strong. Interestingly, mDCs have been previously shown to adapt their motility to the adhesive properties of their microenvironment, alternating distinct modes of migration that sustain fast speed (22). Altogether, these observations indicate the existence of different types of migratory machineries in mDCs that depending on the properties of their microenvironment can compensate to ensure their migratory function.

Migration under strong confinement (small channels and constrictions) required MyoII activity. This indicates that despite the existence of different modes of motility in mDCs, extreme confinement needs a specific migratory mechanism that relies on cell contractility. This mechanism also applies for mDCs migration in dense collagen gels, showing that this need is maintained during migration in more complex landscapes (7). This adaptation is not universal, since some tumor cells and human mesenchymal stem cells have been shown to use a contractility-independent mode of motility under confinement (23,24). Interestingly, the MyoII requirement to migrate in small holes seems specific to mDCs, since we have shown that passage of immature DCs through constrictions was independent of cell contractility and required Arp2/3-mediated actin nucleation (9). These differences might result in an additional level of control for the migration of mDCs, in which the regulation of MyoII contractility by inflammatory or environmental factors might participate in the fine tuning of

their migration to LNs. This MyoII-dependency might be a global requirement for leukocyte migration between tissues, since neutrophils and T lymphocytes also require contractility to squeeze through confined landscapes (13,35).

Our study also showed that the geometry of the microenvironment has a strong impact on mDCs migration, especially in irregular spaces where the size of the pores limits mDCs passage. Thus, modification in the density of the extracellular matrix may also modulate mDCs arrival at LNs. This property can be particularly relevant during mDCs migration through distinct organs, which display intrinsic differences in their stiffness (26) or during inflammation, known to alter the physical properties of the tissue (27). The same principle can apply during cancer progression, that often alter the properties of the extracellular matrices surrounding the core of the tumor (28,29) and might prevent immune cells infiltration (30). Thus, modulation of contractility could be used as a general approach to optimize mDCs motility in pathological conditions.

Importantly, the behavior of mDCs relative to the different degrees of confinement suggests a mechano-response in these cells. However, the mechanism(s) that sense the geometry of the tissue and adapt MyoII activity remain unknown. A local control of mDCs contractility has been already reported to promote their transmigration, where MyoII activity was modulated by chemical signals from lymphatic endothelial cells (31). Also, a possible specific regulatory mechanism might come from lysosomal signaling, that we have recently shown to regulate MyoII-induced contractility at the back of mDCs (6). Understanding how MyoII activity is modulated in response to confinement might provide molecular tools to modulate cell migration through specific tissues. In particular, in inflammatory diseases such as auto-immune encephalopathies or allergic contact dermatitis, down regulation of MyoII activity prevents mDCs migration to LNs and limits inflammation (8), while in other situations, such as tumors, increasing their migration might be beneficial (32). A better understanding of the mechanisms regulating mDCs contractility under confinement can create new routes to the development of molecules to tune the adaptive immune response with therapeutic purposes.

Methods

Cells. Bone marrow derived dendritic cells (BMDCs) were obtain by differentiation of bone morrow precursors for 10 days in DCs medium (IMDM-Glutamax, FCS 10%, pen-strep 100U ml-1, and 2-ME 50 µM) supplemented with granulocyte-macrophage colony stimulating factor (GM-CSF)-containing supernatant (50 ng ml-1) obtained from transfected J558 cell line, as previously described (33). Briefly, at day 10 of differentiation, semi-adherent DCs were treated with LPS (100 ng ml-1) for 30 min, then washed 3 times with DCs medium and cultured overnight (ON) to reach full DC maturation. Migration of mDCs was recorded between 24h and 34h post LPS treatment.

Mice. BMDCs were obtained from wild-type C57BL/B6 mice (Charles River). In the case of MyoII KO, BMDCs were differentiated from MyoIIA-flox/flox-CD11c-Cre+ mice, as previously described (15,25,34). Littermate MyoIIA-flox/flox CD11c-Cre- were used as a control. In general, 6 to 10 weeks old mice were used as source for bone marrows; 4 to 6 weeks old mice were used as ear explant donors. For animal care, we strictly followed the European and French National Regulation for the Protection of Vertebrate Animals used for Experimental and other Scientific Purposes (Directive 2010/63; French Decree 2013-118). The present experiments, which used mouse strains displaying non-harmful phenotypes, did not require a project authorization and benefited from guidance of the Animal Welfare Body, Research Centre, Institut Curie.

Antibodies and reagents. For drug treatment, Blebbistatin (50µM, Tocris Bioscience) and the equivalent amount of DMSO (Sigma-Aldrich), or Y-27632 (10µM, Tocris Bioscience) and the equivalent amount of distillated water were used. For labeling of lymphatic vessels in mouse era explants, Alexa Fluor 655-coupled anti-Lyve-1 antibody was used (R&D System, 1/50). To label BMDCs for migration in ear explants we used Hoechst 33342 (200 ng ml-1, Life Technologies) and CellMask CFSE or CMTMR (2,5 µM) (Life Technologies). For western blot, Non-muscle Myosin Heavy Chain II-A Antibody (Biolegend, clone Ply19098, 1/200) and GAPDH Antibody (Cell Signaling, clone 14c10, 1/5000). For flow cytometry analysis : Mouse CCL19-Fc Fusion Recombinant Protein (1/400, eBioscience) and Alexa-Fluor 488 -coupled anti-human Fc (1/400, eBioscience)

Migration in ear explant. Migration of DCs was performed as previously described (14) but modified to work with fixed samples. Briefly, ears were excised from C57BL/6 mice and the ventral part of the

skin was peeled off to expose their dermal side. 100 000 colored LPS-activated BMDCs were added on the top of the exposed dermal side of the skin explant. After 1 h of incubation, explants were washed to remove the loosely attached mDCs and fixed during 20 min on a drop of 4 % paraformaldehyde (Sigma-Aldrich). In the case of Blebbistatin treatment, the cells were colored and pre-incubated 2h with the drug before seeding in the ear and was further maintained during migration in the explants. In the case of MyoII WT and KO mDCs, 75 000 colored LPS-MyoII KO BMDCs were mixed with 75 000 colored LPS-MyoII WT BMDCs and added on the top of the exposed dermal side of the skin explant. After fixation, the explants were washed in PBS 2%-BSA and the lymphatic vessels were stained with Alexa Fluor 655-coupled anti-Lyve-1 antibody 1 h at 4°C. After three washes, skin explants were mounted in a microscopy slide using fluoromount-G (Invitrogen) and imaged on a Spinning disk confocal CSU X1 inverted microscope (Leica) and a ×20 dry objective (NA 0.75). For Blebbistatin experiments, mDCs overlapping or not with the lymphatic system were manually count on a SUM z-projection. For MyoII-KO experiments, a custom ImageJ macro was used to count the number of nucleus corresponding to each phenotype. Briefly, a SUM z-projection was made and, using appropriated thresholding, we detected MyoII-WT and MyoII-KO nucleus. Then, using a mask obtained from the lymphatic vessels, we counted the numbers of nucleus of MyoII-WT and MyoII-KO mDCs overlapping or not with the lymphatic system. The ratio of mDCs in the lymphatic vessels was calculated as the number of nucleus in the lymphatic vessel divided by the number of nucleus outside the lymphatic vessels.

Migration in collagen gels. Collagen experiments were performed as previously described (16). Briefly, mDCs were mixed at 4°C with rat tail collagen type I (Corning) at 3 mg ml-1 at basic pH and loaded in the custom-made chamber in polydimethylsiloxane (PDMS). The sample was incubated at 37°C for 30 min to allow gel polymerization. Then, 2 ml of DC medium containing 200 ng ml-1 CCL21 (R&D Systems) was added in the dish, generating a chemokine gradient that triggered directed mDC migration. When indicated, cells were pre-incubated 1h with Blebbistatin at 50 µM or Y27632 at 10 µM, and then maintained in the media during their chemotaxis. Cells were imaged overnight with a DMi8 inverted microscope (Leica) at 37 °C with 5% CO2 atmosphere and a ×10 dry objective (NA 0.40 phase). Resulting movies were processed with average subtraction, mean filter and Gaussian Blur filter to obtain cells as white round object on a dark background. Tracking was performed with Imaris software in the first 400 µm from the border of the chamber, where the gradient is stable.

Tracks of objects moving less than 10 µm length or lasting less than 10 min were removed from the analysis to avoid artifacts.

Migration in micro-channels. Micro-channels experiments were performed as previously described (18). Briefly, PDMS (RTV615, Neyco) was used to make microchannels of the different geometries from custom-made molds. The micro-channels were coated with bovine plasma fibronectin (10 µg ml-1) (Sigma-Aldrich) for 1 h at RT and washed 3 times with PBS before incubating with DC medium for at least 1 h at 37°C and 5% CO2 before cell loading. When indicated, this media also contained 50 µM blebbistatin or 10µM Y27632. Migrating cells were recorded overnight with a DMi8 inverted microscope (Leica) at 37 °C with 5% CO2 atmosphere and a ×10 dry objective (NA 0.40 phase). One image every 2 min during 16 h was recorded.

Quantification of cell migration in micro-channels. Kymographs for each channel were generated using a semi-automated ImageJ macro. For velocity measurements, kymographs from isolated migrating cells were manually extracted and analyzed using a custom Matlab program as previously described (33). For cell passage through constrictions, kymographs from each channel were analyzed using a semi-automated ImageJ macro. We focused on the passage of the first constriction encountered by the cell. The percentage of passage represents the ratio between the number of cells that passed a constriction respect to the number of cells that encountered a constriction. The passage time represents the time between the time at which the cell front reaches the constriction and the time at which the cell back exits the constriction.

Immunoblotting. 1.5 millions of mDCs were lysed for 30 min in 40µl of lysis buffer containing 100 mM Tris, 150 mM NaCl, 0.5% NP-40 and a protease inhibitor cocktail tablet (Roche). 10µl of extracts were loaded onto a 4–20% TGX gradient gel (BioRad) and transferred onto an Ethanol-activated PVDF membrane by over-night wet transfer (BioRad). The membrane was blocked, incubated sequentially with the appropriate antibodies and revealed using the SuperSignal West Pico Chemiluminescent substrate (Thermo Scientific). Membranes were cut accordingly to the molecular weight of the protein of interest. This allowed us to evaluate different labelling in the same run. As consequence, full membranes were in most cases only fragments.

Flow cytometry analysis. 750 000 mDCs pre-incubated 2h with Blebbistaitin or DMSO as a control were resuspended in 50µl of PBS 2% BSA alone as unstained control or with Mouse CCL19-Fc Fusion Recombinant Protein. After 1h of staining at 4 °C, cells were then washed two times and incubated for 1h with Alexa Fluor 488-coupled anti-human Fc at room temperature. After two washes, cells were resuspended in 200µl of PBS 2% BSA. Single cell fluorescence were measured on a Accuri flow cytometer and analyses with FCS Express 6 software. Appropriated gating was made of SSC/FFC signal.

Acknowledgments

We thank Guilherme F.P. Nader, Mathieu Deygas, Bianca Cali and Mathilde Bernard for the critical reading of the manuscript. LB was funded by a Ph.D. fellowship from the Ministere de l'Education Nationale, de l'Enseignement Superieur et de la Recherche. This work was supported by grants from the DCBIOL Labex (ANR-10-IDEX-0001-02-PSL and ANR-11-LABX-0043) to A.M.L.-D., as well as the ANR (PhyMax), the Fondation pour la Recherche Médicale and the Institut National du Cancer to A.-M.L.-D and M.P. This work also received the support of the Association Nationale pour la Recherche (MOTILE project, ANR-16-CE13-0009) and Labex-IPGG attributed to PV as well as the support of "Institut Pierre-Gilles de Gennes" (laboratoire d'excellence, "Investissements d'avenir" program ANR-10-IDEX-0001-02 PSL and ANR-10-LABX-31.).

Author contributions

L.B. performed and analyzed most experiments, prepared manuscript figures and strongly participated in article writing; P.J.S. performed and analyzed collagen gels experiments and contributed to article writing; R.A. designed the microchannels and performed photolithography; A.M.L provided animal models and contributed to article writing; I.L wrote the code to analyze cell trajectories in collagen gels; M.P. participated in experiment design and contributed to article writing. P.V. designed the overall research and wrote the manuscript.

References

1. Cella M, Sallusto F, Lanzavecchia A. Origin, maturation and antigen presenting function of dendritic cells. Curr Opin Immunol. 1997;9 (1):10–16.

2. West MA, Wallin RPA, Matthews SP, Svensson HG, Zaru R, Ljunggren H-G, et al. Enhanced Dendritic Cell Antigen Capture via Toll-Like Receptor-Induced Actin Remodeling. Science. 2004 Aug 20;305 (5687):1153.

3. Martín-Fontecha A, Lanzavecchia A, Sallusto F. Dendritic Cell Migration to Peripheral Lymph Nodes. In: Lombardi G, Riffo-Vasquez Y, editors. Dendritic Cells [Internet]. Berlin, Heidelberg: Springer Berlin Heidelberg; 2009. p. 31–49. Available from: https://doi.org/10.1007/978-3-540-71029-5_2

4. Vargas P, Maiuri P, Bretou M, Sáez PJ, Pierobon P, Maurin M, et al. Innate control of actin nucleation determines two distinct migration behaviours in dendritic cells. Nat Cell Biol. 2016 Jan;18 (1):43–53.

5. Sáez PJ, Vargas P, Shoji KF, Harcha PA, Lennon-Duménil A-M, Sáez JC. ATP promotes the fast migration of dendritic cells through the activity of pannexin 1 channels and P2X7 receptors. Sci Signal [Internet]. 2017 Nov 21;10 (506). Available from: http://stke.sciencemag.org/content/10/506/eaah7107.abstract

6. Bretou M, Sáez PJ, Sanséau D, Maurin M, Lankar D, Chabaud M, et al. Lysosome signaling controls the migration of dendritic cells. Sci Immunol [Internet]. 2017 Oct 27;2 (16). Available from: http://immunology.sciencemag.org/content/2/16/eaak9573.abstract

7. Lämmermann T, Bader BL, Monkley SJ, Worbs T, Wedlich-Söldner R, Hirsch K, et al. Rapid leukocyte migration by integrin-independent flowing and squeezing. Nature. 2008 May 1;453 (7191):51–5.

8. Ufer F, Vargas P, Engler JB, Tintelnot J, Schattling B, Winkler H, et al. Arc/Arg3.1 governs inflammatory dendritic cell migration from the skin and thereby controls T cell activation. Sci Immunol. 2016 Sep 23;1 (3):eaaf8665–eaaf8665.

9. Thiam H-R, Vargas P, Carpi N, Crespo CL, Raab M, Terriac E, et al. Perinuclear Arp2/3-driven actin polymerization enables nuclear deformation to facilitate cell migration through complex environments. Nat Commun. 2016 Mar 15;7:10997.

10. Hung WC, Chen SH, Paul CD, Stroka KM, Lo YC, Yang JT, Konstantopoulos K. Distinct signaling mechanisms regulate migration in unconfined versus confined spaces. J Cell Biol. 2013 Sep 2;202 (5):807-24. doi: 10.1083/jcb.201302132. Epub 2013 Aug 26.

11. Hung WC, Yang JR, Yankaskas CL, Wong BS, Wu PH, Pardo-Pastor C, Serra SA, Chiang MJ, Gu Z, Wirtz D, Valverde MA, Yang JT, Zhang J, Konstantopoulos K. Confinement Sensing and Signal Optimization via Piezo1/PKA and Myosin II Pathways. Cell Rep. 2016 May 17;15 (7):1430-1441. doi: 10.1016/j.celrep.2016.04.035. Epub 2016 May 5.

12. Doyle AD, Wang FW, Matsumoto K, Yamada KM. One-dimensional topography underlies three-dimensional fibrillar cell migration. J Cell Biol. 2009 Feb 23;184 (4):481-90. doi: 10.1083/jcb.200810041. Epub 2009 Feb 16.

13. Liu YJ, Le Berre M, Lautenschlaeger F, Maiuri P, Callan-Jones A, Heuzé M, Takaki T, Voituriez R, Piel M. Confinement and low adhesion induce fast amoeboid migration of slow mesenchymal cells. Cell. 2015 Feb 12;160 (4):659-672. doi: 10.1016/j.cell.2015.01.007.

14. Weber M, Hauschild R, Schwarz J, Moussion C, de Vries I, Legler DF, et al. Interstitial Dendritic Cell Guidance by Haptotactic Chemokine Gradients. Science. 2013 Jan 18;339 (6117):328–32.

15. Chabaud M, Heuzé ML, Bretou M, Vargas P, Maiuri P, Solanes P, et al. Cell migration and antigen capture are antagonistic processes coupled by myosin II in dendritic cells. Nat Commun [Internet]. 2015 Dec [cited 2018 Oct 25];6 (1).

16. Sáez PJ, Barbier L, Attia R, Thiam H-R, Piel M, Vargas P. Leukocyte Migration and Deformation in Collagen Gels and Microfabricated Constrictions. In: Gautreau A, editor. Cell Migration: Methods and Protocols [Internet]. New York, NY: Springer New York; 2018. p. 361–73. Available from: https://doi.org/10.1007/978-1-4939-7701-7_26

17. Heuzé ML, Collin O, Terriac E, Lennon-Duménil A-M, Piel M. Cell Migration in Confinement: A Micro-Channel-Based Assay. In: Wells CM, Parsons M, editors. Cell Migration: Developmental Methods and Protocols [Internet]. Totowa, NJ: Humana Press; 2011. p. 415–34. Available from: https://doi.org/10.1007/978-1-61779-207-6_28

18. Vargas P, Terriac E, Lennon-Duménil A-M, Piel M. Study of cell migration in microfabricated channels. J Vis Exp JoVE. 2014 Feb 21; (84):e51099–e51099.

19. Vargas P, Barbier L, Sáez PJ, Piel M. Mechanisms for fast cell migration in complex environments. Current opinion in cell biology. 2017 Oct 1;48:72–8.

20. Bzymek R, Horsthemke M, Isfort K, Mohr S, Tjaden K, Müller-Tidow C, et al. Real-time two- and three-dimensional imaging of monocyte motility and navigation on planar surfaces and in collagen matrices: roles of Rho. Sci Rep [Internet]. 2016 Jul [cited 2018 Oct 25];6 (1). Available from: http://www.nature.com/articles/srep25016

21. Leithner A, Eichner A, Müller J, Reversat A, Brown M, Schwarz J, et al. Diversified actin protrusions promote environmental exploration but are dispensable for locomotion of leukocytes. Nat Cell Biol. 2016 Oct 24;18:1253.

22. Renkawitz J, Schumann K, Weber M, Lämmermann T, Pflicke H, Piel M, et al. Adaptive force transmission in amoeboid cell migration. Nat Cell Biol. 2009 Dec;11 (12):1438–43.

23. Stroka KM, Jiang H, Chen S-H, Tong Z, Wirtz D, Sun SX, et al. Water permeation drives tumor cell migration in confined microenvironments. Cell. 2014 Apr 24;157 (3):611–23.

24. Doolin MT, Stroka KM. Physical confinement alters cytoskeletal contributions towards human mesenchymal stem cell migration. Cytoskeleton. 2018 Jan 6;75 (3):103–17.

25. Jacobelli J, Friedman RS, Conti MA, Lennon-Dumenil A-M, Piel M, Sorensen CM, et al. Confinement-optimized three-dimensional T cell amoeboid motility is modulated via myosin IIA-regulated adhesions. Nat Immunol. 2010 Oct;11 (10):953–61.

26. Handorf AM, Zhou Y, Halanski MA, Li W-J. Tissue stiffness dictates development, homeostasis, and disease progression. Organogenesis. 2015 Apr 27;11 (1):1–15.

27. Bonnans C, Chou J, Werb Z. Remodelling the extracellular matrix in development and disease. Nat Rev Mol Cell Biol. 2014 Nov 21;15:786.

28. Butcher DT, Alliston T, Weaver VM. A tense situation: forcing tumour progression. Nat Rev Cancer. 2009 Feb 1;9:108.

29. Conklin MW, Eickhoff JC, Riching KM, Pehlke CA, Eliceiri KW, Provenzano PP, et al. Aligned collagen is a prognostic signature for survival in human breast carcinoma. Am J Pathol. 2011 Mar;178 (3):1221–32.

30. Bougherara H, Mansuet-Lupo A, Alifano M, Ngô C, Damotte D, Le Frère-Belda M-A, et al. Real-Time Imaging of Resident T Cells in Human Lung and Ovarian Carcinomas Reveals How Different Tumor Microenvironments Control T Lymphocyte Migration. Front Immunol [Internet]. 2015 Oct 12 [cited 2018 Oct 25];6. Available from: http://journal.frontiersin.org/Article/10.3389/fimmu.2015.00500/abstract

31. Takamatsu H, Takegahara N, Nakagawa Y, Tomura M, Taniguchi M, Friedel RH, et al. Semaphorins guide the entry of dendritic cells into the lymphatics by activating myosin II. Nat Immunol. 2010 Jul;11 (7):594–600.

32. Barnes TA, Amir E. HYPE or HOPE: the prognostic value of infiltrating immune cells in cancer. Br J Cancer. 2017 Aug 8;117 (4):451–60.

33. Faure-André G, Vargas P, Yuseff M-I, Heuzé M, Diaz J, Lankar D, et al. Regulation of Dendritic Cell Migration by CD74, the MHC Class II-Associated Invariant Chain. Science. 2008 Dec 12;322 (5908):1705.

34. Caton ML, Smith-Raska MR, Reizis B. Notch-RBP-J signaling controls the homeostasis of CD8- dendritic cells in the spleen. J Exp Med. 2007 Jul 9;204 (7):1653–64.

35. Stroka KM, Hayenga HN, Aranda-Espinoza H. Human neutrophil cytoskeletal dynamics and contractility actively contribute to trans-endothelial migration. PLoS One. 2013 Apr 23;8 (4):e61377. doi: 10.1371/journal.pone.0061377. Print 2013.

36. Zehrer, A., Pick, R., Salvermoser, M., Boda, A., Miller, M., Stark, K., et al. A Fundamental Role of Myh9 for Neutrophil Migration in Innate Immunity. The Journal of Immunology, 2018 Sep 15;201 (6):1748-1764. doi: 10.4049/jimmunol.1701400.

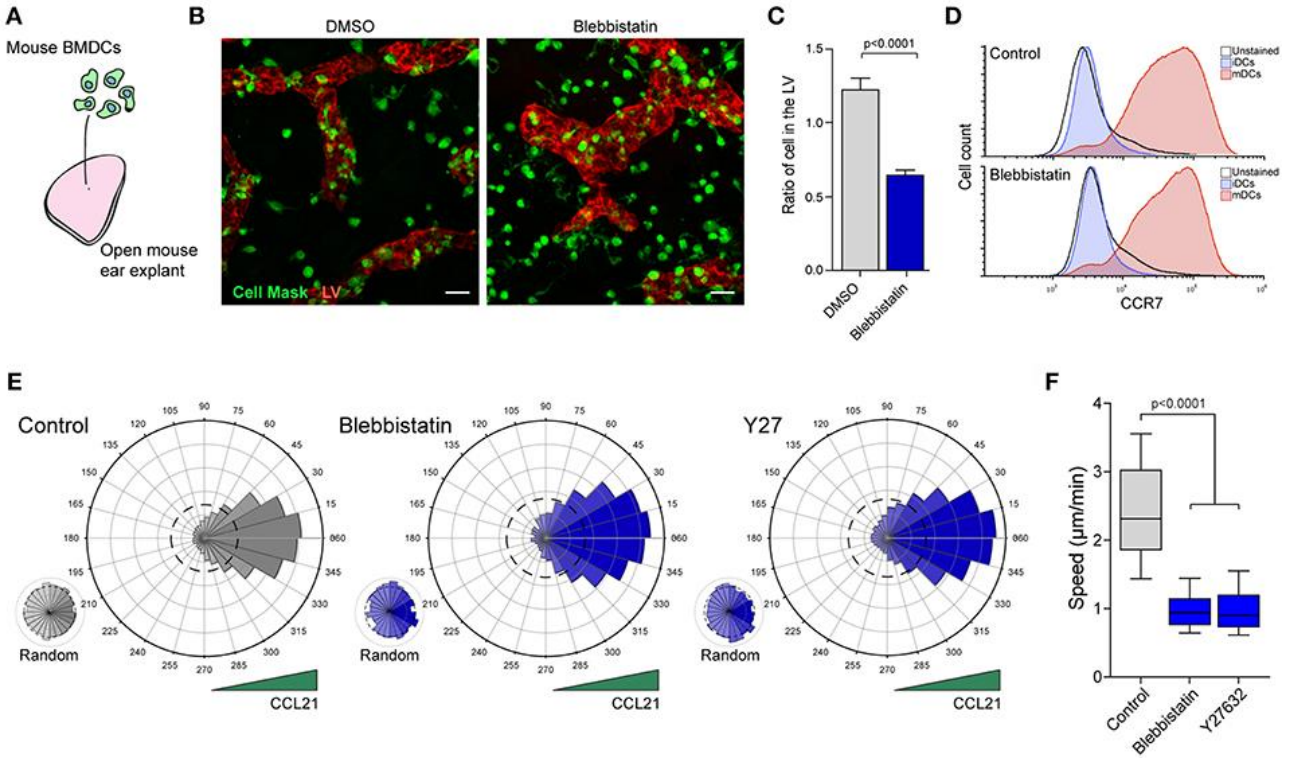

Figure 29 **Figure 1. MyoII activity regulates mDCs migration in dense extracellular matrices**

(A-C) Analysis of mDCs migration in mouse ear explants. **(A)** Schematic representation of the experimental set-up in which in vitro differentiated and labelled mDCs were seeded on the dermal side of mouse ear explants. **(B)** Sum z-projection of a representative field from a skin ear explant imaged at 20X on a spinning disk. mDCs are shown in green, LVs stained with anti Lyve-1 in red. Scale bar=25µm. **(C)** Quantification of the ratio of mDCs overlapping with the LVs versus those in the interstitial space. Data from 2 independent experiments, 2 ears explant per experiment and 4 fields of view per explant. Mean and SEM are showed. Unpaired t-test with Welch's correction was applied for statistical test. **(D)** Flow cytometry analysis of CCR7 surface expression in mDCs treated or not with Blebbistatin. **(E-F)** Analysis of mDCs trajectories in 3D collagen gels along a gradient of CCL21. **(E)** Polar plots show cell directionality during chemotaxis of control, blebbistatin or Y27632 treated mDCs. Random motility was analyzed in the same gels, but in areas with no access to CCL21. The dashed line in the polar plots indicate the theoretical random motility. **(F)** Mean speed of control, blebbistatin or Y27632 treated mDCs migrating in the directional zone of the gel. Data correspond to the same trajectories as shown in E, 3 independent experiments, n=323 in control, 219 in blebbistatin and 199 in Y27632. In the boxplot, the bar and the box include 90% and 75% of the points, respectively. The line inside the box corresponds to the median. The Mann-Whitney test was used as statistical test.

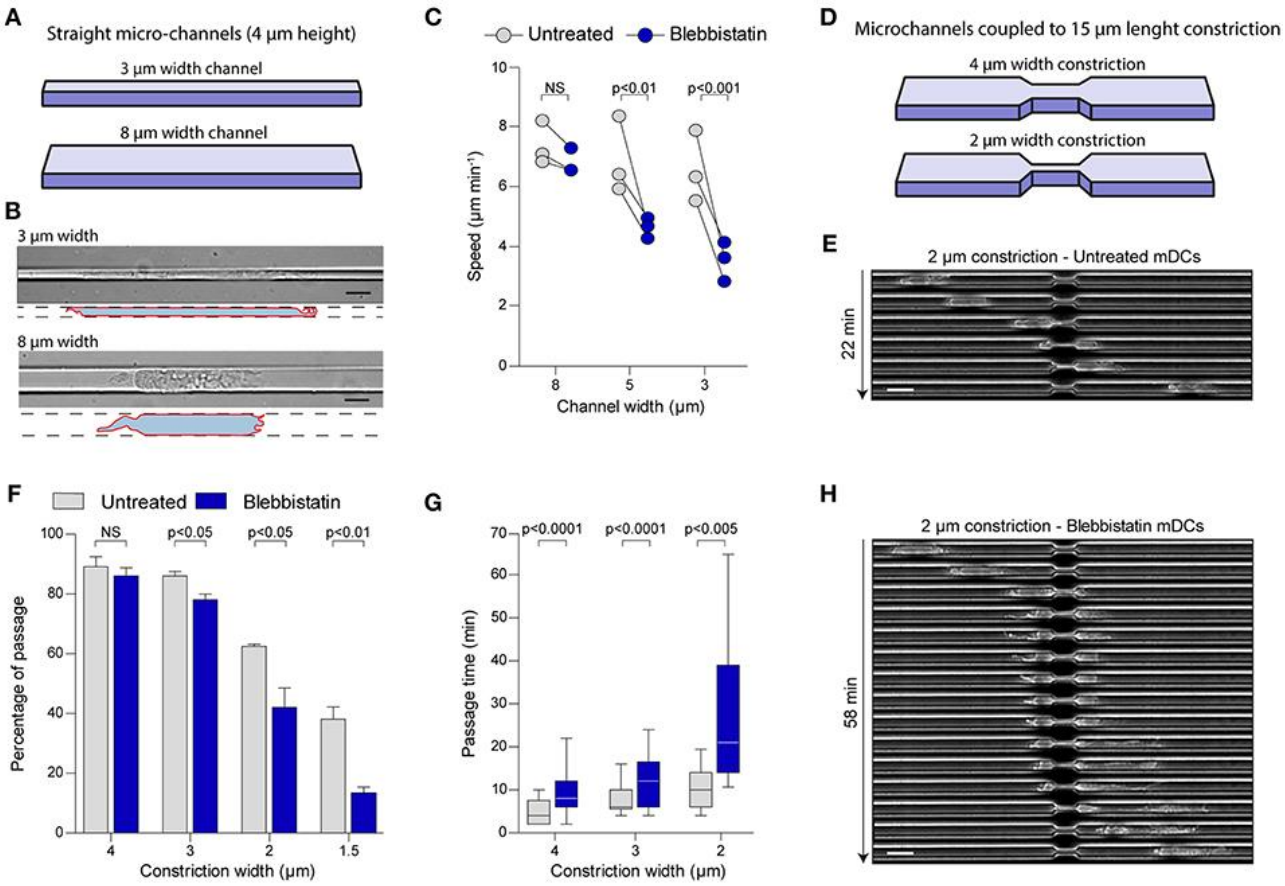

Figure 30: **Figure 2. MyoII motor activity is specifically required for mDCs migration in very confined microenvironments**.

(A-C) Analysis of mDCs migration in straight microchannel of different width. **(A)** Schematic representation of the microchannel used, where the height of the microchannel is fixed at 4 µm, and the width of the channel vary from 3 µm to 8 µm. **(B)** Representative mDCs in 3 and 8 µm width microchannel imaged at 40X with DIC. The drawing highlights the contour of the cells. Scale bar=10 µm. **(C)** Mean instantaneous speed of untreated or blebbistatin treated mDCs in microchannel of 3, 5 and 8 µm width obtained in three independent experiments. Each dot represents the median of one experiment (n>30 cells in 8 µm width channel, n>50 cells in 5 µm and n>60 cells in 3 µm for each experiment). Anova with Tukey's Multiple Comparison Test was applied for statistical test. **(D-H)** Analysis of mDCs passage through constrictions of different sizes. **(D)** Schematic representation of the constrictions added in the microchannel, the height and the length of the constriction are fixed to 4 and 15 µm respectively, the width of the constriction varies from 1,5 to 4 µm. **(E)** Sequential image of a mDCs passing through a 2 µm width constriction acquired with phase contrast and a 10X objective**.** Scale bar=20 µm. **(F)** Percentage of the untreated and treated mDCs passing through the first constriction of the chamber amongst all cells touching it. N=430, 519, 510 and 531 for untreated cells in 1.5, 2, 3 and 4 µm width constrictions; N=346, 389, 362 and 437 for blebbistatin treated cells in 1.5, 2, 3 and 4 µm width constrictions, from three independent experiments. Unpaired t-test was applied for statistical test. **(G)** Time spent in the constriction by mDCs passing the constriction. N=72, 142 and 156 untreated mDCs in 2, 3 and 4 µm width constrictions; n= 42, 70 and 142 for blebbistatin treated mDCs in 2, 3 and 4 µm width constrictions. The bar and the box include respectively 90% and 75% of the points, the center corresponds to the median. One representative experiment out of 3 is shown. Unpaired t-test with Welch's correction was applied for statistical test. **(H)** Sequential image of a blebbistatin treated mDCs passing through a 2 µm width constriction acquired with phase contrast and a 10X objective**.** Scale bar=20 µm.

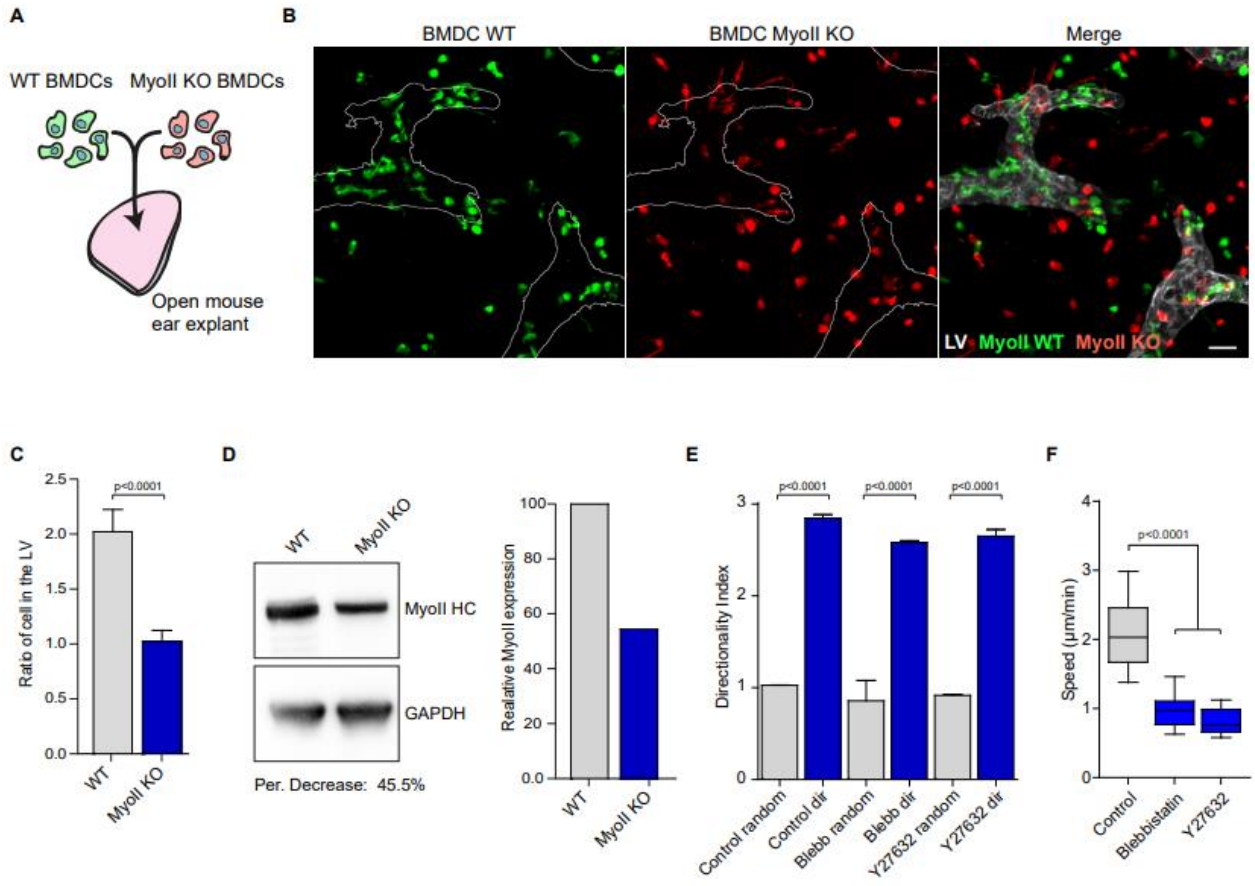

Figure 31. **Sup. Figure 1.**

(A-B) Analysis of mDCs migration in mouse ear explants. **(A)** Schematic representation of the experimental set-up in which *in vitro* differentiated and labelled mDCs were seeded on the dermal side of mouse ear explants. **(B)** Sum z-projection of a representative field from a skin ear explant imaged at 20X on a spinning disk. mDCs are shown in green, LVs stained with anti Lyve-1 in white. Scale bar=30µm. **(C)** Quantification of the ratio of mDCs overlapping with the LVs versus those in the interstitial space. Data from 2 independent experiments, 3 ears explant per experiment and 3 field of view per explant. Mean and SEM are showed. Paired t-test was used as statistical test. (**D**) Western blot analysis of Myosin II A heavy chain expression in mDCs derived from MyoII-flox/flox/CD11c-Cre- (WT) and MyoII-flox/flox/CD11c-Cre+ (KO) mice. Histogram shows the quantification of the plot. **(E)** Directionality index of mDCs migrating in collagen gels. Grey bars correspond to random trajectories and blue bars to tracks during chemotaxis. This analysis is based on the data shown in figure 1E. **(F)** Representative experiment showing the mean speed of control, Blebbistatin or Y27632 treated mDCs migrating randomly in a collagen gel. Control n=341, Blebbistatin n=104, Y27632 n=90. Three independent experiments were performed. In the boxplot, the bar and the box include 90% and 75% of the points, respectively. The line inside the box corresponds to the median. The Mann-Whitney test was used as statistical test.

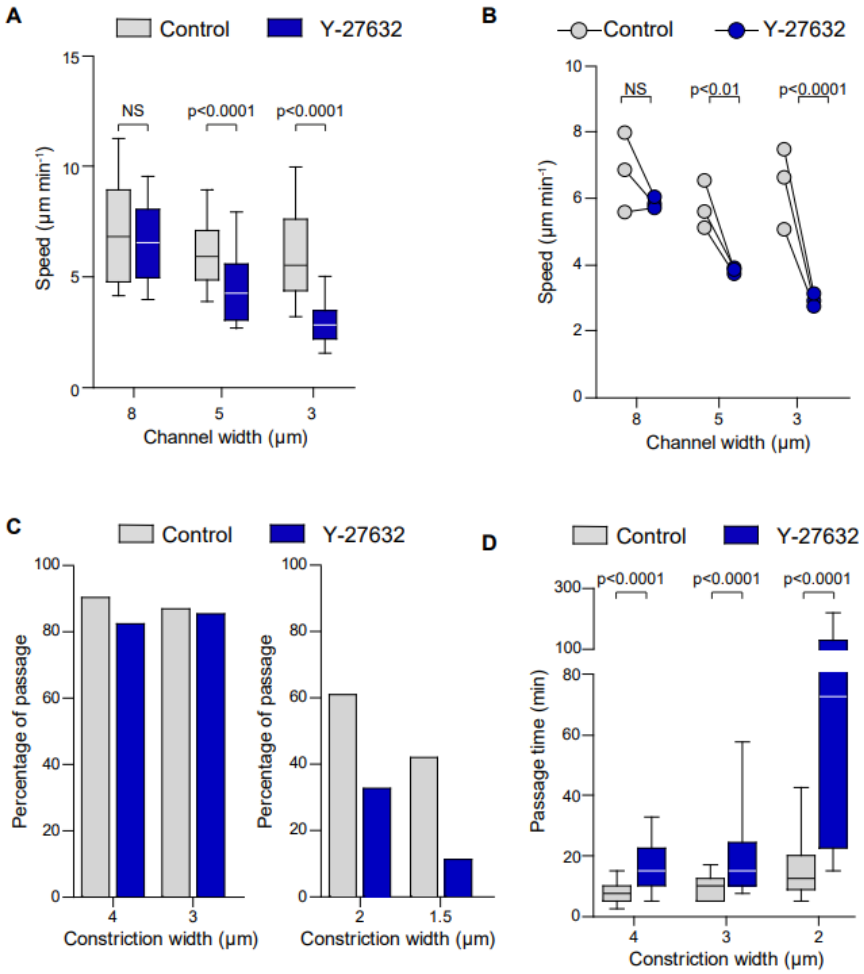

Figure 32: **Sup. Figure 2.**

(**A**) Representative experiment of mDCs migrating in microchannels of different sizes. The figure shows the mean instantaneous speed of untreated or blebbistatin treated mDCs in microchannel of 3, 5 and 8 µm width. N= 91, 109 and 178 untreated mDCs in 8, 5 and 3 µm width microchannel, respectively; n= 53, 85 and 66 for blebbistatin treated mDCs in 8, 5 and 3 µm width microchannels, respectively. Unpaired t-test was applied as statistical test with Welch's correction for 3 µm width microchannel. **(B)** Mean instantaneous speed of untreated or Y27632 treated mDCs in microchannel of 3, 5 and 8 µm width obtained in three independent experiments. Each dot represents the median of one experiment (n>30 cells in 8 µm width channel, n>50 cells in 5 µm and n>60 cells in 3 µm for each experiment). Anova with Tukey's Multiple Comparison Test was applied for statistical test. (**C**) Percentage of the untreated and Y27632 treated mDCs passing through the first constriction of the chamber amongst all cells touching it. More than 50 cells were analyzed from 2 separate experiments for 1.5 and 2 µm width constrictions, and for 3 and 4 µm width constrictions. **(D)** Time spent in the constriction by mDCs passing the constriction in the presence or absence of Y27632. The bar and the box include respectively 90% and 75% of the points, the center corresponds to the median. One experiment with n= 69, 91 and 100 untreated mDCs in 2, 3 and 4 µm width constrictions; n= 32, 104 and 88 for Y-27632 treated mDCs in 2, 3 and 4 µm width constrictions. Unpaired t-test was applied for statistical test.

II. Confinement triggers ROCK-dependent actomyosin reorganization associated with mature dendritic cell speed in confined microchannels.

A noteworthy result of this first study suggested that the microchannel width only slightly affects mDC migration speed. As the narrowing of the microchannels imposes a higher resistance to cell migration, we expected a marked decrease in cell speed in the 3 × 4 µm microchannels compared with the 8 × 4 µm microchannels. Thus, we investigated whether speed maintenance is related to an adaptation of the mDC migration machinery to produce higher force in narrow spaces.

A. Characterization of actomyosin organization at different degrees of confinement

We focused on actin and MyoII since they constitute the main driving force for mDC locomotion. We used LifeAct- and MyoII-GFP-mDCs to study the localization of these cytoskeletal components in cells migrating in microchannels of varying dimensions. Results showed that confinement triggered a complete reorganization of the actin and MyoII structures in the cell (Fig.33 A and B).

Actin organization in wide microchannels (i.e., 8 × 4 µm) has been extensively studied (Vargas et al., 2016). Actin fluctuated; however, in general, was localized immediately posterior to the center of the cell (Fig.33 A and C, upper panel). This actin pool is essential for the rapid mDC migration to the lymph node. In comparison, mDCs migrating in 3 x 4 µm microchannels were characterized by complete actin depletion in the anterior of the cell and the appearance of an actin structure at the extreme posterior end of the cell (Fig.33 A, C, and E).

Narrowing of microchannels also affected MyoII localization. However, the different structures were difficult to distinguish at the cell population level owing to the high cytoplasmic signal. In the 8 × 4 µm microchannels, the MyoII-GFP signal was weak in the center of the cell, which corresponds to signal exclusion from the nucleus (image not shown). As already described (Bretou et al., 2017), in wide microchannels, MyoII-GFP was enriched in the posterior end of the cell (Fig.33 B and D, top panel). In mDCs migrating in 3 × 4 µm microchannels, this MyoII-GFP signal imbalance between the cell anterior and posterior regions was enhanced (Fig.33 B, D, and F). Moreover, MyoII appeared to accumulate in the posterior 15% of the cell length, similar to the actin structure

triggered by cell confinement (Fig.33 E and F).

To quantify actin and MyoII accumulation at the cell posterior, we measured the average LifeAct and MyoII-GFP signal intensity over the posterior 15% of the cell length relative to the average intensity in the whole cell (Fig.33 G and H). The results confirmed that mDCs migrating in 3 × 4 µm microchannels accumulated significantly more actomyosin cytoskeleton in the posterior end than cells migrating in 8 × 4 µm microchannels. Moreover, cell speed did not differ significantly in microchannels of different dimensions (Fig.33 I), as shown in our previous study. Thus, these results characterize a reinforced actomyosin structure at the cell rear in mDCs migrating in 3 × 4 µm microchannels. This contractile structure may produce the force necessary to counteract the microchannel resistance.

Figure 33 Actomyosin accumulation in the posterior end of the cell under confinement

(A-B) *Representative montage of an image sequence of a LifeAct-mDC* ***(A)*** *or MyoII-GFP-mDC* ***(B)*** *migrating in 8 × 4 µm (top) and 3 × 4 µm (bottom) microchannels.* ***(C-D)*** *Mean LifeAct* ***(C)*** *or MyoII-GFP* ***(D)*** *signal density map of mDCs migrating in 8 × 4 µm (top), 5 × 4 µm (middle), and 3 × 4 µm (bottom) microchannel. One representative example of three independent experiments for LifeAct and two independent experiments for MyoII-GFP.* ***(F-E)*** *Intensity profile of mean LifeAct* ***(E)*** *or MyoII-GFP* ***(F)*** *signal density map. Curve and error bars represent the mean and standard error of the mean of three independent experiments for LifeAct or the mean and range of two independent experiments for MyoII-GFP. The dotted bar indicates the posterior 15% of the cell length.* ***(G-H)*** *Quantification of LifeAct* ***(G)*** *or MyoII-GFP* ***(H)*** *signal accumulation in the posterior 15% of the cell length for mDCs migrating in 8 × 4 µm, 5 × 4 µm, and 3 × 4 µm microchannels. Each dots and error bars represent the mean and standard deviation (SD), respectively, of one independent experiment (see methods).* ***(I)*** *Speed of mDCs migrating in 8 × 4 µm, 5 × 4 µm, and 3 × 4 µm microchannels. The dots and error bars represent the mean and SD, respectively, of one independent experiment. ANOVA with Tukey's multiple comparison test was used; **p < 0.01.*

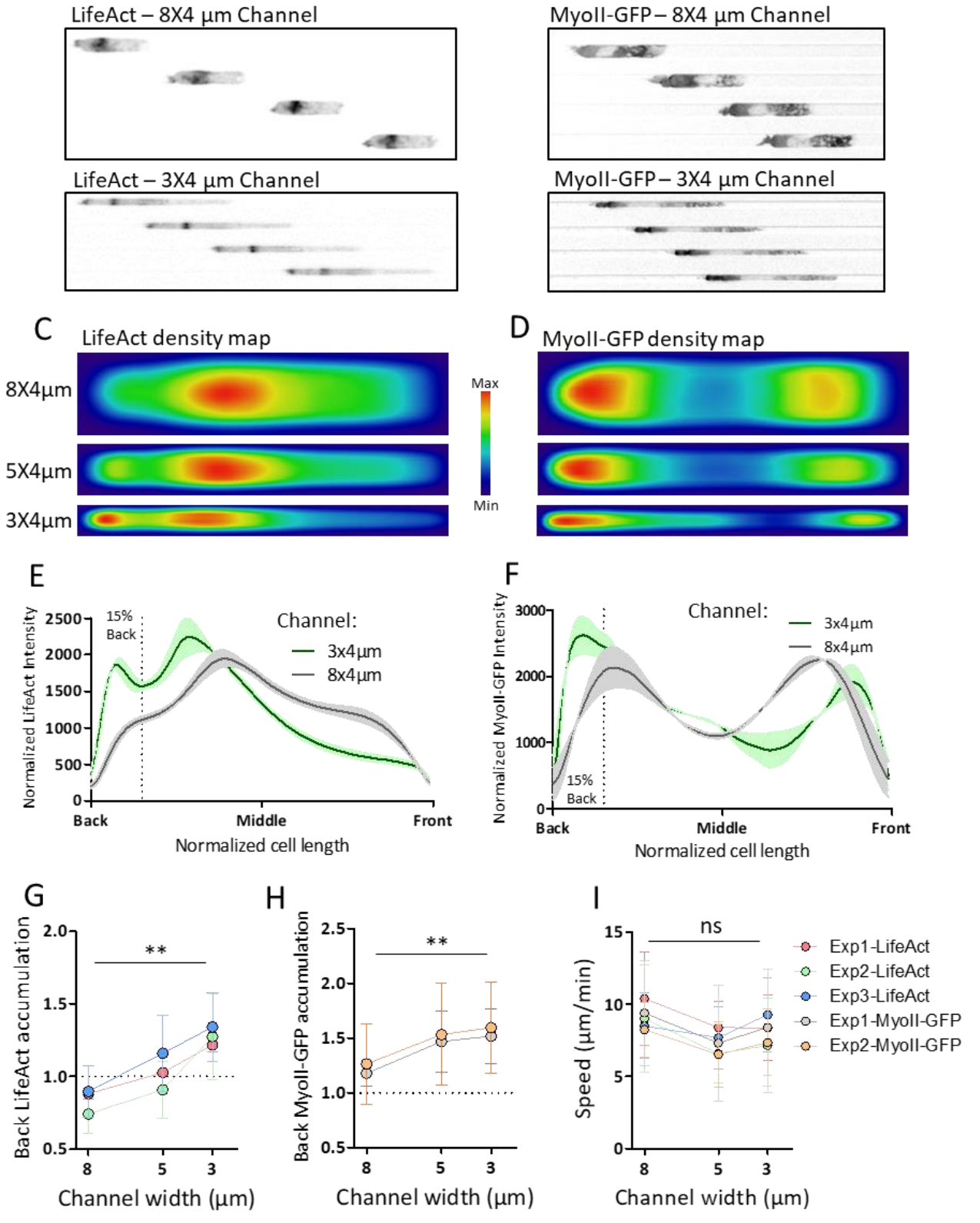
LifeAct – 8X4 µm Channel
MyoII-GFP – 8X4 µm Channel
LifeAct – 3X4 µm Channel
MyoII-GFP – 3X4 µm Channel
C
LifeAct density map
D
MyoII-GFP density map
8X4µm
5X4µm
3X4µm
Max
Min
E
Normalized LifeAct Intensity
15% Back
Channel:
3x4µm
8x4µm
Back
Middle
Front
Normalized cell length
F
Normalized MyoII-GFP Intensity
Channel:
3x4µm
8x4µm
15% Back
Back
Middle
Front
Normalized cell length
G
Back LifeAct accumulation
**
Channel width (µm)
H
Back MyoII-GFP accumulation
**
Channel width (µm)
I
Speed (µm/min)
ns
Exp1-LifeAct
Exp2-LifeAct
Exp3-LifeAct
Exp1-MyoII-GFP
Exp2-MyoII-GFP
Channel width (µm)

B. Dynamic cytoskeleton remodeling in microchannels of varying dimensions

Previous results raise a question regarding whether cytoskeletal remodeling is dynamic and whether mDCs can adapt their migration machinery to varying dimensions as observed in the interstitial space. Thus, we challenged mDCs in microchannels with a constriction at which the microchannel width decreases from 8 to 3 µm. This configuration facilitates the study of cell deformation at the transition between wide and narrow channels as well as the subsequent cellular adaptations to confinement.

The speed of mDCs decreased significantly at the constriction. However, the mDCs regained a speed similar to that before the constriction within the first 100 µm after the transition (Fig.34 A to D). This finding demonstrates the ability of mDCs to adapt to increased confinement and highlights the cell deformation phase at the constriction as a factor limiting cell motility in varying dimensions.

The actomyosin accumulation in the posterior end of the cell observed in straight microchannels was formed at the constriction (Fig.34 A to D). Accumulation of actin and myosin began at the position where mDCs reached their minimum velocity. We have already shown that MyoII inhibition increases cell passage time through the constriction. Thus, this observation suggests that this contractile structure is involved in cell deformation through narrowing.

LifeAct signal accumulation in the posterior end of the cell reached a maximum (~1.4 fold) when the nucleus was at a 50 µm distance after the constriction. The average cell length (80 µm - see Methods) suggests that this distance corresponds approximately to the position where the posterior of the cell enters the 3 × 4 µm part. Then, the value decreased slowly to reach the level observed in the straight microchannels (~1.25 fold; Fig.34 C). MyoII remodeling was more rapid than actin remodeling; and reached a plateau only 15 µm after nucleus entry (Fig.34 D). Remarkably, cell speed after the constriction was significantly correlated with actin accumulation at the posterior of the cell but not with MyoII accumulation (Fig.34 E and F), which suggests that the roles of these two cytoskeleton components differ. MyoII contractility would be necessary for cell deformation through constrictions, whereas the actin dynamic is involved in cell speed recovery after compression. However, MyoII-GFP signal accumulation at the posterior of the cell may not be a direct indication of its activity. Indeed, a previous study has shown that MyoII contractility plays a role in accelerating the retrograde actin flow and modulates the actin pool in the posterior end of the cell (Bretou et al., 2017; Liu et al., 2015). Thus, actin overshoot in the posterior end of the cell

after the constriction may also indicate an increase in MyoII activity even if MyoII-GFP signal accumulation has already plateaued.

Therefore, actin and myosin accumulation in the posterior end of the cell is triggered by cell entry into 3 × 4 µm microchannels. Correlation between actin accumulation and cell speed suggests that this contractile structure is involved in the dynamic adaptation of mDCs to confinement. A complete understanding of the role of MyoII-dependent contractility in cell deformation and cell speed recovery requires the measurement of MyoII activity. One approach is to focus on the study of its flow rate (Bretou et al., 2017). However, visualization of MyoII-GFP retrograde movement in 3 × 4 µm microchannels can be challenging owing to cell crowding. Another potential approach is to quantify the phosphorylation of the MyoII regulatory light chain (RLC) during cell squeezing. Different biosensors based on fluorescence resonance energy transfer (FRET) have been developed to quantify RLC phosphorylation dynamics in living cells (Markwardt et al., 2018; Yamada et al., 2005). However, they correspond to genetically encoded biosensors, and their complicated expression in DCs may limit their use. The first step would be to quantify RLC phosphorylation by IF in mDCs migrating in 3 × 4 µm and 8 × 4 µm microchannels separately. Different levels of MyoII activation, depending on the microchannel dimensions, would provide an insight into its dynamic modulation during mDC deformation. Higher RLC phosphorylation in 3 × 4 µm microchannels would suggest an active mechano-response leading to MyoII activation and remodeling. In contrast, equivalent RLC phosphorylation levels would indicate that the actomyosin structure in the posterior end of the cell is a passive effect of geometric variations in the microenvironment.

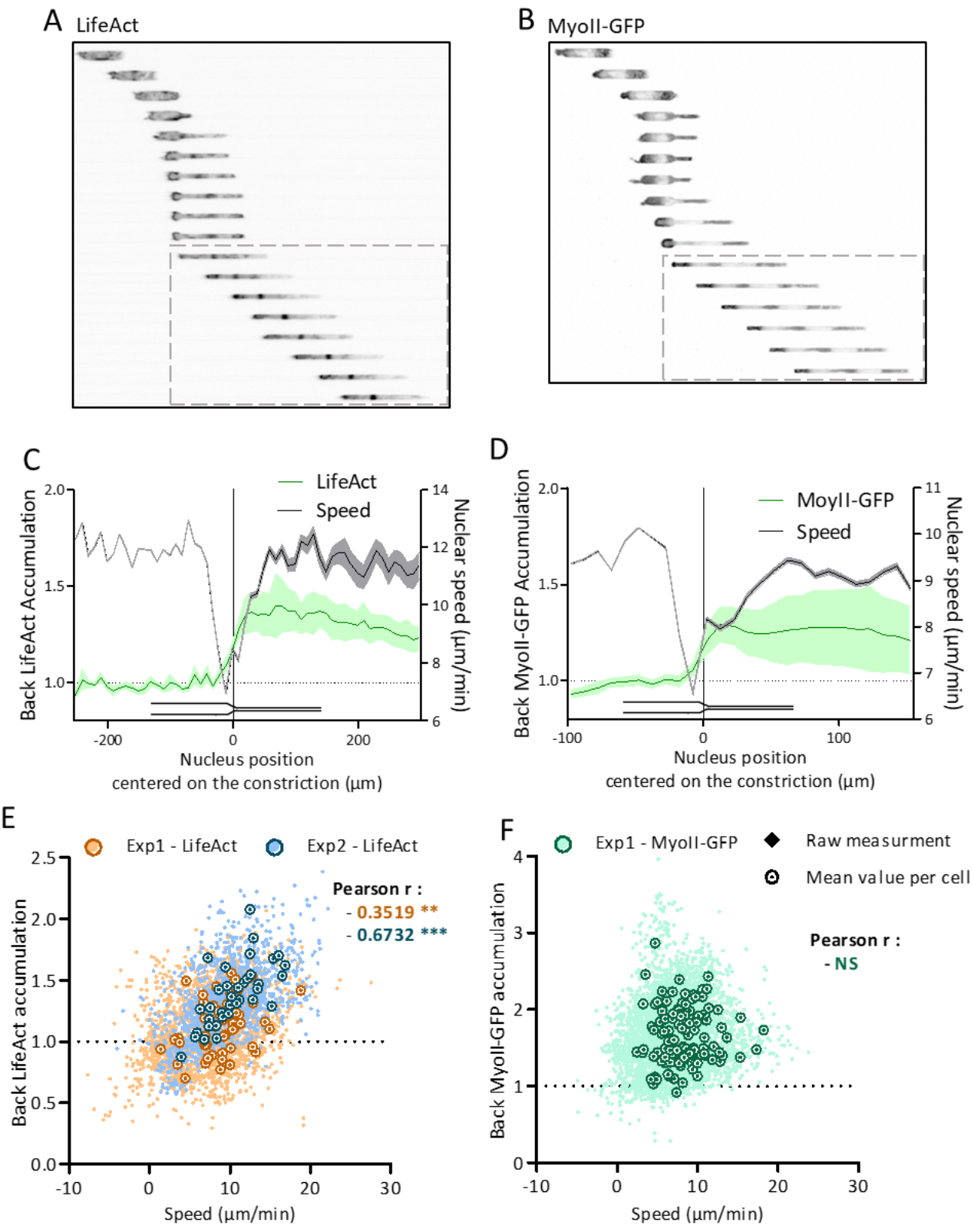
A LifeAct
B MyoII-GFP
C
LifeAct
Speed
Back LifeAct Accumulation
Nuclear speed (µm/min)
Nucleus position
centered on the constriction (µm)
D
MoyII-GFP
Speed
Back MyoII-GFP Accumulation
Nuclear speed (µm/min)
Nucleus position
centered on the constriction (µm)
E
Exp1 - LifeAct
Exp2 - LifeAct
Pearson r :
- 0.3519 **
- 0.6732 ***
Back LifeAct accumulation
Speed (µm/min)
F
Exp1 - MyoII-GFP
Raw measurment
Mean value per cell
Pearson r :
- NS
Back MyoII-GFP accumulation
Speed (µm/min)

Figure 34 Dynamic actomyosin reorganization upon cell confinement

(A-B) Representative montage of an image sequence of a LifeAct-mDC **(A)** and MyoII-GFP-mDC **(B)** migrating in microchannel varying from 8 × 4 µm to 3 × 4 µm. The dotted rectangle highlights the area analyzed in E and F. **(C-D)** Mean speed and LifeAct **(C)** or MyoII-GFP **(D)** signal accumulation in the posterior 15% of the cell length for mDCs migrating in microchannels varying from 8 × 4 µm to 3 × 4 µm as a function of the nuclear position from the constriction. The curves and error bars represent the mean and standard deviation, respectively, of 36 cells for **(C)** and 112 cells for **(D)** from one experiment. **(E-F)** Correlation between cell speed and LifeAct **(E)** or MyoII-GFP **(F)** signal accumulation in the posterior 15% of the cell length measured in the first 250 µm after the width variation from 8 µm to 3 µm (dotted rectangle in A and B). **p-value < 0.01; ***p-value < 0.0001.

C. ROCK activity controls actin remodeling during confined migration

To better characterize the role of MyoII in cytoskeletal remodeling triggered by confined migration of mDCs, we used pharmacological inhibitors. We focused on the ROCK inhibitor, Y-27632. ROCK phosphorylates the RLC, leading to MyoII activation. Y-27632 has the advantage of being non-phototoxic (compared to the direct MyoII inhibitor blebbistatin) and water soluble, which limits its absorption by PDMS.

ROCK inhibition affected the actin organization in 8 × 4 µm and 3 × 4 µm microchannels (Fig.35 A to C). Y-27632-treated cells showed an increase in actin accumulation anterior to the nucleus compared with control cells. This increase was enhanced in the 3 × 4 µm microchannels (Fig.35 E and F). Actin remodeling observed in all microchannel sizes suggests that the MyoII contractility is involved in mDC movement in both 8 × 4 µm and 3 × 4 µm microchannels. Thus, the absence of a significant effect of Y-27632 on mDC speed in the 8 × 4 µm microchannels could be due to compensation by other migration mechanisms that are not efficient in the 3 × 4 µm microchannels.

A significant effect of ROCK inhibition was the loss of actin accumulation at the cell posterior normally induced by mDC migration in 3 × 4 µm microchannels (Fig.35 G). The loss of the actin pool in the posterior end of the cell was correlated with a decrease in velocity with the narrowing of the microchannels under Y-27632 conditions (Fig.35 H).

The effects of Y-27632 on cell speed are similar to those observed with blebbistatin treatment. Thus, we hypothesized that the impact of ROCK inhibition depends on its MyoII activator function.

The results obtained confirm the link between the rapid mDC migration in narrow microchannels and the increase in actin accumulation in the posterior end of the cell. The loss of this structure upon ROCK inhibition suggests that it is triggered by a mechano-response activated by cell confinement. This signaling pathway would be ROCK-dependent.

Actin remodeling with Y-27632 in 8 × 4 µm microchannels suggests a change in the mode of migration even if the cell velocity is preserved. The treated cells seem to switch from a contractile behavior pushing the nucleus to a protruding mode dragging the nucleus. This hypothesis is also supported by the change in the nuclear position, which is backward in Y-27632-treated cells (Fig.35 E and F). This raises a question regarding the molecular motor driving the actin-rich protrusion. In iDCs, Arp2/3 is the main actin nucleator in the anterior of the cell. However, its activity is downregulated during DC maturation (Vargas et al., 2016). The role of Arp2/3 in protrusive migration could be tested with a combined treatment of Y-27632 and CK666, an Arp2/3 inhibitor. Arp2/3 inhibition alone does not affect mDC speed or actin organization in wide microchannels (Vargas et al., 2016). Thus, if this drug decreases mDC velocity in combination with Y-27632, it would highlight Arp2/3-dependent protrusive migration as a compensatory mechanism triggered by MyoII inhibition

Remarkably, the protrusive migration mode is sufficient to drive efficient mDC movement in 8 × 4 µm microchannels but not in 3 × 4 µm microchannels. We can hypothesize that protrusion produces fewer forces than MyoII-dependent contractility. Therefore, it would not be sufficient to overcome the increased resistance to cell migration induced by narrowing of the microchannel. It is also possible that MyoII activity affects the mechanical properties of the cell acting on the nucleus or cell adhesion. It would then allow migration in confined spaces without the need for increased force.

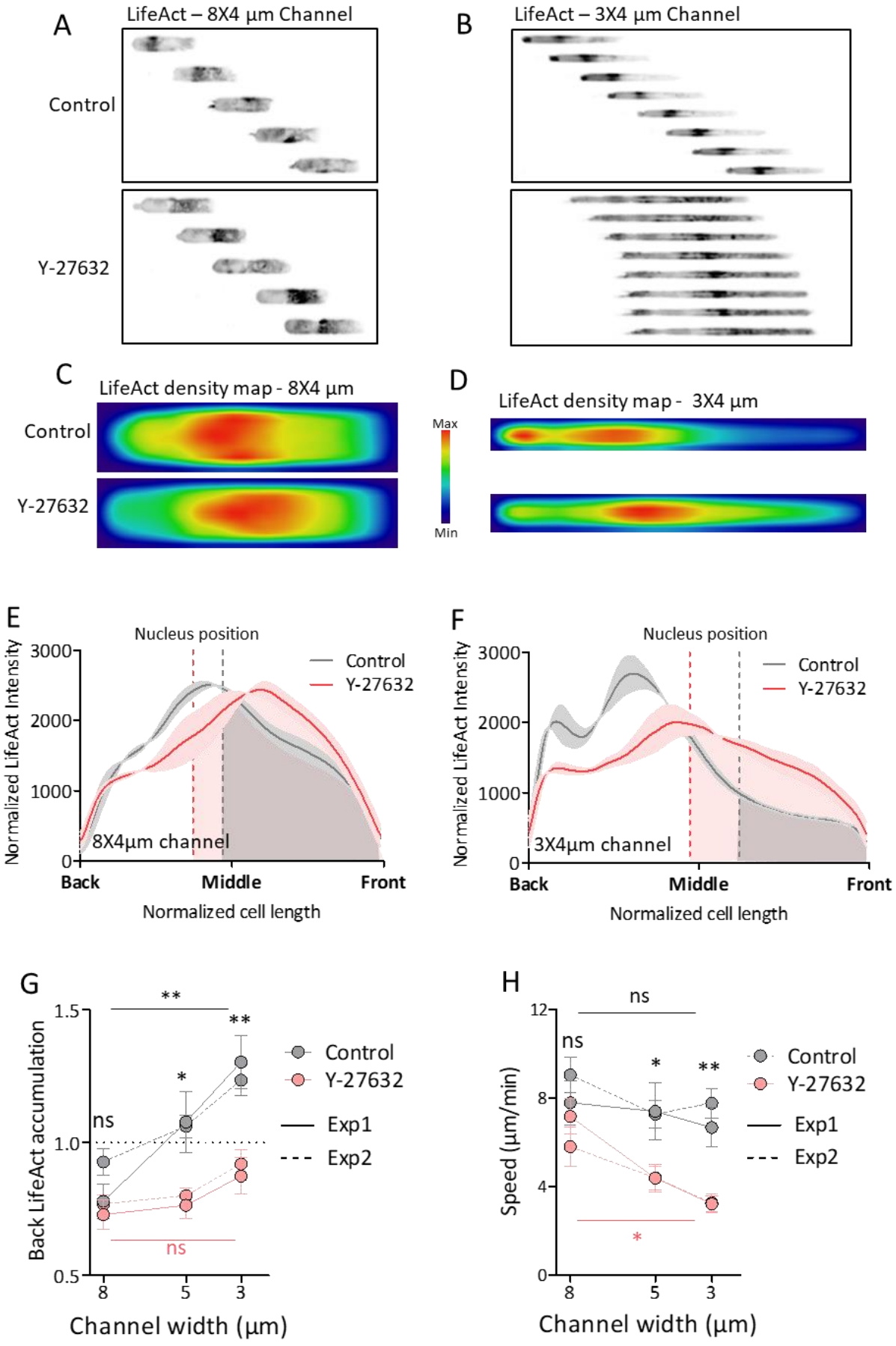
A
LifeAct – 8X4 µm Channel
Control
Y-27632
B
LifeAct – 3X4 µm Channel
C
LifeAct density map - 8X4 µm
Control
Y-27632
D
LifeAct density map - 3X4 µm
Max
Min
E
Nucleus position
Normalized LifeAct Intensity
3000
2000
1000
0
Control
Y-27632
8X4µm channel
Back
Middle
Front
Normalized cell length
F
Nucleus position
Normalized LifeAct Intensity
3000
2000
1000
0
Control
Y-27632
3X4µm channel
Back
Middle
Front
Normalized cell length
G
Back LifeAct accumulation
1.5
1.0
0.5
**
**
*
ns
ns
Control
Y-27632
Exp1
Exp2
8
5
3
Channel width (µm)
H
Speed (µm/min)
12
8
4
0
ns
ns
*
**
*
Control
Y-27632
Exp1
Exp2
8
5
3
Channel width (µm)

Figure 35 Actin accumulation in the posterior end of the cell is dependent on ROCK activity

(A-B) Representative montage of an image sequence of a control LifeAct-mDC (top) and LifeAct-mDC treated with 10 µM Y-27632 (ROCK inhibitor; bottom) migrating in 8 × 4 µm **(A)** and 3 × 4 µm **(B)** microchannels. **(C-D)** Mean LifeAct signal density map of control mDCs (top) and mDCs treated with 10 µM Y-27632 (bottom) migrating in 8 × 4 µm **(C)** and 3 × 4 µm **(D)** microchannels. One representative example of two independent experiments. **(F-E)** Intensity profile of mean LifeAct signal density map of mDCs migrating in 8 × 4 µm (F) and 3 × 4 µm (E) microchannels. The curves and error bars represent the mean and range, respectively, of two independent experiments. The dotted line indicates the mean relative position of the nucleus and the filled area indicates the actin in front of the nucleus. **(G)** Quantification of LifeAct **(G)** signal accumulation in the posterior 15% of the cell length for control mDCs or mDCs treated with 10 µM Y-27632 migrating in 8 × 4 µm, 5 × 4 µm, and 3 × 4 µm microchannels. Each dots and error bars represent the mean and 95% confidence interval, respectively, of one independent experiment. **(H)** Speed of control mDCs or mDCs treated with 10 µM Y-27632 migrating in 8 × 4 µm, 5 × 4 µm, and 3 × 4 µm microchannels. Each dot and error bars represent the mean and 95% confidence interval, respectively, of one independent experiment. ANOVA with Tukey's multiple comparison test was used; **p < 0.05, **p < 0.01, *above data points indicates the comparison between Control and* Y-27632 conditions for each microchannel sizes, *with bars indicates the comparison between 8 × 4 µm and 3 × 4 µm microchannels for each treatment condition. Dataset re-analyzed from Barbier et al., 2019; supplementary figure 2 A and B.

To conclude this section, mDCs adapt their mode of migration to varying dimensions. This plasticity is associated with cytoskeleton reorganization and accumulation of actin and myosin at the posterior of the cell. Cytoskeleton remodeling is dynamic and controlled by ROCK signaling. This cell reaction to varying dimensions suggests the presence of a mechano-response and a cellular sensor for confinement. The next section focuses on the effect of mDC confinement in microchannels of different sizes on the intracellular organization of mDCs to identify a mechanosensitive structure.

III. Impact of confinement on the intracellular organization of mature dendritic cells.

A. Confined migration decreases actin fraction at the nucleus and triggers rupture of the perinuclear lamina

First, we focused on the nucleus because it has been described as the main factor limiting cell migration in confined spaces. Immature DCs have a specific Arp2/3-dependent actin network that promotes nuclear deformation in narrow pores (Thiam et al., 2016). However, this mechanism has not been studied in mDCs. Moreover, it has recently been shown that cells can rely on their nuclei to modulate their contractility in confined spaces. Cell confinement below the resting nuclear size activates cortical MyoII through nuclear envelope stretch-sensitive signaling pathways (Lomakin et al., 2019). In our system, microchannel narrowing affects the nuclear dynamics. As mentioned in the methods, the nuclear shape may fluctuate in the 8 × 4 µm microchannels, and the nucleus is elongated and constrained in the 3 × 4 µm microchannels. This raises a question regarding whether this mechano-response could be involved in the adaptation of mDCs to microchannel sizes.

As mentioned above, the MyoII-GFP signal is not detected in the nuclear zone; therefore, we focused on actin and its interaction with the nucleus in microchannels of different sizes. In the 8 × 4 µm microchannels, the location of actin fluctuated and it was localized, on average, at the nucleus position in the center of the cell (Fig.36 A and B). In 3 × 4 µm microchannels, the nucleus was displaced toward the anterior of the cell and is devoid of actin (Fig.36 C and D). The actin fraction in the nuclear area was significantly reduced in microchannels smaller than 5 × 4 µm (Fig.36 E). This threshold suggests a specific effect of high degrees of confinement.

In width-varying microchannels, the actin fraction in the nuclear area began to decrease at the position where the nucleus entered the constriction and reached a minimum value 100 µm after the constriction (Fig.36. H and G). This distance corresponds to the average distance at which mDCs recover their pre-constriction velocity. This remodeling was slower than the actin structure in the posterior end of the cell. The loss of nuclear actin does not appear to be a rapid response induced by cell confinement but is rather related to cell movement in narrow spaces.

The behavior of nuclear actin seems to be the opposite of the behavior observed in iDCs facing shorter (15 µm length) but narrower (2 µm width) constrictions. Therefore, we evaluated the actin dynamics in iDCs in our set-up. We observed a transient actin accumulation around the nucleus at

the constriction. This observation is consistent with the Arp2/3-dependent structure already characterized in iDCs but not observed in mDCs. However, the nuclear actin fraction in iDCs also decreased after the constriction (Fig.36 G). The different actin dynamics at the constriction confirms the specific needs for nuclear deformation in immature or mature DCs. Immature DCs rely on the Arp2/3-dependent network, whereas mDCs require MyoII-dependent forces and do not assemble an actin lattice around the nucleus.

However, in both states, the nuclear area is depleted of actin after prolonged deformation, which suggests long-term adaptation to migration in confinement. Remarkably, iDC nuclei without lamin A/C do not induce actin recruitment in narrow pores (Thiam et al., 2016). Therefore, we investigated whether the decrease in the nuclear actin fraction would be associated with nucleoskeletal remodeling. We studied the effect of migration in microchannels of different sizes on the nuclear lamin A/C envelope using immunofluorescence staining. As the equivalent diffusion of antibodies was not controlled for each microchannel geometry, our system did not allow us to compare lamin A/C quantities between different conditions. However, we were still able to study its organization. Migration of mDCs in microchannels triggers the rupture of the nuclear lamina envelope and DNA herniation. The percentage of cells showing interrupted staining of the perinuclear laminar increased with microchannel narrowing, from 20% in 8 × 4 µm microchannels to 70% in 3 × 4 µm microchannels. This first result suggests that the loss of nuclear actin could be due to lamina network disruption. It should be noted that we had reduced the length of the microchannel to only 100 µm to ensure sufficient antibody diffusion. Therefore, we could not confirm whether the rupture is maintained during mDC migration and whether it is actively associated with the loss of nuclear actin. In addition, the lamina rupture may be followed by a complete remodeling of the nuclear skeleton. We could complete this study by staining the phosphorylated lamin A/C an early step of perinuclear lamina disassembly (Ward and Kirschner, 1990).

Based on these observations, we could wonder whether lamina rupture is associated with nuclear envelope openings. Indeed, successive blebbing and ruptures of the nuclear envelope could have a long-term impact on mDC biology as they trigger DNA damage. Nuclear envelope disruption followed by DNA damage has been observed in iDCs migrating in microchannels and also in mouse skin ear explants. However, it occurs in only 55% or 10% of the iDCs migrating through 3 or 5 µm width constrictions, respectively (Raab et al., 2016). Therefore, these events may be more frequent in mDCs.

The nuclear envelope rupture could be further investigated using mDCs expressing a fluorescent protein linked to a nuclear localization sequence (NLS). When the nuclear envelope is ruptured, the NLS signal leaks into the cytoplasm. Such cells would facilitate the detection of potential nuclear envelope rupture in living mDCs (Raab et al., 2016). We could investigate whether the nuclear envelope rupture is associated with a decrease in the nuclear actin fraction, but also with the speed recovery after the constriction. Indeed, lamin A/C-dependent nuclear rigidity is an obstacle to cell migration under confinement (Harada et al., 2014). Lamina rupture may soften the nucleus, thus decreasing the nuclear resistance to mDC migration in narrow microchannels.

This raises a question regarding the interplay between MyoII and perinuclear lamina rupture. Indeed, in iDCs, the Arp2/3 network weakens the lamin A/C shell to favor nuclear deformation (Thiam et al., 2016). We could test the hypothesis that MyoII plays this role in mDCs by assessing the percentage of interrupted staining of the perinuclear lamina in blebbistatin- or Y-27632-treated cells. Thus, MyoII may be required to weaken the lamin A/C shell and reduce nuclear resistance to mDC migration in narrow space. We can also use lamin A/C-depleted mDCs and study their requirement for MyoII-dependent contractility in microchannels of different dimensions. Preliminary experiments have shown that lamin A/C depletion does not affect mDC velocity in any of the microchannels (data not shown). The experiments should be combined with blebbistatin or Y-27632 to established whether lamin A/C-depleted cells require MyoII activity in 3 × 4 µm microchannels. This set of experiments would demonstrate whether nuclear stiffness is the main obstacle to mDC migration under confinement and whether contractile forces produced by MyoII are specifically required to deform mDC nuclei.

Regarding the question of the mechano-response, the nuclear envelope stretch-sensitive signaling pathway depends on the lamina integrity as it governs nuclear envelope tension (Lomakin et al., 2019). Thus, the presence of breaks in the lamin A/C lattice and the efficient migration of lamin A/C-depleted cells suggest that this signaling pathway is not involved in the adaptation of mDCs to different microchannel dimensions. In particular, even if the nuclear shape fluctuates in 8 × 4 µm microchannels, the nucleus is already constrained by the 4 µm height. Thus, the variation between the 8 × 4 µm and 3 × 4 µm microchannels could be below the detection threshold of the nucleus and could involve other cell structures. In previous experiments, we were intrigued by the actin accumulation observed between the nucleus and the posterior of the cell in 3 × 4 µm microchannels. We investigated whether this actin recruitment could be related to the presence of a mechano-sensitive structure in this area.

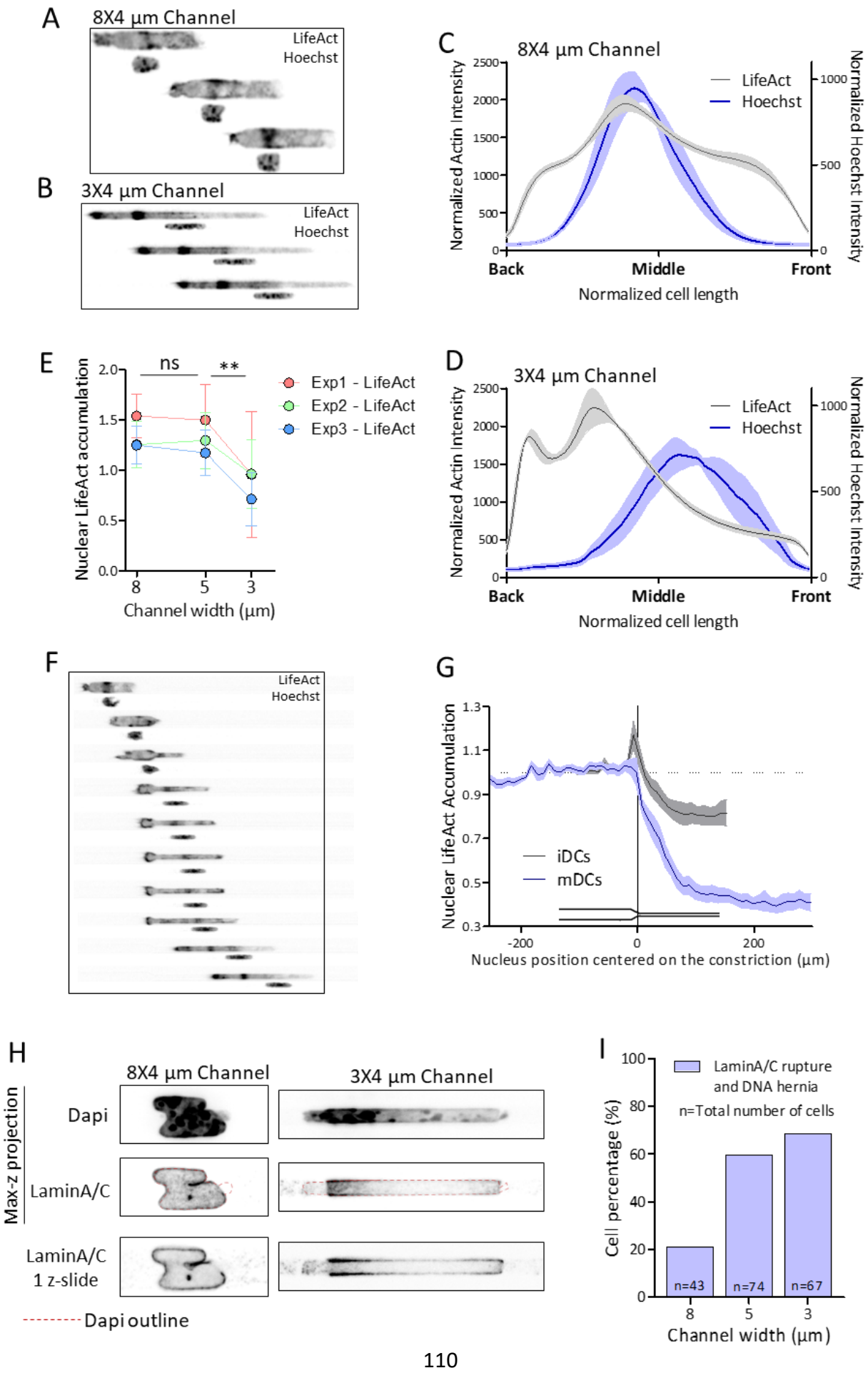
A
8X4 µm Channel
LifeAct
Hoechst
B
3X4 µm Channel
LifeAct
Hoechst
C
8X4 µm Channel
LifeAct
Hoechst
Normalized Actin Intensity
Normalized Hoechst Intensity
Back
Middle
Front
Normalized cell length
D
3X4 µm Channel
LifeAct
Hoechst
Normalized Actin Intensity
Normalized Hoechst Intensity
Back
Middle
Front
Normalized cell length
E
ns
**
Exp1 - LifeAct
Exp2 - LifeAct
Exp3 - LifeAct
Nuclear LifeAct accumulation
Channel width (µm)
F
LifeAct
Hoechst
G
Nuclear LifeAct Accumulation
iDCs
mDCs
Nucleus position centered on the constriction (µm)
H
8X4 µm Channel
3X4 µm Channel
Max-z projection
Dapi
LaminA/C
LaminA/C
1 z-slide
Dapi outline
I
LaminA/C rupture
and DNA hernia
n=Total number of cells
Cell percentage (%)
n=43
n=74
n=67
Channel width (µm)

Figure 36 Confinement decreases actin recruitment at the nucleus and triggers lamina rupture
(A-B) Representative montage of an image sequence of a LifeAct-mDC migrating in 8 × 4 µm **(A)** and 3 × 4 µm **(B)** microchannels. Montages show Hoechst signal under the LifeAct signal. **(C-D**) Intensity profile of mean LifeAct and Hoechst signal density map of mDCs migrating in 8 × 4 µm **(C)** and 3 × 4 µm **(D)** microchannels. The curve and filled area represent the mean and the standard error of the mean (SEM), respectively, of three independent experiments. **(E)** Quantification of the LifeAct signal accumulation in the mask of the nucleus of mDCs migrating in 8 × 4 µm, 5 × 4 µm, and 3 × 4 µm microchannels. Each dot and error bars represent the mean and standard deviation, respectively, of one independent experiment. **(F)** Representative montage of an image sequence of a LifeAct-mDC migrating in microchannels varying from 8 × 4 µm to 3 × 4 µm width. Montages show Hoechst signal under the LifeAct signal**. (G)** Mean LifeAct signal accumulation in the mask of the nucleus of mDCs or iDCs migrating in microchannels varying from 8 × 4 µm to 3 × 4 µm as a function of the nuclear position from the constriction. The curve and error bars represent the mean and the SEM, respectively, of 36 cells for mDCs and 29 cells for iDCs from one experiment. **(H)** Representative confocal spinning-disk images of ruptured nuclei stained with DAPI and antibodies against lamin A/C inside 8 × 4 µm (left) or 3 × 4 µm (right) microchannels. **(I)** Quantification (percentage) of cells showing interrupted staining of perinuclear lamin A/C with DNA herniation inside 8 × 4 µm, 5 × 4 µm, and 3 × 4 µm microchannels. n indicates the total number of cells for each condition in one experiment. ANOVA with Tukey's multiple comparison test was used; **p < 0.01.

B. Confinement triggers actin accumulation around the lysosomes and Golgi apparatus clustered around the microtubule organizing center.

1. Actin and microtubule interplay during confined migration.

Cells using an amoeboid migration mode typically have the microtubule organizing center (MTOC) located posterior to the nucleus (Kopf et al., 2020). Moreover, in B cells, an Arp2/3-dependent actin network nucleates from the centrosome and regulates the relocalization of the microtubule spindle to the immune synapse (Obino et al., 2016). Thus, we hypothesized that the actin accumulation observed posterior to the nucleus in the 3 × 4 µm microchannels could be related to the MTOC. Therefore, we investigated the microtubule network organization and its interplay with actin by immunofluorescence staining.

The microtubule network has never been studied in mDCs migrating in microchannels. Thus, we first focused on its organization in microchannels of different dimensions using super-resolution spinning-disk confocal imaging. The lattice was polarized with more microtubules towards the anterior of the cell than towards the posterior (Fig.37 A-B). This anterior-to-posterior polarization has already been described in two-dimensional migration of mDCs confined between parallel plates (Kopf et al., 2020) and tumor cells confined in microchannels (Balzer et al., 2012). However, confinement in microchannels also induced an anisotropy of the network. Indeed, most of the microtubules were oriented parallel to the migration axis imposed by the microchannel. This anisotropy was enhanced in narrow microchannels (3 × 4 µm or 4 × 4 µm microchannels), particularly at the MTOC. In wide microchannels (8 × 4 µm or 7 × 4 µm microchannels), microtubules radiated in all directions from the MTOC, whereas in narrow microchannels, they were preferentially oriented at an angle close to 0° to the migration axis (Fig.37 C-D).

In addition, we also noticed some dense microtubule bundles between the MTOC and the nucleus in narrow microchannels. Such structures were not observed in wide microchannels (Fig.37 A-B). Changes in the microtubule bundles may be related to their stabilization. We could investigate the relative microtubule dynamics in different microchannels using staining to identify specific tubulins post-translational modifications. In particular, microtubule detyrosination and acetylation are markers of long-lived microtubules (Wloga et al., 2017). However, most antibodies directed against post-translational modifications of tubulins require fixation with ice-cold methanol, which is not compatible with PDMS chambers. As an alternative, we could use micropatterned adherent areas to perform a preliminary screening of microtubule post-translational modifications in mDCs confined on two-dimensional opened surfaces (van den Dries et al., 2012).

Therefore, the results suggest that confinement induces microtubule remodeling, which still requires further characterization and a larger number of imaged cells. The direct effect of this remodeling remains unknown. However, microtubule disassembly increases the number of mDC directional oscillations in the 8 × 4 µm microchannels (Kopf et al., 2020). Therefore, microtubule remodeling may govern persistent mDC migration in confined microenvironments.

Remarkably, constraints on the MTOC result in an area perpendicular to the migration axis devoid of microtubules. We found the central actin structure near this zone in narrow microchannels (Fig.37 A-B). Indeed, on mean intensity profiles, the central actin accumulation was at the mean MTOC position, whereas no actin accumulation was observed in the wide microchannels in this zone (Fig.37 E to H).

We used orthogonal views to precisely characterize this structure. Sections on the MTOC were compared with sections taken between the MTOC and the nucleus (Fig.37 B; markings 1 and 2, respectively, and I-K). In the MTOC section, the tubulin signal was concentrated in the center, which corresponds to the centrosomal network without microtubules perpendicular to the microchannel axis. The mean cortical actin signal in the MTOC section was 50% stronger than the mean value measured over the entire cell length. Remarkably, there was an interval between the tubulin intensity peak and the two cortical actin peaks (Fig.37 I and K). Thus, although the actin structure is localized at the MTOC position, it does not nucleate from the centrosome and is limited to the cell cortex. Anterior to the MTOC, the microtubules were more dispersed throughout the section, with a few filaments close to the cellular cortex. In this area, the mean actin intensity was close to the mean value measured over the entire cell length, without significant accumulation in the cortex (Fig.37 J and L).

Therefore, the central actin structure observed in the narrow microchannels localizes at the MTOC. However, it is limited to the cell cortex and does not nucleate directly from the MTOC. This leads to the question regarding whether other intracellular structures are located in the area between the MTOC and cell cortex and could be associated with the central actin structure.

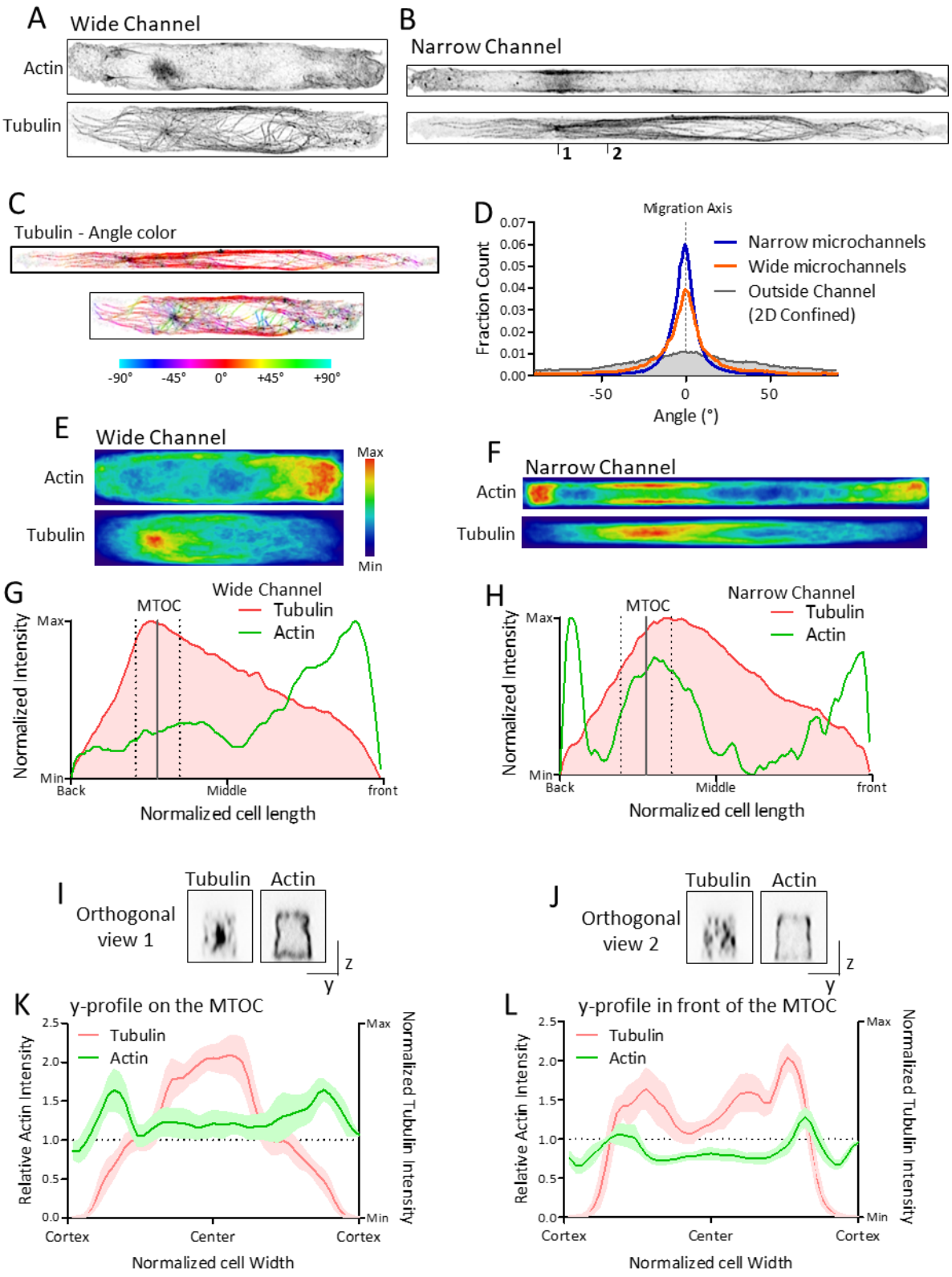
A
Wide Channel
Actin
Tubulin
B
Narrow Channel
1
2
C
Tubulin - Angle color
-90°
-45°
0°
+45°
+90°
D
Migration Axis
Fraction Count
0.07
0.06
0.05
0.04
0.03
0.02
0.01
0.00
-50
0
50
Angle (°)
Narrow microchannels
Wide microchannels
Outside Channel
(2D Confined)
E
Wide Channel
Actin
Tubulin
Max
Min
F
Narrow Channel
Actin
Tubulin
G
Wide Channel
MTOC
Tubulin
Actin
Normalized Intensity
Max
Min
Back
Middle
front
Normalized cell length
H
Narrow Channel
MTOC
Tubulin
Actin
Normalized Intensity
Max
Min
Back
Middle
front
Normalized cell length
I
Orthogonal
view 1
Tubulin
Actin
z
y
J
Orthogonal
view 2
Tubulin
Actin
z
y
K
y-profile on the MTOC
Tubulin
Actin
Relative Actin Intensity
Normalized Tubulin Intensity
Max
Min
2.5
2.0
1.5
1.0
0.5
0.0
Cortex
Center
Cortex
Normalized cell Width
L
y-profile in front of the MTOC
Tubulin
Actin
Relative Actin Intensity
Normalized Tubulin Intensity
Max
Min
2.5
2.0
1.5
1.0
0.5
0.0
Cortex
Center
Cortex
Normalized cell Width

Figure 37 Confinement reinforces microtubule network polarization and triggers cortical actin accumulation around the MTOC.

(A-B) Representative maximum z-projection super-resolution spinning-disk confocal images of fixed mDCs in wide (8 × 4 µm or 7 × 4 µm; **A)** or narrow (4 × 4 µm or 3 × 4 µm; **B)** microchannels stained with phalloidine (Actin; top) and antibodies against α-tubulin (Tubulin; bottom). Markings "1" and "2" indicate the localization of the orthogonal view in I and J. **(C)** Representative tubulin images colored on the basis of the local angle of the stained microtubules. **(D)** Histogram of the angles measured on the tubulin images of cells fixed in narrow (n = 6 cells) and wide (n = 3 cells) microchannels and outside the microchannels (n = 5 cells) from one experiment. Migration axis of the cell was set to 0°. **(E-F)** Mean actin and tubulin signal density map from standard spinning-disk images of fixed mDCs in wide **(E)** and narrow **(F)** microchannels; n = 17 and 19 cells, respectively, pooled from two independent experiments. **(G-H)** Intensity profile of the signal density map shown in E and F, respectively. The vertical line and the dotted line indicate the mean relative position of the MTOC and standard error of the mean (SEM), respectively. **(I-J)** Orthogonal view of the representative cell shown in B, sectioned on the MTOC **(I; marking "1" on the image B)** or anterior to it **(J; marking "2" on the image B). (K-L)** Mean intensity profile measured along the y-axis in a cell section on the MTOC **(K)** or anterior to it **(L)** in cells fixed in narrow microchannels. The actin signal is normalized to the mean intensity profile measured along the y-axis of the entire cell to show relative signal accumulation. The tubulin signal is normalized to the minimum and maximum value to show peak localization. The curve and filled area represent the mean and SEM, respectively, of 6 cells from one experiment.

2. Golgi apparatus and lysosomes form a compact structure clustered on the MTOC surrounded by cortical actin

Both Golgi apparatus and the lysosomal compartment are known to cluster on the MTOC and to associate with actin nucleators.

Lysosomes are dispersed in the cytoplasm. They concentrate in a perinuclear region surrounding the MTOC but are also found at the cell periphery, near the plasma membrane, and in cell protrusions. Their position is mainly regulated by active transport on the microtubule lattice. Kinesins drive vesicle movements toward the cell periphery, whereas dynein-dependent retrograde transport promotes their clustering on the MTOC. At the cell periphery, actin-dependent transport regulates the interaction of lysosomes with the plasma membrane (Pu et al., 2016).

The Arp2/3 activators WASP and WASP and SCAR homolog (WASH) are located on the lysosomal membrane. WASP-dependent polymerization results in actin-rich comet tails that drive lysosome movement within the cell (Taunton et al., 2000). This mechanism is well known to be hijacked by intracellular pathogens such as *Listeria monocytogenes* (Lambrechts et al., 2008). WASH promotes the formation of an actin coating on lysosomal vesicles and regulates their pH by recycling proton pumps (Carnell et al., 2011).

The activation of DCs by LPS sensing triggers lysosomal clustering in the perinuclear region in a Rab34 GTPase-dependent (Alloatti et al., 2015) and TFEB-TRPML1 axis-dependent (Bretou et al., 2017) manner. Lysosomal clustering on the MTOC has not been explicitly demonstrated in mDCs; however, it is the most likely hypothesis. Moreover, the perinuclear lysosomal clustering was found in the vicinity of a dense actin structure dependent on the activation of the TFEB-TRPML1 axis (Bretou et al., 2017).

The Golgi apparatus consists of flat cisternae assembled in a stack. It has been well described as being located near the centrosome in a dynein-dependent manner. Destabilization of the microtubule network triggers fragmentation of the cisternae and disrupts the functions of the Golgi apparatus (Sütterlin and Colanzi, 2010).

The Golgi apparatus is associated with formins and Arp2/3. Some limited actin structures were directly observed on the compartment (Kage et al., 2017b; Zilberman et al., 2011). The formins INF2 (Ramabhadran et al., 2011), FMNL2/3 (Kage et al., 2017b), and FMNL1ϒ (Colón-Franco et al., 2011) promote compaction of the Golgi apparatus, whereas activation of mDia1 triggers its dispersion (Zilberman et al., 2011). Arp2/3-dependent actin polymerization controls vesicle transport to and from the Golgi apparatus, playing a key role in the secretory pathways (Stamnes, 2002). FMNL2/3 is also involved in vesicle trafficking from the Golgi to the plasma membrane (Kage et al., 2017b).

Therefore, the Golgi apparatus and lysosomes are good candidates that could be located near the MTOC and be associated with cortical actin accumulation. To test this hypothesis, we first confirmed their accumulation on the MTOC in mDCs migrating in 3 × 4 µm microchannels using immunofluorescence. We used antibodies specific for LAMP-1 and GM-130 to stain lysosomes and the Golgi apparatus, respectively. We found lysosomes to be concentrated near the MTOC and the Golgi apparatus to be embedded in the lysosomal cluster (Fig.38 A and B). This preliminary structural characterization needs to be confirmed by triple co-staining and accurate three-dimensional colocalization analysis. In addition, we defined the MTOC as the point from which the microtubules

radiate. It should also be further characterized by staining centrosome-related proteins to establish whether it corresponds to the cell centrosome or alternative MTOC.

To study the interaction between cortical actin and this cluster of endomembrane compartments, we used fluorescent wheat germ agglutinin (WGA). Indeed, the WGA signal has been shown to correlate with Lamp-1 positive vesicles in mDCs; thus, WGA staining represents a straightforward method for imaging lysosomes in living mDCs. As observed in fixed samples, a dense cortical actin structure surrounds the lysosomal cluster. However, the area of actin accumulation was not restricted to lysosomal clusters (Fig.38 C). In the orthogonal view, the lysosomes were found in the vicinity of the dense actin cortex. The WGA signal decreased in the center of the cell, which may correspond to the MTOC location (Fig.38 D).

We stained other organelles to examine whether the clustering around the MTOC is specific to lysosomes and the Golgi apparatus. For example, mitochondria were dispersed throughout the cell (Fig.38 E). The study should also be done with ER. Notably, the mitochondrial signal was excluded from the lysosomal area and the nucleus (Fig.38 E and F). This suggests that the endomembrane compartments form a dense cluster around the MTOC. In addition, the lysosomes and nucleus can eventually be confined side by side in a cell constrained by the microchannel, as shown in a cell entering a 3 × 4 µm microchannel. Remarkably, the lysosomal cluster deformed the nucleus (Fig.38 G). Thus, the structure formed by the Golgi apparatus and the lysosomes clustered on the MTOC would have a stiffness equivalent to at least that of the nucleus.

Therefore, we described a compact cluster composed of at least lysosomes and the Golgi apparatus surrounding the MTOC. This structure could be sensitive to confinement, as suggested by its proximity to the dense cortical actin area in the 3 × 4 µm microchannel.

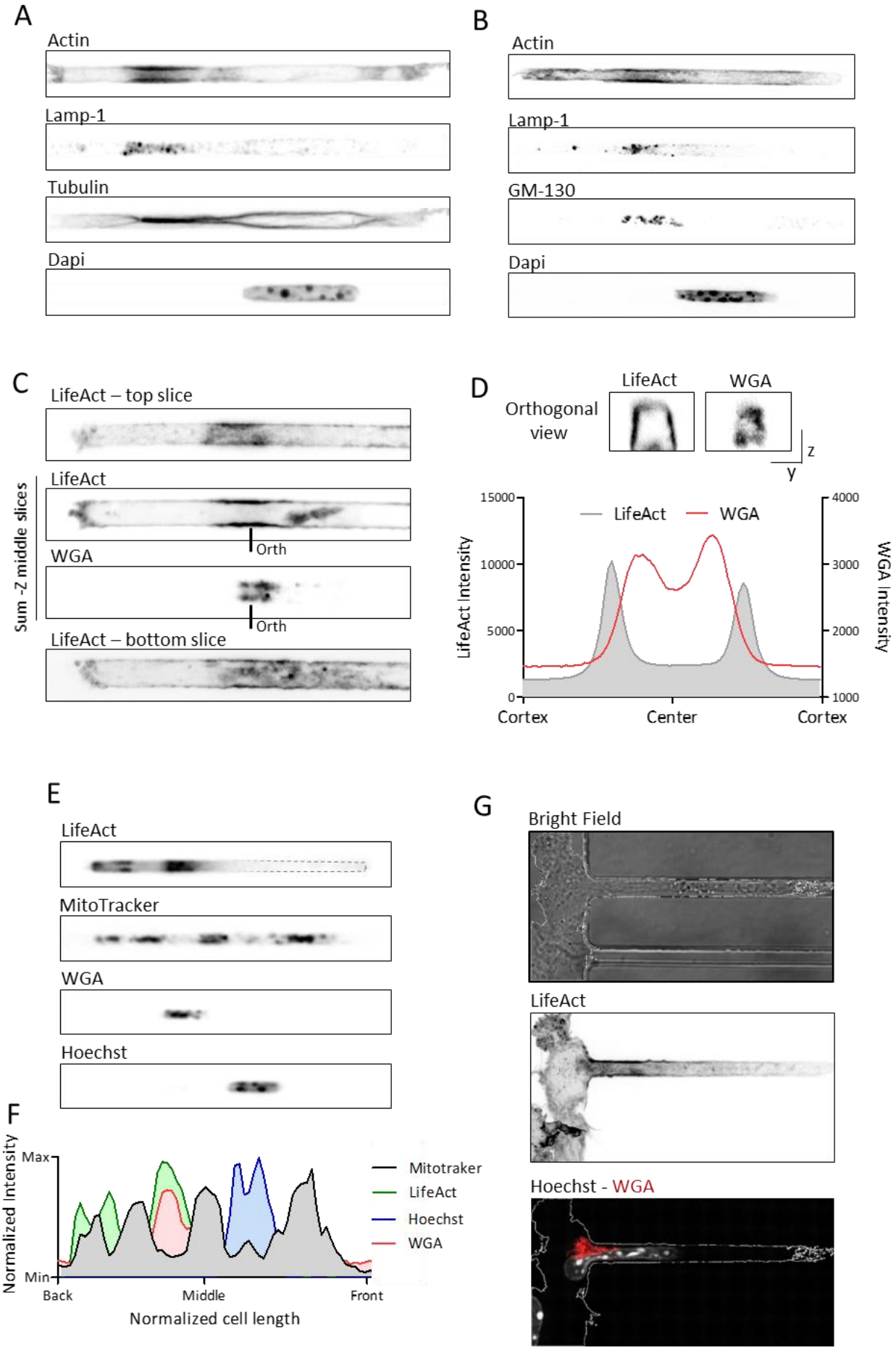
A
Actin
Lamp-1
Tubulin
Dapi
B
Actin
Lamp-1
GM-130
Dapi
C
LifeAct – top slice
LifeAct
Orth
WGA
Orth
LifeAct – bottom slice
Sum -Z middle slices
D
LifeAct
WGA
Orthogonal view
z
y
15000
10000
5000
0
4000
3000
2000
1000
LifeAct
WGA
LifeAct Intensity
WGA Intensity
Cortex
Center
Cortex
E
LifeAct
MitoTracker
WGA
Hoechst
F
Max
Min
Normalized Intensity
Back
Middle
Front
Normalized cell length
Mitotraker
LifeAct
Hoechst
WGA
G
Bright Field
LifeAct
Hoechst - WGA

Figure 38 Lysosomes and the Golgi apparatus form a compact cluster around the MTOC.
(A-B) Representative maximum z-projection spinning-disk confocal images of fixed mDCs in 3 × 4 µm microchannels co-stained with phalloidine (Actin), DAPI, and antibodies against Lamp-1 and α-tubulin (Tubulin; **A**) or Lamp-1 and GM-130 **(B)**. **(C)** Representative z-stack spinning-disk confocal images of a WGA-stained LifeAct-mDC migrating in a 3 × 4 µm microchannel. Only the cell part posterior to the nucleus is shown. **(D)** Orthogonal view of the representative cell shown in C; sections are taken at the marking "Orth" on image C**.** The intensity profile of the orthogonal view measured along the y-axis is shown above. **(E)** Representative images of a LifeAct-mDC stained with WGA, Hoechst and MitoTracker™ (Thermofisher) migrating in a 3 × 4 µm microchannel. **(F)** Intensity profile measured along the x-axis of the four-colored image shown in E. **(G)** Representative images of a LifeAct-mDC stained with WGA and Hoechst entering a 3 × 4 µm microchannel

3. Confinement-induced fast actin accumulation around the lysosomal cluster

To characterize the confinement response of the cluster of lysosomes and Golgi apparatus on the MTOC, we studied its interaction with actin dynamics in the different microfabricated devices. We used WGA staining of the lysosomes as a reporter for the complete structure.

In 8 × 4 µm microchannels, lysosomes were concentrated posterior to the nucleus (Fig.39 A and C; precise measurement not indicated). The lysosomal signal only partially overlapped the actin structure in the center of the cell (Fig.39 C). Confinement in 3 × 4 µm microchannels did not change the relative position of the lysosomes in the cell. Thus, the lysosomal cluster was separated from the forwardly displaced nucleus. The actin structure in the center of the cell colocalized with the WGA signal (Fig.39 B and C). The lysosomal actin fraction tended to increase with the microchannel narrowing; although the statistical test performed on the three experiments did not show significant differences. However, t-tests comparing the lysosomal actin fraction measured in the 3 × 4 µm and 8 × 4 µm microchannels produced a significant p-value within each experiment. Therefore, more experiments should be included to confirm the trend (Fig.39 E).

In width-varying microchannels, the actin fraction in the lysosomal area began to increase at the position where the lysosomes entered the constriction and reached a plateau 70 µm after the constriction (Fig.39 F and G). This actin remodeling was faster than that observed on the nucleus but delayed in comparison with the actomyosin accumulation in the posterior end of the cell. Actin

recruitment in the lysosomal zone is a rapid response to its local confinement and appears to be independent of the constraints applied to the rest of the cell.

Because microbial sensing affects both the structure and the biochemical composition of the lysosomal cluster, we investigated whether iDCs also exhibit this mechanical response. We did not observe a significant increase in the lysosomal actin fraction in iDCs after the constriction (Fig.39 G). Therefore, actin recruitment upon lysosomal confinement is specific to mDCs. The particular feature induced by DC activation responsible for this mechano-response remains to be established. It may be related to lysosomal clustering, modification of actin nucleator activity, or antigen processing and signaling from the lysosomes.

Finally, rapid migration in the interstitial space is a hallmark of mDCs, thus, we explored the potential link between the lysosomal actin fraction and cell velocity after the constriction. Correlation analysis did not reveal a significant relationship between these two parameters (Fig.39 H). Thus, although this actin structure is a response to cell confinement, it does not seem to be involved in the adaptation of the migration machinery to physical constraints. In agreement with this finding, we did not observe any accumulation of MyoII-GFP signals in the lysosomal area after the constriction (Fig.39 I). The actin structure does not correspond to a contractile network.

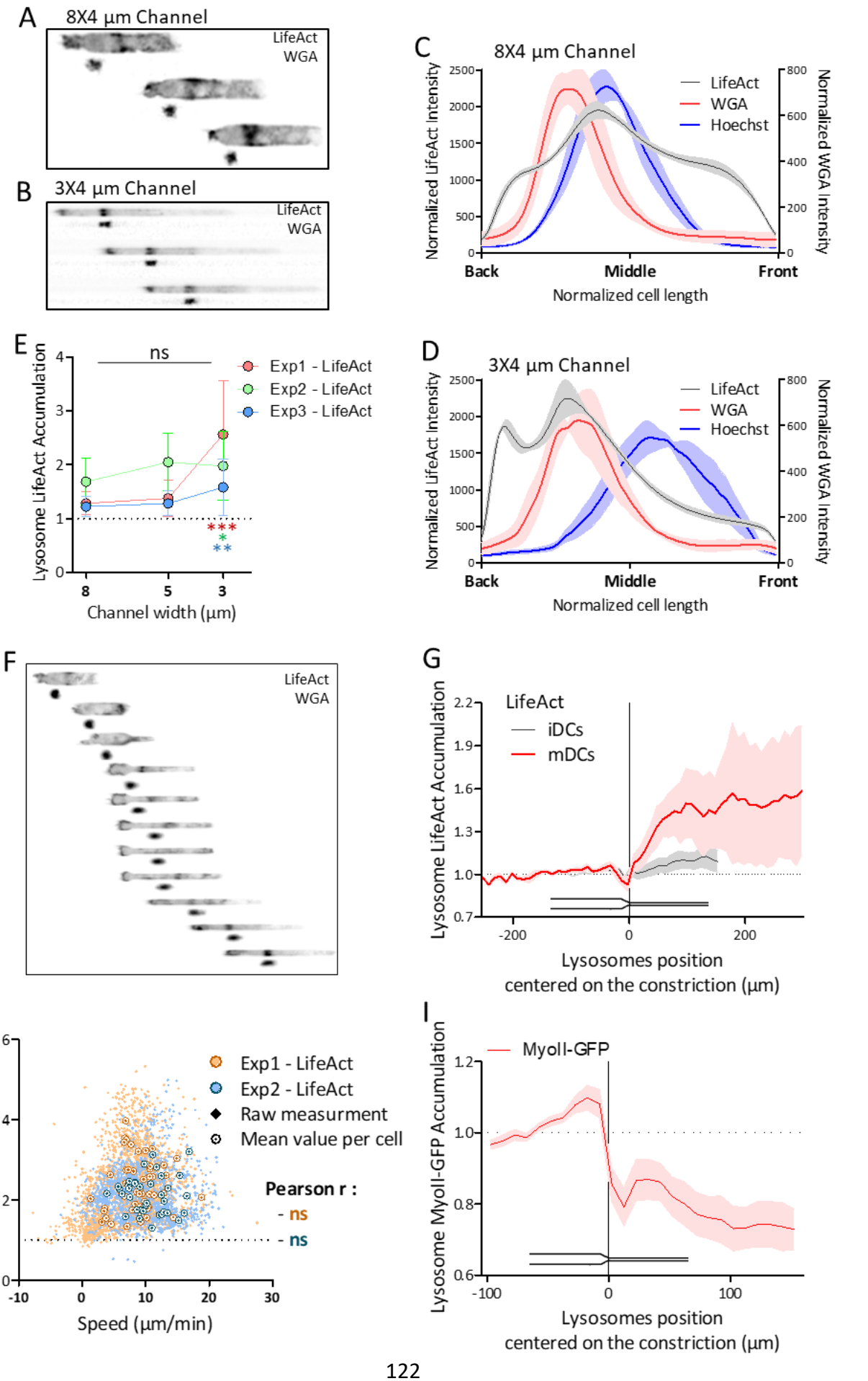
A
8X4 µm Channel
LifeAct
WGA
B
3X4 µm Channel
LifeAct
WGA
C
8X4 µm Channel
Normalized LifeAct Intensity
Normalized WGA Intensity
LifeAct
WGA
Hoechst
Back
Middle
Front
Normalized cell length
D
3X4 µm Channel
Normalized LifeAct Intensity
Normalized WGA Intensity
LifeAct
WGA
Hoechst
Back
Middle
Front
Normalized cell length
E
ns
Exp1 - LifeAct
Exp2 - LifeAct
Exp3 - LifeAct
Lysosome LifeAct Accumulation
Channel width (µm)
F
LifeAct
WGA
G
LifeAct
iDCs
mDCs
Lysosome LifeAct Accumulation
Lysosomes position
centered on the constriction (µm)
H
Exp1 - LifeAct
Exp2 - LifeAct
Raw measurment
Mean value per cell
Pearson r :
- ns
- ns
Lysosome LifeAct Accumulation
Speed (µm/min)
I
MyoII-GFP
Lysosome MyoII-GFP Accumulation
Lysosomes position
centered on the constriction (µm)

Figure 39 Confinement of the lysosomal area triggers a rapid cortical actin accumulation

(A-B) Representative montage of an image sequence of a LifeAct-mDC migrating in 8 × 4 µm **(A)** and 3 × 4 µm **(B)** microchannels. The montages show WGA signal under the LifeAct signal. **(C-D**) Intensity profile of mean LifeAct, WGA, and Hoechst signal density map of mDCs migrating in 8 × 4 µm **(C)** and 3 × 4 µm **(D)** microchannels. The curve and filled area represent the mean and standard error of the mean (SEM), respectively, of three independent experiments. **(E)** Quantification of LifeAct signal accumulation in the lysosomal mask of the lysosomes in mDCs migrating in 8 × 4 µm, 5 × 4 µm, and 3 × 4 µm microchannels. Each dot and error bars represent the mean and standard deviation, respectively, of one independent experiment. **(F)** Representative montage of an image sequence of a LifeAct-mDC migrating in a microchannel varying from 8 × 4 µm to 3 × 4 µm width. The montages show WGA signal under the LifeAct signal**. (G)** Mean LifeAct signal accumulation in the mask of the lysosomes in mDCs or iDCs migrating in a microchannel varying from 8 × 4 µm to 3 × 4 µm as a function of the lysosomal position from the constriction. The curve and error bars represent the mean and the SEM, respectively, of 36 cells for mDCs and 29 cells for iDCs from one experiment. **(H)** Correlation between cell speed and LifeAct signal accumulation in the mask of the lysosomes measured in the first 250 µm after the width variation from 8 µm to 3 µm **(I)** Mean MyoII-GFP signal accumulation in the mask of the lysosomes in mDCs migrating in a microchannel varying from 8 × 4 µm to 3 × 4 µm as a function of the lysosomal position from the constriction. The curve and error bars represent the mean and SEM, respectively, of 112 cells from one experiment. ANOVA with Tukey's multiple comparison test was usedon the three experiments as statistical test. *below data points indicate t-test applied within each experiment to compare between 3 × 4 µm and 8 × 4 µm microchannels *$p < 0.05$, **$p < 0.01$, ***$p < 0.001$

In addition, to confirm actin recruitment in a more physiological setting, we observed mDCs in a collagen gel guided by a gradient of CCL19 (soluble version of CCL21). A transient actin patch appears around the lysosomes each time the cluster deforms between collagen fibers (Fig.40 A).

Finally, we investigated whether actin remodeling requires cell migration or whether it is directly associated with lysosomal confinement in a static set-up. We used the cell confiner developed in the laboratory (Le Berre et al., 2014). In brief, mDCs were plated on a glass-bottom dish coated with fibronectin. A glass slide with sparse PDMS micropillars of a precise height is placed onto the glass-bottom dish. It triggers a rapid uniaxial compression of the cells. The micropillar

height (1.5 µm) define the confinement height. This configuration allowed us to follow an mDC before and a few seconds after the confinement. We observed an actin burst in the lysosomal zone just after compression. It oscillates (not shown) and then stabilizes within the minute following confinement (Fig.40 B). Notably, lysosomes were dispersed upon cell compression, whereas no change in their area was observed in microchannels (data not shown). A longer observation should be made to examine whether the compact cluster re-formed a few minutes after confinement.

Therefore, using lysosomal staining as a reporter, we characterized a cortical actin accumulation dynamically triggered by the confinement of the endomembrane compartments clustered on the MTOC. It corresponds to a rapid, local, and specific response to mDCs confinement.

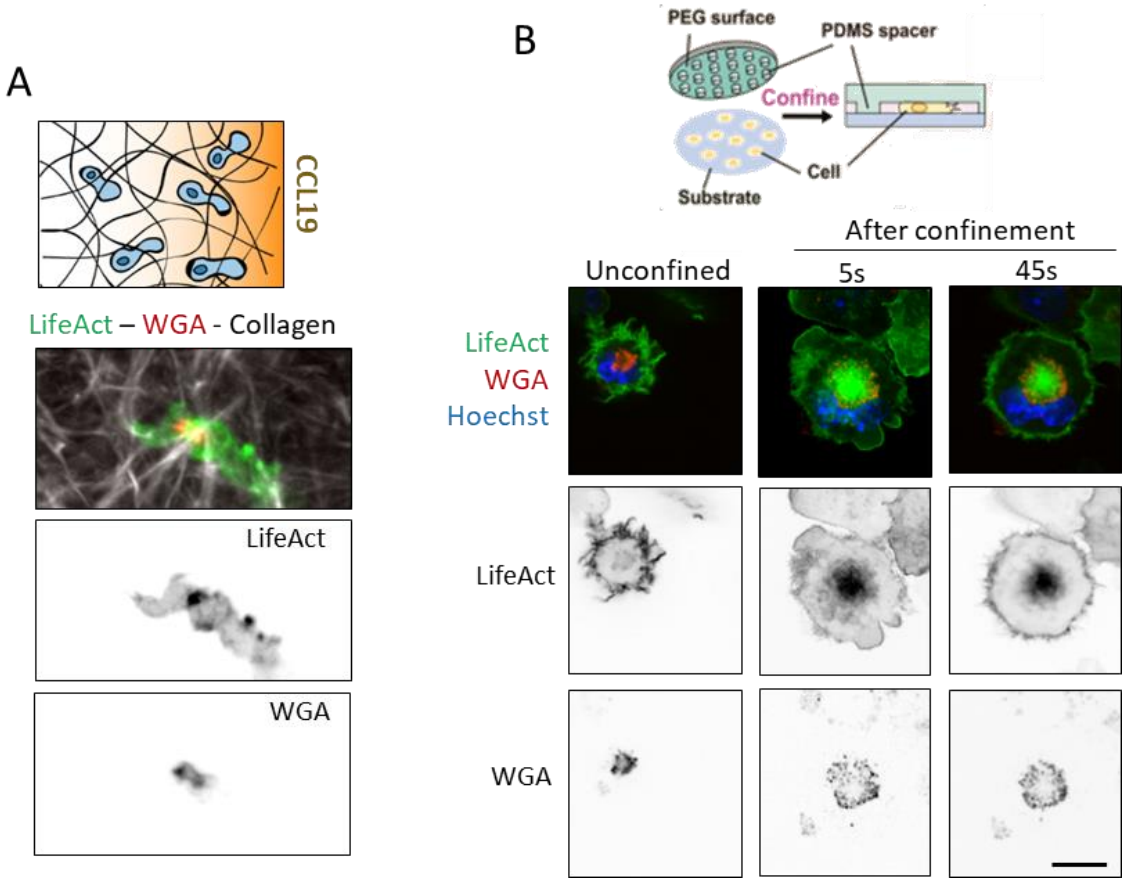

Figure 40 Lysosomal actin accumulation in collagen gels and upon uniaxial confinement

(A) Representative images of a LifeAct-mDC migrating in a collagen gel with CCL19 gradient. **(B)** Representative images of LifeAct-mDC before (right) and 5 seconds (center) and 45 seconds (left) after fast uniaxial compression. Scale bar = 10 µm.

4. Confinement-induced lysosomal actin network is dependent on formin activity.

To study the signaling pathway leading to the accumulation of lysosomal actin upon confinement, we first attempted to identify the actin nucleator involved. In iDCs, the actin network induced by confinement around the nucleus depends on the Arp2/3 activity (Thiam et al., 2016). We evaluated the effect of Arp2/3 in mDCs by using a pharmacological inhibitor, CK666 (Hetrick et al., 2013). Arp2/3 inhibition did not disrupt the overall actin organization in mDCs migrating in 3 × 4 µm microchannels. In particular, the lysosomal actin fraction remained unchanged (Fig.41 A-B).

Microbial detection leads to actin remodeling in mDCs: Arp2/3 activity decreases, whereas formin mDia1 becomes the main actin nucleator in the posterior part of the cell (Vargas et al., 2016). Therefore, we tested the effect of the general formin inhibitor, SMIFH2 (Rizvi et al., 2009). Formin inhibition decreased the lysosomal actin fraction and did not affect the actomyosin structure in the posterior end of the cell (Fig.41 C-D). This finding suggests that formins nucleate the lysosomal actin network and is consistent with the absence of this structure in iDCs. Remarkably, the lysosomal area was larger in SMIFH2-treated cells than in control cells in 3 × 4 µm microchannels (Fig.41 E). This suggests that formin inhibition leads to the dispersion of lysosomal vesicles under confinement. Thus, the cortical actin network may form an enclosure necessary to maintain the organelles clustered around the MTOC under physical constraints. The impact of lysosome dispersion remains unknown but may affect antigen processing (Alloatti et al., 2015).

However, a reduced number of SMIFH2-treated cells was observed in the microchannels, particularly in the 3 × 4 µm microchannels (Fig.41 D-E), suggesting that formin activity favors cell entry into the microchannels. This leads to a limited number of cells being analyzed, and the results need to be confirmed. Moreover, SMFH2 is known as an unstable molecule with several side effects on myosins (Sellers et al., 2020) and on microtubules and the Golgi apparatus through inhibition of p53 (Isogai et al., 2015). In a more specific approach, we tested mDCs depleted of a particular formin. We first focused on mDia1 as its activity is essential for the rapid migration of mDCs into the interstitial space (Vargas et al., 2016). However, a preliminary experiment (data not shown) showed no significant effect. We also tested the formin-like 1 (FMNL1) because its expression level in mDCs is similar to that of mDia1 (Mathilde Bernard; personal communication). Moreover, FMNL1 is essential for the migration of effector T cells to the site of injury. Precisely, FMNL1 nucleates actin in the posterior end of the T lymphocytes and promotes nuclear passage of the nucleus in confined environments (Thompson et al., 2020). In a preliminary experiment, FMNL1 depletion affected

neither mDC velocity in 3 × 4 µm microchannels nor their passage rate through constrictions. However, the presence of the lysosomal actin structure induced in a confined environment needs to be investigated in FMNL1-depleted cells.

From another perspective, the structure of lysosomal actin could not be attributed to local actin polymerization but to the accumulation of already formed actin filaments. Increased actin cross-linking or anchoring to the plasma membrane may induce this local aggregation of cortical actin. This hypothesis can be tested by studying the localization of ezrin, radixin, and moesin proteins and the activity of actin-bundling proteins. Notably, two actin-bundling proteins—fascin-1 and filamin—are overexpressed after DC maturation and are potential candidates (Lamsoul et al., 2013; Yamakita et al., 2011).

Therefore, preliminary results suggest that confinement triggers a formin-dependent accumulation of actin filaments in the lysosomal area. However, this finding should be confirmed, and the specific formin should be identified. Identification of the proteins involved in the assembly of this structure would be a key to study the signaling pathway induced by the confinement and the function of this actin network.

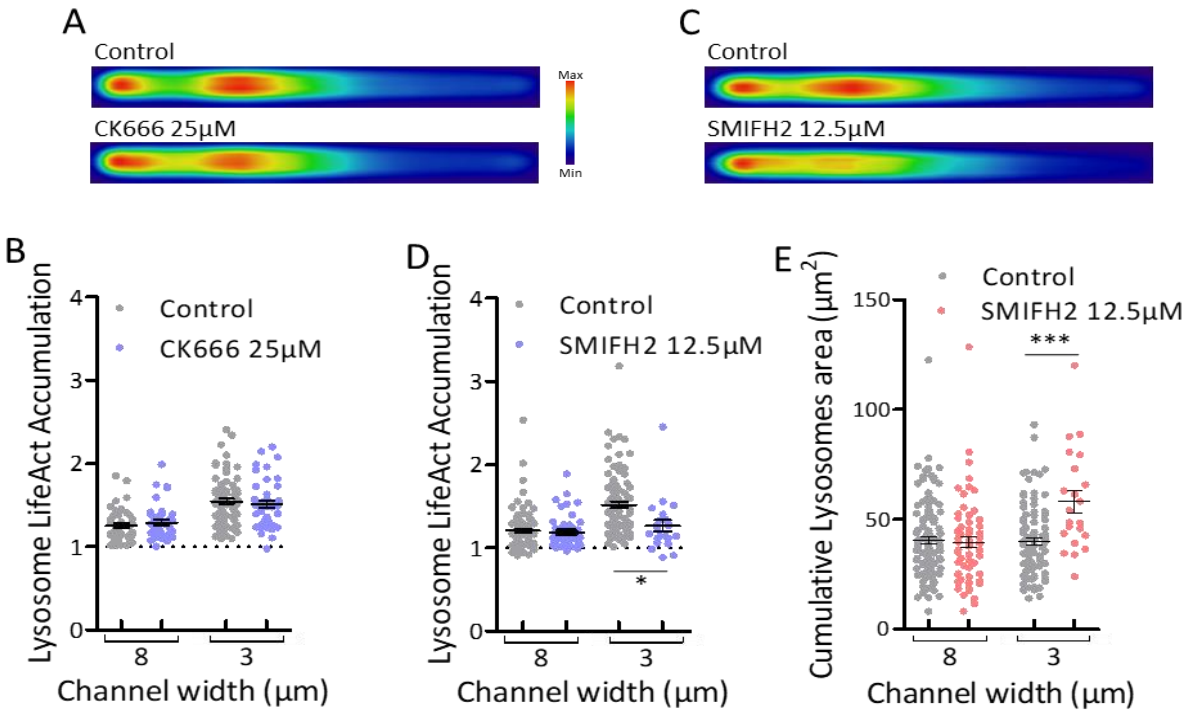

Figure 41 Investigation of the actin nucleator involved in the lysosomal network.
(A and C) *Mean LifeAct signal density map of LifeAct-mDCs migrating in 3 × 4 µm microchannels treated with CK666 (Tocris 25 µM;* ***A****) SMIFH2 (Tocris 12.5 µM;* ***C****), or an equivalent quantity of DMSO as control.* ***(B and D)*** *Quantification of LifeAct signal accumulation in the mask of the lysosomes in mDCs migrating in 8 × 4 µm and 3 × 4 µm microchannels under the same conditions and experiments as those in A and C. The dots represent single cells; the bars and error bars represent the mean and standard error of the mean (SEM), respectively.* ***(E)*** *Total area of the mask of the lysosomes in mDCs migrating in 8 × 4 µm and 3 × 4 µm microchannels under the same conditions and experiment as those in C. The dots represent single cells; the bars and error bars represent the mean and SEM,*

5. Microtubule depolymerization affects the confinement-induced actin network at the center of the cell

As another approach to study the function of the confinement-induced lysosomal actin, we disrupted the organelle cluster on the MTOC. We treated mDCs with 5 µM nocodazole, followed by a 30 min incubation on ice, to achieve complete disruption of the microtubule network (Fig.42 A). As expected, treatment with nocodazole resulted in the dispersion of the lysosomal vesicles. However, they remained posterior to the nucleus (Fig.42 B-D). Microtubule depolymerization increased the number of changes in the cell direction, and mDCs oscillated in the microchannels. This effect is consistent with the role of the microtubule network in maintaining the anterior-to-posterior polarity of leukocytes (Kopf et al., 2020; Prentice-Mott et al., 2016). However, our analysis of actin organization required that cells maintain the same orientation for at least eight time points. Therefore, the number of usable cells was low, particularly for nocodazole-treated cells in the 8 × 4 µm microchannels, and quantitative analysis was not performed under this condition.

The actin fraction in the posterior end of the cell increased in nocodazole-treated cells in both 8 × 4 and 3 × 4 µm microchannels (Fig.42 B-C and E to H). This may be due to the enhanced contractility owing to nocodazole treatment. Indeed, microtubule depolymerization releases RhoA GEFs from the lattice, which activate Rho-dependent contractility (Kopf et al., 2020). In the 3 × 4 µm microchannels, the actin structure in the center of the cell was lost, and no accumulation of actin was observed on the dispersed lysosomes (Fig.42 C and F to H). Approximately 25% of the cells still showed a thin dense structure of actin in the center of the cell but outside the lysosomal area, as shown in Fig.42 C. This structure is often associated with cell pinching and may be due to small

resistant microtubules on a remaining MTOC. This hypothesis can be verified using immunofluorescence staining of cells treated with nocodazole. Moreover, nocodazole treatment should be combined with Y-27632 to decipher whether the loss of the central actin network was due to increased contractility or to depolymerization of microtubules and dispersion of organelles.

We then investigated whether the cell oscillation was related to actin loss in the 3 × 4 µm microchannels. The study of the full cell tracks showed a decrease in cell velocity, persistence time, and persistence length in nocodazole treatment in both 3 × 4 µm and 8 × 4 µm microchannels (Fig.42 I-K). Therefore, loss of central actin in the 3 × 4 µm microchannels may not be responsible for cell oscillation because it occurred in all microchannels. However, more experiments are required to confirm this trend.

Another known effect of nocodazole treatment is fragmentation of mDCs migrating in complex environments. Indeed, the microtubule signal is essential in triggering the retraction of cell branches during decision making in bifurcated microchannels or in a dense porous environment. The MTOC follows the nucleus after the choice of a path, which provokes the depolymerization of the microtubules from the side branches and their retraction. In the absence of microtubules, mDCs extend branches in different directions. They become entangled and eventually get fragmented. The structure of actin in the lysosomal zone may play a role in this process of maintaining cell integrity, particularly when physical constraints increase the distance between the nucleus and the MTOC. Thus, the actin network may be involved in (i) preventing the dispersal of lysosomes and the Golgi apparatus through the different cell branches and/or (ii) ensuring that organelles clustered on the MTOC follow the nucleus after the choice of a trajectory under confinement. This hypothesis can be tested by using bifurcated channels of different sizes and determining whether nocodazole-treated cells tend to get fragmented more in a 3 × 4 µm bifurcated microchannel than in a 8 × 4 µm bifurcated microchannel.

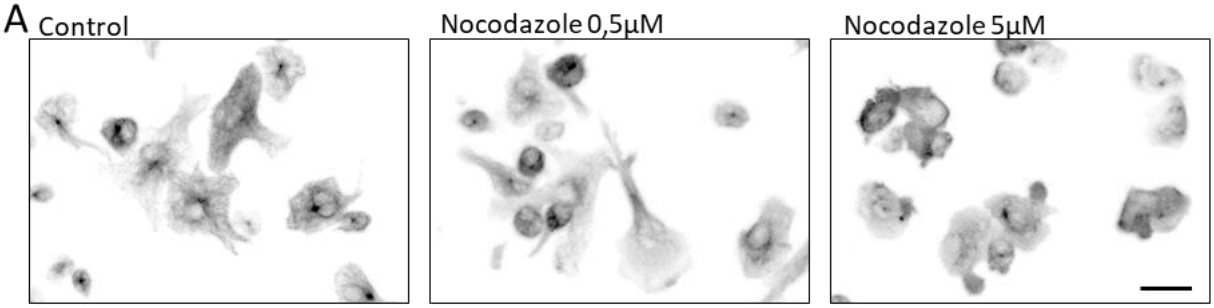
A
Control
Nocodazole 0,5µM
Nocodazole 5µM

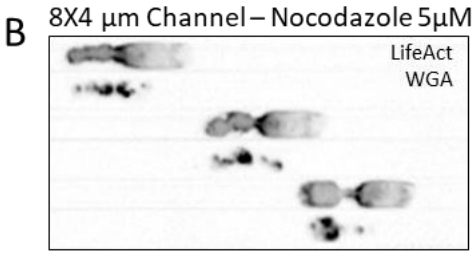
B
8X4 µm Channel – Nocodazole 5µM
LifeAct
WGA

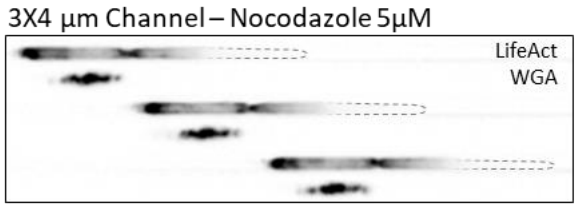
C
3X4 µm Channel – Nocodazole 5µM
LifeAct
WGA

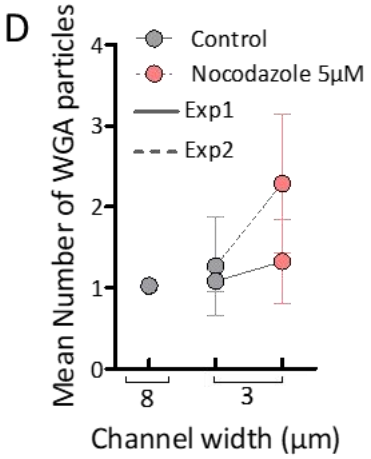
D
Control
Nocodazole 5µM
Exp1
Exp2
Mean Number of WGA particles
Channel width (µm)

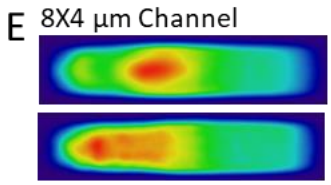
E
8X4 µm Channel
Control
Nocodazole 5µM

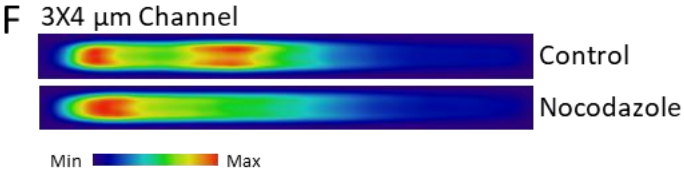
F
3X4 µm Channel
Control
Nocodazole
Min
Max

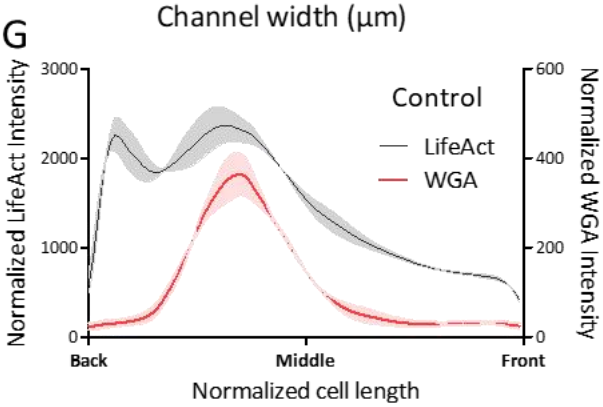
G
Control
LifeAct
WGA
Normalized LifeAct Intensity
Normalized WGA Intensity
Back
Middle
Front
Normalized cell length

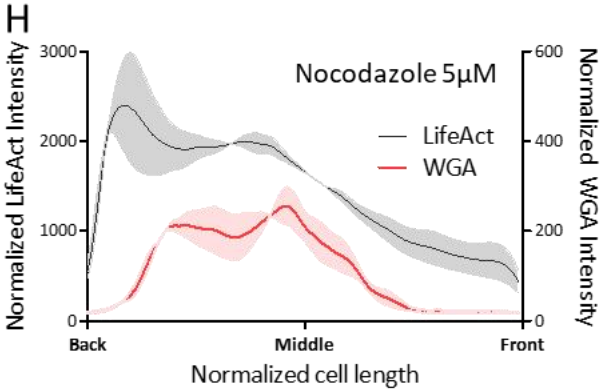
H
Nocodazole 5µM
LifeAct
WGA
Normalized LifeAct Intensity
Normalized WGA Intensity
Back
Middle
Front
Normalized cell length

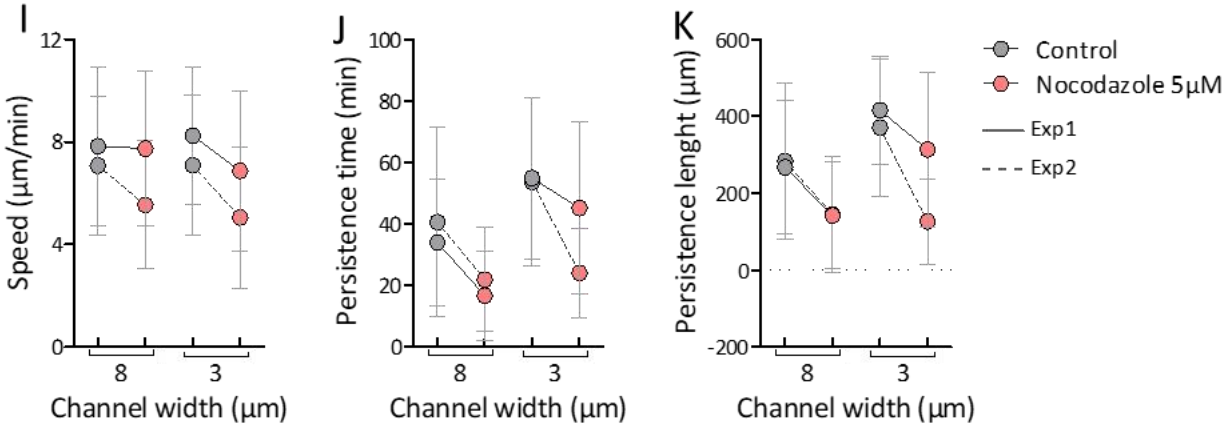
I
Speed (µm/min)
Channel width (µm)
J
Persistence time (min)
Channel width (µm)
K
Persistence lenght (µm)
Channel width (µm)
Control
Nocodazole 5µM
Exp1
Exp2

Figure 42 Microtubule depolymerization provokes cell oscillation and actin remodeling.
(A) Representative images of mDCs treated for 2 h with nocodazole at 0.5 or 5 µM or an equivalent quantity of DMSO as control. Scale bar = 30 µm. **(B-C)** Representative montage of an image sequence of a LifeAct-mDC treated with 5 µM of nocodazole migrating in 8 × 4 µm **(B)** and 3 × 4 µm **(C)** microchannels **(D)** Quantification of mean number of parts of the lysosomal mask in mDCs treated with 5 µM nocodazole or an equivalent quantity of DMSO as control, migrating in 8 × 4 µm and 3 × 4 µm microchannels. The dot and error bars represent the mean and standard deviation (SD), respectively, of one independent experiment. **(E-F)** Mean LifeAct signal density map of LifeAct-mDCs treated with 5 µM nocodazole or an equivalent quantity of DMSO as control, migrating in 8 × 4 µm **(E)** and 3 × 4 µm **(F)** microchannels. One representative experiment out of three is shown**. (G-H)** Intensity profile of mean LifeAct and WGA signal density maps of mDCs treated with 5 µM nocodazole **(H)** or an equivalent quantity of DMSO as control **(G),** migrating in 3 × 4 µm microchannels**.** The curve and filled area represent the mean and range, respectively, of two independent experiments. **(I-K)** Quantification of velocity, persistence length, and persistence time measured on full tracks of mDCs treated with 5 µM nocodazole or an equivalent quantity of DMSO as control, migrating in 8 × 4 µm and 3 × 4 µm microchannels. Each dot and error bars represent the mean and SD of one independent experiment.

6. Fragmentation of the Golgi apparatus does not affect confinement-induced actin remodeling

Finally, we aimed to distinguish which of these structures is responsible for actin accumulation upon confinement by dispersing the cluster of organelles without directly targeting the microtubule network. First, we targeted dyneins, as this molecular motors are essential for the clustering of the Golgi apparatus and lysosomes on the MTOC. However, neither of the two pharmacological inhibitors tested—Ciliobrevin D (Sainath and Gallo, 2015) and Dynarrestin (Höing et al., 2018)—induced significant lysosome dispersal. As an alternative approach, we dispersed the Golgi stacks using Golgicide A (Fig.43 A). Fragmentation of the Golgi apparatus affected neither the lysosomal cluster nor the accumulation of actin in the center of the cell (Fig.43 B-D) suggesting that the cortical actin accumulation induced by confinement is due to the lysosomal cluster or the microtubule lattice. To specifically disperse lysosomes from the MTOC, we could target the Rab34 GTPase known to induce lysosome aggregation after LPS sensing (Alloatti et al., 2015). We could

also exploit the phagocytic property of DCs to modify the size and stiffness of lysosomes. We can investigate whether the presence of latex beads or oil droplets that enlarge lysosomes induces cortical actin accumulation in wider microchannels or in cells treated with nocodazole. In addition, we can use magnetic nanoparticles to confine the lysosomes to one side of the cell cortex with a magnetic field. An asymmetric actin signal would show whether the contact between the lysosomes and the cortex is responsible for the cortical actin accumulation induced by the confinement (Valentin Laplaud; personal communication).

Thus, we characterized a dense cortical actin network formed around the lysosomes clustered on the MTOC during confinement. However, the exact mechanism that triggers this structure, as well as its function, remains to be established.

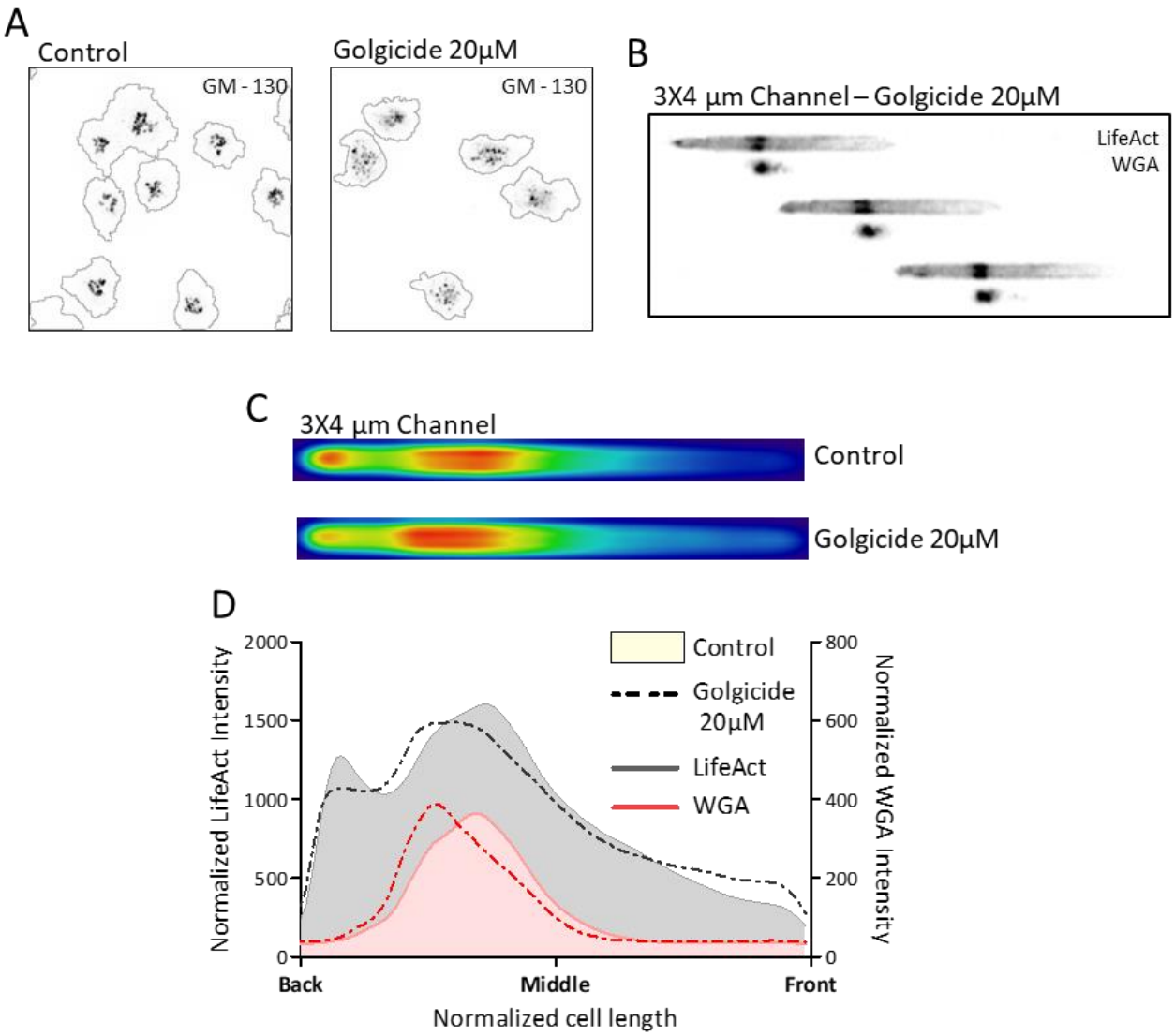

Figure 43 Fragmentation of the Golgi apparatus does not affect confinement-induced actin remodeling

(A) Representative images of mDCs treated for 2 h with 20 µM Golgicide A or an equivalent quantity of DMSO as control. Line highlight cell contour from LifeAct signal. **(B)** Representative montage of an image sequence of a LifeAct-mDC treated with 20 µM of Golgicide A migrating in 3 × 4 µm microchannels **(D)** Mean LifeAct signal density map of LifeAct-mDCs migrating in 3 × 4 µm microchannels treated with 20 µM of Golgicide A or an equivalent quantity of DMSO as control. **(D)** Intensity profile of mean LifeAct and WGA signal density maps of mDCs treated with 20 µM Golgicide A (dotted lines) or an equivalent quantity of DMSO as control (filled curve), migrating in 3 × 4 µm microchannels**.**

DISCUSSION AND PERSPECTIVES

I. Summary of the results

Overall, the present work demonstrates the high plasticity of mDC migration; it is only slightly affected by confinement, and mDCs are able to recover their speed after cell deformation in microchannels of varying width. Our first study showed that MyoII activity is dispensable in unrestricted spaces; however, extreme confinement requires a specific migration mechanism based on cell contractility.

This plasticity is associated with the reorganization of the cytoskeleton and accumulation of actin and myosin in the posterior end of the cell. Actomyosin remodeling is triggered by mDC entry into confined spaces and is correlated with the cell speed after squeezing. This cellular response to varying dimensions suggests the presence of a mechano-response to confinement.

Cytoskeletal remodeling depends on ROCK activity, which controls MyoII contractility. Inhibition of this signaling pathway shifts the mode of migration of mDCs to protrusive migration characterized by actin accumulation at the anterior of the cell and the rearward positioning of the nucleus. However, this compensatory mechanism is not sufficient for mDC migration in restricted areas.

In search of a mechanosensitive structure that would lead to ROCK activation, we explored the effect of physical constraints on the intracellular organization of mDCs. Migration of mDCs in narrow microchannels is associated with nuclear Lamin A/C disruption and actin depletion from the nucleus. The microtubule lattice is also affected by confinement with an increase in microtubule alignment and bundling. Finally, a dense cortical actin network is formed around the lysosomes clustered on the MTOC upon confinement of this structure. This last actin remodeling is specific to mDCs, non-contractile, and dependent on formin activity and microtubule integrity.

The exact mechanisms triggering these cellular remodeling events as well as their function in mDC migration into the interstitial space remain to be established.

II. Mechanisms of cell plasticity

A. Does dendritic cell intra-cellular reorganization favor cell migration in confined areas?

A characteristic of the confinement of mDCs in microchannels is cell elongation. It is interesting to note that the relative position of the MTOC remains constant, whereas the nucleus moves forward. The mechanisms of positioning and movement of the nucleus have been studied in several contexts and are essential to the development of muscles and the nervous system (Osorio and Gomes, 2014). In a migratory context, a wound healing assay done in fibroblasts demonstrated that the nucleus moves backward by a mechanism dependent on the actomyosin cytoskeleton, whereas the MTOC is maintained at the cellular centroid by dyneins (Gomes et al., 2005). In the same manner, the confinement of MDA-MB231 tumor cells leads to the positioning of the MTOC anterior to the nucleus. This relocation of the MTOC is accompanied by the redistribution of endosomes containing metalloproteases and thus promotes the translocation of the nucleus through constricted spaces by local matrix degradation (Infante et al., 2018).

The polarity of the cell observed in the above two examples, with the MTOC anterior to the nucleus, is reversed in DCs. This reversed polarity has recently been linked to the type of migration. Indeed, mesenchymal cells position their MTOC with the degrading machinery anterior to the nucleus to open pores in the matrix (Infante et al., 2018), whereas amoeboid cells, which do not degrade the matrix, position their nuclei anteriorly to select the largest pores in the matrix (Renkawitz et al., 2019). Thus, the frontward positioning of the nucleus is essential for the amoeboid cells to bypass local obstacles and optimize their migration in complex environments. Thus, increased forward positioning of the nucleus in confined microchannels may facilitate this process. However, the mechanism by which the nucleus is positioned at the cell front in mDCs remains unknown.

In T cells, MyoII-dependent contractility promotes the insertion of their nuclei into their lamellipodia (Barzilai et al., 2017). In this line, ROCK inhibition triggers a rearward positioning of the nucleus in mDCs, which suggests that MyoII promotes the forward positioning of the nucleus by generating hydrostatic pressure at the back of the nucleus. In addition, we observed a modification of the lysosome-nucleus axis in ROCK-inhibited mDCs. The mean distance between the nucleus and lysosomes was reduced, and even negative—with the lysosomes positioned anterior to the

nucleus—in Y-27632-treated cells (Fig.44). Although we do not know whether the position of the lysosomes directly reflects the position of the MTOC in ROCK-inhibited mDCs, these results suggest that myosin II activity is also essential in maintaining the nucleus-first migration of mDCs. However, Renkawitz and colleagues found no defects in pore size selection in blebbistatin- or Y-27632-treated mDCs, but they did not characterize the MTOC position in these conditions (Renkawitz et al., 2019).

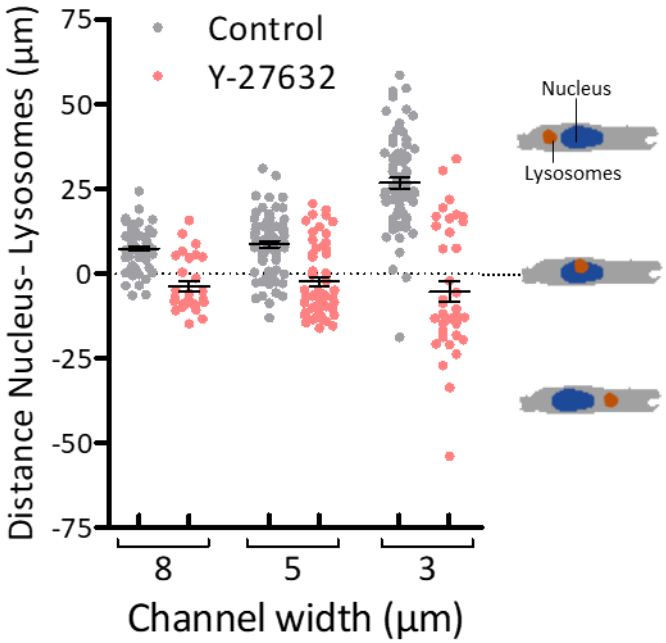

Figure 44 ROCK inhibition reverted the Nucleus-lysosome axis

Quantification of the mean distance between the nuclear centroid and the lysosomal centroid in mDCs treated with Y-27632 (10 µM) or an equivalent quantity of water as control, migrating in 8 × 4 µm, 5 × 4 µm, and 3 × 4 µm microchannels. The dots represent single cells; the bars and error bars represent the mean and standard error of the mean (SEM), respectively.

Therefore, mDC confinement triggers an intracellular reorganization marked by the forward positioning of the nucleus. The mechanisms governing this rearrangement remain to be established; they may be based on MyoII-dependent contractility but may also involve microtubules and dyneins or kinesins, as described in other cell types (Baffet et al., 2015; Infante et al., 2018). More importantly, these mechanisms would provide a better understanding of how mDCs optimize their migration in three-dimensional landscapes and avoid being trapped in constricted areas of the interstitial space.

B. Cytoskeleton reorganization and plasticity of the mode of migration

Our results demonstrate the plasticity of the mDCs cytoskeleton in microchannels with varying dimensions. A decrease in the microchannel cross-section led to an accumulation of actin and myosin in the posterior end of the mDC. Similar results were obtained in other leukocytes, such as T cells (Thompson et al., 2020), iDCs (Raphele Attia; personal communication), and neutrophils, and also in *Dictyostelium* (Mathieu Deygas; personal communication). Thus, this actomyosin remodeling event appears to be a conserved characteristic in migrating amoeboid cells and seems to facilitate their adaptation to varying geometries in their microenvironment.

We also highlight the plasticity of mDCs upon pharmacological manipulation of their migratory machinery. ROCK inhibition shifts the balance from actomyosin contractility towards actin protrusion. Transitions from blebs to lamellipodial or pseudopodial protrusion upon MyoII inhibition have been observed in a wide range of migratory cells, from tumor cells (Bergert et al., 2015; Liu et al., 2015; Petrie et al., 2012) to *Dictyostelium* (Ibo et al., 2016). In T cells, MyoII contractility regulates the balance between the amoeboid and mesenchymal modes of migration (Jacobelli et al., 2009). Although we did not precisely characterize whether mDCs exhibit blebs or Arp2/3-dependent protrusions at their cell front, this plasticity appears to be common to cells evolving in confined three-dimensional microenvironments.

Using a range of microchannel sizes, we demonstrated that tight spaces specifically require MyoII contractility for efficient mDC migration. Thus, the plasticity of mDCs is limited by physical constraints in their microenvironment, and the reasons for this limitation remain to be established. Our results lead us to the hypothesis that MyoII activity could be essential in triggering the rupture of the lamin A/C and promoting nuclear squeezing in confined spaces. Indeed, specific requirements for MyoII to deform the cell nucleus have been previously suggested in mDCs (Lämmermann et al., 2008) and established in T cells (Jacobelli et al., 2013).

In the context of high cell plasticity, microscopic variations in the dimensions of microchannels can completely alter the cellular behavior and effect of pharmacological inhibitors. Thus, the reproducibility of the experiments requires the precise characteristics of the microfabricated device used. In addition, the mechanisms of migration observed in the microchannels may be dependent on the dimensions of the device and may not be generalized to other migration contexts. Thus, assessing the effect of specific molecules or processes would require testing of a wide range of microchannel dimensions.

Nevertheless, it is questionable whether such cellular plasticity is observed in vivo. Indeed, the pore size measured in tissues varies over a wide range, from 2 to 20 µm in diameter (Wolf et al., 2009). We have also observed a variation in collagen structure in ear skin models. Characterization of actomyosin remodeling *in vivo* would confirm the relevance of our observations made in microchannels. In addition, pathological conditions such as fibrosis or tumor development are accompanied by changes in the ECM structures (Bonnans et al., 2014). Our results show that mDCs could adapt and maintain their migration ability in these dense environments by using specific migration modes. Thus, a precise understanding of this adaptation mechanism could lead to novel drug targets that could affect the migration of mDCs in specific pathological microenvironments (de Winde et al., 2020).

C. Potential mechano-responses and confinement sensors in mature dendritic cells

Cytoskeletal remodeling in varying dimensions suggests the presence of a mechano-response in mDCs and a cellular sensor for confinement. We found that actomyosin accumulation in the posterior end of the cell is dependent on ROCK signaling. However, other molecular pathways leading to MyoII activation have not been tested, in particular calcium-dependent myosin light chain kinase (MLCK). In addition, the signaling pathway leading to ROCK activation during cell confinement remains to be established.

Recently, our laboratory identified a nuclear envelope stretch-sensitive signaling leading to MyoII activation upon nuclear deformation (Lomakin et al., 2019). However, the presence of breaks in the lamin A/C lattice of mDCs and the efficient migration of lamin A/C-depleted mDCs suggest that this signaling pathway is not involved in the adaptation of mDCs to different microchannel dimensions. In agreement, no defect in random motility or chemotaxis was observed in lamin A/C knock-down mDCs migrating in collagen gels (Pablo Saez, personal communication).

Besides, we characterized a microtubule network remodeling event induced by cell confinement. A recent study has shown that microtubules are sensitive to the mechanical properties of the microenvironment and that substrate rigidity controls microtubule acetylation. Notably, Seetharaman and colleagues demonstrated that microtubule acetylation results in the release of GEF-H1 and downstream activation of Rho-dependent actomyosin contractility in astrocytes and glioblastoma cells (Seetharaman et al., 2020). These results are consistent with the findings of Kopf

and colleagues. Indeed, they have established that, in mDCs, microtubule depolymerization triggers the activation of MyoII in retracting cell branches by the local release of GEF-H1 (Kopf et al., 2020). Thus, we can hypothesize that microtubule remodeling can trigger mechano-signaling in mDCs through the release of GEF-H1 and downstream activation of Rho-dependent actomyosin contractility. In particular, we should study microtubule dynamics and post-translational modifications during confinement.

Furthermore, our analysis of actin organization in confined mDCs revealed a dense cortical actin structure surrounding the lysosomes and directly induced by the confinement of this zone. This observation suggests that this area of the cell is sensitive to physical constraints. Thus, a mechanical response could come from lysosomal signaling, which we have recently shown to regulate MyoII-induced contractility in mDCs (Bretou et al., 2017).

Finally, we demonstrated that cell length is higher in 3 × 4 µm microchannels than in 8 × 4 µm microchannels. This may be associated with an increase in cell perimeter and stretching of the plasma membrane. Remarkably, different signaling pathways are associated with plasma membrane stretching and actomyosin remodeling. One of the most well-known is based on Piezo1, a stretch-activated cation channel. In *Dictyostelium*, cell confinement sensing depends on Piezo1 signaling, which leads to cortical accumulation of MyoII (Srivastava et al., 2020). Another signaling pathway is associated with caveolae, which are small invaginations in the plasma membrane (60–80 nm) and disassemble rapidly upon cell stretching or osmotic shock (Sinha et al., 2011). Additionally, it has recently been shown that caveolae regulate the mechanical tension of epithelial cells by controlling lipid signaling to the formin FMNL2 and cortical actin remodeling (Teo et al., 2020). Therefore, these two signaling pathways may be involved in the adaptation of mDCs to microchannels of varying dimensions.

III. Microtubules as an integrator of the physical and chemical properties of the microenvironment.

Previous studies have focused on the actin and myosin cytoskeleton as a molecular driver of mDCs migration in the interstitial space. However, mDCs migrating to the lymph vessels must integrate chemical and physical signals from their microenvironment. Indeed, they follow chemokine gradients and overcome physical obstacles imposed by the dense and porous ECM (Vargas et al., 2017). Microtubules could play a key role in this orchestration of mDCs migration

because the network is known to modulate the actomyosin cytoskeleton (Dogterom and Koenderink, 2019) and forms a unique long-range network that can integrate extracellular signals along the entire length of the cell.

A recent study, already mentioned, shows that the network of microtubules controls the retraction of cell branches. Thus, microtubules are essential for maintaining mDCs integrity in porous matrices and for directional migration toward chemokines (Kopf et al., 2020). In addition, our laboratory confirmed that the microtubule lattice is necessary for guided migration toward CCL21 in collagen gels. Microtubules would facilitate the maintenance of a persistent migration toward the chemokine source when mDCs encounter obstacles in confined environments (Pablo Saez, personal communication).

In addition, our work suggests a mechano-response from the microtubule network that could modulate activation of Rho-dependent actomyosin contractility upon confinement by the release of GEF-H1, as already developed in the previous section. We have also noticed that microtubules surround the nucleus and form a cage, even in narrow microchannels (Fig.38 A). Interestingly, microtubules, and in particular acetylated ones, exert forces on the nucleus, leading to its deformation in hematopoietic stem cells (Biedzinski, 2018; Biedzinski et al., 2019). Thus, the microtubule network could also promote nuclear deformation in confined spaces and ensure mDCs adaptation to variable geometries. We did not observe any impact of microtubule depolymerization on mDCs migration through constricted microchannels; however, the effect could be hidden by the hypercontractility induced by nocodazole treatment.

Therefore, the microtubule array is involved in chemokine sensing, cell branch coordination and could also optimize mDCs migration in narrow pores. Thus, microtubules appear as a key network able to integrate chemical and physical signals that are essential to coordinate mDCs migration in interstitial spaces. Microtubules could optimize mDC migration by facilitating the passage of local obstacles while maintaining the overall direction of the cells to the lymphatic vessels. This could be achieved by a stable microtubule bundle towards the front of the cell, allowing nuclear deformation and frontward positioning as well as directional memories, while more dynamic microtubules at the cell rear and in the lateral branches would modulate actomyosin contractility controlling branches retraction and cell propulsion through narrow spaces. Characterization of the impact of physical constraints and chemokines sensing on microtubules dynamic would highlight their specific function and the signaling pathways involved.

IV. Impact of confine migration on mDCs immune functions

A. Dense cortical actin and antigen transport.

We described a dense cortical actin network induced in the cell center by the confinement of mDCs. This structure concentrates around the lysosome cluster on the MTOC and is lost upon microtubules depolymerization. This actin accumulation is independent of the Golgi, and we should establish whether it is related to the lysosomes, the MTOC, or their interaction at the cell center. In contrast to the actin remodeling observed at the back of the cell, this structure was not found in iDCs or in other leukocytes studied in our laboratory. Therefore, the dense cortical actin triggered by confinement should be associated with DC maturation and their specific immune functions.

We used LPS to trigger DC maturation; however, LPS response involves the TLR4 receptor known to signal at the lysosomes (Sanjuan et al., 2009). Thus, we should test whether cortical actin accumulation is also observed with other maturation signals, in particular with ATP, which is known to induce actin remodeling by a pathway independent of TLR4 signaling (Sáez et al., 2017).

Initial results show that actin accumulation is dependent on formins, which is consistent with the modulation of actin nucleator activity during DC maturation. In addition, formin activity is necessary for rapid and directed migration to the lymphatic vessels (Vargas et al., 2016). Thus, this cortical actin structure could facilitate the movement of mDCs in dense environments.

One of the main functions of mDCs is to transport antigens to the lymph node. In the classical view, mDCs mainly carry antigens degraded into small peptides and loaded onto their MHC. However, MDCs have been shown to carry native antigens that are released in the lymph node and activate B cells (El-Barbry et al., 2020). In addition, mDCs carrying apoptotic bodies and melanosomes have been observed in the lymphatic vessels of the skin (Stoitzner et al., 2002). Thus, the lysosomal compartment of mDCs could be filled with large particles that represent an internal obstacle to mDCs migration into interstitial spaces. The dense cortical actin could facilitate the deformation of this compartment through narrow pores. It could also prevent mDCs fragmentation and antigen loss if lysosomes are trapped in a constriction. Therefore, a possible function of this confinement-induced cortical actin is to facilitate the migration of antigen-loaded mDCs to the lymph nodes.

B. Actin and microtubules interplay with antigen processing in lysosomes.

Antigen processing is tightly regulated by vesicle trafficking and determines the adaptive immune response. In particular, the cross-presentation of extracellular antigens on MCHI requires slow endosomal maturation and is essential to trigger cytotoxic T cells in anti-viral or anti-tumor immune responses. (Alloatti et al., 2016)

The dynamics of microtubules and actin regulate endosomal maturation (Belabed et al., 2020). In addition, GEF-H1 released upon microtubules depolymerization triggers DCs maturation and promotes antigen cross-presentation (Kashyap et al., 2019). Thus, cytoskeletal remodeling induced by mDCs confined migration could affect antigen processing.

In addition, the perinuclear clustering of lysosomes prevents their fusion with endocytic compartments and promotes antigen cross-presentation (Alloatti et al., 2015). Interestingly, lysosomes are scattered in narrow microchannels upon formin inhibition. Thus, the dense cortical actin network could preserve lysosome aggregation during confinement and keep them aparate from the endocytic compartment.

Consequently, mDCs migration in confined environments could modulate the processing of antigens and, in particular, their cross-presentation. This is particularly relevant in the context of tumor immunity, which relies on effective cross-presentation and is associated with ECM remodeling.

C. Confined migration impacts the nuclear shell.

Our results reveal LaminA/C ruptures associated with mDCs confinement. We did not observe any actin accumulation around the nucleus at the entry into the 3x4µm microchannels; this suggests that the LaminA/C weakening is not triggered by the arp2/3-dependent actin lattice previously described in iDCs (Thiam et al., 2016). MyoII-dependent contractility promotes mDCs deformation and migration through narrow pores; thus, it could be responsible for the LaminA/C weakening of in mDCs. A possible role of the microtubule network in the induction of these ruptures is also not excluded.

We could wonder whether LaminA/C ruptures are sustained during mDC migration in confined areas and whether they are associated with openings in the nuclear envelope. Indeed, nuclear envelope ruptures have been observed in DCs migrating through 3µm wide constrictions and in the

interstitial space of mouse ear explants (Raab et al., 2016). A breach in the nuclear envelope results in exposure of DNA in the cytoplasm and DNA damages. Since mDCs express cytosolic DNA sensors (Chen et al., 2016), ruptures in the nuclear envelope during confined migration could result in a specific immune response. On the other hand, mechanically induced DNA damages promote an invasive phenotype in breast cancer cells and senescence in untransformed cells (Nader et al., 2020). The effects of DNA damages in DCs have not been studied; however, they may also have a long-term impact on their immune functions.

In addition, Wang and colleagues have recently shown that lymphocyte migration in confined 3D environments leads to increased methylation of histones H3, chromatin decompaction and nuclear softening. This chromatin remodeling depends on MyoII activation by MLCK and facilitates lymphocyte migration in confined spaces (Wang et al., 2018). This work represents an example of nuclear mechanics modulation by MyoII activity that could occur in mDCs. Moreover, chromatin remodeling could also affect gene expression and, in particular, in mDCs, the profile of cytokines and co-stimulating molecules induced by maturation (Boukhaled et al., 2019).

Therefore, confined migration could have an impact on antigen processing and the immune status of mDCs, resulting in specific priming of T cells and modulation of the adaptive immune response. Thus, in addition to antigens and information on the inflammatory context, mDCs could transduce information on the physical properties of the microenvironment at the site of infection to T-cells. This information could favor further homing of effector T cells to the site of infection. Exploration of the idea of physical markers carried by mDCs could have an impact on the development of DC-based vaccines for anti-tumor immunotherapy (Gardner et al., 2020).

ANNEXES

I. Publications list

Reconstitution of cell migration at a glance.

Garcia-Arcos JM, Chabrier R, Deygas M, Nader G, **Barbier Lucie**, Sáez PJ, Mathur A, Vargas P, Piel M. Journal of Cell Science. 2019 Feb 11;132 (4). pii: jcs225565. doi: 10.1242/jcs.225565.

Abstract. Single cells migrate in a myriad of physiological contexts, such as tissue patrolling by immune cells, and during neurogenesis and tissue remodeling, as well as in metastasis, the spread of cancer cells. To understand the basic principles of single-cell migration, a reductionist approach can be taken. This aims to control and deconstruct the complexity of different cellular microenvironments into simpler elementary constrains that can be recombined together. This approach is the cell microenvironment equivalent of in vitro reconstituted systems that combine elementary molecular players to understand cellular functions. In this Cell Science at a Glance article and accompanying poster, we present selected experimental setups that mimic different events that cells undergo during migration in vivo These include polydimethylsiloxane (PDMS) devices to deform whole cells or organelles, micro patterning, nano-fabricated structures like grooves, and compartmentalized collagen chambers with chemical gradients. We also outline the main contribution of each technique to the understanding of different aspects of single-cell migration.

Leukocyte Migration and Deformation in Collagen Gels and Microfabricated Constrictions.

Sáez PJ, **Barbier Lucie**, Attia R, Thiam HR, Piel M, Vargas P.

Methods in Molecular Biology. 2018;1749:361-373. doi: 10.1007/978-1-4939-7701-7_26.

Abstract. In multicellular organisms, cell migration is a complex process. Examples of this are observed during cell motility in the interstitial space, full of extracellular matrix fibers, or when cells pass through endothelial layers to colonize or exit specific tissues. A common parameter for both situations is the fast adaptation of the cellular shape to their irregular landscape. In this chapter, we

describe two methods to study cell migration in complex environments. The first one consists in a multichamber device for the visualization of cell haptotaxis toward the collagen-binding chemokine CCL21. This method is used to study cell migration as well as deformations during directed motility, as in the interstitial space. The second one consists in microfabricated channels connected to small constrictions. This procedure allows the study of cell deformations when single cells migrate through small holes and it is analogous to passage of cells through endothelial layers, resulting in a simplified system to study the mechanisms operating during transvasation. Both methods combined provide a powerful hub for the study of cell plasticity during migration in complex environments.

Mechanisms for fast cell migration in complex environments.

Vargas P, **Barbier Lucie**, Sáez PJ, Piel M.

Current Opinion in Cell Biology 2017 Oct;48:72-78. doi: 10.1016/j.ceb.2017.04.007.

Abstract. Cell migration depends on a combination of the cell's intrinsic capacity to move and the proper interpretation of external cues. This multistep process enables leukocytes to travel long distances in organs in just a few hours. This fast migration is partly due to the leukocytes' high level of plasticity, which helps them to adapt to a changing environment. Here, we review recent progress in understanding the mechanisms used by leukocytes to move rapidly and efficiently in intricate anatomical landscapes. We shall focus on specific cytoskeletal rearrangements used by neutrophils and dendritic cells to migrate within confined environments. Lastly, we will describe the properties that facilitate the rapid migration of leukocyte in complex tissue geometries.

Lysosome signaling controls the migration of dendritic cells.

Bretou M, Sáez PJ, Sanséau D, Maurin M, Lankar D, Chabaud M, Spampanato C, Malbec O, **Barbier Lucie**, Muallem S, Maiuri P, Ballabio A, Helft J, Piel M, Vargas P, Lennon-Duménil AM.

Science Immunology. 2017 Oct 27;2 (16). doi: 10.1126/sciimmunol.aak9573.

Abstract. Dendritic cells (DCs) patrol their environment by linking antigen acquisition by macropinocytosis to cell locomotion. DC activation upon bacterial sensing inhibits macropinocytosis

and increases DC migration, thus promoting the arrival of DCs to lymph nodes for antigen presentation to T cells. The signaling events that trigger such changes are not fully understood. We show that lysosome signaling plays a critical role in this process. Upon bacterial sensing, lysosomal calcium is released by the ionic channel TRPML1 (transient receptor potential cation channel, mucolipin subfamily, member 1), which activates the actin-based motor protein myosin II at the cell rear, promoting fast and directional migration. Lysosomal calcium further induces the activation of the transcription factor EB (TFEB), which translocates to the nucleus to maintain TRPML1 expression. We found that the TRPML1-TFEB axis results from the down-regulation of macropinocytosis after bacterial sensing by DCs. Lysosomal signaling therefore emerges as a hitherto unexpected link between macropinocytosis, actomyosin cytoskeleton organization, and DC migration.

Chercher la lumière - Des expériences pour comprendre le phototropisme des plantes

Barbier Lucie

Revue Découverte, n° 427 (mars-avril 2020), rubrique La science à portée de main.

Article de vulgarisation scientifique.

II. Synthèse en français

A. Préambule

Le déplacement des cellules est un processus essentiel au fonctionnement de notre organisme, en particulier lors du développement embryonnaire, de la réponse immunitaire et de l'homéostasie tissulaire. La migration cellulaire est ainsi finement contrôlée par des signaux intracellulaires mais également extracellulaires. La perturbation de ces mécanismes est impliquée dans de nombreuses maladies immunitaires ou neuronales, et est également associée à la progression métastatique des cancers. Dans ce contexte, l'objectif général de mes recherches est de comprendre comment les propriétés physico-chimiques du microenvironnement qui entoure une cellule peuvent affecter et réguler sa motilité.

B. Contexte

Mes travaux sont centrés sur les cellules dendritiques (DCs), qui sont les principales cellules présentatrices d'antigènes capables d'initier la réponse immunitaire adaptative. En cas d'infection, les cellules dendritiques collectent des antigènes et des informations sur le contexte inflammatoire sur le site de l'infection. Puis, elles les transportent vers les ganglions lymphatiques où elles stimulent les lymphocytes T. Les informations transmises par les cellules dendritiques permettent l'activation et la prolifération des cellules immunitaires effectrices spécifiques au pathogène détecté sur le site de l'infection. Une immunité efficace repose donc sur la migration rapide des DCs entre le tissu infecté et le ganglion lymphatique le plus proche. Cette étape nécessite un ajustement rapide et dynamique des DCs aux propriétés biochimiques et physiques des différents microenvironnements qu'elles traversent. Les DCs doivent donc constamment intégrer différents signaux et, en réponse, adapter leur mode de migration, sujet principal de mes travaux de thèse.

Au niveau cellulaire, les forces qui permettent à la cellule de bouger sont générées par le cytosquelette d'actine et de myosine. La polymérisation des filaments d'actine sous la membrane associée à la contractilité de la myosine non musculaire II A (MyoII) crée un flux rétrograde d'actine le long de la membrane plasmique. Ce flux génère des forces de friction qui sont transmises au

substrat et propulse la cellule.

Les précédents travaux de mon équipe ont montré que les DCs sont capables de détecter les signaux biochimiques associés à un microenvironnement inflammatoire. Ils induisent une relocalisation du cytosquelette d'actine et de MyoII vers l'arrière de la cellule (Sáez et al., 2017; Vargas et al., 2016). Ce remodelage cellulaire est essentiel à la migration des DCs du tissu infecté vers le système lymphatique. En plus des signaux biochimiques, le déplacement des DCs entre différents compartiments du corps leur impose de s'adapter rapidement à l'évolution des propriétés physiques des tissus qu'elles traversent (Thiam et al., 2016; Vargas et al., 2017). En effet, l'espace interstitiel est principalement constitué de protéines de la matrice extra-cellulaire qui forment un réseau en trois dimensions dense, poreux et irréguliers. Les cellules qui se déplacent dans cet environnement doivent (i) coordonner l'extension et la rétraction de leurs différentes branches pour ne pas être piégées entre plusieurs pores et (i) se déformer pour passer dans les pores plus petits que le diamètre de la cellule (Fig.45).

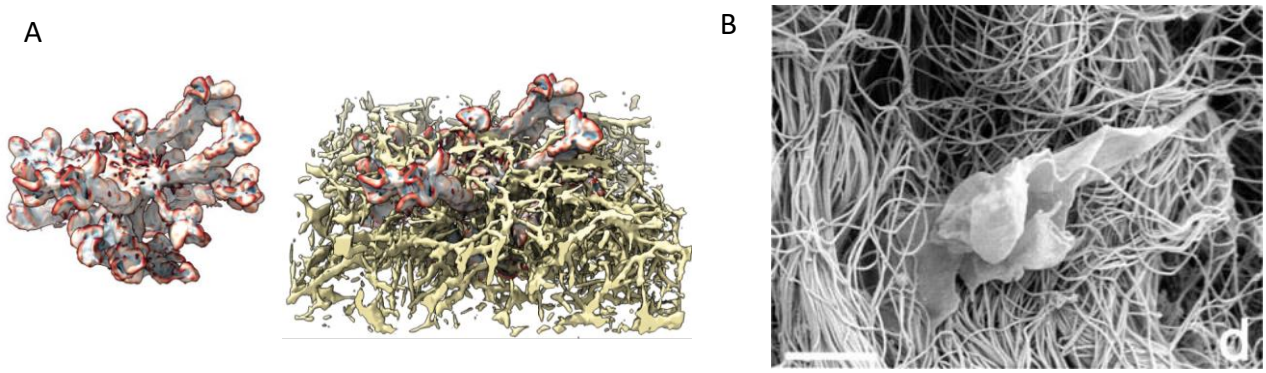

Figure 45 Les DCs se déplaçant dans l'espace interstitiel doivent coordonner l'extension de multiples branches cellulaires et être capables de se déformer dans les pores de la matrice extra cellulaire.
(A) Image d'une DC enchevêtrée dans un gel de collagène. Elle est représentée seule (droite) ou avec la matrice l'entourant (gauche). La cellule forme de multiples branches insérées dans différents pores. Une migration efficace nécessite la coordination de ces extensions pour conduire au passage dans un même pore d'un bras "gagnant" suivi du reste de la cellule et éviter ainsi l'étranglement de la cellule. De Renkawitz J. et al, 2019 (B) Image de microscopie électronique à balayage d'une DC migrant dans l'espace interstitiel du derme. Le passage des cellules à travers le réseau de collagène nécessite une importante déformation cellulaire; De Stoitzner P. et al 2002

Des travaux récents ont montré que le réseau de microtubules assure la coordination des protrusions cellulaires des DCs. Sans ce réseau, les DCs étendent de multiples protrusions sans les rétracter, elles sont donc bloquées dans l'espace interstitiel et peuvent même finir par se fragmenter (Kopf et al., 2020). D'autre part, les DCs utilisent également leur noyau, l'organite le plus rigide de la cellule, pour sélectionner les pores les plus larges et ainsi faciliter leur déplacement dans

l'espace interstitiel (Renkawitz et al., 2019). Cependant, le déplacement des DCs est dirigé vers les vaisseaux lymphatiques par des molécules attractantes. Les DCs sont forcées par ces signaux chimiques de traverser des espaces denses de la matrice où la taille des pores est plus petite que leur diamètre. Des précédents travaux ont montré que dans ces espaces restreints, la contractilité de la MyoII est importante pour propulser le noyau de la cellule. (Lämmermann et al., 2008). Mais, les mécanismes précis qui assurent la déformation et la migration des DCs au travers d'espaces restreints et irréguliers ne sont pas entièrement élucidés. Dans le cadre de mon doctorat, j'ai pour objectif de comprendre comment les propriétés physiques du microenvironnement affectent la migration des DCs lors de la réponse immunitaire. J'ai concentré mes recherches sur la réorganisation du cytosquelette induite par le confinement des DCs dans des espaces restreints et sur les mécanismes qui permettent cette plasticité, favorisant ainsi leur déplacement rapide à travers le corps.

C. Méthodes

Pour comprendre comment les cellules dendritiques adaptent leur migration à différents niveaux de confinement, j'ai conçu un dispositif microfluidique qui reproduit de manière contrôlée les paramètres physiques des tissus que j'étudie (Sáez et al., 2018). Il contient des microcanaux de géométries simples et définies, regroupant différents niveaux de contraintes dans une même puce. Les microcanaux sont de forme rectangulaire, leurs largeurs varient de 3 à 8µm pour une hauteur fixe de 4µm (Fig46 A). Combiné à la microscopie cellulaire et à l'analyse d'images, cet outil me permet de quantifier et de caractériser, au niveau de la cellule unique, la mobilité et l'organisation intracellulaire des DCs pour différents niveaux de confinements.

Le confinement des DCs dans les microcanaux induit une déformation de la cellule ainsi que de son noyau (Fig.46 B). La longueur moyenne des cellules passe de 50 µm dans les microcanaux de 8 x 4 µm à 80 µm dans les microcanaux de 3 x 4 µm (Fig.46 C et D). Le noyau est également allongé et présente moins d'invagination dans les microcanaux de 3 x 4 µm comparés à ceux de 8 x 4 µm (Fig.46 E). Ces modifications de la forme des DCs et de leurs noyaux confirment les contraintes physiques appliquées sur les cellules alors dans la migration dans les microcanaux.

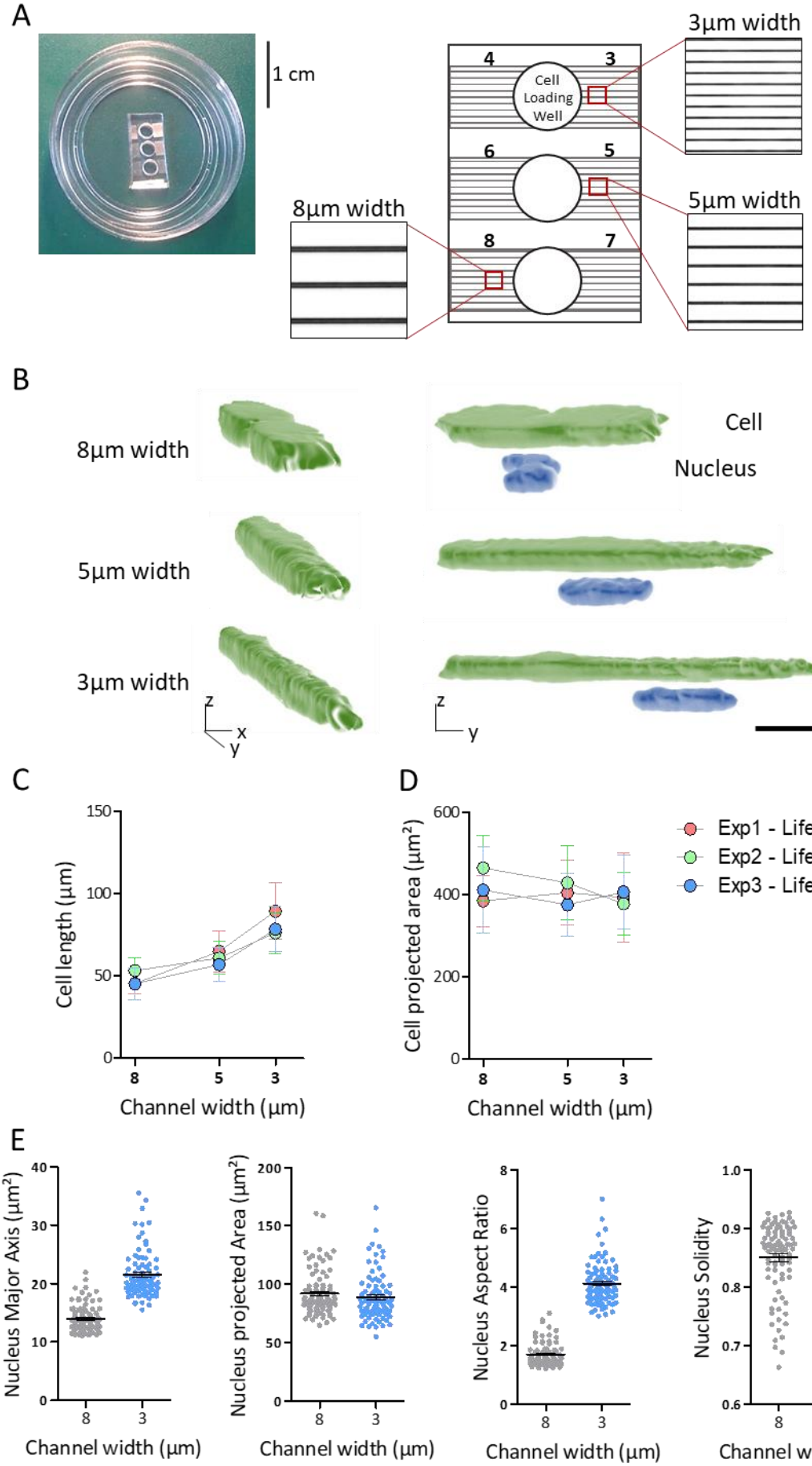
A
1 cm
3µm width
8µm width
5µm width
Cell Loading Well
4
3
6
5
8
7
B
8µm width
5µm width
3µm width
Cell
Nucleus
z
x
y
C
Cell length (µm)
Channel width (µm)
D
Cell projected area (µm²)
Channel width (µm)
Exp1 - LifeAct
Exp2 - LifeAct
Exp3 - LifeAct
E
Nucleus Major Axis (µm²)
Nucleus projected Area (µm²)
Nucleus Aspect Ratio
Nucleus Solidity
Channel width (µm)

Figure 46 Contraintes physiques imposées par des microcanaux de tailles différentes

(A) Image (à gauche) et représentation schématique (à droite) d'un dispositif microfabriqué avec des canaux de différentes tailles. Les chiffres indiquent la largeur des microcanaux dans la zone située dessous. Les encarts montrent des images à contraste de phase des zones avec les microcanaux de 8 × 4 µm, 5 × 4 µm et 3 × 4 µm. **(B)** Vues en perspective d'une reconstruction isosurface tridimensionnelle à partir d'images en microscopie confocale de DC migrant dans les microcanaux 8 × 4 µm, 5 × 4 µm et 3 × 4 µm. La surface du noyau est obtenue à l'aide du signal Hoechst. Barre d'échelle = 10 µm. **(C-D)** Quantification de la longueur **(C)** ou de la surface projetée de la cellule **(D)** des DC migrant à l'intérieur des microcanaux 8 × 4 µm, 5 × 4 µm et 3 × 4 µm. Chaque point et chaque barre d'erreur représentent respectivement la moyenne et l'écart-type d'une expérience indépendante. **(E)** Quantification des paramètres géométriques du noyau à partir du signal de Hoechst des DCs migrant dans les microcanaux 8 × 4 µm et 3 × 4 µm. Chaque point représente la valeur d'une cellule, les lignes et la barre d'erreur correspondent respectivement à la moyenne et à l'écart-type. Les données ont été mises en commun à partir de deux expériences indépendantes.

D.Résultats

Une première partie de mes travaux a montré que l'activité de la MyoII est nécessaire à la migration des DCs vers les vaisseaux lymphatiques dans l'espace interstitiel. En utilisant des gels de collagène, nous avons confirmé que ce défaut est dû à une diminution de la capacité de migration des DCs mais pas à la détection des molécules attractantes. Comme démontré précédemment (Lämmermann et al., 2008), les cellules présentent toujours un mouvement résiduel dans la matrice de collagène après l'inhibition de la MyoII, ce qui suggère que seulement une étape spécifique de la migration des DC dans des environnements complexes est affectée. Ainsi, nous avons utilisé les microcanaux de différentes dimensions pour caractériser avec précision le rôle de la contractilité dépendante de la MyoII dans le mouvement et la plasticité des DCs. Malgré une forte déformation, la vitesse des DCs n'est que légèrement influencée par la taille des microcanaux. En outre, la contractilité dépendante de MyoII est spécifiquement requise pour le mouvement des DCs dans des zones confinées. L'effet de l'inhibition de la MyoII sur la vitesse et la déformation des cellules augmentent avec le rétrécissement des microcanaux et des constrictions. Elle a un fort impact sur le mouvement des cellules dans les microcanaux de 3x4µm et sur le passage des cellules à travers les constrictions de moins de 2µm de large.

Ce travail démontre la grande plasticité de la migration des DCs. Elle n'est que légèrement affectée par le confinement, et l'activité de la MyoII n'est pas indispensable dans des espaces non restreints. Cependant, le confinement extrême nécessite un mécanisme de migration spécifique basé sur la contractilité cellulaire. Ces résultats nous mènent à se questionner sur l'adaptation des

mécanismes de migration des DCs au confinement, ainsi que sur la présence d'une réponse mécano-sensible dans ces cellules. Pour répondre à cette question, j'ai étudié l'effet du confinement des DCs sur l'organisation de leur cytosquelette d'actine.

1. Réorganisation du cytosquelette d'actine induit par le confinement des DCs

Le confinement dans les microcanaux induit un réarrangement rapide et spécifique du cytosquelette des DCs. L'organisation des filaments d'actine dans les microcanaux larges (ie. 8x4 µm) a été abondamment étudiée (Vargas et al., 2016). Cette organisation d'actine fluctue mais se localise globalement au niveau du noyau de la cellule (Fig.47 A-C). En comparaison, dans des microcanaux de 3 x 4 µm, le noyau est déporté vers l'avant de la cellule et est déplété en actine. Après la compression cellulaire, les filaments d'actine se concentrent dans deux parties de la cellule : i) à l'extrémité arrière et ii) au centre où se trouvent le centre organisateur des microtubules (MTOC) et les lysosomes (Fig.47 A, B et D).

Nous avons quantifié précisément l'accumulation d'actine à l'arrière de la cellule (15% arrière de la longueur de la cellule), et dans le masque des lysosomes (Fig.47 E et F). Nos résultats confirment que les DC migrant dans des microcanaux de 3x4 µm accumulent plus de filaments d'actine à l'arrière et de manière plus modérée au niveau des lysosomes que les cellules dans des microcanaux de 8x4 µm. D'autre part, il n'y a pas de différence significative de la vitesse des cellules entre les microcanaux de différentes tailles (Fig.47 G), ce qui confirme notre étude précédente.

Ainsi, ces résultats montrent la présence de structures denses d'actine au niveau des lysosomes et à l'arrière des cellules dans les DCs migrant dans des microcanaux de 3 x 4 µm. La suite de mes travaux a pour but d'identifier la nature et la fonction de ces structures induites par le confinement des DCs.

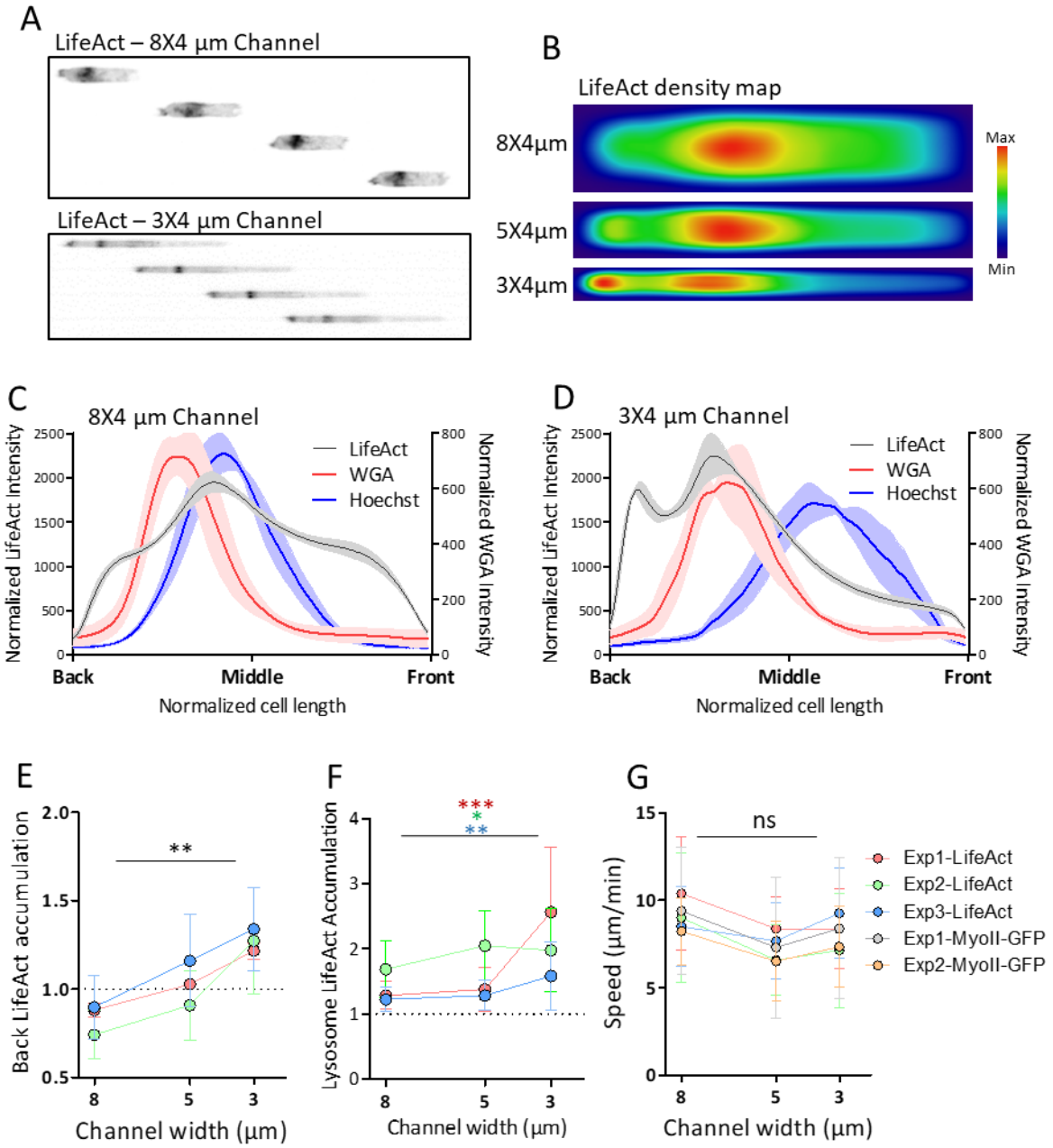

Figure 47 Accumulation d'actine dans les cellules sous confinement

(A) Montage représentatif d'une séquence d'images d'un LifeAct-DC migrant dans des microcanaux de *8 × 4 µm* (en haut) ou de 3X4µm (en bas). **(B)** Carte de densité moyenne du signal LifeAct dans des DCs migrant dans un microcanal de 8X4µm (haut), *5 × 4 µm* (milieu) ou *3 × 4 µm* (bas). Un exemple représentatif de 3 expériences indépendantes **(C-D)** Profil d'intensité moyen pour le signal LifeAct (actine), WGA (lysosomes) et Hoechst (noyau) des DCs migrant dans des microcanaux de *8 × 4 µm* **(C)** ou *3 × 4 µm* **(D).** La courbe et la zone colorée représentent la moyenne et l'écart type de 3 expériences indépendantes.. **(E-F)** Quantification de l'accumulation du signal LifeAct dans les 15% arrière de la longueur de la cellule **(E)** ou dans le masque des lysosomes **(F)** pour les DCs migrant dans des microcanaux de *8 × 4 µm*, *5 × 4 µm* ou *3 × 4 µm*. Chaque point et chaque barre d'erreur représentent respectivement la moyenne et l'écart-type d'une expérience indépendante. **(G)** Vitesse des DCs migrant dans des microcanaux de *8 × 4 µm*, *5 × 4 µm* ou *3 × 4 µm*. Chaque point et barre d'erreur représente respectivement la moyenne et l'écart-type d'une expérience indépendante. Test statistique Anova avec le test de comparaison multiple de Tukey, **p<0,01.

2. La structure d'actine à l'arrière de la cellule est dépendante de l'activité de la kinase ROCK et permet le maintien de la vitesse des DCs dans les espaces restreints.

Des résultats non présentés ici montrent que la structure d'actine à l'arrière de la cellule est associée à la MyoII et est corrélée à la vitesse des DCs après le confinement dans les microcanaux de 3 x 4 µm. Cette accumulation du cytosquelette d'actomyosine à l'arrière des cellules suggère une activation de la contractilité cellulaire provoquée par le confinement. Pour tester l'effet de la contractilité sur la réorganisation du cytosquelette des DC, nous avons utilisé l'inhibiteur chimique de la kinase ROCK, Y-27632. ROCK est une des kinases qui activent la MyoII via la phosphorylation de sa sous-unité régulatrice.

L'inhibition de la ROCK affecte l'organisation de l'actine dans les microcanaux 8 × 4 µm et 3 × 4 µm (Fig.48 A à F). Les cellules traitées au Y-27632 présentent une augmentation de la quantité d'actine à l'avant de leur noyau par rapport aux cellules témoins (Fig.48 C à F). Cette augmentation est renforcée dans les microcanaux de 3 × 4 µm (Fig.48 E et F). Le remodelage de l'actine dans tout les microcanaux, quelle que soit leur taille, suggère que la contractilité dépendante de la MyoII est impliquée dans le mouvement des DCs dans les microcanaux de 8 × 4 µm et de 3 × 4 µm. Ainsi, l'absence d'un effet significatif du Y-27632 sur la vitesse des DCs dans les microcanaux 8 × 4 µm pourrait être due à la compensation par d'autres mécanismes de migration qui ne sont, par contre, pas efficaces dans les microcanaux 3 × 4 µm. Les cellules traitées avec du Y-27632 semblent passer d'un comportement contractile poussant le noyau à un mode de migration protrusif qui tire le noyau. Cette hypothèse est soutenue par la modification de la position du noyau, qui est plus à l'arrière dans les cellules traitées au Y-27632 (Fig48 E et F).

Un second effet significatif de l'inhibition de ROCK est la perte de l'accumulation d'actine à l'arrière de la cellule, normalement induite par la migration des DCs dans les microcanaux de 3 × 4 µm (Fig.48 G). La perte de la fraction d'actine à l'arrière de la cellule est corrélée à une diminution de la vitesse avec le rétrécissement des microcanaux dans les conditions Y-27632 (Fig.48 H). Ces résultats confirment que cette concentration du cytosquelette d'actomyosine à l'arrière de la cellule est essentielle au maintien de la vitesse des DCs dans des espaces restreints.

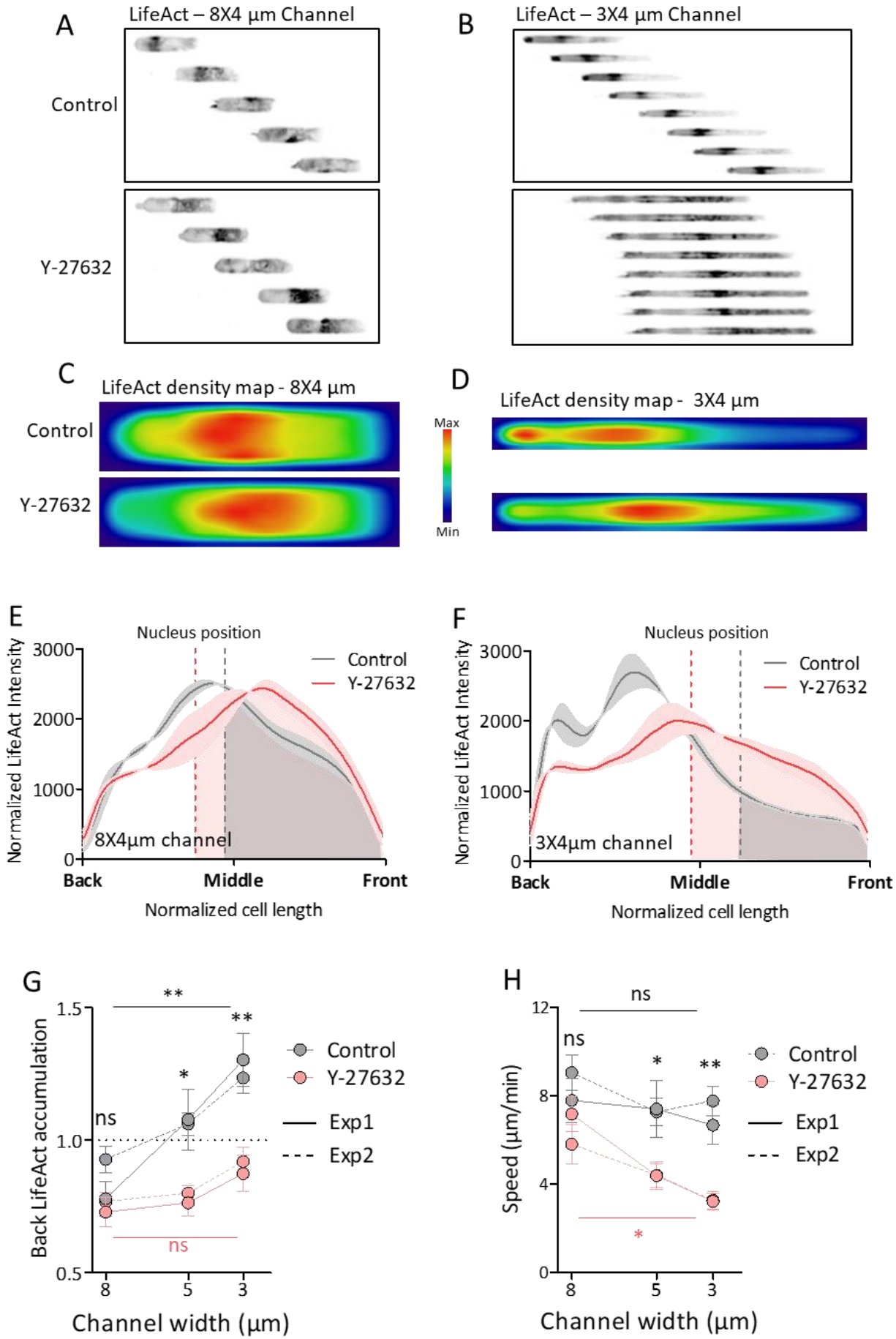
A
LifeAct – 8X4 µm Channel
Control
Y-27632
B
LifeAct – 3X4 µm Channel
C
LifeAct density map - 8X4 µm
Control
Y-27632
Max
Min
D
LifeAct density map - 3X4 µm
E
Nucleus position
Normalized LifeAct Intensity
3000
2000
1000
0
Control
Y-27632
8X4µm channel
Back
Middle
Front
Normalized cell length
F
Nucleus position
Normalized LifeAct Intensity
3000
2000
1000
0
Control
Y-27632
3X4µm channel
Back
Middle
Front
Normalized cell length
G
Back LifeAct accumulation
1.5
1.0
0.5
**
**
*
ns
ns
Control
Y-27632
Exp1
Exp2
8
5
3
Channel width (µm)
H
Speed (µm/min)
12
8
4
0
ns
ns
*
**
*
Control
Y-27632
Exp1
Exp2
8
5
3
Channel width (µm)

Figure 48 L'accumulation d'actine dans les cellules dépend de l'activité de ROCK.

(A-B) Montage représentatif d'une séquence d'images d'une cellule contrôle (haut) ou traité avec 10µM d'inhibiteur ROCK Y-27632 (bas) migrant dans des microcanaux de *8 × 4 µm* **(A)** ou *3 × 4 µm* **(B). (C-D)** Carte de densité moyenne du signal LifeAct dans des DCs contrôles (en haut) ou traitées avec 10µM d'Y-27632 (bas) migrant dans des microcanaux de *8 × 4 µm* **(C)** ou *3 × 4 µm* **(D).** Un exemple représentatif de 2 expériences indépendantes. **(F-E)** Profil d'intensité moyenne du signal LifeAct des DCs migrant dans des microcanaux de *8 × 4 µm* **(F)** ou 3X4µm **(E).** La courbe et les barres d'erreur représentent respectivement la moyenne et la gamme de 2 expériences indépendantes. La ligne pointillée indique la position relative moyenne du noyau et la zone colorée l'actine devant celui-ci. **(G)** Quantification de l'accumulation du signal LifeAct **(G)** à l'arrière de la cellule pour DCs contrôles ou traités avec 10µM de Y-27632 migrant dans des microcanaux de *8 × 4 µm*, *5 × 4 µm* ou *3 × 4 µm*. Chaque point et chaque barre d'erreur représentent la moyenne et l'intervalle de confiance à 95% d'une expérience. **(H)** Vitesse des DCs contrôles ou traités avec 10µM de Y-27632 migrant dans des microcanaux de *8 × 4 µm*, *5 × 4 µm* ou *3 × 4 µm*. Chaque point et chaque barre d'erreur représentent respectivement la moyenne et l'intervalle de confiance à 95% d'une expérience. Un Anova avec le test de comparaison multiple de Tukey a été appliqué comme test statistique, *p<0,05, **p<0,01, *au dessus des point indiquent la comparaison entre les conditions contrôles et d'Y-27632 pour chaque taille de microcanaux, * avec les barres indiquent la comparaison entre les microcanaux *8 × 4 µm* et *3 × 4 µm* pour chaque condition de traitement. Ensemble de données ré-analysées à partir de Barbier et al, 2019, figure supplémentaire 2 A et B.

Par conséquent, le confinement induit une accumulation d'actine et de MyoII dans l'extrémité postérieure des DCs. Ce remaniement du cytosquelette est essentiel à la migration des DCs dans des espaces restreints et est dépendent de l'activité de ROCK. Des travaux complémentaires seront nécessaires pour identifier les voies de signalisation cellulaires mécano-sensibles qui conduisent à l'activation de ROCK lorsque les DCs sont confinées.

3. La dépolymérisation des microtubules affecte l'actine induite par le confinement au centre de la cellule

La structure d'actine au centre des DCs confinées correspond à un épaississement du cortex cellulaire qui entoure les lysosomes regroupés en amas autour du centre organisateur des microtubules (MTOC). Pour étudier cette structure, nous avons utilisé un inhibiteur chimique, le Nocodazole, qui provoque la dépolymérisation des microtubules et la dispersion des lysosomes dans les DCs (Fig.49 A et B). Les DCs traitées au Nocodazole ne présentent plus d'accumulation corticale d'actine au centre des cellules confinées (Fig.49 C à F). De manière surprenante, la suppression de cette structure d'actine n'affecte pas la vitesse de migration des DCs dans les microcanaux. Cependant, nous observons certaines cellules avec un pincement de leur cortex (Fig.49 A et B), ce qui pourrait amener à leur fragmentation dans un microenvironnement plus complexe où les

cellules peuvent générer des protrusions dans différentes directions. L'accumulation d'actine corticale autour des lysosomes pourrait donc éviter le morcellement des DCs lors de leurs déplacements dans des environnements denses et complexes, tel que dans des gels de collagène ou dans l'espace interstitiel des tissus. Cette hypothèse est en accord avec des travaux de Kopf et de ses collègues montrant que la dépolymérisation des microtubules provoque la fragmentation des cellules dans des gels de collagène.

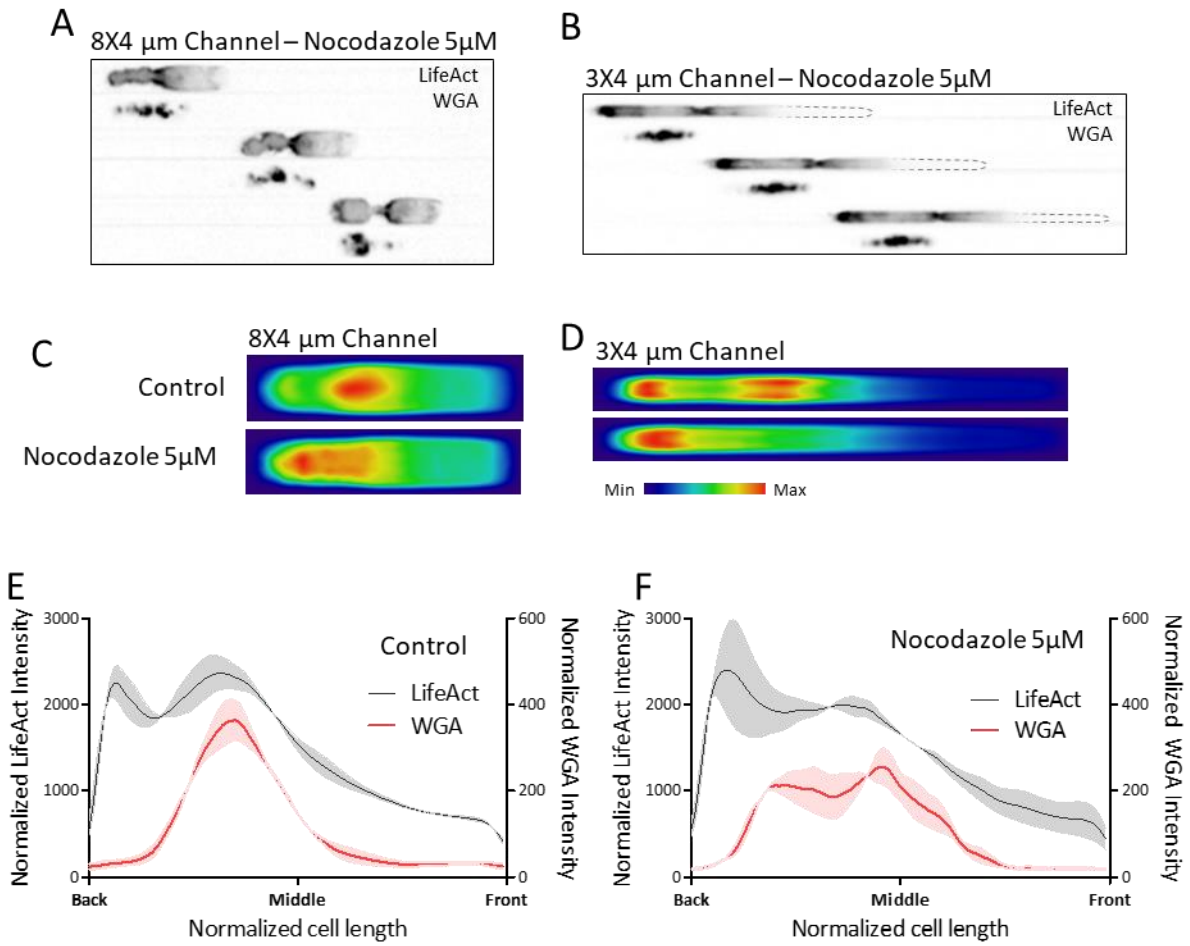

Figure 49 La dépolymérisation des microtubules affecte l'actine induite par le confinement au centre de la cellule.

(A-B) Montage représentatif d'une séquence d'images de DCs traités avec 5µM de nocodazole migrant dans des microcanaux de *8 × 4 µm* **(A)** ou *3 × 4 µm* **(B). (C-D)** Carte de densité moyenne du signal des DCs migrant dans des microcanaux de *8 × 4 µm* **(C)** ou *3 × 4 µm* **(D)** traitées avec du nocodazole 5µM ou une quantité équivalente de DMSO comme contrôle. Une expérience représentative sur trois est présentée. **(E-F)** Profil d'intensité moyen du LifeAct (actine) et WGA (lysosomes) des DCs migrant dans des microcanaux de *3 × 4 µm* traitées avec du nocodazole 5µM **(F)** ou une quantité équivalente de DMSO comme contrôle **(E).** La courbe et l'aire colorée représentent respectivement la moyenne et la gamme de 2 expériences indépendantes.

Ces résultats mettent donc pour la première fois en évidence la région lysosomale comme un détecteur potentiel du degré de confinement qui induit une réponse permettant de garantir l'intégrité cellulaire lors de la migration dans des espaces restreints. Des travaux complémentaires sont cependant nécessaires afin de confirmer le rôle de cette structure d'actine et de déterminer comment elle est induite par le confinement.

E. Conclusions et perspectives

Mes travaux de thèse ont montré que le cytosquelette des DCs est rapidement remanié en cas de modification des contraintes physiques appliquées par le microenvironnement. Cette réorganisation de l'actine et de la myosine est essentielle au maintien de la vitesse de migration des DCs dans des espaces denses et, par conséquent, à leur arrivée dans le système lymphatique suite à la détection d'une d'infection. Cependant, les mécanismes qui sous-tendent ce remodelage cellulaire restent à élucider, ainsi que leur fonction précise dans la migration des DCs dans l'espace interstitiel.

Comprendre comment les DCs répondent au confinement pourrait, dans un futur proche, fournir des outils moléculaires afin de contrôler la migration cellulaire à travers des tissus spécifiques. En particulier, dans les maladies inflammatoires telles que les encéphalopathies auto-immunes ou la dermatite de contact allergique, l'inhibition de la MyoII est déjà connue pour empêcher la migration des DCs vers les ganglions lymphatiques et ainsi limiter l'inflammation (Ufer et al., 2016), mais les mécanismes cellulaires qui sous-tendent cette action anti-inflammatoire restent inconnus. A l'inverse, la progression tumorale est souvent associée à une densification de la matrice extracellulaire entourant le corps de la tumeur qui limite l'infiltration des cellules immunitaires et *in fine* l'efficacité des immunothérapies. Dans ce cas, il serait bénéfique de favoriser l'infiltration des DCs en facilitant leur migration dans un milieu dense. L'approche réductionniste et les systèmes micro-fluidiques que j'utilise aboutiront à une meilleure compréhension des mécanismes qui régulent la mobilité des DCs en milieu confiné et ainsi créeront de nouvelles voies pour le développement de molécules permettant de moduler la réponse immunitaire adaptative à des fins thérapeutiques.

BIBLIOGRAPHY

Abbas, A., Lichtman, A., and Pillai, S. (2017a). Antigen Presentation to T Lymphocytes and the Functions of MHC Molecules. In Cellular and Molecular Immunology, (Elsvier), p.

Abbas, A., Lichtman, A., and Pillai, S. (2017b). Differentiation and Functions of CD4+ Effector T Cells. In Cellular and Molecular Immunology, (Elsvier), p.

Abbas, A., Lichtman, A., and Pillai, S. (2017c). Differentiation and Functions of CD8+ Effector T Cells. In Cellular and Molecular Immunology, (Elsvier), p.

Abbas, A., Lichtman, A., and Pillai, S. (2017d). B Cell Activation and Antibody Production. In Cellular and Molecular Immunology, (Elsvier), p.

Acton, S.E., Astarita, J.L., Malhotra, D., Lukacs-Kornek, V., Franz, B., Hess, P.R., Jakus, Z., Kuligowski, M., Fletcher, A.L., Elpek, K.G., et al. (2012). Podoplanin-Rich Stromal Networks Induce Dendritic Cell Motility via Activation of the C-type Lectin Receptor CLEC-2. Immunity *37*, 276–289.

Alberts, B., Johnson, A., Lewis, J., Raff, M., Roberts, K., and Walter, P. (2002a). Innate Immunity. Mol. Biol. Cell 4th Ed.

Alberts, B., Johnson, A., Lewis, J., Raff, M., Roberts, K., and Walter, P. (2002b). The Adaptive Immune System. Mol. Biol. Cell 4th Ed.

Alloatti, A., Kotsias, F., Pauwels, A.-M., Carpier, J.-M., Jouve, M., Timmerman, E., Pace, L., Vargas, P., Maurin, M., Gehrmann, U., et al. (2015). Toll-like Receptor 4 Engagement on Dendritic Cells Restrains Phago-Lysosome Fusion and Promotes Cross-Presentation of Antigens. Immunity *43*, 1087–1100.

Alloatti, A., Kotsias, F., Magalhaes, J.G., and Amigorena, S. (2016). Dendritic cell maturation and cross-presentation: timing matters! Immunol. Rev. *272*, 97–108.

Amann, K.J., and Pollard, T.D. (2001). The Arp2/3 complex nucleates actin filament branches from the sides of pre-existing filaments. Nat. Cell Biol. *3*, 306–310.

Baffet, A.D., Hu, D.J., and Vallee, R.B. (2015). Cdk1 Activates Pre-mitotic Nuclear Envelope Dynein Recruitment and Apical Nuclear Migration in Neural Stem Cells. Dev. Cell *33*, 703–716.

Bailly, M., Ichetovkin, I., Grant, W., Zebda, N., Machesky, L.M., Segall, J.E., and Condeelis, J. (2001). The F-actin side binding activity of the Arp2/3 complex is essential for actin nucleation and lamellipod extension. Curr. Biol. CB *11*, 620–625.

Bajénoff, M., Granjeaud, S., and Guerder, S. (2003). The Strategy of T Cell Antigen-presenting Cell Encounter in Antigen-draining Lymph Nodes Revealed by Imaging of Initial T Cell Activation. J. Exp. Med. *198*, 715–724.

Bajénoff, M., Egen, J.G., Koo, L.Y., Laugier, J.P., Brau, F., Glaichenhaus, N., and Germain, R.N. (2006). Stromal Cell Networks Regulate Lymphocyte Entry, Migration, and Territoriality in Lymph Nodes. Immunity *25*, 989–1001.

Balzer, E.M., Tong, Z., Paul, C.D., Hung, W.-C., Stroka, K.M., Boggs, A.E., Martin, S.S., and Konstantopoulos, K. (2012). Physical confinement alters tumor cell adhesion and migration phenotypes. FASEB J. *26*, 4045–4056.

Banchereau, J., and Steinman, R.M. (1998). Dendritic cells and the control of immunity. Nature *392*, 245–252.

Barzilai, S., Yadav, S.K., Morrell, S., Roncato, F., Klein, E., Stoler-Barak, L., Golani, O., Feigelson, S.W., Zemel, A., Nourshargh, S., et al. (2017). Leukocytes Breach Endothelial Barriers by Insertion of Nuclear Lobes and Disassembly of Endothelial Actin Filaments. Cell Rep. *18*, 685–699.

Belabed, M., Mauvais, F.-X., Maschalidi, S., Kurowska, M., Goudin, N., Huang, J.-D., Fischer, A., de Saint Basile, G., van Endert, P., Sepulveda, F.E., et al. (2020). Kinesin-1 regulates antigen cross-presentation through the scission of tubulations from early endosomes in dendritic cells. Nat. Commun. *11*, 1817.

Belotti, Y., McGloin, D., and Weijer, C.J. (2020). Chemotaxis overrides Barotaxis during Directional Decision-Making in Dictyostelium discoideum. BioRxiv 2020.01.14.904748.

Benvenuti, F., Hugues, S., Walmsley, M., Ruf, S., Fetler, L., Popoff, M., Tybulewicz, V.L.J., and Amigorena, S. (2004). Requirement of Rac1 and Rac2 expression by mature dendritic cells for T cell priming. Science *305*, 1150–1153.

Bergert, M., Chandradoss, S.D., Desai, R.A., and Paluch, E. (2012). Cell mechanics control rapid transitions between blebs and lamellipodia during migration. Proc. Natl. Acad. Sci. U. S. A. *109*, 14434–14439.

Bergert, M., Erzberger, A., Desai, R.A., Aspalter, I.M., Oates, A.C., Charras, G., Salbreux, G., and Paluch, E.K. (2015). Force transmission during adhesion-independent migration. Nat. Cell Biol. *17*, 524–529.

Biedzinski, S. (2018). Interplay between the nucleus and the microtubules : role in the regulation of chromatin organization in hematopoietic stem cells. These de doctorat. Sorbonne Paris Cité.

Biedzinski, S., Faivre, L., Vianay, B., Delord, M., Blanchoin, L., Larghero, J., Théry, M., and Brunet, S. (2019). Microtubules deform the nucleus and force chromatin reorganization during early differentiation of human hematopoietic stem cells. BioRxiv 763326.

Binamé, F., Pawlak, G., Roux, P., and Hibner, U. (2010). What makes cells move: requirements and obstacles for spontaneous cell motility. Mol. Biosyst. *6*, 648–661.

Bisaria, A., Hayer, A., Garbett, D., Cohen, D., and Meyer, T. (2020). Membrane-proximal F-actin restricts local membrane protrusions and directs cell migration. Science *368*, 1205–1210.

Blanchoin, L., Boujemaa-Paterski, R., Sykes, C., and Plastino, J. (2014). Actin dynamics, architecture, and mechanics in cell motility. Physiol. Rev. *94*, 235–263.

Bonnans, C., Chou, J., and Werb, Z. (2014). Remodelling the extracellular matrix in development and disease. Nat. Rev. Mol. Cell Biol. *15*, 786–801.

Boukhaled, G.M., Corrado, M., Guak, H., and Krawczyk, C.M. (2019). Chromatin Architecture as an Essential Determinant of Dendritic Cell Function. Front. Immunol. *10*.

Bousso, P. (2008). T-cell activation by dendritic cells in the lymph node: lessons from the movies. Nat. Rev. Immunol. *8*, 675–684.

Bousso, P., and Robey, E. (2003). Dynamics of CD8 + T cell priming by dendritic cells in intact lymph nodes. Nat. Immunol. *4*, 579–585.

Bovellan, M., Fritzsche, M., Stevens, C., and Charras, G. (2010). Death-associated protein kinase (DAPK) and signal transduction: blebbing in programmed cell death. FEBS J. *277*, 58–65.

Bretou, M., Sáez, P.J., Sanséau, D., Maurin, M., Lankar, D., Chabaud, M., Spampanato, C., Malbec, O., Barbier, L., Muallem, S., et al. (2017). Lysosome signaling controls the migration of dendritic cells. Sci. Immunol. *2*.

Campbell, I.D., and Humphries, M.J. (2011). Integrin structure, activation, and interactions. Cold Spring Harb. Perspect. Biol. *3*.

Carnell, M., Zech, T., Calaminus, S.D., Ura, S., Hagedorn, M., Johnston, S.A., May, R.C., Soldati, T., Machesky, L.M., and Insall, R.H. (2011). Actin polymerization driven by WASH causes V-ATPase retrieval and vesicle neutralization before exocytosis. J. Cell Biol. *193*, 831–839.

Case, L.B., and Waterman, C.M. (2015). Integration of actin dynamics and cell adhesion by a three-dimensional, mechanosensitive molecular clutch. Nat. Cell Biol. *17*, 955–963.

Cassimeris, L. (2009). Microtubule Associated Proteins in Neurons. In Encyclopedia of Neuroscience, L.R. Squire, ed. (Oxford: Academic Press), pp. 865–870.

Cella, M., Sallusto, F., and Lanzavecchia, A. (1997a). Origin, maturation and antigen presenting function of dendritic cells. Curr. Opin. Immunol. *9*, 10–16.

Cella, M., Engering, A., Pinet, V., Pieters, J., and Lanzavecchia, A. (1997b). Inflammatory stimuli induce accumulation of MHC class II complexes on dendritic cells. Nature *388*, 782–787.

Chabaud, M., Heuzé, M.L., Bretou, M., Vargas, P., Maiuri, P., Solanes, P., Maurin, M., Terriac, E., Le Berre, M., Lankar, D., et al. (2015). Cell migration and antigen capture are antagonistic processes coupled by myosin II in dendritic cells. Nat. Commun. *6*.

Charras, G., and Paluch, E. (2008). Blebs lead the way: how to migrate without lamellipodia. Nat. Rev. Mol. Cell Biol. *9*, 730–736.

Charras, G., and Sahai, E. (2014). Physical influences of the extracellular environment on cell migration. Nat. Rev. Mol. Cell Biol. *15*, 813–824.

Chen, Q., Sun, L., and Chen, Z.J. (2016). Regulation and function of the cGAS-STING pathway of cytosolic DNA sensing. Nat. Immunol. *17*, 1142–1149.

Colón-Franco, J.M., Gomez, T.S., and Billadeau, D.D. (2011). Dynamic remodeling of the actin cytoskeleton by FMNL1γ is required for structural maintenance of the Golgi complex. J. Cell Sci. *124*, 3118–3126.

Copos, C.A., Walcott, S., Del Álamo, J.C., Bastounis, E., Mogilner, A., and Guy, R.D. (2017). Mechanosensitive Adhesion Explains Stepping Motility in Amoeboid Cells. Biophys. J. *112*, 2672–2682.

Cougoule, C., Lastrucci, C., Guiet, R., Mascarau, R., Meunier, E., Lugo-Villarino, G., Neyrolles, O., Poincloux, R., and Maridonneau-Parini, I. (2018). Podosomes, But Not the Maturation Status, Determine the Protease-Dependent 3D Migration in Human Dendritic Cells. Front. Immunol. *9*.

Cramer, L.P. (1997). Molecular mechanism of actin-dependent retrograde flow in lamellipodia of motile cells. Front. Biosci. J. Virtual Libr. *2*, d260-270.

Cramer, L.P. (2013). Mechanism of cell rear retraction in migrating cells. Curr. Opin. Cell Biol. *25*, 591–599.

Curreli, S., Wong, B.S., Latinovic, O., Konstantopoulos, K., and Stamatos, N.M. (2016). Class 3 semaphorins induce F-actin reorganization in human dendritic cells: Role in cell migration. J. Leukoc. Biol. *100*, 1323–1334.

De Bruyn, P.P.H. (1946). The amoeboid movement of the mammalian leukocyte in tissue culture. Anat. Rec. *95*, 177–191.

Devreotes, P., and Horwitz, A.R. (2015). Signaling networks that regulate cell migration. Cold Spring Harb. Perspect. Biol. *7*, a005959.

Diz-Muñoz, A., Krieg, M., Bergert, M., Ibarlucea-Benitez, I., Muller, D.J., Paluch, E., and Heisenberg, C.-P. (2010). Control of directed cell migration in vivo by membrane-to-cortex attachment. PLoS Biol. *8*, e1000544.

Diz-Muñoz, A., Thurley, K., Chintamen, S., Altschuler, S.J., Wu, L.F., Fletcher, D.A., and Weiner, O.D. (2016). Membrane Tension Acts Through PLD2 and mTORC2 to Limit Actin Network Assembly During Neutrophil Migration. PLOS Biol. *14*, e1002474.

Dogterom, M., and Koenderink, G.H. (2019). Actin–microtubule crosstalk in cell biology. Nat. Rev. Mol. Cell Biol. *20*, 38–54.

van den Dries, K., van Helden, S.F.G., Riet, J. te, Diez-Ahedo, R., Manzo, C., Oud, M.M., van Leeuwen, F.N., Brock, R., Garcia-Parajo, M.F., Cambi, A., et al. (2012). Geometry sensing by dendritic cells dictates spatial organization and PGE2-induced dissolution of podosomes. Cell. Mol. Life Sci. *69*, 1889–1901.

El-Barbry, H., Capitao, M., Barrin, S., Amziani, S., Paul, P.P., Borreill, S., Guilbert, T., Donnadieu, E., Niedergang, F., and Ouaaz, F. (2020). Extracellular Release of Antigen by Dendritic Cell Regurgitation Promotes B Cell Activation through NF-κB/cRel. J. Immunol.

Etienne-Manneville, S. (2013). Microtubules in cell migration. Annu. Rev. Cell Dev. Biol. *29*, 471–499.

Faix, J., and Rottner, K. (2006). The making of filopodia. Curr. Opin. Cell Biol. *18*, 18–25.

Faure-André, G., Vargas, P., Yuseff, M.-I., Heuzé, M., Diaz, J., Lankar, D., Steri, V., Manry, J., Hugues, S., Vascotto, F., et al. (2008). Regulation of Dendritic Cell Migration by CD74, the MHC Class II-Associated Invariant Chain. Science *322*, 1705.

Friedl, P., and Bröcker, E.B. (2000). The biology of cell locomotion within three-dimensional extracellular matrix. Cell. Mol. Life Sci. CMLS *57*, 41–64.

Frittoli, E., Matteoli, G., Palamidessi, A., Mazzini, E., Maddaluno, L., Disanza, A., Yang, C., Svitkina, T., Rescigno, M., and Scita, G. (2011). The Signaling Adaptor Eps8 Is an Essential Actin Capping Protein for Dendritic Cell Migration. Immunity *35*, 388–399.

Fritz-Laylin, L.K., Riel-Mehan, M., Chen, B.-C., Lord, S.J., Goddard, T.D., Ferrin, T.E., Nicholson-Dykstra, S.M., Higgs, H., Johnson, G.T., Betzig, E., et al. (2017). Actin-based protrusions of migrating neutrophils are intrinsically lamellar and facilitate direction changes. ELife *6*.

Fu, H., Ward, E.J., and Marelli-Berg, F.M. (2016). Mechanisms of T cell organotropism. Cell. Mol. Life Sci. *73*, 3009–3033.

Garcia-Arcos, J.M., Chabrier, R., Deygas, M., Nader, G., Barbier, L., Sáez, P.J., Mathur, A., Vargas, P., and Piel, M. (2019). Reconstitution of cell migration at a glance. J. Cell Sci. *132*.

Gardner, A., de Mingo Pulido, Á., and Ruffell, B. (2020). Dendritic Cells and Their Role in Immunotherapy. Front. Immunol. *11*.

Gerner, M.Y., Casey, K.A., Kastenmuller, W., and Germain, R.N. (2017). Dendritic cell and antigen dispersal landscapes regulate T cell immunity. J. Exp. Med. *214*, 3105–3122.

Goley, E.D., and Welch, M.D. (2006). The ARP2/3 complex: an actin nucleator comes of age. Nat. Rev. Mol. Cell Biol. *7*, 713–726.

Gomes, E.R., Jani, S., and Gundersen, G.G. (2005). Nuclear movement regulated by Cdc42, MRCK, myosin, and actin flow establishes MTOC polarization in migrating cells. Cell *121*, 451–463.

Harada, T., Swift, J., Irianto, J., Shin, J.-W., Spinler, K.R., Athirasala, A., Diegmiller, R., Dingal, P.C.D.P., Ivanovska, I.L., and Discher, D.E. (2014). Nuclear lamin stiffness is a barrier to 3D migration, but softness can limit survival. J. Cell Biol. *204*, 669–682.

Harada, Y., Tanaka, Y., Terasawa, M., Pieczyk, M., Habiro, K., Katakai, T., Hanawa-Suetsugu, K., Kukimoto-Niino, M., Nishizaki, T., Shirouzu, M., et al. (2012). DOCK8 is a Cdc42 activator critical for interstitial dendritic cell migration during immune responses. Blood *119*, 4451–4461.

Helft, J., Böttcher, J., Chakravarty, P., Zelenay, S., Huotari, J., Schraml, B.U., Goubau, D., and Reis e Sousa, C. (2015). GM-CSF Mouse Bone Marrow Cultures Comprise a Heterogeneous Population of CD11c (+)MHCII (+) Macrophages and Dendritic Cells. Immunity *42*, 1197–1211.

Hetmanski, J.H.R., de Belly, H., Busnelli, I., Waring, T., Nair, R.V., Sokleva, V., Dobre, O., Cameron, A., Gauthier, N., Lamaze, C., et al. (2019). Membrane Tension Orchestrates Rear Retraction in Matrix-Directed Cell Migration. Dev. Cell *51*, 460-475.e10.

Hetrick, B., Han, M.S., Helgeson, L.A., and Nolen, B.J. (2013). Small molecules CK-666 and CK-869 inhibit Arp2/3 complex by blocking an activating conformational change. Chem. Biol. *20*, 701–712.

Heuzé, M.L., Collin, O., Terriac, E., Lennon-Duménil, A.-M., and Piel, M. (2011). Cell migration in confinement: a micro-channel-based assay. Methods Mol. Biol. Clifton NJ *769*, 415–434.

Heuzé, M.L., Vargas, P., Chabaud, M., Le Berre, M., Liu, Y.-J., Collin, O., Solanes, P., Voituriez, R., Piel, M., and Lennon-Duménil, A.-M. (2013). Migration of dendritic cells: physical principles, molecular mechanisms, and functional implications. Immunol. Rev. *256*, 240–254.

Higashida, C., Miyoshi, T., Fujita, A., Oceguera-Yanez, F., Monypenny, J., Andou, Y., Narumiya, S., and Watanabe, N. (2004). Actin polymerization-driven molecular movement of mDia1 in living cells. Science *303*, 2007–2010.

Hilligan, K.L., and Ronchese, F. (2020). Antigen presentation by dendritic cells and their instruction of CD4+ T helper cell responses. Cell. Mol. Immunol. *17*, 587–599.

Hind, L.E., Vincent, W.J.B., and Huttenlocher, A. (2016). Leading from the Back: The Role of the Uropod in Neutrophil Polarization and Migration. Dev. Cell *38*, 161–169.

Höing, S., Yeh, T.-Y., Baumann, M., Martinez, N.E., Habenberger, P., Kremer, L., Drexler, H.C.A., Küchler, P., Reinhardt, P., Choidas, A., et al. (2018). Dynarrestin, a Novel Inhibitor of Cytoplasmic Dynein. Cell Chem. Biol. *25*, 357-369.e6.

Houk, A.R., Jilkine, A., Mejean, C.O., Boltyanskiy, R., Dufresne, E.R., Angenent, S.B., Altschuler, S.J., Wu, L.F., and Weiner, O.D. (2012). Membrane tension maintains cell polarity by confining signals to the leading edge during neutrophil migration. Cell *148*, 175–188.

Ibo, M., Srivastava, V., Robinson, D.N., and Gagnon, Z.R. (2016). Cell Blebbing in Confined Microfluidic Environments. PLOS ONE *11*, e0163866.

Inaba, K., Inaba, M., Romani, N., Aya, H., Deguchi, M., Ikehara, S., Muramatsu, S., and Steinman, R.M. (1992). Generation of large numbers of dendritic cells from mouse bone marrow cultures supplemented with granulocyte/macrophage colony-stimulating factor. J. Exp. Med. *176*, 1693–1702.

Infante, E., Castagnino, A., Ferrari, R., Monteiro, P., Agüera-González, S., Paul-Gilloteaux, P., Domingues, M.J., Maiuri, P., Raab, M., Shanahan, C.M., et al. (2018). LINC complex-Lis1 interplay controls MT1-MMP matrix digest-on-demand response for confined tumor cell migration. Nat. Commun. *9*, 2443.

Irimia, D., and Ellett, F. (2016). Big insights from small volumes: deciphering complex leukocyte behaviors using microfluidics. J. Leukoc. Biol. *100*, 291–304.

Isogai, T., van der Kammen, R., and Innocenti, M. (2015). SMIFH2 has effects on Formins and p53 that perturb the cell cytoskeleton. Sci. Rep. *5*, 9802.

Iwasaki, A., and Medzhitov, R. (2015). Control of adaptive immunity by the innate immune system. Nat. Immunol. *16*, 343–353.

Jacobelli, J., Bennett, F.C., Pandurangi, P., Tooley, A.J., and Krummel, M.F. (2009). Myosin-IIA and ICAM-1 Regulate the Interchange between Two Distinct Modes of T Cell Migration. J. Immunol. *182*, 2041–2050.

Jacobelli, J., Matthews, M.E., Chen, S., and Krummel, M.F. (2013). Activated T Cell Trans-Endothelial Migration Relies on Myosin-IIA Contractility for Squeezing the Cell Nucleus through Endothelial Cell Barriers. PLOS ONE *8*, e75151.

Kage, F., Winterhoff, M., Dimchev, V., Mueller, J., Thalheim, T., Freise, A., Brühmann, S., Kollasser, J., Block, J., Dimchev, G., et al. (2017a). FMNL formins boost lamellipodial force generation. Nat. Commun. *8*, 14832.

Kage, F., Steffen, A., Ellinger, A., Ranftler, C., Gehre, C., Brakebusch, C., Pavelka, M., Stradal, T., and Rottner, K. (2017b). FMNL2 and -3 regulate Golgi architecture and anterograde transport downstream of Cdc42. Sci. Rep. *7*, 9791.

Kambayashi, T., and Laufer, T.M. (2014). Atypical MHC class II-expressing antigen-presenting cells: can anything replace a dendritic cell? Nat. Rev. Immunol. *14*, 719–730.

Kashyap, A.S., Fernandez-Rodriguez, L., Zhao, Y., Monaco, G., Trefny, M.P., Yoshida, N., Martin, K., Sharma, A., Olieric, N., Shah, P., et al. (2019). GEF-H1 Signaling upon Microtubule Destabilization Is Required for Dendritic Cell Activation and Specific Anti-tumor Responses. Cell Rep. *28*, 3367-3380.e8.

Kawasaki, Y., Senda, T., Ishidate, T., Koyama, R., Morishita, T., Iwayama, Y., Higuchi, O., and Akiyama, T. (2000). Asef, a link between the tumor suppressor APC and G-protein signaling. Science *289*, 1194–1197.

Keren, K., Pincus, Z., Allen, G.M., Barnhart, E.L., Marriott, G., Mogilner, A., and Theriot, J.A. (2008). Mechanism of shape determination in motile cells. Nature *453*, 475–480.

Khurana, S., and George, S.P. (2011). The role of actin bundling proteins in the assembly of filopodia in epithelial cells. Cell Adhes. Migr. *5*, 409–420.

Kienle, K., and Lämmermann, T. (2016). Neutrophil swarming: an essential process of the neutrophil tissue response. Immunol. Rev. *273*, 76–93.

Kissenpfennig, A., Henri, S., Dubois, B., Laplace-Builhé, C., Perrin, P., Romani, N., Tripp, C.H., Douillard, P., Leserman, L., Kaiserlian, D., et al. (2005). Dynamics and function of Langerhans cells in vivo: dermal dendritic cells colonize lymph node areas distinct from slower migrating Langerhans cells. Immunity *22*, 643–654.

Kopf, A., Renkawitz, J., Hauschild, R., Girkontaite, I., Tedford, K., Merrin, J., Thorn-Seshold, O., Trauner, D., Häcker, H., Fischer, K.-D., et al. (2020). Microtubules control cellular shape and coherence in amoeboid migrating cells. J. Cell Biol. *219*.

Kovar, D.R., and Pollard, T.D. (2004). Insertional assembly of actin filament barbed ends in association with formins produces piconewton forces. Proc. Natl. Acad. Sci. U. S. A. *101*, 14725–14730.

Kular, J.K., Basu, S., and Sharma, R.I. (2014). The extracellular matrix: Structure, composition, age-related differences, tools for analysis and applications for tissue engineering. J. Tissue Eng. *5*.

Lambrechts, A., Gevaert, K., Cossart, P., Vandekerckhove, J., and Van Troys, M. (2008). Listeria comet tails: the actin-based motility machinery at work. Trends Cell Biol. *18*, 220–227.

Lammerding, J., Fong, L.G., Ji, J.Y., Reue, K., Stewart, C.L., Young, S.G., and Lee, R.T. (2006). Lamins A and C but not lamin B1 regulate nuclear mechanics. J. Biol. Chem. *281*, 25768–25780.

Lämmermann, T., and Germain, R.N. (2014). The multiple faces of leukocyte interstitial migration. Semin. Immunopathol. *36*, 227–251.

Lämmermann, T., and Kastenmüller, W. (2019). Concepts of GPCR-controlled navigation in the immune system. Immunol. Rev. *289*, 205–231.

Lämmermann, T., and Sixt, M. (2008). The microanatomy of T-cell responses. Immunol. Rev. *221*, 26–43.

Lämmermann, T., and Sixt, M. (2009). Mechanical modes of “amoeboid” cell migration. Curr. Opin. Cell Biol. *21*, 636–644.

Lämmermann, T., Bader, B.L., Monkley, S.J., Worbs, T., Wedlich-Söldner, R., Hirsch, K., Keller, M., Förster, R., Critchley, D.R., Fässler, R., et al. (2008). Rapid leukocyte migration by integrin-independent flowing and squeezing. Nature *453*, 51–55.

Lämmermann, T., Renkawitz, J., Wu, X., Hirsch, K., Brakebusch, C., and Sixt, M. (2009). Cdc42-dependent leading edge coordination is essential for interstitial dendritic cell migration. Blood *113*, 5703–5710.

Lämmermann, T., Afonso, P.V., Angermann, B.R., Wang, J.M., Kastenmüller, W., Parent, C.A., and Germain, R.N. (2013). Neutrophil swarms require LTB4 and integrins at sites of cell death in vivo. Nature *498*, 371–375.

Lamsoul, I., Métais, A., Gouot, E., Heuzé, M.L., Lennon-Duménil, A.-M., Moog-Lutz, C., and Lutz, P.G. (2013). ASB2α regulates migration of immature dendritic cells. Blood *122*, 533–541.

Lawson, C.D., and Ridley, A.J. (2018). Rho GTPase signaling complexes in cell migration and invasion. J. Cell Biol. *217*, 447–457.

Le Berre, M., Liu, Y.-J., Hu, J., Maiuri, P., Bénichou, O., Voituriez, R., Chen, Y., and Piel, M. (2013). Geometric Friction Directs Cell Migration. Phys. Rev. Lett. *111*, 198101.

Le Berre, M., Zlotek-Zlotkiewicz, E., Bonazzi, D., Lautenschlaeger, F., and Piel, M. (2014). Chapter 14 - Methods for Two-Dimensional Cell Confinement. In Methods in Cell Biology, M. Piel, and M. Théry, eds. (Academic Press), pp. 213–229.

Lee, J.-H., Katakai, T., Hara, T., Gonda, H., Sugai, M., and Shimizu, A. (2004). Roles of p-ERM and Rho–ROCK signaling in lymphocyte polarity and uropod formation. J. Cell Biol. *167*, 327–337.

Leithner, A., Eichner, A., Müller, J., Reversat, A., Brown, M., Schwarz, J., Merrin, J., de Gorter, D.J.J., Schur, F., Bayerl, J., et al. (2016). Diversified actin protrusions promote environmental exploration but are dispensable for locomotion of leukocytes. Nat. Cell Biol. *18*, 1253.

Lele, T.P., Dickinson, R.B., and Gundersen, G.G. (2018). Mechanical principles of nuclear shaping and positioning. J. Cell Biol. *217*, 3330–3342.

Li, R., and Gundersen, G.G. (2008). Beyond polymer polarity: how the cytoskeleton builds a polarized cell. Nat. Rev. Mol. Cell Biol. *9*, 860–873.

Lindquist, R.L., Shakhar, G., Dudziak, D., Wardemann, H., Eisenreich, T., Dustin, M.L., and Nussenzweig, M.C. (2004). Visualizing dendritic cell networks in vivo. Nat. Immunol. *5*, 1243–1250.

Liu, Y., Belkina, N.V., Park, C., Nambiar, R., Loughhead, S.M., Patino-Lopez, G., Ben-Aissa, K., Hao, J.-J., Kruhlak, M.J., Qi, H., et al. (2012). Constitutively active ezrin increases membrane tension, slows migration, and impedes endothelial transmigration of lymphocytes in vivo in mice. Blood *119*, 445–453.

Liu, Y.-J., Le Berre, M., Lautenschlaeger, F., Maiuri, P., Callan-Jones, A., Heuzé, M., Takaki, T., Voituriez, R., and Piel, M. (2015). Confinement and low adhesion induce fast amoeboid migration of slow mesenchymal cells. Cell *160*, 659–672.

Lodish, H., Berk, A., and Zipursky, S.L. (2000). Molecular Cell Biology. 4th edition (New York).

Lomakin, A.J., Cattin, C.J., Cuvelier, D., Alraies, Z., Molina, M., Nader, G., Srivastava, N., Garcia-Arcos, J.M., Zhitnyak, I.Y., Bhargava, A., et al. (2019). The nucleus acts as a ruler tailoring cell responses to spatial constraints. BioRxiv 863514.

Lorentzen, A., Bamber, J., Sadok, A., Elson-Schwab, I., and Marshall, C.J. (2011). An ezrin-rich, rigid uropod-like structure directs movement of amoeboid blebbing cells. J. Cell Sci. *124*, 1256–1267.

Luster, A.D., Alon, R., and von Andrian, U.H. (2005). Immune cell migration in inflammation: present and future therapeutic targets. Nat. Immunol. *6*, 1182–1190.

Maiuri, P., Rupprecht, J.-F., Wieser, S., Ruprecht, V., Bénichou, O., Carpi, N., Coppey, M., De Beco, S., Gov, N., Heisenberg, C.-P., et al. (2015). Actin flows mediate a universal coupling between cell speed and cell persistence. Cell *161*, 374–386.

Malawista, S.E., de Boisfleury Chevance, A., and Boxer, L.A. (2000). Random locomotion and chemotaxis of human blood polymorphonuclear leukocytes from a patient with leukocyte adhesion deficiency-1: normal displacement in close quarters via chimneying. Cell Motil. Cytoskeleton *46*, 183–189.

Markwardt, M.L., Snell, N.E., Guo, M., Wu, Y., Christensen, R., Liu, H., Shroff, H., and Rizzo, M.A. (2018). A Genetically Encoded Biosensor Strategy for Quantifying Non-muscle Myosin II Phosphorylation Dynamics in Living Cells and Organisms. Cell Rep. *24*, 1060-1070.e4.

van Meer, B.J., de Vries, H., Firth, K.S.A., van Weerd, J., Tertoolen, L.G.J., Karperien, H.B.J., Jonkheijm, P., Denning, C., IJzerman, A.P., and Mummery, C.L. (2017). Small molecule absorption by PDMS in the context of drug response bioassays. Biochem. Biophys. Res. Commun. *482*, 323–328.

Mescher, A.L. (2016). The Immune System & Lymphoid Organs. In Junqueira's Basic Histology, (New York, NY: McGraw-Hill Education), p.

Miki, H., Sasaki, T., Takai, Y., and Takenawa, T. (1998). Induction of filopodium formation by a WASP-related actin-depolymerizing protein N-WASP. Nature *391*, 93–96.

Mogensen, T.H. (2009). Pathogen Recognition and Inflammatory Signaling in Innate Immune Defenses. Clin. Microbiol. Rev. *22*, 240–273.

Molinie, N., and Gautreau, A. (2018). The Arp2/3 Regulatory System and Its Deregulation in Cancer. Physiol. Rev. *98*, 215–238.

Moreau, H.D., Blanch-Mercader, C., Attia, R., Maurin, M., Alraies, Z., Sanséau, D., Malbec, O., Delgado, M.-G., Bousso, P., Joanny, J.-F., et al. (2019). Macropinocytosis Overcomes Directional Bias in Dendritic Cells Due to Hydraulic Resistance and Facilitates Space Exploration. Dev. Cell *49*, 171-188.e5.

Mseka, T., and Cramer, L.P. (2011). Actin depolymerization-based force retracts the cell rear in polarizing and migrating cells. Curr. Biol. CB *21*, 2085–2091.

Muroyama, A., and Lechler, T. (2017). Microtubule organization, dynamics and functions in differentiated cells. Development *144*, 3012–3021.

Nader, G.P.F., Agüera-Gonzalez, S., Routet, F., Gratia, M., Maurin, M., Cancila, V., Cadart, C., Gentili, M., Yamada, A., Lodillinsky, C., et al. (2020). Compromised nuclear envelope integrity drives tumor cell invasion. BioRxiv 2020.05.22.110122.

Neefjes, J., Jongsma, M.L.M., Paul, P., and Bakke, O. (2011). Towards a systems understanding of MHC class I and MHC class II antigen presentation. Nat. Rev. Immunol. *11*, 823–836.

Ng, L.G., Qin, J.S., Roediger, B., Wang, Y., Jain, R., Cavanagh, L.L., Smith, A.L., Jones, C.A., de Veer, M., Grimbaldeston, M.A., et al. (2011). Visualizing the Neutrophil Response to Sterile Tissue Injury in Mouse Dermis Reveals a Three-Phase Cascade of Events. J. Invest. Dermatol. *131*, 2058–2068.

de Noronha, S., Hardy, S., Sinclair, J., Blundell, M.P., Strid, J., Schulz, O., Zwirner, J., Jones, G.E., Katz, D.R., Kinnon, C., et al. (2005). Impaired dendritic-cell homing in vivo in the absence of Wiskott-Aldrich syndrome protein. Blood *105*, 1590–1597.

Obeidy, P., Ju, L.A., Oehlers, S.H., Zulkhernain, N.S., Lee, Q., Galeano Niño, J.L., Kwan, R.Y., Tikoo, S., Cavanagh, L.L., Mrass, P., et al. (2020). Partial loss of actin nucleator actin-related protein 2/3 activity triggers blebbing in primary T lymphocytes. Immunol. Cell Biol. *98*, 93–113.

Obino, D., Farina, F., Malbec, O., Sáez, P.J., Maurin, M., Gaillard, J., Dingli, F., Loew, D., Gautreau, A., Yuseff, M.-I., et al. (2016). Actin nucleation at the centrosome controls lymphocyte polarity. Nat. Commun. *7*, 10969.

Ohl, L., Mohaupt, M., Czeloth, N., Hintzen, G., Kiafard, Z., Zwirner, J., Blankenstein, T., Henning, G., and Förster, R. (2004). CCR7 governs skin dendritic cell migration under inflammatory and steady-state conditions. Immunity *21*, 279–288.

Osmani, N., Peglion, F., Chavrier, P., and Etienne-Manneville, S. (2010). Cdc42 localization and cell polarity depend on membrane traffic. J. Cell Biol. *191*, 1261–1269.

Osorio, D.S., and Gomes, E.R. (2014). Connecting the nucleus to the cytoskeleton for nuclear positioning and cell migration. Adv. Exp. Med. Biol. *773*, 505–520.

Overstreet, M.G., Gaylo, A., Angermann, B.R., Hughson, A., Hyun, Y.-M., Lambert, K., Acharya, M., Billroth-MacLurg, A.C., Rosenberg, A.F., Topham, D.J., et al. (2013). Inflammation-induced interstitial migration of effector CD4+ T cells is dependent on integrin αV. Nat. Immunol. *14*, 949–958.

Palecek, S.P., Loftus, J.C., Ginsberg, M.H., Lauffenburger, D.A., and Horwitz, A.F. (1997). Integrin-ligand binding properties govern cell migration speed through cell-substratum adhesiveness. Nature *385*, 537–540.

Parsons, J.T., Horwitz, A.R., and Schwartz, M.A. (2010). Cell adhesion: integrating cytoskeletal dynamics and cellular tension. Nat. Rev. Mol. Cell Biol. *11*, 633–643.

Pejoski, D., Ballester, M., Auderset, F., Vono, M., Christensen, D., Andersen, P., Lambert, P.-H., and Siegrist, C.-A. (2019). Site-Specific DC Surface Signatures Influence CD4+ T Cell Co-stimulation and Lung-Homing. Front. Immunol. *10*.

Perdiguero, E.G., and Geissmann, F. (2016). The development and maintenance of resident

macrophages. Nat. Immunol. *17*, 2–8.

Petrie, R.J., Gavara, N., Chadwick, R.S., and Yamada, K.M. (2012). Nonpolarized signaling reveals two distinct modes of 3D cell migration. J. Cell Biol. *197*, 439–455.

Pflicke, H., and Sixt, M. (2009). Preformed portals facilitate dendritic cell entry into afferent lymphatic vessels. J. Exp. Med. *206*, 2925–2935.

Pober, J.S., and Sessa, W.C. (2007). Evolving functions of endothelial cells in inflammation. Nat. Rev. Immunol. *7*, 803–815.

Pollard, T.D., and Borisy, G.G. (2003). Cellular motility driven by assembly and disassembly of actin filaments. Cell *112*, 453–465.

Ponti, A., Machacek, M., Gupton, S.L., Waterman-Storer, C.M., and Danuser, G. (2004). Two distinct actin networks drive the protrusion of migrating cells. Science *305*, 1782–1786.

Prentice-Mott, H.V., Chang, C.-H., Mahadevan, L., Mitchison, T.J., Irimia, D., and Shah, J.V. (2013). Biased migration of confined neutrophil-like cells in asymmetric hydraulic environments. Proc. Natl. Acad. Sci. *110*, 21006–21011.

Prentice-Mott, H.V., Meroz, Y., Carlson, A., Levine, M.A., Davidson, M.W., Irimia, D., Charras, G.T., Mahadevan, L., and Shah, J.V. (2016). Directional memory arises from long-lived cytoskeletal asymmetries in polarized chemotactic cells. Proc. Natl. Acad. Sci. *113*, 1267–1272.

Pruyne, D., Evangelista, M., Yang, C., Bi, E., Zigmond, S., Bretscher, A., and Boone, C. (2002). Role of formins in actin assembly: nucleation and barbed-end association. Science *297*, 612–615.

Pu, J., Guardia, C.M., Keren-Kaplan, T., and Bonifacino, J.S. (2016). Mechanisms and functions of lysosome positioning. J. Cell Sci. *129*, 4329–4339.

Raab, M., Gentili, M., de Belly, H., Thiam, H.R., Vargas, P., Jimenez, A.J., Lautenschlaeger, F., Voituriez, R., Lennon-Duménil, A.M., Manel, N., et al. (2016). ESCRT III repairs nuclear envelope ruptures during cell migration to limit DNA damage and cell death. Science *352*, 359–362.

Ramabhadran, V., Korobova, F., Rahme, G.J., and Higgs, H.N. (2011). Splice variant–specific cellular function of the formin INF2 in maintenance of Golgi architecture. Mol. Biol. Cell *22*, 4822–4833.

Ramalingam, N., Franke, C., Jaschinski, E., Winterhoff, M., Lu, Y., Brühmann, S., Junemann, A., Meier, H., Noegel, A.A., Weber, I., et al. (2015). A resilient formin-derived cortical actin meshwork in the rear drives actomyosin-based motility in 2D confinement. Nat. Commun. *6*, 8496.

Renkawitz, J., Schumann, K., Weber, M., Lämmermann, T., Pflicke, H., Piel, M., Polleux, J., Spatz, J.P., and Sixt, M. (2009). Adaptive force transmission in amoeboid cell migration. Nat. Cell Biol. *11*, 1438–1443.

Renkawitz, J., Kopf, A., Stopp, J., de Vries, I., Driscoll, M.K., Merrin, J., Hauschild, R., Welf, E.S., Danuser, G., Fiolka, R., et al. (2019). Nuclear positioning facilitates amoeboid migration along the path of least resistance. Nature *568*, 546–550.

Reversat, A., Gaertner, F., Merrin, J., Stopp, J., Tasciyan, S., Aguilera, J., de Vries, I., Hauschild, R., Hons, M., Piel, M., et al. (2020). Cellular locomotion using environmental topography. Nature 1–4.

Ridley, A.J. (2011). Life at the leading edge. Cell *145*, 1012–1022.

Riedl, J., Flynn, K.C., Raducanu, A., Gärtner, F., Beck, G., Bösl, M., Bradke, F., Massberg, S., Aszodi, A., Sixt, M., et al. (2010). Lifeact mice for studying F-actin dynamics. Nat. Methods *7*, 168–169.

Riese, R.J., Mitchell, R.N., Villadangos, J.A., Shi, G.P., Palmer, J.T., Karp, E.R., De Sanctis, G.T., Ploegh, H.L., and Chapman, H.A. (1998). Cathepsin S activity regulates antigen presentation and immunity. J. Clin. Invest. *101*, 2351–2363.

Rizvi, S.A., Neidt, E.M., Cui, J., Feiger, Z., Skau, C.T., Gardel, M.L., Kozmin, S.A., and Kovar, D.R. (2009). Identification and Characterization of a Small Molecule Inhibitor of Formin-Mediated Actin Assembly. Chem. Biol. *16*, 1158–1168.

Roche, P.A., and Furuta, K. (2015). The ins and outs of MHC class II-mediated antigen processing and presentation. Nat. Rev. Immunol. *15*, 203–216.

Rowat, A.C., Jaalouk, D.E., Zwerger, M., Ung, W.L., Eydelnant, I.A., Olins, D.E., Olins, A.L., Herrmann, H., Weitz, D.A., and Lammerding, J. (2013). Nuclear envelope composition determines the ability of neutrophil-type cells to passage through micron-scale constrictions. J. Biol. Chem. *288*, 8610–8618.

Ruprecht, V., Wieser, S., Callan-Jones, A., Smutny, M., Morita, H., Sako, K., Barone, V., Ritsch-Marte, M., Sixt, M., Voituriez, R., et al. (2015). Cortical contractility triggers a stochastic switch to fast amoeboid cell motility. Cell *160*, 673–685.

Russo, E., Teijeira, A., Vaahtomeri, K., Willrodt, A.-H., Bloch, J.S., Nitschké, M., Santambrogio, L., Kerjaschki, D., Sixt, M., and Halin, C. (2016). Intralymphatic CCL21 Promotes Tissue Egress of Dendritic Cells through Afferent Lymphatic Vessels. Cell Rep. *14*, 1723–1734.

Sáez, P.J., Vargas, P., Shoji, K.F., Harcha, P.A., Lennon-Duménil, A.-M., and Sáez, J.C. (2017). ATP promotes the fast migration of dendritic cells through the activity of pannexin 1 channels and $P2X_7$ receptors. Sci. Signal. *10*.

Sáez, P.J., Barbier, L., Attia, R., Thiam, H.-R., Piel, M., and Vargas, P. (2018). Leukocyte Migration and Deformation in Collagen Gels and Microfabricated Constrictions. In Cell Migration: Methods and Protocols, A. Gautreau, ed. (New York, NY: Springer New York), pp. 361–373.

Sainath, R., and Gallo, G. (2015). The Dynein Inhibitor Ciliobrevin D Inhibits the Bi-directional Transport of Organelles along Sensory Axons and Impairs NGF-Mediated Regulation of Growth Cones and Axon Branches. Dev. Neurobiol. *75*, 757–777.

Salbreux, G., Charras, G., and Paluch, E. (2012). Actin cortex mechanics and cellular morphogenesis. Trends Cell Biol. *22*, 536–545.

Sallusto, F., Schaerli, P., Loetscher, P., Schaniel, C., Lenig, D., Mackay, C.R., Qin, S., and Lanzavecchia, A. (1998). Rapid and coordinated switch in chemokine receptor expression during dendritic cell maturation. Eur. J. Immunol. *28*, 2760–2769.

Samie, M., and Cresswell, P. (2015). The transcription factor TFEB acts as a molecular switch that regulates exogenous antigen-presentation pathways. Nat. Immunol. *16*, 729–736.

Sanjuan, M.A., Milasta, S., and Green, D.R. (2009). Toll-like receptor signaling in the lysosomal pathways. Immunol. Rev. *227*, 203–220.

Seetharaman, S., Vianay, B., Roca, V., Pascalis, C.D., Boëda, B., Dingli, F., Loew, D., Vassilopoulos, S., Théry, M., and Etienne-Manneville, S. (2020). Microtubules tune mechanosensitive cell responses. BioRxiv 2020.07.22.205203.

Sellers, J.R. (2000). Myosins: a diverse superfamily. Biochim. Biophys. Acta BBA - Mol. Cell Res. *1496*, 3–22.

Sellers, J.R., Shi, S., Nishimura, Y., Zhang, F., Liu, R., Takagi, Y., Viasnoff, V., and Bershadsky, A.D. (2020). The Formin Inhibitor, SMIFH2, Inhibits Members of the Myosin Superfamily. Biophys. J. *118*, 125a.

Shi, Z., Graber, Z.T., Baumgart, T., Stone, H.A., and Cohen, A.E. (2018). Cell Membranes Resist Flow. Cell *175*, 1769-1779.e13.

Sinha, B., Köster, D., Ruez, R., Gonnord, P., Bastiani, M., Abankwa, D., Stan, Radu.V., Butler-Browne, G., Vedie, B., Johannes, L., et al. (2011). Cells Respond to Mechanical Stress by Rapid Disassembly of Caveolae. Cell *144*, 402–413.

Srivastava, N., Traynor, D., Piel, M., Kabla, A.J., and Kay, R.R. (2020). Pressure sensing through Piezo channels controls whether cells migrate with blebs or pseudopods. Proc. Natl. Acad. Sci. *117*, 2506–2512.

Stamnes, M. (2002). Regulating the actin cytoskeleton during vesicular transport. Curr. Opin. Cell Biol. *14*, 428–433.

Stephens, A.D., Banigan, E.J., Adam, S.A., Goldman, R.D., and Marko, J.F. (2017). Chromatin and lamin A determine two different mechanical response regimes of the cell nucleus. Mol. Biol. Cell *28*, 1984–1996.

Stoitzner, P., Pfaller, K., Stössel, H., and Romani, N. (2002). A close-up view of migrating Langerhans cells in the skin. J. Invest. Dermatol. *118*, 117–125.

Sun, S.X., Walcott, S., and Wolgemuth, C.W. (2010). Cytoskeletal cross-linking and bundling in motor-independent contraction. Curr. Biol. CB *20*, R649-654.

Sütterlin, C., and Colanzi, A. (2010). The Golgi and the centrosome: building a functional partnership. J. Cell Biol. *188*, 621–628.

Svitkina, T. (2018). The Actin Cytoskeleton and Actin-Based Motility. Cold Spring Harb. Perspect. Biol. *10*.

Svitkina, T.M., Verkhovsky, A.B., McQuade, K.M., and Borisy, G.G. (1997). Analysis of the actin-myosin II system in fish epidermal keratocytes: mechanism of cell body translocation. J. Cell Biol. *139*, 397–415.

Takamatsu, H., Takegahara, N., Nakagawa, Y., Tomura, M., Taniguchi, M., Friedel, R.H., Rayburn, H., Tessier-Lavigne, M., Yoshida, Y., Okuno, T., et al. (2010). Semaphorins guide the entry of dendritic cells into the lymphatics by activating myosin II. Nat. Immunol. *11*, 594–600.

Takenawa, T., and Miki, H. (2001). WASP and WAVE family proteins: key molecules for rapid rearrangement of cortical actin filaments and cell movement. J. Cell Sci. *114*, 1801–1809.

Takesono, A., Heasman, S.J., Wojciak-Stothard, B., Garg, R., and Ridley, A.J. (2010). Microtubules Regulate Migratory Polarity through Rho/ROCK Signaling in T Cells. PLoS ONE *5*.

Taunton, J., Rowning, B.A., Coughlin, M.L., Wu, M., Moon, R.T., Mitchison, T.J., and Larabell, C.A. (2000). Actin-Dependent Propulsion of Endosomes and Lysosomes by Recruitment of N-Wasp✪. J. Cell Biol. *148*, 519–530.

Teo, J.L., Gomez, G.A., Weeratunga, S., Davies, E.M., Noordstra, I., Budnar, S., Katsuno-Kambe, H., McGrath, M.J., Verma, S., Tomatis, V., et al. (2020). Caveolae Control Contractile Tension for Epithelia to Eliminate Tumor Cells. Dev. Cell *54*, 75-91.e7.

Theriot, J.A., and Mitchison, T.J. (1991). Actin microfilament dynamics in locomoting cells. Nature *352*, 126–131.

Thiam, H.-R., Vargas, P., Carpi, N., Crespo, C.L., Raab, M., Terriac, E., King, M.C., Jacobelli, J., Alberts, A.S., Stradal, T., et al. (2016). Perinuclear Arp2/3-driven actin polymerization enables nuclear deformation to facilitate cell migration through complex environments. Nat. Commun. *7*, 10997.

Thompson, S.B., Sandor, A.M., Lui, V., Chung, J.W., Waldman, M.M., Long, R.A., Estin, M.L., Matsuda, J.L., Friedman, R.S., and Jacobelli, J. (2020). Formin-like 1 mediates effector T cell trafficking to inflammatory sites to enable T cell-mediated autoimmunity. ELife *9*.

Trombetta, E.S., Ebersold, M., Garrett, W., Pypaert, M., and Mellman, I. (2003). Activation of lysosomal function during dendritic cell maturation. Science *299*, 1400–1403.

Tsai, T.Y.-C., Collins, S.R., Chan, C.K., Hadjitheodorou, A., Lam, P.-Y., Lou, S.S., Yang, H.W., Jorgensen, J., Ellett, F., Irimia, D., et al. (2019). Efficient Front-Rear Coupling in Neutrophil Chemotaxis by Dynamic Myosin II Localization. Dev. Cell *49*, 189-205.e6.

Tybulewicz, V.L.J., and Henderson, R.B. (2009). Rho family GTPases and their regulators in lymphocytes. Nat. Rev. Immunol. *9*, 630–644.

Ueno, H., Klechevsky, E., Morita, R., Aspord, C., Cao, T., Matsui, T., Di Pucchio, T., Connolly, J., Fay, J.W., Pascual, V., et al. (2007). Dendritic cell subsets in health and disease. Immunol. Rev. *219*, 118–142.

Ufer, F., Vargas, P., Engler, J.B., Tintelnot, J., Schattling, B., Winkler, H., Bauer, S., Kursawe, N., Willing, A., Keminer, O., et al. (2016). Arc/Arg3.1 governs inflammatory dendritic cell migration from the skin and thereby controls T cell activation. Sci. Immunol. *1*, eaaf8665–eaaf8665.

Vaahtomeri, K., Brown, M., Hauschild, R., De Vries, I., Leithner, A.F., Mehling, M., Kaufmann, W.A., and Sixt, M. (2017). Locally Triggered Release of the Chemokine CCL21 Promotes Dendritic Cell Transmigration across Lymphatic Endothelia. Cell Rep. *19*, 902–909.

Vargas, P., Maiuri, P., Bretou, M., Sáez, P.J., Pierobon, P., Maurin, M., Chabaud, M., Lankar, D., Obino, D., Terriac, E., et al. (2016). Innate control of actin nucleation determines two distinct migration behaviours in dendritic cells. Nat. Cell Biol. *18*, 43–53.

Vargas, P., Barbier, L., Sáez, P.J., and Piel, M. (2017). Mechanisms for fast cell migration in complex environments. Cell Dyn. *48*, 72–78.

Venturini, V., Pezzano, F., Castro, F.C., Häkkinen, H.-M., Jiménez-Delgado, S., Colomer-Rosell, M.,

Sánchez, M.M., Tolosa-Ramon, Q., Paz-López, S., Valverde, M.A., et al. (2019). The nucleus measures shape deformation for cellular proprioception and regulates adaptive morphodynamics. BioRxiv 865949.

Verkhovsky, A.B., Svitkina, T.M., and Borisy, G.G. (1999). Self-polarization and directional motility of cytoplasm. Curr. Biol. CB *9*, 11–20.

Vestweber, D. (2015). How leukocytes cross the vascular endothelium. Nat. Rev. Immunol. *15*, 692–704.

Vicente-Manzanares, M., Webb, D.J., and Horwitz, A.R. (2005). Cell migration at a glance. J. Cell Sci. *118*, 4917–4919.

Vicente-Manzanares, M., Ma, X., Adelstein, R.S., and Horwitz, A.R. (2009). Non-muscle myosin II takes centre stage in cell adhesion and migration. Nat. Rev. Mol. Cell Biol. *10*, 778–790.

Vogel, S.K., Petrasek, Z., Heinemann, F., and Schwille, P. (2013). Myosin motors fragment and compact membrane-bound actin filaments. ELife *2*, e00116.

Wang, P., Dreger, M., Madrazo, E., Williams, C.J., Samaniego, R., Hodson, N.W., Monroy, F., Baena, E., Sánchez-Mateos, P., Hurlstone, A., et al. (2018). WDR5 modulates cell motility and morphology and controls nuclear changes induced by a 3D environment. Proc. Natl. Acad. Sci. U. S. A. *115*, 8581–8586.

Watts, C., West, M.A., and Zaru, R. (2010). TLR signalling regulated antigen presentation in dendritic cells. Curr. Opin. Immunol. *22*, 124–130.

Weber, M., and Sixt, M. (2013). Live Cell Imaging of Chemotactic Dendritic Cell Migration in Explanted Mouse Ear Preparations. In Chemokines: Methods and Protocols, A.E. Cardona, and E.E. Ubogu, eds. (Totowa, NJ: Humana Press), pp. 215–226.

Weber, M., Hauschild, R., Schwarz, J., Moussion, C., de Vries, I., Legler, D.F., Luther, S.A., Bollenbach, T., and Sixt, M. (2013). Interstitial dendritic cell guidance by haptotactic chemokine gradients. Science *339*, 328–332.

Weiner, O.D., Neilsen, P.O., Prestwich, G.D., Kirschner, M.W., Cantley, L.C., and Bourne, H.R. (2002). A PtdInsP (3)- and Rho GTPase-mediated positive feedback loop regulates neutrophil polarity. Nat. Cell Biol. *4*, 509–513.

Weninger, W., Biro, M., and Jain, R. (2014). Leukocyte migration in the interstitial space of non-lymphoid organs. Nat. Rev. Immunol. *14*, 232–246.

Wessels, D., Soll, D.R., Knecht, D., Loomis, W.F., De Lozanne, A., and Spudich, J. (1988). Cell motility and chemotaxis in Dictyostelium amebae lacking myosin heavy chain. Dev. Biol. *128*, 164–177.

West, M.A., Wallin, R.P.A., Matthews, S.P., Svensson, H.G., Zaru, R., Ljunggren, H.-G., Prescott, A.R., and Watts, C. (2004). Enhanced Dendritic Cell Antigen Capture via Toll-Like Receptor-Induced Actin Remodeling. Science *305*, 1153.

Westman, J., Grinstein, S., and Marques, P.E. (2020). Phagocytosis of Necrotic Debris at Sites of Injury and Inflammation. Front. Immunol. *10*.

Wilson, C.A., Tsuchida, M.A., Allen, G.M., Barnhart, E.L., Applegate, K.T., Yam, P.T., Ji, L., Keren, K., Danuser, G., and Theriot, J.A. (2010). Myosin II contributes to cell-scale actin network treadmilling through network disassembly. Nature *465*, 373–377.

Wilson, K., Lewalle, A., Fritzsche, M., Thorogate, R., Duke, T., and Charras, G. (2013). Mechanisms of leading edge protrusion in interstitial migration. Nat. Commun. *4*, 2896.

de Winde, C.M., Matthews, A.L., van Deventer, S., van der Schaaf, A., Tomlinson, N.D., Jansen, E., Eble, J.A., Nieswandt, B., McGettrick, H.M., Figdor, C.G., et al. (2018). C-type lectin-like receptor 2 (CLEC-2)-dependent dendritic cell migration is controlled by tetraspanin CD37. J. Cell Sci. *131*.

de Winde, C.M., Munday, C., and Acton, S.E. (2020). Molecular mechanisms of dendritic cell migration in immunity and cancer. Med. Microbiol. Immunol. (Berl.) *209*, 515–529.

Wittmann, T., Bokoch, G.M., and Waterman-Storer, C.M. (2003). Regulation of leading edge microtubule and actin dynamics downstream of Rac1. J. Cell Biol. *161*, 845–851.

Wloga, D., Joachimiak, E., and Fabczak, H. (2017). Tubulin Post-Translational Modifications and Microtubule Dynamics. Int. J. Mol. Sci. *18*.

Wolf, K., Alexander, S., Schacht, V., Coussens, L.M., von Andrian, U.H., van Rheenen, J., Deryugina, E., and Friedl, P. (2009). Collagen-based cell migration models in vitro and in vivo. Semin. Cell Dev. Biol. *20*, 931–941.

Wolf, K., te Lindert, M., Krause, M., Alexander, S., te Riet, J., Willis, A.L., Hoffman, R.M., Figdor, C.G., Weiss, S.J., and Friedl, P. (2013). Physical limits of cell migration: Control by ECM space and nuclear deformation and tuning by proteolysis and traction force. J. Cell Biol. *201*, 1069–1084.

Worbs, T., Mempel, T.R., Bölter, J., von Andrian, U.H., and Förster, R. (2007). CCR7 ligands stimulate the intranodal motility of T lymphocytes in vivo. J. Exp. Med. *204*, 489–495.

Xie, J., Tato, C.M., and Davis, M.M. (2013). How the immune system talks to itself: the varied role of synapses. Immunol. Rev. *251*, 65–79.

Yamada, K.M., and Sixt, M. (2019). Mechanisms of 3D cell migration. Nat. Rev. Mol. Cell Biol. *20*, 738–752.

Yamada, A., Hirose, K., Hashimoto, A., and Iino, M. (2005). Real-time imaging of myosin II regulatory light-chain phosphorylation using a new protein biosensor. Biochem. J. *385*, 589–594.

Yamakita, Y., Matsumura, F., Lipscomb, M.W., Chou, P., Werlen, G., Burkhardt, J.K., and Yamashiro, S. (2011). Fascin1 Promotes Cell Migration of Mature Dendritic Cells. J. Immunol.

Yang, C., Czech, L., Gerboth, S., Kojima, S., Scita, G., and Svitkina, T. (2007). Novel roles of formin mDia2 in lamellipodia and filopodia formation in motile cells. PLoS Biol. *5*, e317.

Yolland, L., Burki, M., Marcotti, S., Luchici, A., Kenny, F.N., Davis, J.R., Serna-Morales, E., Müller, J., Sixt, M., Davidson, A., et al. (2019). Persistent and polarized global actin flow is essential for directionality during cell migration. Nat. Cell Biol. *21*, 1370–1381.

Yoshida, K., and Soldati, T. (2006). Dissection of amoeboid movement into two mechanically distinct modes. J. Cell Sci. *119*, 3833–3844.

Zhang, J., Guo, W.-H., and Wang, Y.-L. (2014). Microtubules stabilize cell polarity by localizing rear signals. Proc. Natl. Acad. Sci. *111*, 16383–16388.

Zhang, Y., Conti, M.A., Malide, D., Dong, F., Wang, A., Shmist, Y.A., Liu, C., Zerfas, P., Daniels, M.P., Chan, C.-C., et al. (2012). Mouse models of MYH9-related disease: mutations in nonmuscle myosin II-A. Blood *119*, 238–250.

Zilberman, Y., Alieva, N.O., Miserey-Lenkei, S., Lichtenstein, A., Kam, Z., Sabanay, H., and Bershadsky, A. (2011). Involvement of the Rho–mDia1 pathway in the regulation of Golgi complex architecture and dynamics. Mol. Biol. Cell *22*, 2900–2911.

Zlotnik, A., and Yoshie, O. (2012). The Chemokine Superfamily Revisited. Immunity *36*, 705–716.

université PARIS-SACLAY
ÉCOLE DOCTORALE
Structure et dynamique des systèmes vivants (SDSV)

Titre : Etude des mécanismes cellulaires permettant la migration des cellules dendritiques dans des espaces restreints

Mots clés : Leukocytes, Actine, Myosine, Contrainte Physique, Dispositif Microfabriqué

Résumé : En cas d'infection, les cellules dendritiques matures (CDm) migrent des tissus périphériques vers les ganglions lymphatiques où ils déclenchent la réponse immunitaire adaptative. Ce déplacement impose une série de contraintes physiques sur les CDm. Au niveau cellulaire, la migration des CDm repose sur la contractilité du cytosquelette d'actine et de myosine. Toutefois, la réponse mécanique spécifique qui permet aux CDm d'adapter leur mode de migration aux contraintes physiques n'a pas été entièrement caractérisée. Dans ce travail, nous avons combiné une série d'approches, des outils microfluidiques aux modèles ex vivo, pour disséquer les réarrangements du cytosquelette nécessaires à l'adaptation du mode de migration des cellules dendritiques aux propriétés physiques de leur microenvironnement. Nous avons montré que les CDm sont capables de maintenir une vitesse constante tout en migrant à différents niveaux de confinement. Cela révèle la capacité des CDm à adapter leur mode de migration en réponse aux changements dans la géométrie de leur microenvironnement. Au niveau cellulaire, le confinement dans les microcanaux induit un remodelage rapide et spécifique du cytosquelette d'actine et de myosine. Il est essentiel à la plasticité migratoire des CDm et optimise le déplacement de ces cellules dans des environnements 3D complexes. Ces travaux conduisent à une meilleure compréhension des mécanismes permettant aux CDm d'adapter leur motilité face à des structures tissulaires spécifiques. Ils permettront de mieux appréhender le contrôle de la migration des leucocytes dans des espaces confinés et pouvoir ainsi la moduler avec précision afin de favoriser ou de prévenir les réponses immunitaires.

Title : Study of cellular mechanisms allowing dendritic cell migration in restricted spaces

Keywords : Leukocytes, Actin, Myosin, Physical constraints, Microfabricated devices

Abstract : Upon infection, mature dendritic cells (mDCs) migrate from peripheral tissue to lymph nodes and initiate the adaptive immune response. This fast and tightly regulated process imposes a series of physical constraints and is tuned by different microenvironmental factors, such as the physical properties of the tissue. Mechanistically, mDCs migration relies on actomyosin flow and contractility, which are dependent on non-muscular Myosin IIA activity. However, the specific mechanoresponse that allows mDCs to adapt their migration machinery to irregular 3D landscapes has not been fully characterized. In this work, we combined a series of approaches, from micro-fabricated devices to ex vivo skin models, to dissect the cytoskeleton rearrangements used by mDCs to overcome the physical barriers imposed by the tissue. We have shown mDCs are able to maintain a constant speed while migrating at different levels of confinement. This reveals the extreme capacity of mDCs to adapt their migration machinery in response to changes in the geometry of their microenvironment. At the cellular level, confinement in microchannels induces a fast and specific actomyosin remodeling in mDCs. This reveals a complete actomyosin rearrangement triggered by confinement, which is essential for mDCs migratory plasticity that allows these cells to move in intricate 3D geometries. The full understanding of how mDCs and other leukocytes adapt their motility to specific tissue structures will provide better knowledge on how cell migration is controlled in confined spaces and new insight to finely tune their migration to promote or prevent immune responses.

Université Paris-Saclay
Espace Technologique / Immeuble Discovery
Route de l'Orme aux Merisiers RD 128 / 91190 Saint-Aubin, France